



UNIVERSITY OF
LIVERPOOL

**Reconstructing historical sea-level trends for the Croatian coast of
the Adriatic Sea using salt-marsh foraminifera**

Thesis submitted in accordance with the requirements of the
University of Liverpool for the degree of Doctor in Philosophy

Timothy Adam Shaw

November 2013

ABSTRACT

The application of salt-marsh foraminifera to reconstruct historical sea-level trends was investigated for the Croatian coast of the Adriatic Sea using a transfer function approach. This technique, whilst well practised from north Atlantic sites along the shores of America and UK, has previously evaded any published study in the Mediterranean region. A total of 70 surface samples were collected across separate transects established at two micro-tidal salt-marsh sites from the central Croatian coastline to establish a modern dataset of foraminifera. In addition, environmental variables were also investigated including salinity, pH, organic matter, particle size, distance (from open water) and altitude, relative to the Croatian national datum. Three sediment cores were sampled for fossil foraminifera and composite chronologies involving short-lived radionuclides, radiocarbon dating and pollution indicators from XRF. Age-depth models were created using classical and Bayesian approaches. Quantitative analysis of the foraminiferal assemblages revealed on average three faunal zones in which characteristic species occurred. This comprised a faunal zone composed almost exclusively of agglutinated species; *J. macrescens*, *T. inflata* and *M. fusca* extending between mean tidal level (MTL) and beyond MHWST (higher altitude). A second faunal zone was more variable and comprised of a mixed assemblage of agglutinated species described above in addition to calcareous species; *Ammonia* spp., *Elphidium* spp., *Haynesina germanica* and *Quinqueloculina* spp. This zone spanned a large vertical range above and below MTL. In a third faunal zone calcareous species dominated and was restricted to the lower altitudes of the salt-marsh environments. Further quantitative measures were employed to test the hypothesis that foraminiferal distributions were controlled by altitude. Partial ordination techniques revealed altitude as a statistically significant control confirming their suitability as proxies for sea-level in transfer function reconstructions. An analysis of species environment relationships revealed strong linear response suggesting the use of PLS regression models. Transfer functions were then developed for both site specific and a total combined dataset, where small r^2_{jack} values largely reflected the short environmental gradients despite relatively low predictions errors ($\text{RMSEP}_{\text{jack}} = <0.11$). The total combined dataset was chosen and screened to remove sample outliers improving model performance ($r^2_{\text{jack}} = 0.54$ and $\text{RMSEP}_{\text{jack}} = 0.08$). Finally, the transfer function model was applied to core sediments to reconstruct mean sea-level where an inflexion observed at AD 1940 showed acceleration comparable to other proxy reconstructions. Indeed this trend was similar to instrumental data from Trieste tide-gauge records. Similarly the transfer function reconstruction identifies the dramatic increases in MSL observed in both tide-gauge (Split and Trieste) and satellite observations since the early 1990s.

ACKNOWLEDGMENTS

I would like to begin by saying how thankful I am to my supervisory team, Prof. Andrew Plater, Dr. Jason Kirby and Dr. Simon Holgate, for their help, guidance and encouragement throughout the past four years. I have many fond memories, too many to write here but I thoroughly enjoyed working with you all and will be forever grateful. I am particularly appreciative to Andy for his help, advice and continued support throughout the PhD, especially during the later stages of the final write up. I could not have asked for a better supervisor.

I would also like to thank all of my family and friends for their continued support. I am indebted to my parents, who have always encouraged me throughout my studies and provided much needed financial support, particularly during the final few months of the thesis. I certainly would not have made it through without your help. At this point I'd also like to acknowledge my better half, Jennifer, who was always there for me. How we managed to do two PhD's at the same time, live and work together and raise Isaac I'll never know but I'm glad we came through and thanks for putting up with me. I should also like to mention Isaac, who provided much needed play time, sleep deprivation and reflection that the PhD wasn't everything. Watching you grow up has been another highlight of the past four years.

I am very grateful to the Geography department, University of Liverpool and its staff that have helped me over the past few years, most notably Sandra Mather, Susanne Yee, Tinho Da Cruz, Mike O'Conner, Alan Henderson and Irene Copper. I would also like to thank Dr. John Boyle for his help regarding XRF and for inviting me along to Santa Cruz every year. It provided a much welcomed break to my studies and was my guaranteed trip abroad over the past four years. I am also very appreciative to Prof. Richard Chiverrell for his time, comments and assistance in constructing age-depth models and also for our many tennis sessions which helped take my mind off my studies (if only for a short period of time).

I would also like to thank my fellow post-graduate students (past and present) in the Geography department for the many coffee, lunch and at times much needed pub sessions. I would especially like to thank Dr. Jennifer Clear, (soon to be) Dr. Beverly Todd, Dr. David Clarke and Dr. Hayley Mills. I thank Jenny and Bev for our time in the office and putting up with my loud and select music tastes while David is acknowledged for his 'words of wisdom' and IPA recommendations, particularly during our visits to Santa Cruz. I thank Hayley for her help and patience with the statistical analyses. I don't think I would have made it through without your help.

I would like to thank the NERC radiocarbon facility (East Kilbride), in particular Dr. Steve Morton, and the steering committee, for their helpful comments and finally granting the radiocarbon dates. Prof. Peter Appleby and Dr. Gayane Piliposyan from the University of Liverpool are also acknowledged for their help regarding the radionuclide chronology. I am also grateful to Dr. Srdjan Cupic from the Hydrographic Institute of the Republic of Croatia for providing the tidal data used in this thesis. I would also like to say a special thank you to Dr. Pero Tutman from the Institute of Oceanography and Fisheries, Split for his time, help and advice (including food – in particular the fresh oysters!) during our fieldwork trips in Croatia. I will always keep a watchful eye on Hajduk Split FC - go Torcida!

Lastly I would like to thank my internal and external examiners, Dr. Fabienne Marret-Davies, University of Liverpool and Dr. Robin Edwards, Trinity College Dublin for the discussions we had during the viva and for their constructive comments which undoubtedly improved the final thesis.

Thank you to you all.

TABLE OF CONTENTS

Title Page	i
Abstract	ii
Acknowledgments	iii
Table of Contents	v
List of Figures	x
Lit of Tables	xvi
1. INTRODUCTION AND AIMS	1
1.1. BACKGROUND	1
1.2. RESEARCH AIMS	3
1.2.1. Objectives	4
1.3. OUTLINE OF THESIS	4
2. RESEARCH CONTEXT	6
2.1. INTRODUCTION	6
2.2. MEDITERRANEAN SEA-LEVEL	6
2.2.1. Instrumental records of sea-level change	6
2.2.2. Long-term recorders of sea-level change	8
2.3. PROXY SEA-LEVEL RECONSTRUCTIONS	10
2.3.1. Salt-marsh environments	10
2.3.2. Microfossil indicators	11
2.3.3. Reconstructing sea-level	14
2.3.4. Microfossil-based transfer functions	15
3. STUDY AREA AND RESEARCH METHODS	21
3.1. INTRODUCTION	21
3.2. STUDY AREA	21
3.2.1. The Mediterranean Sea	21
3.2.2. The Adriatic Sea	23
3.2.2.1. Oceanographic setting	23
3.2.2.2. Tectonic setting	25
3.2.2.3. Glacial isostatic adjustment	26

3.3. STUDY SITES	27
3.3.1. Rationale for site selection	27
3.3.2. Site selection – The Croatian Coast	28
3.3.3. Jadrtovac	30
3.3.4. Blace	31
3.4. RESEARCH METHODS	33
3.5. FIELD METHODS	33
3.5.1. Salt-marsh stratigraphy	33
3.5.2. Salt-marsh sampling	33
3.5.3. RBR temporary tide-gauge	35
3.5.4. Levelling survey	36
3.6. LABORATORY METHODS	37
3.6.1. Foraminiferal analyses (fossil and contemporary)	37
3.6.2. Environmental variable analyses	38
3.6.2.1. Salinity and pH	38
3.6.2.2. Organic matter	39
3.6.2.3. Particle size analysis	39
3.6.2.4. Dry bulk density	40
3.7. CORE CHRONOLOGY	40
3.7.1. Short-lived radionuclides	44
3.7.2. Radiocarbon dating	44
3.7.3. X-ray fluorescence	46
3.7.4. Age-depth modelling	47
3.8. MULTIVARIATE STATISTICAL ANALYSES	49
3.8.1. Zonation	49
3.8.2. Ordination	50
4. RESULTS I	
CONTEMPORARY SALT-MARSH DATA	52
4.1. INTRODUCTION	52
4.2. ENVIRONMENTAL VARIABLES	52
4.2.1. Jadrtovac site 1	52
4.2.2. Jadrtovac site 2	55
4.2.3. Blace transect 1	57
4.2.4. Blace transect 2	59
4.3. THE DISTRIBUTION OF CONTEMPORARY FORAMINIFERA	62
4.3.1. Jadrtovac site 1	62

4.3.2. Jadrtovac site 2.....	65
4.3.3. Jadrtovac random sampling.....	67
4.3.4. Blace transect 1.....	69
4.3.5. Blace transect 2.....	71
4.4. THE VERTICAL DISTRIBUTION OF CONTEMPORARY SALT-MARSH FORAMINIFERA.....	73
4.4.1. Jadrtovac site 1.....	74
4.4.2. Jadrtovac site 2.....	76
4.4.3. Jadrtovac random sampling.....	78
4.4.4. Blace transect 1.....	80
4.4.5. Blace transect 2.....	82
4.4.6. Jadrtovac transects 1 & 2.....	84
4.4.7. Blace transects 1 & 2.....	86
4.5. CONTROLS GOVERNING CONTEMPORARY SALT-MARSH FORAMINIFERAL DISTRIBUTIONS.....	88
4.5.1. Jadrtovac transects 1 & 2.....	89
4.5.2. Blace transects 1 & 2.....	91
4.5.3. Total combined dataset.....	93
4.6. SUMMARY OF CONTEMPORARY SALT-MARSH DATA.....	95
 5. RESULTS II	
 <i>FOSSIL SALT-MARSH DATA AND CHRONOLOGY.....</i>	<i>99</i>
5.1. INTRODUCTION.....	99
5.2. SEDIMENT STRATIGRAPHY.....	99
5.2.1. Jadrtovac site 1.....	100
5.2.2. Jadrtovac site 2.....	101
5.2.3. Blace.....	102
5.3. FOSSIL FORAMINIFERA.....	103
5.3.1. Jadrtovac site 1.....	103
5.3.2. Jadrtovac site 2.....	104
5.3.3. Blace.....	105
5.4. ENVIRONMENTAL VARIABLES.....	106
5.4.1. Organic matter.....	106
5.4.2. Dry bulk density.....	107
5.4.3. Particle size analysis.....	108
5.5. CORE CHRONOLOGY.....	110
5.5.1. Short-lived radionuclides.....	110

5.5.2.	X-ray fluorescence.....	114
5.5.3.	Jadrtovac site 1 chronology.....	116
5.5.3.1.	Radiocarbon dating.....	117
5.5.3.2.	Clam age-depth model.....	121
5.5.3.3.	OxCal age-depth model.....	122
5.5.4.	Jadrtovac site 2 chronology.....	124
5.5.5.	Blace chronology.....	124
5.6.	SUMMARY OF FOSSIL SALT-MARSH DATA	126
6.	RESULTS III	
	<i>TRANSFER FUNCTION ANALYSIS AND SEA-LEVEL RECONSTRUCTION</i>	<i>128</i>
6.1.	INTRODUCTION.....	128
6.2.	TRANSFER FUNCTION METHODOLOGY.....	129
6.2.1.	Species-environment response model.....	129
6.2.2.	Model selection.....	129
6.2.3.	Assessing model performance.....	130
6.2.4.	Data screening.....	131
6.2.5.	Component selection.....	132
6.2.6.	Modern analogue technique.....	133
6.2.7.	Transfer function application.....	134
6.3.	TRANSFER FUNCTION RESULTS	135
6.3.1.	Jadrtovac transects 1 & 2.....	135
6.3.2.	Blace transects 1 & 2.....	137
6.3.3.	Total combined dataset.....	139
6.3.4.	Local versus regional training set.....	141
6.3.5.	Training set screening.....	142
6.3.6.	Modern analogues.....	147
6.3.7.	Palaeo-marsh altitudereconstruction.....	149
6.3.8.	Unscreened total dataset comparison.....	153
6.4.	SEA-LEVEL RECONSTRUCTION.....	155
6.4.1.	Jadrtovac site 1.....	156
6.4.2.	Jadrtovac site 2.....	156
6.4.3.	Blace.....	157
6.5.	SUMMARY OF TRANSFER FUNCTION RECONSTRUCTION.....	161

7.	INTERPRETATIONS AND DISCUSSION	163
7.1.	INTRODUCTION	163
7.2.	FOSSIL ENVIRONMENTS AND SITE EVOLUTION	163
7.3.	CONTEMPORARY FORAMINIFERA DISTRIBUTIONS	165
7.3.1.	Foraminiferal assemblages	165
7.3.2.	Dead <i>versus</i> living assemblages	167
7.3.3.	Foraminiferal and environmental controls	168
7.4.	TRANSFER FUNCTION PERFORMANCE	171
7.5.	COMPARISON WITH INSTRUMENTAL RECORDS	173
7.6.	FURTHER WORK	182
7.6.1.	Improving chronological constraints	182
7.6.2.	Increasing modern analogues	182
8.	CONCLUSIONS	184
	REFERENCES	187
	APPENDICIES	211
	APPENDIX A. TROELS SMITH CORE DESCRIPTIONS	211
	APPENDIX B. FORAMINIFERAL RAW COUNTS	217
	APPENDIX C. RADIOCARBON ANALYTICAL REPORT	227
	APPENDIX D. TRANSFER FUNCTION RESULTS	229
	APPENDIX E. SCANNING ELECTRON MICROSCOPE IMAGES	232
	APPENDIX F. TIDAL LEVELS	234

LIST OF FIGURES

Figure 1.1 Map showing (a) global distribution of tide-gauge stations included in the PSMSL database and (b) stations with records longer than 40 years (Holgate et al., 2013).....	1
Figure 1.2 Annual averages of global mean sea level taken from the latest IPCC report (Bindoff et al., 2007). The red curve showing reconstructed sea level fields since 1870 (Church and White, 2006); the blue curve shows coastal tide-gauge measurements since 1950 (Holgate and Woodworth, 2004) and the black curve showing satellite altimetry data from 1993 to 2001 (Leuliette et al., 2004).....	2
Figure 2.1 Tide-gauge stations in the Mediterranean with records longer than 35 years (black dots). Study area also shown (rectangle). <i>After</i> Marcos and Tsimplis (2008).....	7
Figure 2.2 Sea-level change from tide-gauges in the Adriatic Sea (Tsimplis et al., 2012).....	8
Figure 2.3 Schematic diagram to illustrate the distribution of foraminiferal assemblages across a salt-marsh environment.	12
Figure 2.4 Principles of quantitative palaeoenvironmental reconstruction showing X_0 , the unknown environmental variable to be reconstructed from fossil assemblage Y_0 , and the role of a modern training set consisting of modern biological Y (foraminifera) and environmental data X (elevation). Modified <i>after</i> Birks (1995).	15
Figure 2.5 Taxon-environment response models showing (a) Gaussian unimodal distribution, (b) linear distribution between species abundance (y) and the environmental variable(x). u = optimum and t = tolerance (Horton and Edwards, 2006; modified after Birks, 1995).....	18
Figure 3.1 Map showing sub-divisions of the eastern and western Mediterranean Sea including the study area (highlighted in the black box) within the Adriatic Sea.....	22
Figure 3.2 Map of (a) Adriatic Sea showing location of tide-gauge stations, study site areas (square boxes) and (b) approximate location of bathymetry profile (dashed line) redrawn <i>after</i> Piva et al. (2008).	24
Figure 3.3 Tectonic setting of the Mediterranean region (Morhange and Pirazzoli, 2005).....	26
Figure 3.4 Study area map showing relative locations of sample sites (a) Jadrtovac and (b) Blace along the Croatian coastline, eastern Adriatic Sea	29
Figure 3.5 Study site map showing (a) location of salt-marsh environment within Morinje Bay with surface transects, random sampling area and core sties, (b) photo of JD1 sample site, and (c) photo of JD2 sample	31
Figure 3.6 Study site map showing (a) location of salt-marsh environment at Blace with surface transect and core sties, (b) photo of BL1 and (c) BL2 sample sites	32

Figure 3.7 Details and photos of the national geodetic benchmark used near to Jadrtovac	36
Figure 3.8 <i>Scirpus holoschoenus</i> seeds analysed for ^{14}C from JD1 core (26-27 cm)	45
Figure 4.1 Measured environmental variables (altitude m HVR571, salinity, pH, LOI and mean grain size) across JD1 transect	54
Figure 4.2 Measured environmental variables (altitude m HVR571, salinity, pH, LOI and mean grain size) across JD2 transect	56
Figure 4.3 Measured environmental variables (altitude m HVR571, salinity, pH, LOI and mean grain size) across Blace transect 1	58
Figure 4.4 Measured environmental variables (altitude m HVR571, salinity, pH, LOI and mean grain size) across Blace transect 2	60
Figure 4.5 Substrate composition showing total sand, silt and clay percentage across transects (a) JD1, (b) JD2, (c) BL1 and (d) BL2. Sample locations also shown	61
Figure 4.6 Relative abundance (%) of 'dead' foraminifera and concentration (per 5 cm ³) across JD1 transect. Altitude (m HVR571) also shown	64
Figure 4.7 Relative abundance (%) of 'dead' foraminifera and concentration (per 5 cm ³) across JD2 transect. Altitude (m HVR571) also shown	66
Figure 4.8 Relative abundance (%) of 'dead' foraminifera and concentration (per 5 cm ³) from JDR ordered by altitude from high (1) to low (10)	68
Figure 4.9 Relative abundance (%) of 'dead' foraminifera and concentration (per 5 cm ³) across BL1 transect. Altitude (m HVR571) also shown	70
Figure 4.10 Relative abundance (%) of 'dead' foraminifera and concentration (per 5 cm ³) across BL2 transect. Altitude (m HVR571) also shown	72
Figure 4.11 (a) Unconstrained cluster analysis based on unweighted Euclidean distance identifying faunal zones, (b) detrended correspondence analysis displaying faunal zones, and (c) altitude of faunal zones (m HVR571) based on relative percentages of 'dead' assemblages from JD1 with tidal levels superimposed	75
Figure 4.12 (a) Unconstrained cluster analysis based on unweighted Euclidean distance identifying faunal zones, (b) detrended correspondence analysis displaying faunal zones, and (c) altitude of faunal zones (m HVR571) based on relative percentages of 'dead' assemblage from JD2 with tidal levels superimposed	77
Figure 4.13 (a) Unconstrained cluster analysis based on unweighted Euclidean distance identifying faunal zones, (b) detrended correspondence analysis displaying faunal zones, and (c) altitude of faunal zones (m HVR571) based on relative percentages of 'dead' assemblage from JDR with tidal levels superimposed	79
Figure 4.14 (a) Unconstrained cluster analysis based on unweighted Euclidean distance identifying faunal zones, (b) detrended correspondence analysis displaying faunal zones,	

and (c) altitude of faunal zones (m HVR571) based on relative percentages of 'dead' assemblage from BL1 with tidal levels superimposed.....	81
Figure 4.15 (a) Unconstrained cluster analysis based on unweighted Euclidean distance identifying faunal zones, (b) detrended correspondence analysis displaying faunal zones, and (c) altitude of faunal zones (m HVR571) based on relative percentages of 'dead' assemblage from BL2 with tidal levels superimposed.....	83
Figure 4.16 (a) Unconstrained cluster analysis based on unweighted Euclidean distance identifying faunal zones, (b) detrended correspondence analysis displaying faunal zones, and (c) altitude of faunal zones (m HVR571) based on relative percentages of 'dead' assemblage from the combined transect dataset at Jadrtovac with tidal levels superimposed.....	85
Figure 4.17 (a) Unconstrained cluster analysis based on unweighted Euclidean distance identifying faunal zones, (b) detrended correspondence analysis displaying faunal zones, and (c) altitude of faunal zones (m HVR571) based on relative percentages of 'dead' assemblage from the combined Blace dataset with tidal levels superimposed.....	87
Figure 4.18 Redundancy Analysis biplots of (a) samples relative to environmental variables and (b) species relative to environmental variables from JDT. Pie charts showing (c) total explained and unexplained variance and (d) unique contributions of tested environmental variables as identified from pRDA.....	90
Figure 4.19. Canonical correspondence analysis biplots of (a) samples relative to environmental variables and (b) species relative to environmental variables from BLT. Pie charts showing (c) total explained and unexplained variance and (d) unique contributions of tested environmental variables as identified from pCCA.....	92
Figure 4.20 Canonical correspondence analysis biplots of (a) samples relative to environmental variables and (b) species relative to environmental variables from a total combined transect dataset. Pie charts showing (c) total explained and unexplained variance and (d) unique contributions of tested environmental variables as identified from pCCA....	94
Figure 5.1 Simplified sediment stratigraphy at JD1, plotted relative to altitude (m HVR571) from high (1) to low (12) marsh. 'Type' core JD1 also highlighted (4).....	100
Figure 5.2 Photograph of JD1 42 cm 'type' core illustrating the up-core transition of basal minerogenic silts and clays to highly organic peat sediments towards the surface.....	101
Figure 5.3 Simplified sediment stratigraphy at BL, plotted relative to altitude (m HVR571) from high (1) to low (7) salt-marsh. 'Type' core BL also highlighted (2).....	102
Figure 5.4 Photograph of BL 32 cm 'type' core.....	102
Figure 5.5 Fossil foraminiferal stratigraphy from core JD1 expressed as a percentage, ordered by depth (cm) and altitude (m HVR571). Simplified sediment stratigraphy, foraminiferal abundance (per 5 cm ³) and LOI _{450°C} are also displayed.....	104

Figure 5.6 Fossil foraminiferal stratigraphy from core JD2 expressed as a percentage, ordered by depth (cm) and altitude (m HVRS71). Simplified sediment stratigraphy, foraminiferal abundance (per 5 cm ³) and LOI _{450°C} are also displayed.....	105
Figure 5.7 Fossil foraminiferal stratigraphy from core BL expressed as a percentage, ordered by depth (cm) and altitude (m HVRS71). Simplified sediment stratigraphy, foraminiferal abundance (per 5 cm ³) and LOI _{450°C} are also displayed.....	106
Figure 5.8 Down-core trends of LOI (%) for cores (a) JD1, (b) JD2 and (c) BL.....	107
Figure 5.9 Down-core trends of DBD (g/cm ³) for cores (a) JD1, (b) JD2 and (c) BL.....	108
Figure 5.10 Down-core particle size data for cores (a) JD1, (b) JD2 and (c) BL showing percentage sand, silt, clay, mean grain size (µm), sorting (φ), skewness and kurtosis.....	109
Figure 5.11 Fallout radionuclides of the JD1 core showing (a) total ²¹⁰ Pb, (b) unsupported ²¹⁰ Pb, (c) ¹³⁷ Cs concentrations and (d) ¹³⁷ Cs/ ²¹⁰ Pb activity ratio versus depth.....	111
Figure 5.12 Fallout radionuclides of the JD2 core showing (a) total ²¹⁰ Pb, (b) unsupported ²¹⁰ Pb and (c) ¹³⁷ Cs concentrations versus depth.....	112
Figure 5.13 Fallout radionuclides of the BL core showing (a) total ²¹⁰ Pb, (b) unsupported ²¹⁰ Pb, (c) ¹³⁷ Cs and (d) ²⁴¹ AMS concentrations versus depth.....	113
Figure 5.14 Cu, Pb and Zn profiles for (a) JD1, (b) JD2 and (c) BL cores.....	115
Figure 5.15 Radiometric chronology for JD1 showing CRS model ²¹⁰ Pb dates, sedimentation rate (g cm ⁻² y ⁻¹) and the 1963 and 1986 depths suggested by ¹³⁷ Cs record.....	116
Figure 5.16 OxCal (Bronk Ramsey, 2009) calibration of ¹⁴ C ages showing (a) ¹⁴ C ages intercepting IntCal 09 calibration curve (Reimer et al., 2009) and (b, c and d) individual calibration plots displaying Gaussian distribution of uncalibrated ¹⁴ C ages (red curve), IntCal 09 calibration curve (blue curve) (Reimer et al., 2009) and highest <i>posterior</i> density ranges (2σ c. 95% probability) of calibrated ages (dark grey curve). Median age (AD) and agreement level indexes are also provided.....	120
Figure 5.17 Smooth spline (smoothing=0.6) age-depth model produced by <i>Clam</i> (Blaauw, 2010) for core JD1 combining ²¹⁰ Pb and ¹³⁷ Cs analyses and calibrated ¹⁴ C age distributions.....	122
Figure 5.18 P_Sequence age-depth model with $k = 0.5 \text{ mm}^{-1}$ produced by <i>OxCal</i> (Bronk Ramsey, 2009) for core JD1 combining ²¹⁰ Pb and ¹³⁷ Cs analyses and calibrated ¹⁴ C age distributions to 2σ (95% confidence level). Agreement indexes [A: #] and median ages also highlighted (crosshair).....	123
Figure 5.19 Radiometric chronology of the JD2 core showing the 1963 and possible 1986 depths suggested by the ¹³⁷ Cs stratigraphy and also the CRS model ²¹⁰ Pb dates and sedimentation rates calculated using the 1963 ¹³⁷ Cs date as a reference point.....	125

Figure 5.20 Radiometric chronology of the BL core showing CRS model ^{210}Pb dates, sedimentation rate ($\text{g cm}^{-2} \text{y}^{-1}$) and the 1963 and 1986 depths suggested by the ^{137}Cs stratigraphy.....	125
Figure 6.1 Transfer function (PLS) observed versus predicted altitude (m HVR571) and residual values for JDT training set (component 2; jack-knife measures).....	137
Figure 6.2 Transfer function (PLS) observed versus predicted altitude (m HVR571) and residual values for BLT training set (component 2; jack-knife measures).....	139
Figure 6.3 Transfer function (PLS) observed versus predicted altitude (m HVR571) and residual values for TCD training set (component 2; jack-knife measures).....	140
Figure 6.4 Transfer function PLS (component 3) and WA-PLS (component 2) observed versus predicted altitude (m HVR571) and residual values for the screened TCD training set.....	145
Figure 6.5 Transfer function (PLS) observed versus predicted altitude (m HVR571) and residual values for agglutinated only TCD training set (component 3).....	146
Figure 6.6 Summary MAT results showing ‘good’, ‘close’ and ‘poor’ analogues in cores (a) JD1, (b) JD2 and (c) BL.....	148
Figure 6.7 Palaeo-marsh altitude (m HVR571) estimated using PLS (component 3), WA-PLS (component 2) and ML transfer functions for core JD1 including sample specific errors estimated by bootstrapping. Good/close and poor modern analogues also displayed.....	150
Figure 6.8 Palaeo-marsh altitude (m HVR571) estimated using PLS (component 3), WA-PLS (component 2) and ML transfer functions for core JD2 including sample specific errors estimated by bootstrapping. Good/close and poor modern analogues also displayed.....	152
Figure 6.9 Palaeo-marsh altitude (m HVR571) estimated using PLS (component 3), WA-PLS (component 2) and ML transfer functions for core BL including sample specific errors estimated by bootstrapping. Good/close and poor modern analogues also displayed.....	153
Figure 6.10 Palaeo-marsh altitude (m HVR571) estimated using PLS (component 3), WA-PLS (component 2) including sample specific errors estimated by bootstrapping for an unscreened total training set. Good/close and poor modern analogues also displayed.....	154
Figure 6.11 PLS transfer function reconstruction of MSL using the TCD screened training set plotted against (a) core depth (cm) and (b) OxCal age-depth model (AD) for core JD1 including bootstrap prediction errors (m) and model uncertainties (2σ).....	158
Figure 6.12 PLS transfer function reconstruction of MSL using the TCD screened training set plotted against (a) core depth (cm) and (b) chronology (AD) for core JD2 including bootstrap prediction errors (m) and age uncertainties (AD).....	159
Figure 6.13 PLS transfer function reconstruction of MSL using the TCD screened training set plotted against (a) core depth (cm) and (b) chronology (AD) for core BL including bootstrap prediction errors (m) and age uncertainties (AD).....	160

Figure 7.1 Yearly average mean sea-level from Split tide-gauge (Holgate et al., 2013).....	174
Figure 7.2 Yearly average mean sea-level from Trieste tide-gauge (Holgate et al., 2013).....	174
Figure 7.3 Transfer function reconstruction of MSL for core JD1 compared with (a) Split tide-gauge data from AD 1955 and (b) extrapolated back through time including bootstrap prediction errors (m) and model uncertainties (2σ). Good/close and poor modern analogues also displayed.....	175
Figure 7.4 Transfer function reconstruction of MSL for core JD compared with Split tide-gauge data from AD 1955 including bootstrap prediction errors (m) and age uncertainties (AD).....	176
Figure 7.5 Transfer function reconstruction of MSL for core BL compared with (a) Split tide-gauge data from AD 1955 and (b) extrapolated back through time including bootstrap prediction errors (m) and model uncertainties (AD). Good/close and poor modern analogues also displayed.....	177
Figure 7.6 Transfer function reconstruction of MSL for core JD1. Altitudes of fossil samples were increased in line with tide-gauge where the altitude was raised 14 cm.....	178
Figure 7.7 Transfer function reconstruction of MSL for core JD1 compared with (a) Trieste tide-gauge data from AD 1875 and (b) extrapolated back through time including bootstrap prediction errors (m) and model uncertainties (2σ). Good/close and poor modern analogues also displayed. Note core altitude was raised 14cm.....	179
Figure 7.8 Transfer function reconstruction of MSL for core BL compared with Trieste tide-gauge data from AD 1875 including bootstrap prediction errors (m) and model uncertainties (AD). Good/close and poor modern analogues also displayed.....	180

LIST OF TABLES

Table 3.1 Mean daily tidal range along Croatian coast of the Adriatic Sea (Hydrographic Institute, 1955–2002). Location of tide-gauge stations are shown in figure 3.2.....	25
Table 3.2 ICE-5G (v.1.3) model predictions of GIA-induced sea-level change and vertical land motion (mm/yr) for PSMSL tide-gauge records >35 yr located along the eastern Adriatic shoreline for the past 250 years, next 250 years and average present-day rate. Location of tide-gauge stations are shown in figure 3.2.....	27
Table 3.3 Details and period of relative sea-level trends (mm yr ⁻¹) for tide gauge stations along the eastern Adriatic coastline with records longer than 35 years (<i>after</i> Marcos and Tsimplis, 2008). Location of tide-gauge stations are shown in figure 3.2.....	28
Table 3.4 Tidal levels (relative to m HVRS71) derived from Split tide-gauge (Hydrographic Institute, 1955–2002).....	31
Table 3.5 Summary of sampling at study sites Jadrtovac and Blace.....	35
Table 4.1 Pearson's correlation coefficients (<i>r</i>) for environmental variables at JD1.....	53
Table 4.2 Pearson's correlation coefficients (<i>r</i>) for environmental variables at JD2.....	55
Table 4.3 Pearson's correlation coefficients (<i>r</i>) for environmental variables at BL1.....	57
Table 4.4 Pearson's correlation coefficients (<i>r</i>) for environmental variables at BL2.....	59
Table 4.5 Summary of contemporary surface samples used in the modern training set.....	74
Table 4.6 Altitude and distance of samples 16, 17 and 18 added to the BL1 dataset.....	79
Table 4.7 Summary DCA results for dead foraminiferal assemblages for JDT.....	89
Table 4.8 Summary RDA results from dead foraminiferal assemblages for JDT.....	89
Table 4.9 Summary DCA results for dead foraminiferal assemblages for BLT.....	91
Table 4.10 Summary CCA results from dead foraminiferal assemblages for BLT.....	91
Table 4.11 Summary DCA results for dead foraminiferal assemblages for TCD.....	93
Table 4.12 Summary CCA results for dead foraminiferal assemblages for TCD.....	93
Table 5.1 Lithology of JD1 'type' core following the Troëls-Smith (1955) classification.....	101
Table 5.2 Lithology of JD2 'type' core following Troëls-Smith (1955) classification.....	101
Table 5.3 Lithology of BL 'type' core following Troëls-Smith (1955) classification.....	103
Table 5.4 Fallout radionuclide activities of the JD1 core.....	112
Table 5.5 Fallout radionuclide activities of the JD2 core.....	113
Table 5.6 Fallout radionuclide activities of the BL core.....	114
Table 5.7 Combined ²¹⁰ Pb (CRS) and ¹³⁷ Cs chronology of the JD1 core.....	117
Table 5.8 Depths and dry weights (mg) at which <i>Scirpus holoschoenus</i> seeds were found in core JD1.....	118

Table 5.9 AMS ^{14}C results for core JD1 (NERC allocation number 1678.1012).....	118
Table 5.10 Revised ^{210}Pb chronology of the JD2 core.....	126
Table 5.11 Combined ^{210}Pb (CRS) and ^{137}Cs chronology of the BL core.....	126
Table 6.1 Summary of the number of surface samples included in each training set.....	129
Table 6.2 Summary DCCA results for JDT training set. Length of gradient is in SD units..	135
Table 6.3 Statistical summary of PLS transfer function performance from modern dead foraminiferal assemblages using the JDT training set.....	136
Table 6.4 Summary DCCA results for BLT training set. Length of gradient is in SD units..	137
Table 6.5 Statistical summary of PLS and WA-PLS transfer function performance for dead foraminiferal assemblages using the BLT training set.....	138
Table 6.6 Summary DCCA results for TCD training set. Length of gradient is in SD units..	139
Table 6.7 Statistical summary of PLS and WA-PLS transfer function performance for dead foraminiferal assemblages using a total combined transect training set.....	140
Table 6.8 Comparison of training set size with published literature.....	141
Table 6.9 Summary of surface samples removed through screening process. The standard deviation of altitude for unscreened TCD training set was 0.141	142
Table 6.10 Summary DCCA results for a screened TCD training set.....	143
Table 6.11 Statistical summary of transfer function performance for screened dead foraminiferal assemblages from a total combined training set	144
Table 6.12 Statistical summary of PLS and WA-PLS transfer function performance for screened dead agglutinated species only foraminiferal assemblages from a total combined transect training set.....	146
Table 6.13 Summary of MAT percentiles using dissimilarities in the TCD training set.....	147
Table 6.14 Statistical summary of ML transfer function performance for screened dead foraminiferal assemblages from a total combined training set.....	149
Table 6.15 Summary of palaeo-marsh altitude and average errors for core JD1.....	151
Table 6.16 Summary of palaeo-marsh altitude and average errors for core JD2.....	152
Table 6.17 Summary of palaeo-marsh altitude and average errors for core BL	153
Table 6.18 Statistical summary of transfer function performance for an unscreened total training set including samples from JDR. C = component.....	154
Table 7.1 Summary table highlighting the amount elevation accounts for in the explained variance for microfossil distributions from salt-marsh environments.....	170
Table 7.2 Comparison table of microfossil transfer function prediction errors ($\text{RMSEP}_{\text{jack}}$) and as a percentage of the tidal range with published studies.....	173
Table 7.3 Summary information for Split and Trieste tide-gauge stations (Holgate et al., 2013).....	174

INTRODUCTION AND AIMS

1.1. BACKGROUND

Measurements of global sea-level have shown significant increases in the rate of change during the 20th century in comparison to the 19th century and this trend is expected to accelerate through the 21st century in-line with human-induced climate change (Nicholls and Cazenave, 2010). Tide-gauge measurements have formed a significant contribution to this understanding, where the Permanent Service for Mean Sea Level (PSMSL) database contains monthly and annual observations from stations spanning most of the world's coastline (Holgate et al., 2013). However, the temporal scale of these records is inconsistent and indeed there lies a geographic deficiency, with many longer records biased towards the northern hemisphere (Douglas, 1991) as shown figure in 1.1b. The past 20-30 years have witnessed the development of proxy sea-level records derived from salt-marsh sediments to provide complementary data with which to assess the timing of modern sea-level rise (Gehrels and Woodworth, 2013). A significant benefit of these records is that their temporal resolution often allows extrapolation beyond the instrumental period as far back in time as the sediments allow (e.g. Donnelly et al., 2004; Leorri et al., 2008; Kemp et al., 2009b). In this way salt-marshes can be regarded as 'natural' archives of sea-level change comparable to tide-gauge records (Barlow et al., 2013).

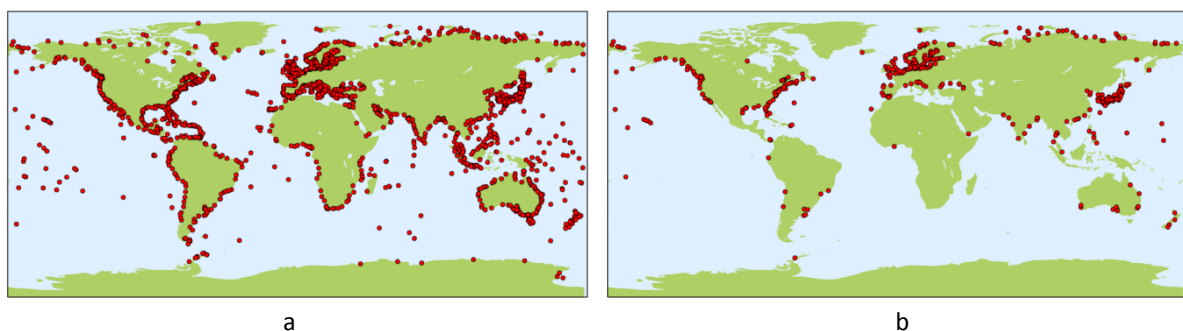


Figure 1.1. Map showing (a) global distribution of tide-gauge stations included in the PSMSL database and (b) stations with records longer than 40 years (Holgate et al., 2013).

The many fields of sea-level rise comprise a major area of climate research (Cazenave and Llovel, 2010) which forms a significant component of the Intergovernmental Panel on Climate Change (IPCC) report (Bindoff et al., 2007). In an analysis of the few high quality long-term tide-gauge records available, the average rate of global sea-level rise throughout the twentieth century varied between 1-2 mm/yr as shown in figure 1.2 (Douglas, 1991; Church and White, 2006; Jevrejeva et al., 2006; Holgate, 2007) and is primarily associated with the thermal expansion of the oceans (Church et al., 2001). Whilst the magnitude of sea-level rise was greatest during the 20th century, recent observations from satellite altimetry since the early 1990s have shown a further increase, with some areas experiencing up to ten times the global mean rate (Cazenave and Nerem, 2004; Cazenave and Llovel, 2010). The latest (AR5) IPCC report confirms this increase quoting global mean sea-level rise to vary from 2.8-3.6 mm/yr based on averaged altimeter values for the period 1993-2010 (Church et al., 2013).

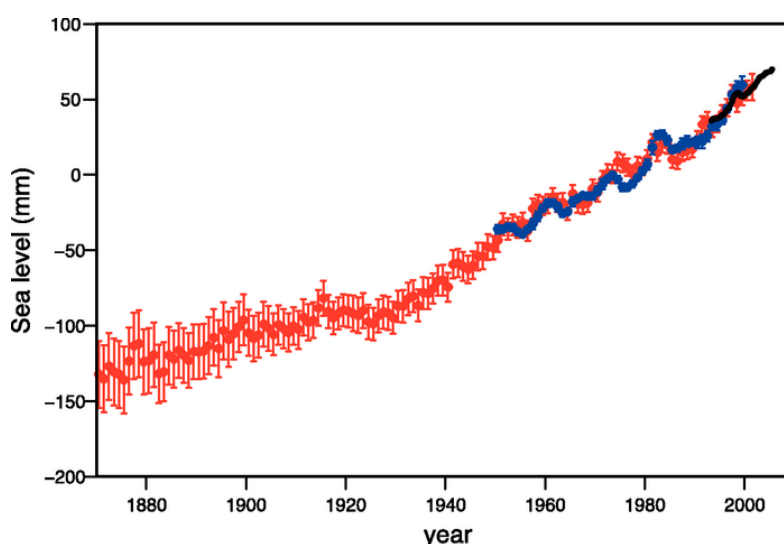


Figure 1.2. Annual averages of global mean sea level taken from the latest IPCC report (Bindoff et al., 2007). The red curve showing reconstructed sea level fields since 1870 (Church and White, 2006); the blue curve shows coastal tide-gauge measurements since 1950 (Holgate and Woodworth, 2004) and the black curve showing satellite altimetry data from 1993 to 2001 (Leuliette et al., 2004).

The utility of salt-marsh environments to contribute to these sea-level histories stems from a quantifiable relationship of microfossils (e.g. benthic foraminifera and diatoms) contained within salt-marsh sediments with elevation (Scott and Medioli, 1978; 1980). Quantitative studies using tidal-level transfer functions have applied this relationship to fossil samples that record past changes in salt-marsh altitude. When combined with chronological data (e.g.

radiocarbon dating) estimates of paleo-sea-level are produced, with tide-gauge data often used to validate the reconstruction before it is extended back through time (e.g. Gehrels et al., 2005). The application of microfossil assemblages in transfer function-based sea-level reconstructions is well established for sites from Atlantic coasts of north America and UK (Horton et al., 1999; Zong and Horton, 1999; Edwards and Horton, 2000; Gehrels, 2000; Edwards, 2001; Charman et al., 2002; Gehrels et al., 2002; Edwards et al., 2004; Gehrels et al., 2005; Horton and Edwards, 2005; Gehrels et al., 2006; Kemp et al., 2009a; Kemp et al., 2011; Barlow et al., 2013). Similarly their vertical distribution and reconstructive potential is also well explored from sites across Indonesia, Australasia and the Pacific Ocean (e.g. Hayward et al., 1990; Scott et al., 1996; Haslett, 2001; Horton et al., 2005; Woodroffe et al., 2005; Southall et al., 2006; Engelhart et al., 2007; Gehrels et al., 2008; Woodroffe, 2009; Callard et al., 2011; Grenfell et al., 2012).

By comparison, the Mediterranean region has received less attention, with very little published on the use of microfossil assemblages from intertidal environments for the purpose of sea-level studies (e.g. Petrucci et al., 1983). Other studies have analysed the vertical zonation of benthic foraminifera from coastal habitats but this has primarily focused on using them as bioindicators for studying pollution and anthropogenic impacts in the Venice lagoon area, northern Adriatic Sea (e.g. Albani et al., 2007; Serandrei-Barbero et al., 2011). Whilst foraminifera based transfer function reconstructions have also been widely applied, their attention has focused on reconstructing other environmental parameters such as paleo-bathymetry (Rossi and Horton, 2009; Milker et al., 2011), paleoclimate (Luz and Bernstein, 1976), sea-surface temperatures and salinities (Hayes et al., 2005; Penaud et al., 2011). This distinct lack of research is perhaps surprising given the wealth and range of sea-level information available. The Adriatic Sea in particular offers a number of tide-gauge records with observations greater than 50 years (Tsimplis et al., 2012). Indeed Trieste has one of the longest instrumental records in the world dating back to AD 1875 (Raicich, 2007). The Adriatic region also has a microtidal regime (Hydrographic Institute, 1955–2002). Transfer function studies based on microtidal salt-marshes are generally of good quality as vertical uncertainties associated with the technique are minimised (Edwards and Horton, 2006; Callard et al., 2011; Barlow et al., 2013). The Adriatic Sea therefore offers an ideal location for a study of this type.

1.2. RESEARCH AIMS

The overriding aim of this thesis is to reconstruct relative sea-level change for the Croatian coast of the Adriatic by using a foraminiferal-based transfer function from micro-tidal salt-

marsh environments. By achieving this aim it will contribute to our understanding of sea-level change for this region, allowing an extension of the record as far back in time as the sediments allow. By comparing the reconstruction with instrumental records, it may serve as an independent test of sea-level trends observed throughout the Adriatic Sea and much of the Mediterranean region. In particular the increased sea-level trends observed during the 20th century and further increases after ~AD 1990. The ability of the reconstruction to identify reduced rates of change and perhaps even negative sea-level tendencies during the period 1960-1990 will also be assessed (e.g. Marcos and Tsimplis, 2008). Further details regarding sea-level trends for this region are discussed in chapter 2.

1.2.1. Objectives

To address the research aim outlined above, the objectives of this study are to:

- Establish a contemporary dataset of salt-marsh foraminifera and assess their utility as proxy indicators for use in transfer function reconstructions of sea level in the Adriatic region by confirming elevation as a statistically significant control.
- Investigate sediment cores for fossil foraminifera and establish chronologies to determine age constraints for the reconstruction and sedimentation rate changes.
- Developed transfer functions to calibrate fossil samples and produce a record of relative sea-level change.
- Provide an independent assessment of tide-gauge records by comparing the proxy reconstruction with instrumental data to assess the synchronicity in sea-level changes.

1.3. OUTLINE OF THESIS

This thesis is subdivided into eight chapters beginning with an introduction to the main research objectives and is structured as follows. Chapter 2 details the current understanding of Mediterranean sea-level change followed by an overview of salt-marsh environments and how microfossil indicators can serve as proxies for sea-level change in transfer functions reconstructions. Chapter 3 introduces the Mediterranean and Adriatic study area, before descriptions of the sample sites are provided. The methods used to address the research

aims are then described, including field, laboratory and statistical techniques. There are three results chapters which begin with a qualitative overview of the contemporary salt-marsh environments, including analysed environmental variables and the distribution of foraminiferal assemblages in chapter 4. A more quantitative approach is then adopted to assess the foraminiferal data and their relationship with tidal levels and environmental variables. Chapter 5 provides the results of fossil salt-marsh data, including sediment stratigraphy, fossil foraminifera and chronologies established for salt-marsh cores. In chapter 6 the data are used to construct transfer functions which are then applied to fossil samples to reconstruct palaeo-marsh altitude and changes in mean sea-level. Chapter 7 discusses the main findings of the thesis. In this chapter the transfer function reconstruction is critically examined and compared with previous work before a final independent assessment is made by comparing the reconstruction results with local tide-gauge records. Further avenues of research are also provided. Finally the thesis finishes with a summary of the research and the implications it has for sea-level studies in the Adriatic and Mediterranean regions.

RESEARCH CONTEXT

2.1. INTRODUCTION

The aim of this chapter is to provide an overview of the main research themes covered by this thesis, beginning with a summary of sea-level change within the Mediterranean and Adriatic region. This begins with detail regarding sea-level changes spanning the instrumental period as recorded by tide gauges and satellite altimetry, followed by the longer term rate of sea-level change provided by archaeological and geomorphological evidence. Consideration is also given to glacial isostatic adjustment (GIA) measurements. The utility of proxy sea-level records constructed from salt-marsh sediments is then reviewed, including details on the use of microfossils and their intrinsic link with the elevation within tidal frame. Finally reconstructing sea-level changes from these environments using the transfer function approach is discussed.

2.2. MEDITERRANEAN SEA-LEVEL

2.2.1. Instrumental Records of Sea-Level Change

The Mediterranean Sea offers an excellent base for sea-level studies thanks to the numerous tide-gauge stations distributed along its coastline, the majority of which are focused around the northern shores (figure 2.1). Whilst interpreting sea-level change from these records might not be representative of the Mediterranean basin as a whole, due to their uneven spatial distribution (Tsimplis and Spencer, 1997) and limited availability from the African Mediterranean coastline (Woodworth, 2003), the records are of good quality with minimal gaps (1-6 %) (Marcos and Tsimplis, 2008). Indeed Trieste and Venice together present two of the longest and most detailed records available in the world.

Sea-level trends in the Mediterranean, over the instrumental period, are not homogeneous in space or time. Observations from the longest tide-gauges record sea-level rise throughout the 20th century up to 1.1-1.3 mm/yr, within the lower boundary of estimated global sea-level rise for the same period (Tsimplis and Baker, 2000). However, between 1960-1990, an increase in atmospheric pressure over the region caused a negative sea-levels trend of up to

1.3 mm/yr (Tsimplis and Baker, 2000; Tsimplis and Josey, 2001; Marcos and Tsimplis, 2008; Tsimplis et al., 2012) whilst sea-level stations in the Atlantic and Black seas continued to rise, albeit at reduced rates of 1.0-1.2 mm/yr (Tsimplis and Baker, 2000). Whilst global sea-level appears to have increased from the 1980s onwards (Holgate and Woodworth, 2004; Holgate, 2007), it wasn't until the 1990s that similar trends were observed in the Mediterranean (Cazenave et al., 2001; Fenoglio-Marc, 2002).

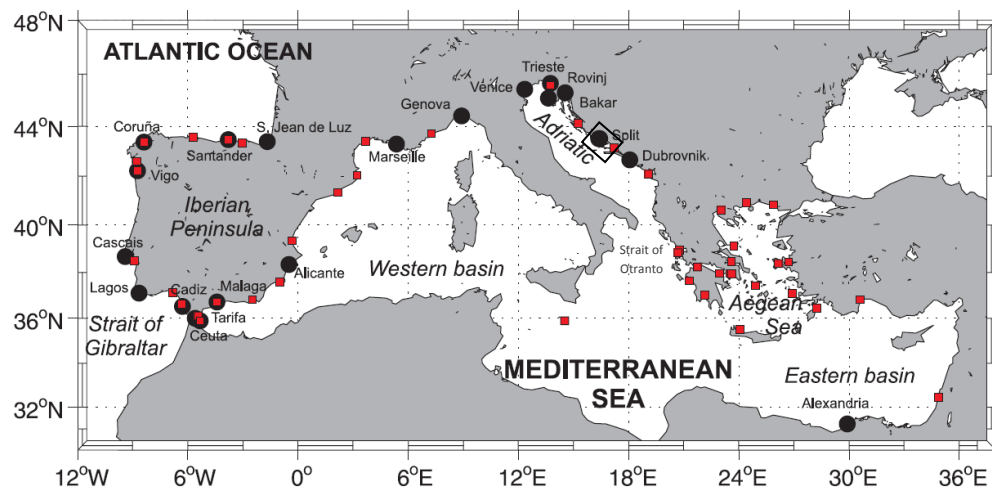


Figure 2.1. Tide-gauge stations in the Mediterranean with records longer than 35 years (black dots). Study area also shown (rectangle). *After Marcos and Tsimplis (2008).*

During the period of 1992 to 2000 satellite observations and tide-gauge measurements revealed a linear sea-level change of 2.2 mm/yr over the entire basin (Fenoglio-Marc, 2002). However, substantial spatial variability was revealed between the western and eastern basins. Relatively small increases are recorded in the western Mediterranean Sea whilst in the eastern Mediterranean basin, sea levels have simultaneously recorded large increases and decreases (Cazenave et al., 2001; 2002; Fenoglio-Marc, 2002). Over a six-year period sea-level trends in the eastern basin showed increases of up to 30 mm/yr whilst negative trends of 15-20 mm/yr are recorded in the Ionian Sea (Cazenave et al., 2002). The altimetry data also revealed the strong correlation between the observed sea-level trends and sea-surface temperatures (Cazenave et al., 2001; Fenoglio-Marc et al., 2012) suggesting recent change is primarily associated with a heating of surface layers (Cazenave et al., 2002) whilst the negative trends are probably more related to mass redistribution (Del Río Vera et al., 2009).

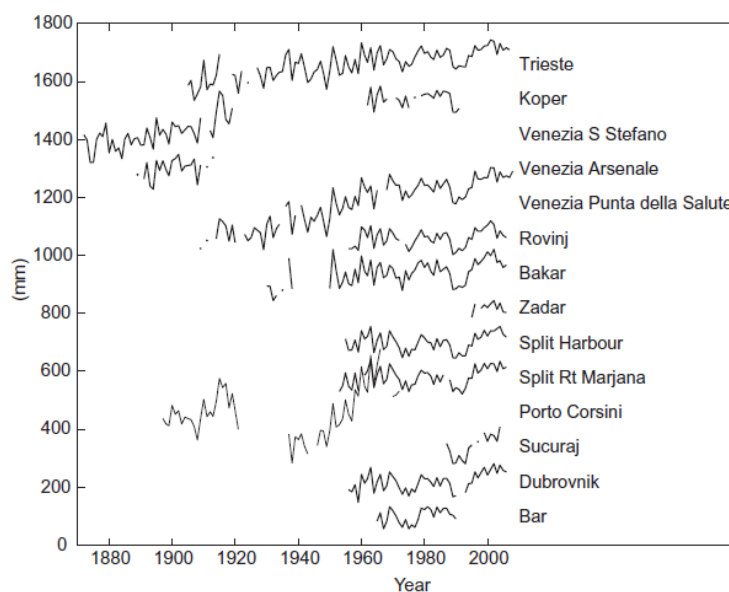


Figure 2.2. Sea-level change from tide-gauges in the Adriatic Sea (Tsimplis et al., 2012).

The Adriatic Sea contains seven tide-gauge stations which have been operational for over 50 years (Tsimplis et al., 2012). The long-term RSL rise from these records during the 20th century varies between 0.5 ± 0.2 and 1.2 ± 0.1 mm/yr, with trends in excess of 2.5 mm/yr recorded in Venice (Marcos and Tsimplis, 2008). The latter, however, is related with local anthropogenic subsidence primarily associated with water abstraction and thus is often regarded unsuitable for regional or global studies (Woodworth, 2003). Between 1960-2000 small rates of change have been recorded in the Adriatic, with values ranging from -0.4 ± 0.4 and 0.3 ± 0.4 mm/yr (Marcos and Tsimplis, 2008; Tsimplis et al., 2012). The higher rates occurring towards the end of the 20th century (figure 2.2) are confirmed through satellite observations where TOPEX/Poseidon altimetry data revealed sea-level rise between 10 and 15 mm/yr between 1993 and 1999 (Cazenave et al., 2001). However whilst the TOPEX/Poseidon and Jason-1 altimetry missions have provided high spatial resolution data (e.g. Cazenave et al., 2001; 2002; Fenoglio-Marc, 2002; García et al., 2007; Fenoglio-Marc et al., 2012), the relatively short period since its operation may not accurately reflect the longer-term rates of sea-level change in this region due to interannual and decadal variations such as water temperature, salinity and atmospheric pressure that can cause dramatic sea-level oscillations (Buble et al., 2010).

2.2.2. Long-Term Recorders of Sea-Level Change

While yearly fluctuations in sea-level can be related to climatic forcing (e.g. wind and atmospheric pressure) and/or steric variation (e.g. Tsimplis et al., 2008), longer-term millennial sea-level trends are attributed to differential GIA and tectonic movements (e.g.

Lambeck et al., 2004; Lambeck and Purcell, 2005; Antonioli et al., 2009; Stocchi and Spada, 2009b; Stocchi et al., 2009; Furlani et al., 2011). Geological evidence can provide useful information to infer relative sea-level changes dating back to the last interglacial (e.g. Ferranti et al., 2006; 2008). The low tidal range in the Mediterranean region again offers an ideal environment for studying long-term sea-level changes as an abundance of archaeological evidence and geomorphological features, coupled with instrumental records, can be used to fill the gap in between the geological and instrumental data (Anzidei et al., 2010). When combined with robust chronologies (usually acquired through radiocarbon and U-series dating, amongst other techniques), well preserved archaeological coastal structures such as ancient fish tanks, piers and harbour slipways have the potential to provide a wealth of information regarding late Holocene sea-level over the past two millennia because of their strong relationship with sea-level at the time of construction (e.g. Flemming and Webb, 1986; Lambeck et al., 2004; Antonioli et al., 2007). Using archaeological evidence, Lambeck et al. (2004) showed sea-level was up to 1.35 (± 0.07) m lower 2000 years ago in the central Mediterranean region attributing part of this change to ongoing glacio-hydro isostatic adjustment. Similarly an abundance of marine features such as tidal notches have provided evidence of former sea-level due to their relationship with mean sea-level whilst also highlighting regional variability in tectonic movements throughout the Mediterranean (e.g. Pirazzoli, 1986; 1996; Antonioli et al., 2004; 2007; Benac et al., 2008; Faivre et al., 2010a; 2010b; Furlani et al., 2010).

The effects of glacio- and hydro-isostatic readjustment of the Earth in response to the melting of Pleistocene ice sheets since the end of the last glacial period is an important mechanism driving long-term sea-level change. This process is not constant, however, and varies throughout the Mediterranean and indeed within the Adriatic itself. For example, a number of studies have shown land subsidence in the northern Adriatic region to vary. An uplift rate is observed in the area surrounding Trieste, whilst Venice reports a negative trend and Marina di Ravenna (north-east Adriatic) an even greater negative trend (Zerbini et al., 1996; Orlić and Pasarić, 2000; Antonioli et al., 2009). Whilst vertical movements in the northern Adriatic are controlled by both natural and anthropogenic effects (Stocchi and Spada, 2009a), the contribution of GIA to sea-level rise in the Adriatic can also have implications for observed sea-level rates from tide-gauge records. For example, it has been suggested that the long time-series of Trieste may comprise a GIA induced sea-level component comprising ~30% of the observed rate (Stocchi and Spada, 2009b). A summary of recent and projected GIA movements for tide-gauges, including those near to the study presented in this thesis are included in section 3.2.2.3 using data provided by the PSMSL (Holgate et al., 2013) and Peltier (2004).

2.3. PROXY SEA-LEVEL RECONSTRUCTIONS

2.3.1. Salt-Marsh Environments

Salt-marshes are vegetated areas which develop in low energy environments of the coastal zone where wave energy is minimized (Bartholdy, 2012). They are located in the upper region of the intertidal zone and differ from bordering tidal mudflat and sandflat environments through colonization by halophytic grasses, herbs and shrubs that are subject to intermittent flooding from the tide (Adam, 1978; 1990). Indeed where the frequency and amplitude of tidal inundation is limited, trees such as Alder (*Alnus*), Willow (*Salix*) and Oak (*Quercus*) may also colonize (Ranwell, 1974). Most salt-marshes are flooded by the higher tides during a spring-neap tidal cycle. However some salt-marshes can sustain a level above the highest astronomical tide (HAT) where strong winds can amplify water level (Bartholdy, 2012). Salt-marsh environments, which are replaced by mangrove communities in low latitude subtropical regions, have significant ecological and economic value as they sustain a highly dynamic and variable habitat of floral and faunal species whilst also acting as a natural defence mechanism to coastal process by absorbing wave energy (Allen, 2000; Doody, 2008). They characteristically have an inclined surface, declining in altitude in a seaward direction, and form through the accretion of fine-grained minerogenic sediment driven primarily from the marine environment, but also through additional organic deposits from above and below ground salt-marsh vegetation (Allen, 2000).

With these characteristics in mind, salt-marsh environments provide an ideal settings for palaeo-sea-level investigations where ecological zones are created on the salt-marsh surface that can be linked to tidal inundation duration and frequency (Murray, 1971; 2006). In the northern hemisphere, salt-marsh deposits from the Atlantic coast of Northern America are distinctly more organic then their European counterparts where meters of highly organic peat deposits have accumulated during the past 3000 to 4000 years (Gehrels, 2000). In contrast, salt-marshes from European sites are typically more minerogenic, particularly during the late Holocene (Horton and Edwards, 2006) where tidally introduced sediments results in an organic component rarely exceeding 10% (dry weight) (Allen, 2000). With reference to sea-level studies from European salt-marsh sites, this has impeded studies of similar timescales due to the lack of material suitable for radiocarbon dating (Allen, 2000; Edwards, 2001).

2.3.2. Microfossil Indicators

The utility of salt-marsh sediments to provide high-resolution sea-level records stems from their intrinsic relationship with the tidal frame where distinct microfossil assemblages occupy narrow vertical niches (Scott and Medioli, 1978; 1980). The frequency and duration of tidal inundation creates a vertical zonation of flora and fauna allowing sub-environments to be identified (Horton and Edwards, 2006) which is based on the tolerance or preference of individual species to limiting ecological parameters, such as frequency and duration of tidal flooding and consequently sub-aerial exposure, salinity, substrate composition and food availability (de Rijk, 1995; de Rijk and Troelstra, 1997; Berkeley et al., 2007). As a result, microfossil indicators (e.g. foraminifera, diatoms, testate amoebae and pollen) preserved within salt-marsh sediments have provided a wealth of information regarding Holocene RSL (Gehrels, 1994; Horton et al., 1999a; Zong and Horton, 1999; Edwards, 2001; Gehrels et al., 2001; Edwards et al., 2004; Gehrels et al., 2005; Horton and Edwards, 2006; Gehrels et al., 2008; Kemp et al., 2009a; Charman et al., 2010; Kemp et al., 2011).

Of all microfossil groups contained within salt-marsh environments, it is foraminifera that have probably received the most widespread attention in palaeo-sea-level studies. Found solely in marine environments, all intertidal foraminifera are benthic, living either on the sediment surface (epifaunal) or just below it (infaunal) and are readily preserved in salt-marsh sediments (Gehrels, 2002). They are single-celled organism (protists) of which there are around 900 modern genera and 10,000 modern species (Murray, 2006). They are formed of a single cell (which is not preserved), encased in a shell (test) that is composed of detrital sediment particles cemented together by organic material (agglutinated taxa) or of secreted calcium carbonate (calcareous taxa) (Murray, 1991). Salt-marsh foraminiferal assemblages are mostly composed of agglutinated taxa which, unlike calcareous species that can suffer from dissolution (e.g. Murray, 1989), are able to withstand the acidic conditions generally found in salt-marsh environments. The rise and fall of the tides results in low salt-marsh intertidal areas being more frequently submerged than upper intertidal areas where prolonged periods of subaerial exposure occur (Gehrels, 2002). The ability to which benthic foraminifera can withstand exposure and conversely tidal submergence results in a distinct zonation pattern throughout many salt-marshes around the world as they compete for space during tidal cycles (Scott and Medioli, 1980).

Pheleger and Walton (1950) first observed a relationship between salt-marsh foraminiferal distributions and elevation, identifying four ecological zones. It was not however until the late 1970s that Scott and Medioli (1978) first highlighted their use as potential proxies for RSL studies. They showed that monospecific assemblages of *Trochammina macrescens* were

vertically zoned high in the upper intertidal zone, just below mean high high water (MHHW), and close to the landward limit of the salt-marsh environment. The authors argued that former sea levels could be reconstructed to within ± 0.05 m which has since been confirmed from other marsh environments (e.g. Southall et al., 2006; Kemp et al., 2009a). The relative proportion of different foraminiferal taxa can be used to distinguish faunal zones across the salt-marsh surface (figure 2.3). Additionally, a distinct advantage of using foraminifera from these environments is that while species abundance is high, species diversity is generally low (Gehrels, 2007). This phenomenon of foraminiferal zonation with respect to the tidal frame is central to the theme of palaeo-sea-level reconstructions using microfossil evidence from salt-marsh environments. With this in mind and due to their intrinsic link with the tidal frame, salt-marsh foraminifera have become a widely used as tool for reconstructing Holocene sea-level changes (Thomas and Varekamp, 1991; Gehrels, 1994; Horton, 1999; Horton et al., 1999b; Gehrels, 2000; Edwards, 2001; Gehrels et al., 2001; 2002; Edwards et al., 2004; Gehrels et al., 2005; Horton and Edwards, 2006; Southall et al., 2006; Leorri et al., 2008; 2010; Callard et al., 2011; Kemp et al., 2011; Wright et al., 2011; Barlow et al., 2013; Mills et al., 2013).

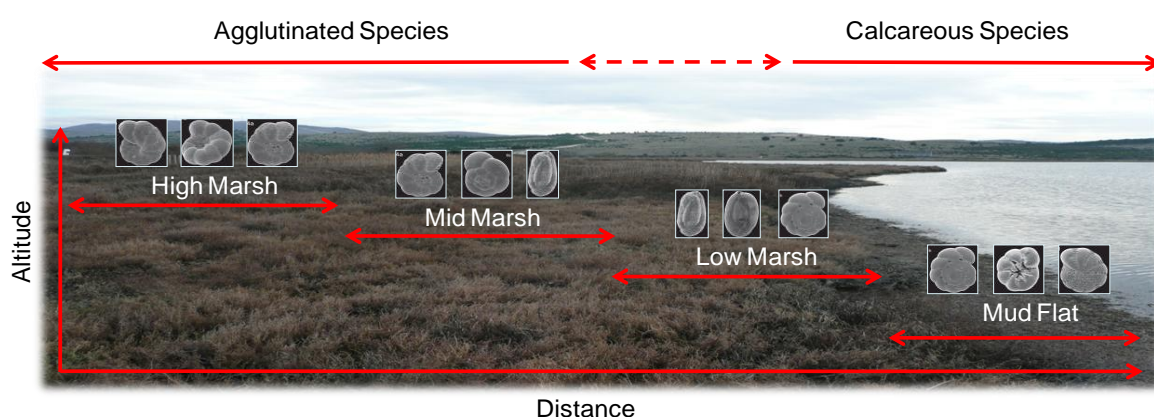


Figure 2.3. Schematic diagram to illustrate the distribution of foraminiferal assemblages across a salt-marsh environment.

Sometimes the relationship between foraminiferal distributions and elevation as a controlling factor is not entirely clear. For example, de Rijk (1995) and de Rijk and Troelstra (1997) analysed foraminiferal distributions along surface transects from the Great Marshes, Massachusetts showing foraminiferal assemblages to vary with salinity, displaying no clear relationship with elevation above sea-level. In this instance, the authors conclude that whilst foraminiferal distributions may be used for paleoecological purposes, they are unsuitable as proxies for sea-level change. It is therefore paramount that a thorough understanding of contemporary surface distributions at each sample site is investigated prior to their application in palaeo-sea-level studies as a degree of variability to which other

environmental factors such as salinity, organic matter, pH, grain size and vegetation cover may affect foraminiferal distributions could exist (e.g. de Rijk and Troelstra, 1997; Woodroffe et al., 2005; Mills et al., 2013).

Like foraminifera, diatoms have also commonly been used to study Holocene sea-level changes (e.g. Devoy, 1979; Plater and Shennan, 1992; Zong and Tooley, 1996; Zong, 1997; Zong and Horton, 1999; Plater et al., 2000; Hill et al., 2007; Horton et al., 2007; Barlow et al., 2013). They are abundant in virtually all aquatic environments, both fresh and marine, and similarly have high presentation potential within intertidal sediments. Their application is similar to foraminifera, due to their ecological preferences with respect to the tidal frame. Analysis of diatom assemblages reveals that they can provide good evidence of changes in the marine influence through changes in the relative proportion of polyhalobus (fully marine), mesohalobus (brackish), oligohalobus (brackish-fresh) and halophobus (fresh) species within lithological sequences (Haslett, 2002). Whilst foraminiferal and diatom RSL reconstructions have undoubtedly dominated palaeo-sea-level investigations in recent years, other proxy indicators such as testate amoebae and pollen are available that offer additional benefits in sea-level research conducted in intertidal environments. Indeed a multi proxy approach incorporating some or all of the above proxy indicators has proved successful in improving the accuracy of quantitative sea-level reconstructions in comparison to a single micro-organism group (e.g. Gehrels et al., 2001; Kemp et al., 2009a).

Testate amoebae, which flourish in a range of terrestrial and aquatic environments including peat bogs, lakes, soils and salt-marshes (Gehrels, 2007) show particular promise for sea-level studies. Species diversity is a lot higher than foraminifera while similarly occurring in abundance with high preservation potential within salt-marsh sediments (Charman et al., 1998; Charman et al., 2002; Roe et al., 2002; Charman et al., 2010). They have proven particularly useful due to their ability to extend beyond the highest limit reached by foraminifera but also thanks to the narrower vertical range testate amoebae assemblages occupy in comparison to other microfossil groups within high marsh zones (Charman et al., 1998; Gehrels et al., 2001; 2006). As a result, quantitative analyses of modern testate amoebae assemblages reveal sea-level reconstructions possible to within an accuracy of ± 0.04 m when conducted under microtidal settings (Gehrels et al., 2006), thus highlighting their strong potential in sea-level studies.

Other studies utilising pollen evidence have also long been applied in sea-level research (e.g. Godwin, 1940; Tooley, 1978; Shennan, 1982; Ellison, 1989; Roe and van de Plassche, 2005; Engelhart et al., 2007) despite pollen not necessarily being produced *in situ* like other microfossil groups as they are transported by wind or water (Gehrels, 2007). This proxy

shows particular benefits when used in mangrove environments (e.g. Horton et al., 2005) where preservation issues of foraminifera can be affected by taphonomic processes (Debenay et al., 2002; 2004; Woodroffe et al., 2005) limiting their application in these environments. Pollen may however supply additional, very useful information in sea-level studies, by providing independently dated age markers when establishing chronologies for salt-marsh sediment cores (e.g. Gehrels et al., 2005; Marshall et al., 2007) (see section 3.7 for further details on the utility of independent age markers).

2.3.3. Reconstructing Sea Level

Assessing changes in sea-level through an age-altitude trend requires plotting a series of sea-level index points (SLIPs) (Shennan, 1982) which contain information on location, age (e.g. radiocarbon dating), the height of original deposition (to a vertical datum e.g. OD) and the 'indicative meaning'. This term is used to describe the vertical relationship between the height at which the sample accumulated in and a reference tidal level with an associated error range (Shennan, 1986; van de Plassche, 1986). Until recently, sea-level studies were confined to the sedimentary boundary between transgressive and regressive contacts reflecting changes in terrestrial and marine sedimentation (Shennan, 1982; Tooley, 1982). Salt-marsh sediments record a transgressive trend when sea-level rise outpaces accretion and conversely a regression when accretion is faster than sea-level rise. Limitations in this approach however restricted its application to lithostratigraphic boundaries of changing marine and terrestrial sedimentation, providing no information about changes in sea-level between these points (Edwards, 2001). Other distinct disadvantages of using SLIPs from organic-minerogenic contacts is their spatial and temporal availability in late Holocene sediments (Edwards, 2001) and the long-term consolidation often associated with coastal deposits (e.g. Brain et al., 2011). In particular this process, referred to as 'autocompaction', leads to a lowering of SLIPs from their original height of deposition which, in turn, can lead to an overestimation of the rate of relative sea-level rise (Gehrels, 2007). In some extreme cases this process can lead to the displacement of coastal deposits by up to 1 m (Gehrels, 1999).

In addition to lithostratigraphic changes in coastal sedimentation, biostratigraphic indicators (e.g. foraminifera and diatoms) can provide further evidence of sea-level change (e.g. Thomas and Varekamp, 1991). A distinct advantage of using biological indicators is that they respond much more sensitively to sea-level change in comparison to their lithostratigraphic counterparts (Edwards, 2001). They also are not restricted to transgressive and regressive stratigraphic contacts but can be applied to a continuous core sequence. In this approach, more detailed, 'higher resolution' records of sea-level change can be obtained using transfer

functions that offer robustly quantification of the indicative meaning and its associated errors (Gehrels, 2007).

2.3.4. Microfossil-Based Transfer Functions

Imbrie and Kipp (1971) were first to utilize the transfer function methodology whereby deep-sea foraminiferal assemblages were employed to reconstruct paleo-sea-surface temperatures from sediment cores. Its application in salt-marsh environments however did not occur until much later in the 1990s when Guilbault et al. (1995) used the approach to quantify the amount of subsidence during a late Holocene earthquake using fossil tidal salt-marsh foraminifera from Vancouver Island, Canada. The term 'transfer function' is used to describe a set of regression equations that attempts to model the contemporary distribution of microfossil assemblages and their relationship with an associated environmental variable. Essentially the goal of a transfer function is to mathematically relate the species abundance of biological data as a function of an environmental variable, as illustrated in figure 2.4 (Birks, 1995). Its success in quantifying microfossil assemblages and reconstructing palaeoenvironmental change has since spawned numerous papers investigating Holocene sea-level change to become the mainstay in quantitative sea-level reconstructions conducted in salt-marsh environments (Horton et al., 1999a; Zong and Horton, 1999; Gehrels, 2000; Edwards, 2001; Gehrels et al., 2001; Gehrels et al., 2002; Edwards et al., 2004; Gehrels et al., 2005; Horton and Edwards, 2006; Kemp et al., 2009b; Leorri and Cearreta, 2009; Woodroffe, 2009; Woodroffe and Long, 2010; Callard et al., 2011).

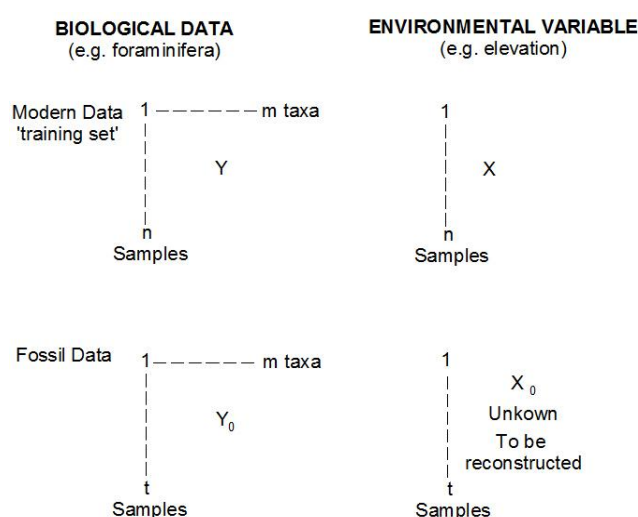


Figure 2.4. Principles of quantitative palaeoenvironmental reconstruction showing X_0 , the unknown environmental variable to be reconstructed from fossil assemblage Y_0 , and the role of a modern training set consisting of modern biological Y (foraminifera) and environmental data X (elevation). Modified after Birks (1995).

With reference to foraminifera-based transfer function reconstructions from salt-marsh environments, the method is centered around fossil foraminifera preserved in sediment cores that can be quantitatively related to their modern counterparts found on the contemporary salt-marsh surface (Gehrels et al., 2001). As the vertical zonation of contemporary foraminifera have been shown to be strongly influenced by tidal level, they can be used as 'proxies' for elevation in which the faunal data are converted into environmental data and applied to fossil analogues found in sediment cores to reconstruct relative sea-level changes when combined with chronostratigraphic techniques (e.g. radiocarbon dating) (Gehrels, 2000).

A detailed investigation into the contemporary environment and the relationship between microfossil assemblages and environmental variables is therefore prerequisite in transfer function based sea-level reconstructions. The relationship between foraminiferal assemblages and elevation must first be investigated to confirm their suitability before they can be confidently used as 'proxy' indicators of sea-level change. The development of a transfer function begins with the compilation a modern dataset, commonly referred to as a 'training set', that accurately depicts the modern environment which is reflected in the fossil sequence (Barlow et al., 2013). It contains information on the relative abundance of foraminiferal taxa and associated environmental data (e.g. elevation, pH, salinity etc). Whilst there are no strict guidelines as to an ideal size of a training set, it should be as large as possible since smaller training sets will be more susceptible to errors (Horton and Edwards, 2006). More importantly however is that it should contain foraminiferal assemblages that are from the same environmental conditions repeated in the fossil sequence to be reconstructed (Horton and Edwards, 2006). With this in mind, the spatial scale from which a training set is derived, collectively termed 'local' or 'regional', can have a significant effect on transfer function performance (e.g. Woodroffe and Long, 2010; Watcham et al., 2013).

Where a training set has been collected in close proximity to the fossil sequence (i.e. a local training set), assumptions are made in that the modern data is a true analogue for environmental conditions similar to that preserved in a sediment core. However where the depositional environment is not represented by the modern day environment or has significantly changed through time, a local training set may be inadequate to account for the changes in palaeoenvironment and microfossil assemblages (Barlow et al., 2013). To compensate for such variations, regional training sets that are comprised of foraminiferal assemblages and associated environmental data from a wide range of sites may provide better analogues of environmental change permitting a more accurate reconstruction (Edwards and Horton, 2000; Gehrels, 2000; Edwards et al., 2004; Horton and Edwards,

2005; Leorri et al., 2008; Watcham et al., 2013). When regional training sets are used in transfer function reconstructions they are able to capture much wider spatial variability and are capable of achieving reliable results where modern environmental conditions differ from those in the past (Horton and Edwards, 2005). Merging datasets together to form a regional training set however necessitates the need for elevation to be standardized to a water level index (SWLI) to account for differences in tidal range between the sample sites (Horton, 1999). An example of such procedure from Horton and Edwards (2006) is presented below where Alt_{ab} is the altitude of sample a at site b (measured to vertical datum m OD); $MLWST_b$ is the mean low water spring tide level at site b (m OD); and $MHWST_b$ is the mean high water spring tide at site b (m OD). Whilst other tidal parameters are available (e.g. HAT) and are indeed employed by different authors (e.g. Woodroffe and Long, 2010), in this instance MHWST and MLWST were used as they improved correlations with tide levels from lower elevation environments (Horton and Edwards, 2006). Care must be taken when choosing tidal levels for this process however as transfer function performance can be impeded where tidal levels do not accurately standardize water levels in the tidal frame being reconstructed (Woodroffe and Long, 2010).

$$SWLI = \frac{Alt_{ab} - MLWS}{MHWST_b - MLWST_b}$$

Establishing a modern training set that is deemed suitable for palaeosea-level studies is followed by an analysis of the species response along the environmental gradient to derive 'ecological response functions' (Horton and Edwards, 2006). As the transfer function models the relationship between microfossil assemblages and the environmental variable to be reconstructed (e.g. elevation), it is important to understand whether the modern species-environment response is linear or unimodal so that the appropriate statistical technique can be applied (Birks, 1995; 2010). To achieve this, regression methods are applied to express the biological data as a function of elevation (the 'classical' approach) or elevation as a function of biological data (the 'inverse' approach) (Horton and Edwards, 2006). Detrended canonical correspondence analysis (DCCA) is used to quantify this relationship to provide a measure of gradient length which is measured in standard deviation (SD) units (ter Braak and Juggins, 1993; Birks, 1995). Assessment of this gradient length provides information concerning the species response (Telford and Birks, 2005). Generally, where the gradient length is greater than two SD units, the species data are regarded as unimodal where assemblages have their optima along the environmental gradient displaying a Gaussian distribution (Gauch and Whittaker, 1972). Standard deviations units less than two however

suggests several taxa increase or decrease with the environmental variable of interest and therefore the data are linear (figure 2.5) (ter Braak and Prentice, 1988; Birks, 1995; 2010).

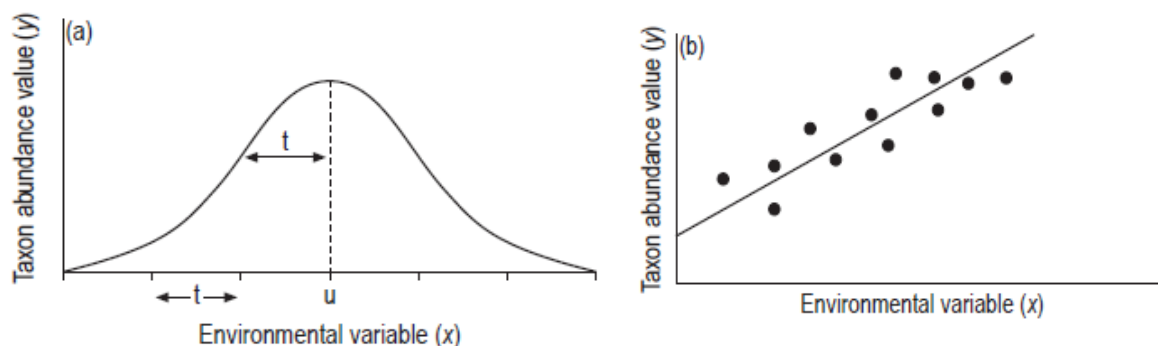


Figure 2.5. Taxon-environment response models showing (a) Gaussian unimodal distribution and (b) linear distribution between species abundance (y) and the environmental variable (x). u = optimum and t = tolerance (Horton and Edwards, 2006; ; modified after Birks, 1995).

In most Holocene sea-level investigations however, species distributions are generally unimodal due the nature of foraminiferal assemblages displaying a Gaussian distribution in relation to the environmental variable of interest (Barlow et al., 2013). Indeed unimodal response models such as Weighted Averaging (WA) (Ter Braak and Barendregt, 1986) and Weighted Averaging Partial Least Squares (WA-PLS) (ter Braak and Juggins, 1993) are considered robust and reliable reconstruction techniques (ter Braak and Juggins, 1993; ter Braak et al., 1993; Birks, 1995; Telford et al., 2004; Telford and Birks, 2005) and are widely applied in salt-marsh microfossil based sea-level reconstructions (e.g. Edwards and Horton, 2000; Edwards et al., 2004; Gehrels et al., 2005; Horton and Edwards, 2005; 2006; Woodroffe and Long, 2010; Leorri et al., 2011; Kemp et al., 2012; Barlow et al., 2013).

Unimodal regression models such as WA consider the variance along a single environmental gradient where foraminiferal taxa are assigned an ecological optimal elevation and tolerance in which they may be observed (Horton and Edwards, 2006). However there are several disadvantages associated with this approach, for example WA considers each environmental variable separately and also disregards the residual correlations in the biological data when other variables affecting the data are not considered after fitting the environmental variable of interest (Birks, 1995). Whilst the environmental controls that govern contemporary foraminiferal distributions in salt-marsh environments show a strong correlation with elevation, other environmental factors such as salinity (e.g. de Rijk and Troelstra, 1997) can introduce 'noise' and disrupt the unimodal response of species data to

the environmental variable of interest (e.g. elevation) (Horton and Edwards, 2006). In WA, these correlations are not taken into account and as a result WA-PLS (ter Braak and Juggins, 1993; ter Braak et al., 1993), was developed to allow for such variability. WA-PLS is an extension of WA where the incorporation of partial least squares (PLS) considers the residual correlations in the biological data to improve estimation of the optima for the taxa (Birks, 1995) by considering the effect of other potentially influential environmental variables (ter Braak and Juggins, 1993). Indeed ter Braak and Juggins (1993) consider WA-PLS to be a simple and robust method and recommend its use until other more sophisticated methods are developed. Where the lengths of gradient fall between 2 and 3 SD units, suggesting species response is neither strongly linear or unimodal, Birks (1998) states WA-PLS will in most instances, outperform linear techniques due to the fewer components required by WA-PLS to create an adequate model.

Linear-based regressions models, including Imbrie and Kipp Factor Analysis (IKFA), principal components regression (PCR) and PLS, are suitable for use where data exhibit a linear distribution in relation to the tested environmental variable (i.e. less than 2 SD units as identified from DCCA). In PLS regression, developed by Wold et al. (1984), components are maximised to the covariance with the response variable and thus requires fewer components usually giving lower prediction errors in comparison to other linear methods such as PCR. More importantly however are the added benefits of cross-validation procedures available in PLS which are not possible with PCR (Birks, 1995). Using the same number of components a PLS model always improves on the coefficient of determination (r^2) in comparison to PCR and is thus the preferred reconstruction technique (Birks, 1995). Linear-based regression and calibration models are comparatively rare in proxy sea-level studies due to the unimodal relationship commonly observed between foraminifera and elevation. It has however been successfully applied in regions where foraminiferal training sets are derived from short vertical ranges in relationship to the tidal frame (Barlow et al., 2013) such as Leorri et al. (2010) and Rossi et al. (2011).

Following the construction of a transfer function, calibration is performed in which the developed regression linear or unimodal statistical models are applied to fossil counterparts found in sediment cores to reconstruct estimates of paleo-marsh surface (Birks, 1995; Horton and Edwards, 2006). When combined with detailed chronological information (e.g. Marshall et al., 2007), usually acquired through radiocarbon dating and/or short-lived radionuclides, changes in relative sea-level can then be investigated (Horton and Edwards, 2006). Statistical parameters produced from the transfer function models allow an assessment of the reconstruction performance and predictive ability of the training set in

reconstructing past environmental change (further details regarding these parameters are provided in section 6.2). However, quantitative transfer function reconstructions will produce a result regardless of the data used and so the accuracy of the reconstruction should be tested (Birks, 1995). In microfossil-based sea-level reconstructions from salt-marsh environments a common goal of the transfer function technique is to reconstruct relative sea-level over the history of deposition for a core sequence.

As a validation tool and to assess the reconstruction performance it is useful to compare the reconstructed results with direct observations from local instrumental records (e.g. tide gauges). This has proved successful in a number of studies where rates of change are comparable to instrumental records, but provides the added ability of extrapolating the sea-level record further back into the Holocene (Gehrels, 2000; Edwards, 2001; Gehrels et al., 2002; Donnelly et al., 2004; Gehrels et al., 2005; Edwards and Horton, 2006; Kemp et al., 2011). In this respect salt-marsh environments can be regarded as natural archives of sea-level change comparable to tide-gauge records (e.g. Barlow et al., 2013) permitting sea-level observations as far back in time as the sediments allow. Significantly, the transfer function approach has the potential to bridge the crucial gap that exists between instrumental and geological records of sea-level change (Edwards and Horton, 2006).

STUDY AREA AND RESEARCH METHODS

3.1. INTRODUCTION

The aim of this chapter is to first introduce the study area and specific salt-marsh sites chosen for this study and, secondly, to provide an illustration of the research methods detailing the field, laboratory, chronological and statistical techniques applied. It begins with an introduction to the Mediterranean region and more specifically the Adriatic Sea, focusing on its oceanographic and tectonic setting, and including information regarding regional glacio-isostatic adjustment. The rationale for site selection and a detailed description of each study site is then provided before all methods employed in the research are presented. First, the field methodology, incorporating modern sampling strategy, stratigraphic and levelling surveys are outlined before the individual laboratory techniques are described, which include foraminiferal analyses (surface and core), analysis of tested environmental variables and the methods used to establish chronologies for 'type' cores. The chapter finishes with some detail on the multivariate statistical analyses applied to the modern foraminiferal datasets.

3.2. STUDY AREA

3.2.1. The Mediterranean Sea

The Mediterranean Sea, situated between the continents of Europe and Africa, is a semi-enclosed basin covering approximately 2.5×10^6 km² with an average and maximum water depth of 1500 m and 5150 m, respectively (Lionello, 2012). The Mediterranean Sea can be divided into two nearly equal sized basins known simply as the eastern and western Mediterranean basins which are separated by the Strait of Sicily (figure 3.1) at a depth of 330 m (Robinson et al., 2001). To the west, communication with the Atlantic Ocean occurs through the narrow 14.5 km-wide Strait of Gibraltar at an approximate depth of 345 m (Lionello et al., 2004) whilst to the east, communication with the Black Sea occurs through the Bosphorus Strait. Both eastern and western basins are similarly sub-divided into a number of basins and seas as shown in figure 3.1. The western Mediterranean Sea is characterised by the Alboran Basin to the far west and the Tyrrhenian Basin towards the Italian coastline in

the east. The eastern Mediterranean Sea is separated into the Levantine and Ionian Basins and also the Aegean and Adriatic Seas.

Four main water masses characterise the Mediterranean Sea. An inflow of surface Atlantic water (up to 200 m depth) circulates throughout the whole basin increasing in temperature and salinity from west to east, which is replaced by an intermediate layer known as the Levantine Intermediate Waters (LIW) between 300 – 800 m depth. This warm (15 – 16°C), salty intermediate layer is formed in the Levantine sub-basin of the eastern Mediterranean and similarly circulates throughout the whole of the Mediterranean (Lascaratos et al., 1999; Lionello, 2012). Below 800 m depth, cold, dense water masses are formed within selected areas of both the eastern and western Mediterranean basins (Rixen et al., 2005) where favourable oceanic conditions and interactions between the air and sea result in downward mixing deep into the water column (Lascaratos et al., 1999). As Atlantic waters move into the eastern Mediterranean through the Strait of Sicily, evaporation exceeds precipitation and runoff, creating more saline waters and a negative water balance (Tsimplis and Baker, 2000), which is amplified to the east in the Black Sea (Millot and Taupier-Letage, 2005).

The small tidal ranges that are experienced throughout the Mediterranean Sea are the direct result of its narrow connection with the Atlantic Ocean via the Strait of Gibraltar, limiting the inflow of strong oceanic tidal energy (Pugh, 1996). In the west, tides are influenced by the Atlantic tidal wave penetrating through the Strait of Gibraltar, resulting in a tidal component rarely exceeding 10 cm, namely in the northern Adriatic and Aegean Seas (Tsimplis et al., 1995). In the east, the effects on tidal dynamics of the small openings through the Bosphorus (N-E Aegean) and Suez (S-E Mediterranean) canals are negligible (Arabelos et al., 2011).

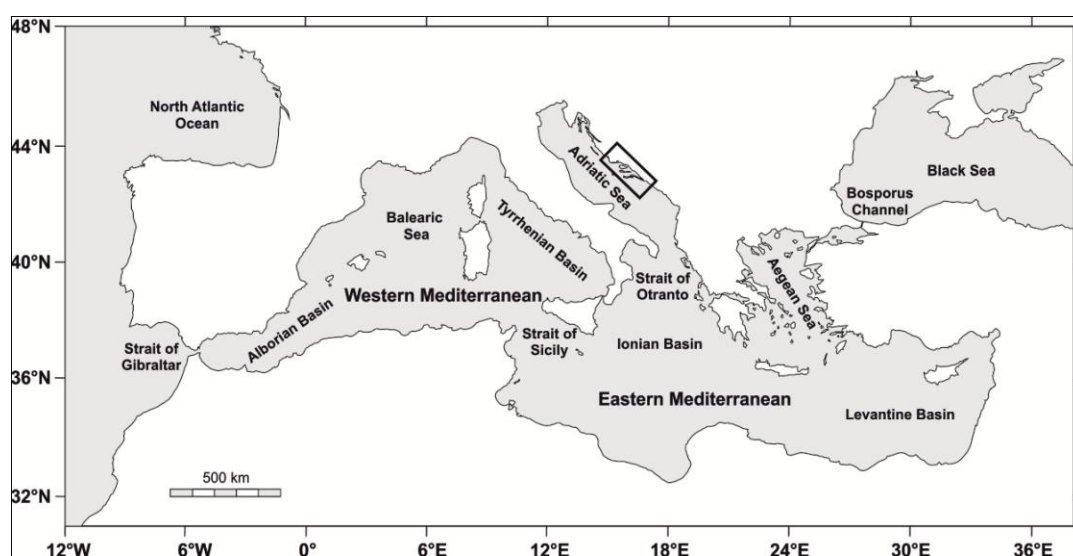


Figure 3.1. Map showing sub-divisions of the eastern and western Mediterranean Sea including the study area (highlighted in the black box) within the Adriatic Sea.

3.2.2. The Adriatic Sea

3.2.2.1. Oceanographic Setting

Covering an approximate area of 160,000 km², the Adriatic Sea is a relatively shallow (average depth 160 m) elongated basin, measuring roughly 800 km long by 200 km wide. Communication with the Mediterranean Sea occurs through the Strait of Otranto which is marked by a sill at 800 m water depth (Artegiani et al., 1997). The bathymetry of the basin (figure 3.2) is similarly subdivided into sub-basins comprising a shallow (35 m), gently sloping 300 km northern section before extending down to 270 m in the Mid Adriatic Pit (also known as the Jabuka Pit) before reaching a maximum water depth of 1200 m in the southern Adriatic Pit near to Dubrovnik (Ciabatti et al., 1987; Orlić et al., 1992).

There are three main water masses that circulate within the Adriatic Sea, including the Adriatic Surface Water, the LIW, and Adriatic Deep Water, with each sub-basin having its own characteristic deep water system (Artegiani et al., 1997). The cold dense water masses of the Adriatic Sea form a significant component of the Mediterranean Deep Water transferring to the eastern Mediterranean through the Strait of Otranto. The formation of this water mass in the shallow northern shelf region occurs during winter months when meteorological conditions characterised by cold strong winds (known as Bora events) persist over the region (Orlic et al., 1992; Lascaratos et al., 1999). This dense water then propagates south along the western Adriatic coast where it is stored and mixed in the Jabuka Pit (Lascaratos et al., 1999). The formation of dense water in the southern Adriatic pit similarly occurs during cold winter months and the mixing of both dense water masses forms the Adriatic Deep Water (Manca et al., 2002). While the formation of each deep water mass is a distinct but linked process (Tsimplis et al., 2012) it is generally agreed that it is the southern Adriatic deep water mass that transfers through the Strait of Otranto to fill the deepest regions of Ionian and then the Levantine Basins respectively (Orlić et al., 1992; Lascaratos et al., 1999).

The Adriatic experiences a general cyclonic circulation, flowing in a south-easterly direction along the western side which is strongly influenced by both seasonal fluctuations in climate (Franco et al., 1982) and discharge from a number of significant rivers, most notably the Po River in northern shelf region (figure 3.2) (Artegiani et al., 1997) with a mean annual runoff of 1700 m³/s (Orlić et al., 1992). Seasonal and year-to-year changes in relative sea-level in the Adriatic Sea shows strong correlation with atmospheric pressure where sea-level fluctuations correspond with variations in air pressure (Orlić and Pasarić, 2000; Vilibić,

2006b). A 1 mbar increase or decrease in atmospheric pressure causes the lowering or rising of sea-level of up to 2.0 cm (Orlić and Pasarić, 2000).

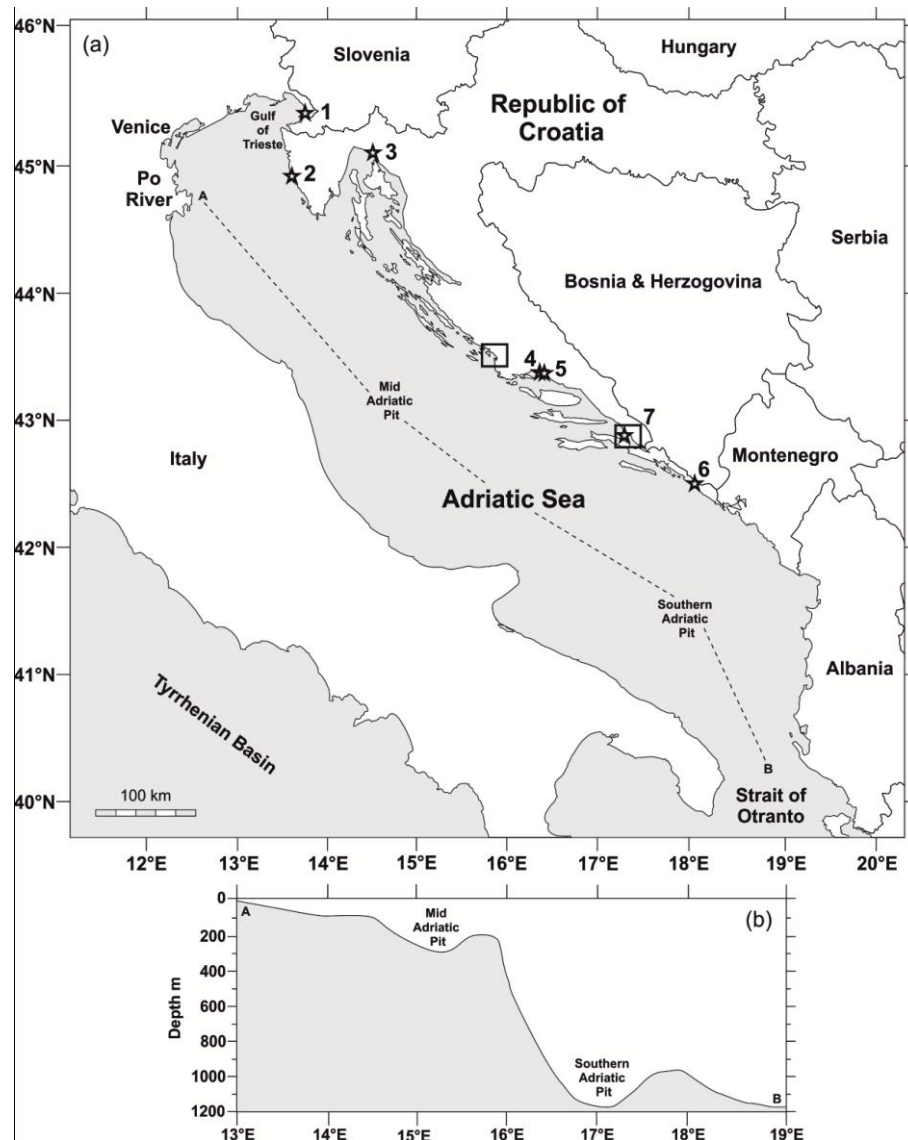


Figure 3.2. Map of (a) Adriatic Sea showing location of tide-gauge stations, study site areas (square boxes) and (b) approximate location of bathymetry profile (dashed line) redrawn after Piva et al. (2008). 1= Trieste, 2= Rovinj, 3=Bakar, 4=Split (Harbour), 5= Split (Rt. Marjana), 6=Dubrovnik, 7=Ploče.

In comparison with the rest of the Mediterranean Sea, where tides are weak, the Adriatic features moderate semi- and diurnal-tides (Tsimplis et al., 1995). Due to the decrease in water depth, an increasing trend in tidal amplitude propagating north along the eastern coast occurs with the highest amplitudes in the relatively shallow waters in the Gulf of Trieste (Cushman-Roisin and Naimie, 2002). Diurnal tidal amplitudes can vary from 18 cm in the Gulf of Trieste to just 5 cm in the south at Dubrovnik. The mean daily (diurnal) tidal range

from tide-gauge sites based on long-term sea-level measurements for the Croatian coast of the eastern Adriatic Sea is provided in table 3.1 below. Tidal levels in the Adriatic Sea are also able to be significantly raised due to meteorological forcing (known as a meteotsunami) associated with strong depressions over the region (Ferla et al., 2007) while peaks in extreme events (Vilibić, 2006a) also coincide with peaks in mean sea-level for the Adriatic Sea during months November and December (Crisciani et al., 1994). The threat of meteotsunamis also represents a significant hazard for the eastern Adriatic coast (Vilibić and Šepić, 2009), where sixteen tsunami-like sea-level oscillations have been documented between 1955-2010 alone, creating wave heights of up to 60 cm (Šepić et al., 2012).

Table 3.1.

Mean daily tidal range along Croatian coast of the Adriatic Sea (Hydrographic Institute, 1955–2002). Location of tide-gauge stations are shown in figure 3.2.

Tide-gauge site	Tidal range (cm)
(2) Rovinj	47
(3) Bakar	30
(4&5) Split	23
(6) Dubrovnik	23

3.2.2.2. Tectonic Setting

The Mediterranean region is situated across a major tectonic boundary where deformation occurs as a result of the near head-on collision between the continental plates of Africa (Nubia) and Europe (Eurasia) (figure 3.3) (Anderson and Jackson, 1987; Battaglia et al., 2004) with Nubia moving north towards Eurasia at a rate of 10 mm/yr (Barka and Reilinger, 1997). Contained within this relatively simple system, however, is a more complex tectonic network of collisional mountain belts, oceanic lithosphere and rift basins, subduction zones and microplates (Weber et al., 2010). The existence of a microplate in the Adriatic region that moved independently of both Nubia and Eurasia in the Mediterranean was first proposed by McKenzie (1972). This microplate or lithosphere block, which can itself be subdivided into northern and southern microplates, includes areas of the Adriatic Sea, eastern part of Italy and the Apennines, the Po River valley and the area of western Dinarides and Hellenides along the eastern Adriatic coast (Marjanović et al., 2012). It is thought to have originated from a larger Paleozoic outcrop of the Nubia plate that collided with Eurasia during the Cretaceous, and subsequently fragmented into independent microplates during the Cenozoic period (Anderson and Jackson, 1987; Battaglia et al., 2004). Deformation of the earth's crust in this region is the direct result of the African plate being forced north into Eurasia (Marjanović et al., 2012) and this interaction varies

accordingly along the eastern Adriatic coastline (Buble et al., 2010). Continuous GPS measurements of coastal rocks show vertical motion to vary from -1.7 ± 0.4 mm/yr in the southern Adriatic to 0.0 ± 0.4 mm/yr in the northern Adriatic (Buble et al., 2010).

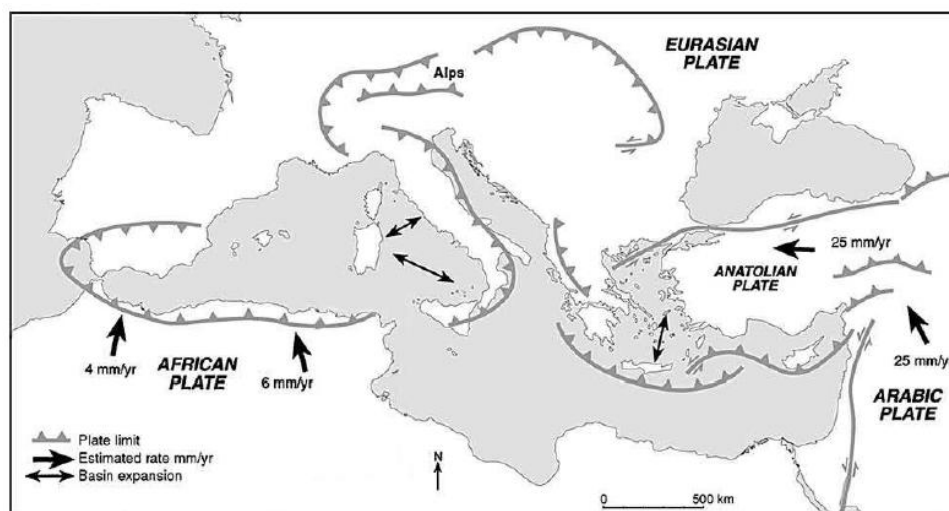


Figure 3.3. Tectonic setting of the Mediterranean region (Morhange and Pirazzoli, 2005).

3.2.2.3. Glacial-Isostatic Adjustment (GIA)

The far-field location of the Adriatic Sea from former late Pleistocene ice sheets does not preclude this region from the effects of post-glacial rebound or associated meltwater loading (e.g. hydro-isostatic adjustment). Whilst it is beyond the scope of this thesis to precisely model the GIA component of sea-level change for the Croatian coast of the Adriatic, it is important to recognise this process and its potential effects on sea-level reconstructions from this area. An understanding this process will ultimately help further constrain the various components of sea-level change in order to identify a eustatic sea-level signal (Tamisiea and Mitrovica, 2011).

Data provided by the Permanent Service for Mean Sea Level (PSMSL) (Holgate et al., 2013) were used to assess both the predicted rate of GIA induced sea-level change and vertical motion of the solid earth (mm/yr) for PSMSL tide-gauge sites located along the eastern Adriatic shoreline covering a time period spanning the last 250 years, the next 250 years and finally an average present-day rate (table 3.2). The ice-model used throughout, ICE-5G (VM2) version 1.3, is based on an elastic, compressible 90 km lithosphere (Peltier, 2004) and follows an extended theory of the sea-level equation by Farrell and Clark (1976). Model predictions show an increasing trend in the average rate of sea-level fall moving north up through the Adriatic Sea towards Rovinj (-0.13 mm/yr) and Trieste (-0.14 mm/yr). Rates of

GIA-induced change (land and sea) are very similar between tide-gauge stations at Split and Dubrovnik, implying an almost homogenous change over the past 250 years for the sample sites considered in this thesis.

Table 3.2. ICE-5G (v.1.3) model predictions of GIA-induced sea-level change and vertical land motion (mm/yr) for PSMSL tide-gauge records >35 yr located along the eastern Adriatic shoreline for the past 250 years, next 250 years and average present-day rate. Location of tide-gauge stations are shown in figure 3.2. Av = Average.

Name	PMSL ref	Lat	Long	Sea-Level			Vertical Land Motion		
				<250 yr	> 250 yr	Av	< 250 yr	> 250 yr	Av
(1) Trieste	270061	45.65	13.76	-0.14	-0.14	-0.14	-0.07	-0.06	-0.06
(2) Rovinj	280006	45.08	13.63	-0.13	-0.12	-0.13	-0.09	-0.08	-0.09
(3) Bakar	280011	45.30	14.53	-0.13	-0.12	-0.12	-0.08	-0.07	-0.08
(4) Split I	280021	43.51	16.39	-0.06	-0.06	-0.06	-0.15	-0.14	-0.14
(5) Split II	280031	43.51	16.44	-0.06	-0.06	-0.06	-0.14	-0.14	-0.14
(6) Dubrovnik	280081	42.66	18.06	-0.06	-0.05	-0.06	-0.14	-0.13	-0.13
(7) Ploče*	280075	43.05	17.42	-0.06	-0.06	-0.05	-0.14	-0.13	-0.14

*Ploče included due to its close proximity to sample site at Blace.

3.3. STUDY SITES

3.3.1. Rationale for Site Selection

Foraminiferal and other ecological sea-level reconstructions from intertidal environments have received widespread attention throughout Atlantic sites in northern Europe and America. However, the Mediterranean, and specifically the Adriatic Sea, has received little attention utilising this technique. Research in the Adriatic region has primarily been focused on the use of foraminifera as indicators of recent pollution histories (e.g. Coccioni, 2000; Albani et al., 2007; Frontalini and Coccioni, 2008; Frontalini et al., 2010; Frontalini and Coccioni, 2011; 2012) and palaeoenvironmental and climate change (e.g. Jorissen et al., 1993; Rohling and Gieskens, 1993; Oldfield et al., 2003; Di Bella et al., 2008; Piva et al., 2008; Di Bella and Casieri, 2011) covering the broader Holocene and Late Quaternary period. Whilst the distribution of benthic foraminifera in the Adriatic Sea has been well documented (e.g. Jorissen, 1987; 1988), their vertical zonation across intertidal environments for the purpose of sea-level studies is limited. This is perhaps surprising for a number of reasons. First, an almost unanimous conclusion from microfossil-based reconstructions is the improved accuracy of the transfer function when conducted under microtidal settings in reducing the error uncertainties involved in the technique (e.g. Horton and Edwards, 2006; Southall et al., 2006; Leorri and Cearreta, 2009; Callard et al., 2011; Barlow et al., 2013). In this respect, tidal ranges in the Adriatic Sea (as described above) are microtidal, ranging between 20 cm to approximately 50 cm moving north up through the

basin (table 3.1). Secondly, the plethora of information regarding temporal and spatial patterns of Holocene sea-level change available in the Mediterranean is perhaps unmatched worldwide, offering an ideal base for sea-level studies. Abundant geological, geomorphological and archaeological evidence is accompanied more recently by a dense network of tide-gauge stations, some of which offer the longest, most detailed records in the world. Indeed the eastern Adriatic coastline includes seven tide-gauge stations which have been operational for longer than 50 years, with Trieste extending back to the 19th Century (Marcos and Tsimplis, 2008). Tide-gauge data are often used in foraminiferal transfer function sea-level reconstructions as a validation tool allowing the accuracy of the sea-level reconstruction to be assessed before it is extended back beyond the instrumental period and as far back in time as the sediments allow. With this in mind, the eastern Adriatic coastline represents a perfect setting for a study of this type, where high resolution, long (>35 years) tide-gauge records exist within a relatively small geographical region (figure 3.2 and table 3.3).

Table 3.3.

Details and period of relative sea-level trends (mm yr^{-1}) for tide gauge stations along the eastern Adriatic coastline with records longer than 35 years (*after* Marcos and Tsimplis, 2008). Location of tide-gauge stations are shown in figure 3.2.

Name	PMSL ref	Lat	Long	Period	Length (years)	Relative Trend mm yr^{-1}
(1) Trieste	270061	45.65	13.76	1905 - 2006	106	1.2 ± 0.1
(2) Rovinj	280006	45.08	13.63	1955 - 2004	53.58	0.6 ± 0.2
(3) Bakar	280011	45.30	14.53	1930 - 2004	79.00	1.1 ± 0.1
(4) Split I	280021	43.51	16.39	1952 - 2004	56.67	0.7 ± 0.2
(5) Split II	280031	43.51	16.44	1954 - 2004	54.83	0.5 ± 0.2
(6) Dubrovnik	280081	42.66	18.06	1956 - 2004	53.00	0.9 ± 0.2

3.3.2. Site Selection - The Croatian Coast

The eastern Adriatic coastline is the second most indented coastline in Europe, of which Croatia hosts the longest part (Pikelj and Juračić, 2013). With a total length of approximately 5800 km, the Croatian coastline is predominantly rocky and steep with numerous pockets of sand and gravel beaches and few alluvial zones (Baric et al., 2008). The coastal zone is generally very narrow (between 1 – 5 km) where high Dinaric mountain ranges often protrude straight out of the sea (Pikelj and Juračić, 2013). Population density is significantly higher in the coastal zone compared to the hinterland, housing 25.6 % of the total population (Baric et al., 2008). Ten relatively large rivers flow out into the Adriatic Sea along the Croatian coastline, the largest of which is the Neretva River in the Dubrovnik-Neretva

County, with an average discharge of $332 \text{ m}^3\text{s}^{-1}$ which peaks in December (Orlić et al., 2006).

As a result of the highly indented karstic nature of the coastline, vegetated coastal sedimentary environments are a rare habitat in this region, with only one large alluvial plain along the coastline at Neretva in the south. A limited amount of research exists on salt-marsh environments in the Adriatic, with most studies focusing on the Italian and northern side due karstic nature of the eastern coastline. However, a review of salt-marsh vegetation by Pandža et al. (2007) identified eight ecologically important sites in central and south-eastern Adriatic, and two of the sites, Jadrtovac and Blace (figure 3.4), are the focus of this research. Their selection is also based on the close proximity of Jadrtovac and Blace to tide gauge stations at Split, Ploče and Dubrovnik respectively (figure 3.4) where tidal ranges are of comparable amplitude as shown in table 3.1.

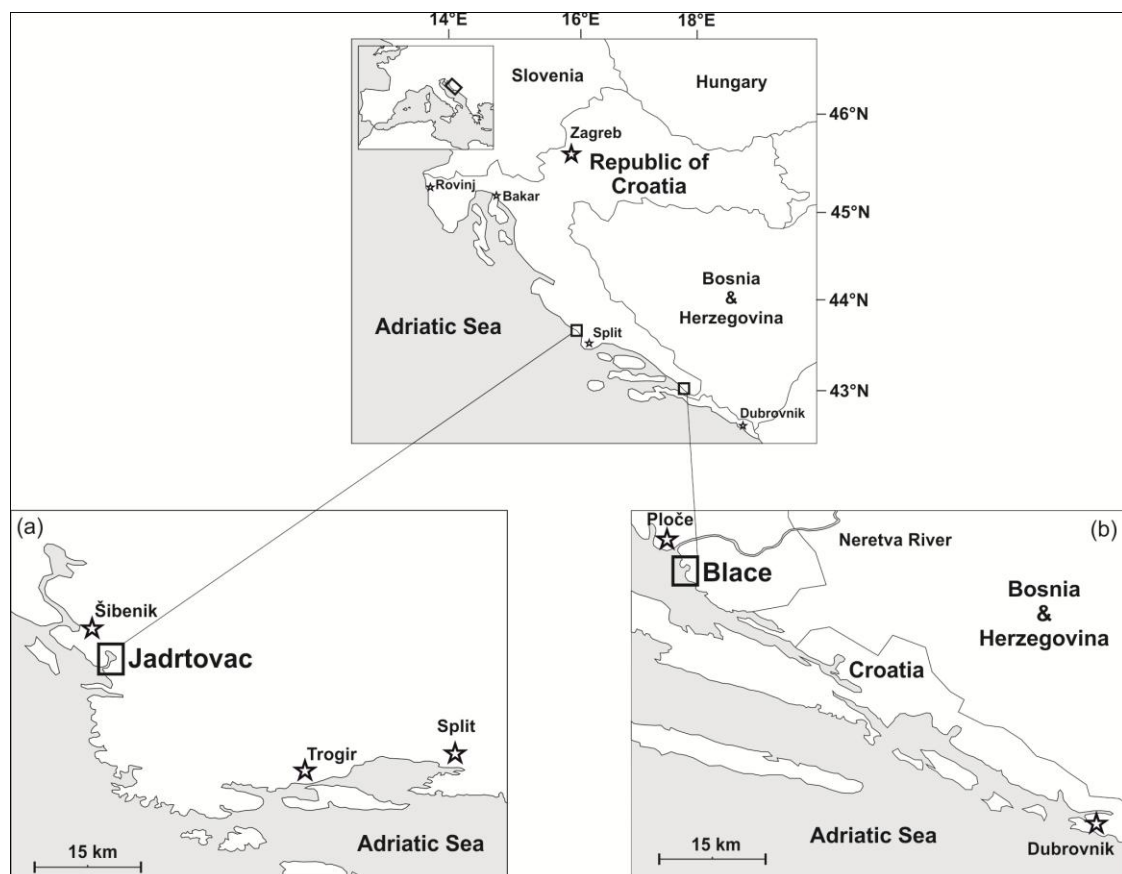


Figure 3.4. Study area map showing relative locations of sample sites (a) Jadrtovac and (b) Blace along the Croatian coastline, eastern Adriatic Sea.

3.3.3. Jadrtovac

The salt-marsh is located on the outskirts Jadrtovac (population 200) situated within Morinje Bay (43°40'48"N, 15°57'24"E), approximately 3 km south of Šibenik and 50 km north of Split, central Croatia (figure 3.4). Communication with the open Adriatic Sea occurs through a narrow (150-350 m), 2.5 km-long channel at a depth of 23 m, while at the entrance to the Bay the depth is reduced to 2 m (Šparica et al., 2005a). With a surface area of 3.5 km² and a maximum water depth of 21 m, the bay can be divided into two sections, with a shallow northern region and a deeper southern channel (Mihelčić et al., 2006). A relatively high sedimentation rate of 1.0 m/ka has resulted in the accumulation of 4.5 m of organic-rich sediment which began approximately 4.5 ka BP as the Morinje depression was inundated during the latter stages of the Holocene transgression (Bačani et al., 2004; Šparica et al., 2005a). The Morinje ecosystem is characterised by varying seawater temperatures (0-35°C) and fluctuating salinities (up to 42‰) as a result of seasonally enhanced evaporation, continuous freshwater supply from onshore and submarine springs and surface runoff events (Bačani et al., 2004; Šparica et al., 2005a). At present, there are no permanent inflows to the bay, and current activities in the surrounding environment are primarily associated with seasonal tourism and agriculture (Mihelčić et al., 2006).

The Jadrtovac salt-marsh is located on the eastern side of the bay (figure 3.5) and is roughly 130 m at its widest point before thinning out moving north around the bay. The mean daily tidal range at this site is approximately 23 cm, derived from values obtained at the nearby Split tide-gauge (Hydrographic Institute, 1955–2002). A table of tidal levels for this site is provided in table 3.4. The salt-marsh environment displays distinct zones of vegetation with *Juncus* spp., *Halimione*, *Atriplex*, *Scirpus* spp., *Phragmites* and occasional *Suaeda* spp. colonising higher elevations in the upper salt-marsh zone, whilst mid-to-low salt-marsh zones are dominated by *Halimione* spp., *Salicornia* spp. and again occasional *Suaeda* spp. The salt-marsh is intersected by a narrow (~2 m) man-made channel presumably for local fishing access within the bay. Two sample sites were established at Jadrtovac (JD1 and JD2), as shown in figure 3.5, where surface transects were established perpendicular to the coast incorporating all sub-environments from the high salt-marsh zone to the salt-marsh/sea interface. The low salt-marsh/sea interface at JD1 is characterised by a small cliff edge (~10-20 cm). Details regarding the sampling at JD1 and JD2 are provided in table 3.6.

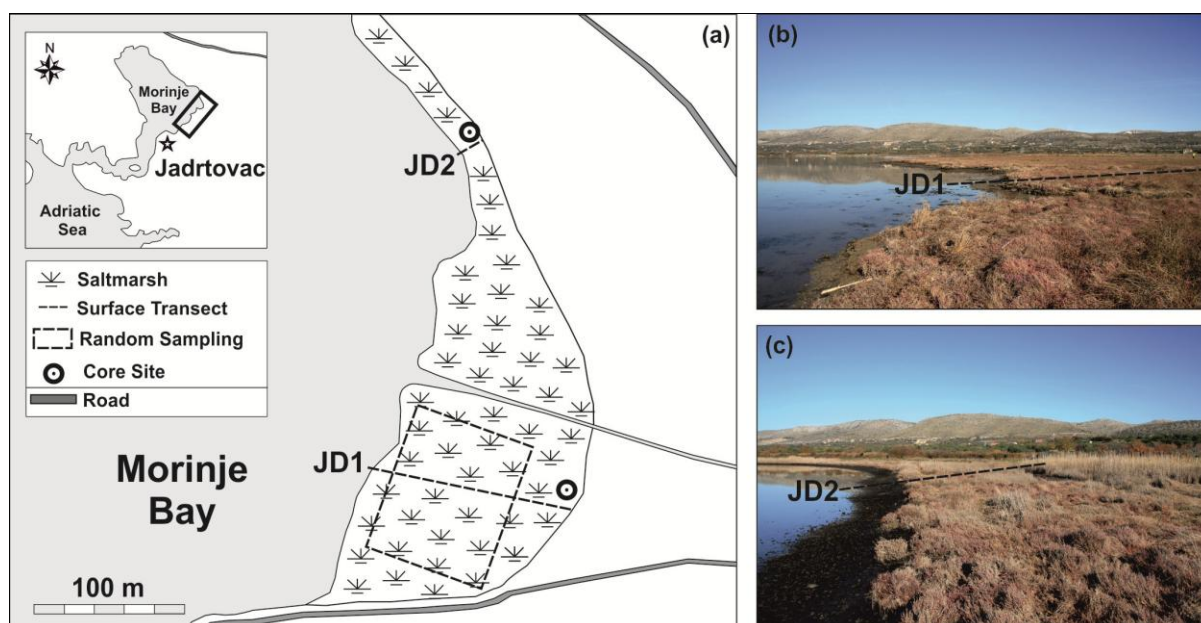


Figure 3.5. Study site map showing (a) location of salt-marsh environment within Morinje Bay with surface transects, random sampling area and core sites, (b) photo of JD1 sample site, and (c) photo of JD2 sample.

Table 3.4.

Tidal levels (relative to m HVR571) derived from Split tide-gauge (Hydrographic Institute, 1955–2002).

Lowest astronomical tide	Mean low water springs	Mean low water neap	Mean tidal-level	Mean high water neap	Mean high water springs	Highest astronomical tide
- 0.203	-0.036	+0.034	+ 0.128	+0.233	+0.256	+ 0.284

3.3.4. Blace

Blace is situated approximately 120 km south of Jadrtovac (43°00'15"N, 17°28'27"E) and comprises a remote small pocket salt-marsh just north of a small fishing village (population 200) approximately 10 km south of Ploče (figure 3.4). The salt-marsh is located south of the Neretva River Delta, the largest outflow along the Croatian coastline with a large, 12 000 hectare alluvial plain, representing an important ecological and agricultural site (Romić et al., 2008) and recognised by the Ramsar Convention since 1993. The river originates in Bosnia & Herzegovina and is approximately 255 km long within a catchment area covering over 13000 km² (Jurina et al., 2013). The lower course of the river however, which flows through the Republic of Croatia, is only 36 km long, flowing through Quaternary alluvial deposits (Orlić et al., 2006). Rising sea level is a particular risk to this region and, combined with

surge-induced flooding, the intrusion of saline waters could have devastating effects on the agricultural practices that dominate this landscape (Baric et al., 2008).

The salt-marsh is located approximately 3 km south of the river's mouth in a sheltered embayment from the open Adriatic Sea and is roughly 40 m wide. The mean daily tidal range at this site is again 23 cm, as taken from values from the Ploče tide-gauge (Hydrographic Institute, 1955–2002). Indeed, analysis of admiralty tide-tables (Admiralty, 2010) for Ploče revealed an almost identical tidal regime to Split (table 3.4). Distinct zones of vegetation are again apparent at Blace, with *Juncus* spp., *Halimione*, *Atriplex* and *Chenopodiaceae* spp. dominating high-to-mid salt-marsh zones and *Limonium* spp. and *Salicornia* spp. dominating mid-to-low salt-marsh. Two sample sites were established at Blace (BL1 and BL2), as shown in figure 3.6, where surface transects were again established perpendicular to the coast incorporating all sub-environments from the high salt-marsh zone to the salt-marsh/sea interface. Specific details regarding the sampling at BL1 and BL2 are provided in table 3.6.

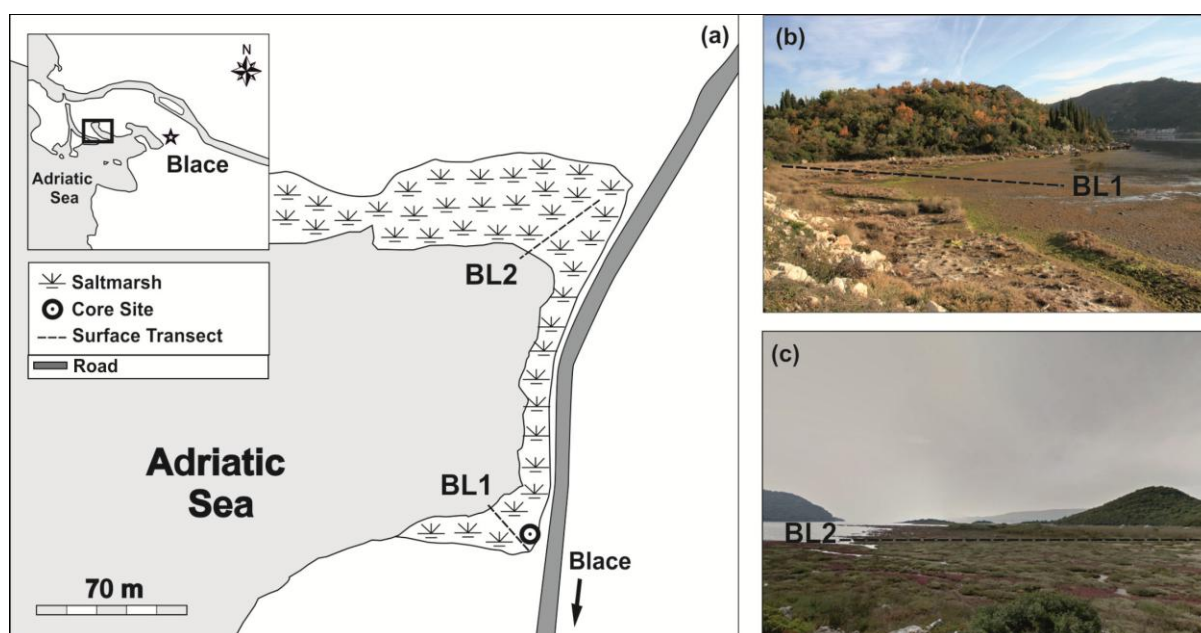


Figure 3.6. Study site map showing (a) location of salt-marsh environment at Blace with surface transect and core sites, (b) photo of BL1 and (c) BL2 sample sites.

3.4. RESEARCH METHODS

To reduce the potential effects of seasonality on surface foraminiferal distributions (i.e. seasonal blooms), as discussed by Horton and Edwards (2006), field work was conducted during winter months (January 2010), collecting all surface transect and ‘type’ core material. A second visit during December 2011 permitted the collection of a randomly sampled contemporary dataset from JD1, as discussed below. It is therefore considered that the presented foraminiferal datasets are representative of the salt-marsh environments at the time of sampling.

3.5. FIELD METHODS

3.5.1. Salt-Marsh Stratigraphy

The majority of Quaternary coastal research employs a standardised sediment classification scheme (Troëls-Smith, 1955) for the semi-quantitative recording of sediment stratigraphy. This scheme provides a rapid and detailed analysis of sediment records, allowing direct comparisons to be made across the Holocene sea-level research community. The Troëls-Smith (1955) classification system was therefore utilised to describe the underlying sediments at Jadrtovac and Blace to understand the pattern and history of deposition at the study sites. This procedure permitted ‘type’ cores to then be selected, and thus analysed, based on their sediment composition (i.e. typical of the stratigraphy found at the site in question) and location within the salt-marsh environment. Using a 25 mm diameter, 1 m-long Eijkelkamp hand gouge corer, overlapping sequences of sediment were analysed and described in detail, with all cores drilled to the underlying limestone bedrock. Whilst the sampling frequency varied between each site, sediment coring incorporated all sub-environments from the high salt-marsh zone to the seaward edge. Transect locations are depicted on the study site maps for both Jadrtovac and Blace in figures 3.5 and 3.6, respectively. For clarity and ease of interpretation, a simplified form of the salt-marsh stratigraphy at both study sites is presented in chapter 5, while a full Troëls-Smith (1955) description for each core analysed is provided in Appendix A. Core locations were flagged, and subsequently surveyed relative to m HVR571 as described below.

3.5.2. Salt-Marsh Sampling

Following the analysis of the salt-marsh stratigraphy, ‘type’ cores were then selected from within the upper salt-marsh zone. In addition to the analysis of fossil foraminifera, other analyses included organic matter, pH, particle size, sediment geochemistry and dating

(^{210}Pb , ^{137}Cs and AMS ^{14}C) as outlined below. Details regarding the location of these cores are shown in figures 3.5 and 3.6 whilst the length and altitude of each core is provided in table 3.5. Using a large-diameter (50 mm), 1 m-long Eijkelpkamp hand gouge corer, 'type' cores were again drilled to the underlying bedrock, with the outer surface of the core carefully cleaned to prevent contamination prior to sub-sampling of the undisturbed internal section at 1 cm intervals. Samples were placed in sealed sample bags and refrigerated at 4°C until ready for analysis.

Contemporary surface samples for foraminiferal analyses followed a similar strategy to that of transects established during the sediment stratigraphy survey. Although site-specific in terms of detail, this again incorporated all sub-environments of the salt-marsh environment from the high salt-marsh zone to the low salt-marsh-sea interface, but at a higher resolution focusing on distinct changes in topography and/or floral community, following Scott and Medioli (1980). The locations of these transects are displayed on study site maps in figures 3.5 and 3.6 while the exact distance and altitudes between the sample stations are shown in the transect altitude profiles in chapter 4. At JD1, a random sampling approach was also performed, but again incorporating all sub-environments of the salt-marsh environment. A standardised sample volume of 10 cm³ (10 cm² x 1 cm thick) was retrieved allowing for a direct comparison to previous research on foraminifera from other intertidal environments (Horton and Edwards, 2006). In some instances the salt-marsh surface was heavily root bound, thus a sharp serrated knife was used to extract the sample, keeping the blade firmly against the sample pot before placing into sealed sample bags containing buffered ethanol (95%) and protein stain Rose Bengal. This was used to help differentiate between live and dead foraminifera at the time of collection during the analysis stage (Walton, 1952). Whilst this technique has been scrutinised (Bernhard, 2000; Bernhard et al., 2006), it is widely adopted amongst the research community and still represents the most effective way of staining live foraminifera (Figueira et al., 2012). Finally, all sample stations were again flagged and surveyed relative to m HVR571.

This sampling procedure, in which the upper centimetre of sediment is collected, follows the commonly adopted sampling depth for studies analysing modern foraminiferal distributions from salt-marsh environments (e.g. Gehrels, 1994; Horton, 1999; Horton et al., 1999b; Gehrels et al., 2001; Edwards et al., 2004; Gehrels and Newman, 2004; Duchemin et al., 2005; Tobin et al., 2005; Southall et al., 2006). This approach assumes that the modern training data set used is composed of intertidal foraminifera which are primarily epifaunal. Some studies however have highlighted the importance of infaunal populations and their potential implications for sea-level reconstructions (e.g. mixing of live foraminifera with fossil

assemblages). Indeed this has shown to be particularly evident from studies of Northern America saltmarshes where infaunal populations can be significant (Goldstein and Harben, 1993; Ozarko et al., 1997; Goldstein and Watkins, 1998; Hippensteel et al., 2002; Duchemin et al., 2005; Tobin et al., 2005). In contrast to this, studies of modern foraminiferal distributions from European saltmarshes have found infaunal populations to be less significant, where foraminiferal assemblages are generally restricted to the upper few centimetres of sediment surface (Horton, 1997; Horton et al., 1999a; Alve and Murray, 2001; Horton and Edwards, 2006). The differences in these observations may in part reflect the organic nature of northern American salt-marsh environments compared to their more minerogenic European counterparts restricting the penetration of subsurface foraminifera (Horton et al., 1999a). Whilst the population of infaunal foraminifera may be variable and site specific, using a depth interval incorporating the upper 1 cm of the marsh sediment surface, provides an adequate model from which palaeoenvironmental reconstructions can be based (Culver and Horton, 2005; Horton and Edwards, 2006) and is thus adopted in this study.

Immediately adjacent to samples retrieved for contemporary foraminiferal distributions, 30 cm³ (30 cm² x 1 cm thick) of surface sediment was retrieved for the analysis of tested environmental variables. These included salinity, pH, organic matter and particle size. Additional environmental variables recorded were altitude and distance from water's edge. Distance was simply assessed using a 30 m tape, measuring each sample's location relative to the water's edge at the time of sampling (low tide). These variables are important as they were tested for their influence on the modern foraminiferal datasets, allowing an assessment to be made of the main controls governing foraminiferal distributions on the present-day marsh surface. The aim of this is to identify altitude (and hence tidal level) as an important control, permitting the contemporary foraminifera data to be used as a proxy for sea level.

Table 3.5. Summary of sampling at study sites Jadrtovac and Blace.

Site Name	Transect length (m)	Surface samples collected	'Type' core length (m)	'Type' core altitude (m HVR571)
JD1	122	22	0.42	0.165
JD2	16.5	10	0.56	0.245
JDR	-	10	-	-
BL1	29.2	15	0.32	0.300
BL2	46	9	-	-

JDR=Random sampling approach.

3.5.3. RBR Temporary Tide-Gauges

At both Jadrtovac and Blace, RBR submersible temporary tide-recorders were installed to acquire local tidal data. The autonomous instruments were kept horizontal and fully



submerged at all times to allow continuous tidal measurements, which are achieved by averaging pressure data. An in-built averaging function eliminates interference from localised wave action. This information could then be later used to assess the correspondence between the sample sites and high frequency tidal data obtained from nearby tide-gauge stations (e.g. Split) and to detect any local tidal distortion relative to the reference tide-gauge site.

3.5.4. Levelling Survey

To establish absolute altitudes for the stratigraphic transects, 'type' cores and surface sample stations, each location was surveyed relative to the vertical datum used in the Republic of Croatia (HVRs71). This was achieved using a Leica Na820 optical level and staff in conjunction with TopCon Hiper Pro Precision GPS+ positioning system. National geodetic benchmarks (figure 3.7), levelled to HVRs71, in close proximity to the field sites were surveyed back to temporary benchmarks established at each site, allowing the absolute altitude of each location to thus be calculated. The logistical problems caused by the remote location of Blace, meant that reference water levels (low-tide) were also recorded and later converted into absolute altitudes relative to HVRs71 using tidal levels provided by the Hydrographic Institute of the Republic of Croatia (Hydrographic Institute, 1955–2002) (table A12). Similar to the national vertical datum used in the UK (Ordnance Datum Newlyn), the national vertical datum used in the Republic of Croatia relates to mean sea-level over a known period of time from tide-gauge station(s). Previously, the old vertical datum used was defined by the mean sea-level at the Trieste tide-gauge for 1875. In comparison, HVRs71 is defined by the mean sea-level level from five tide gauge stations distributed along the Croatian coastline (Dubrovnik, Split, Bakar, Rovinj and Kopar) for 1971.5 over a measurement interval of 18.6 years (Rožić, 2001).

Figure 3.7. Details and photos of the national geodetic benchmark used near to Jadrtovac.

Benchmark ID	Identification #	Latitude	Longitude	Height (m HVRs71)
58/705	2 008 897	43N 41' 3.91"	15E 58' 2.14"	9.6448

3.6. LABORATORY METHODS

3.6.1. Foraminiferal Analyses (Fossil and Contemporary)

Sample preparation followed that outlined by Scott and Medioli (1980) and de Rijk (1995), wet sieving 10 cm³ of sediment through 500 µm and 63 µm sieves before transferring the >63 µm fraction into a wet splitter (Scott and Hermelin, 1993) and allowing the sample to settle out of suspension. Using a pipette, known volumes (usually 1/8th) of the >63 µm fraction (live and dead) were placed onto a spiral counting tray and counted wet under a Leica S8APO Stereo microscope at a magnification of x63 until a minimum of 100 (dead) counts was achieved (Patterson and Fishbein, 1989; Fatela and Taborda, 2002). The >500 µm fraction and supernatant was also checked for foraminifera before being discarded.

Samples for foraminiferal analysis were stored in buffered ethanol with Rose Bengal added to aid in the identification of live specimens at the time of collection. As the protoplasm is stained bright red, it was assumed that any tests containing protoplasm were either alive or only recently dead at the time of collection (Murray, 1991). A continuing debate exists in modern foraminifera studies as to which assemblage best reflects a reliable model for the sampled environment. Several authors (Horton and Edwards, 2003; Leorri et al., 2010; Rossi et al., 2011) advise using dead assemblages for analogues of palaeoenvironmental change as they more accurately depict the modern environment in comparison with total or living assemblages which are more susceptible to seasonal (Murray, 1991) and/or post-depositional changes (Horton and Edwards, 2006). The number of live specimens counted in each sample was significantly lower than the dead fraction, and the majority of surface samples analysed were void of any living foraminifera. Where present, numbers of live foraminifera were below statistically confident limits even when considering the low species diversity of the studied environments. This observation confirms previous findings by Cosovic et al. (2006) who analysed recent foraminifera along the Croatian Adriatic seacoast concluding that dead tests are substantially more common compared to living assemblages, regardless of season when sampling took place. Similarly in a study of foraminiferal populations from the Gulf of Venice, dead foraminiferal assemblages were not only more diverse, but much more abundant in comparison to the living component (Serandrei-Barbero et al., 2003). As a result, only the 'dead' datasets were employed in the results and interpretation of the contemporary study as discussed in chapter 4. Raw counts of both surface (live and dead) and core foraminifera are provided Appendix B.

Foraminiferal taxonomy was confirmed through comparison with primary resources (e.g. Murray, 1973; 1979; 1991) and the vast array of scanning-electron microscope (SEM)

images of intertidal foraminifera in the published literature (e.g. Horton and Edwards, 2006). The lack of previous research on salt-marsh foraminifera from the eastern Adriatic coastline limits comparisons, however comprehensive studies of benthic foraminifera in the Adriatic Sea were frequently referenced (e.g. Jorissen, 1987; 1988) to aid the identification of calcareous taxa. The various calcareous species of *Ammonia*, *Elphidium* and *Quinqueloculina* are grouped together at genus level as *Ammonia* spp., *Elphidium* spp. and *Quinqueloculina* spp., respectively, following Hayward et al. (2004) and Horton and Edwards (2006). Using a Hitachi TM3000 Tabletop microscope, high-resolution 'SEM' style images of the main foraminiferal taxa encountered were captured and are presented in Appendix E.

3.6.2. Environmental Variable Analyses

To explore the potential mechanisms influencing surface foraminifera distributions, sediment samples were sub-sampled and analysed for environmental variables so that their significance on the foraminiferal dataset could be determined through multivariate statistical analyses, as presented in chapter 4. Where applicable, the same procedures were repeated for both contemporary and core material (e.g. loss-on-ignition, laser granulometry). Results from surface environmental variables are presented in chapter 4 whilst down-core trends are presented in chapter 5.

3.6.2.1. Salinity and pH

Conductivity (as an indicator of salinity) and pH were analysed simultaneously after creating a 1:2 soil to water mixture comprising 35 ml of sediment and 70 ml double distilled water. The mixture was thoroughly stirred using a glass rod and allowed to settle for approximately one hour before measurements commenced. The solution was then measured and repeated three times before an average was taken for each sample station. Measurements of pH were performed using a HANNA HI-98115 pH meter while conductivity measurements were recorded using a HANNA HI-9033 multi-range conductivity probe. Calibration solutions were first used, and periodically thereafter, to ensure the correct measurement of pH and conductivity, using pH solutions 4.01 and 7.01 and conductivity solution 1413 $\mu\text{S}/\text{cm}$ (H170031). As the probe measures conductivity, which is used as a direct indication of salinity levels at each sample station, the equation given below was used to express conductivity as a function of salinity, presented as parts per thousand (‰) following Gehrels and Newman (2004). To ensure consistent results, the temperature of the analysed solution was also readily recorded.

$$\text{Salinity } \text{‰} = 0.6679 (\text{conductivity in } \text{mS cm}^{-1} - 0.1513)$$

3.6.2.2. Organic Matter

The organic matter of each sample was determined by loss-on-ignition (LOI) (Ball, 1964) whereby the organic content in each sample is combusted to ash and carbon dioxide. To remove hygroscopic moisture, approximately 5 g of sediment from each sample was left overnight (typically 12 hours) in a Sanyo Convection Oven at 105°C. The samples were then re-weighed before ignition at 450°C for approximately four hours in a pre-heated muffle furnace. Samples were allowed to cool in desiccators before weighing using a Mettler Toledo high-precision analytical balance allowing down-core and surface trends of LOI to be calculated using the following equation:

$$LOI_{450} = \frac{(DW_{105} - DW_{450})}{DW_{450}} \times 100$$

where;

LOI_{450} = Loss-on-ignition at 450°C expressed as a percentage.

DW_{105} = Dry-weight (g) of the sample before ignition (after drying at 105°C).

DW_{450} = Dry-weight (g) of the sample after ignition.

3.6.2.3. Particle Size Analysis

Substrate particle size distribution of both contemporary and core material was analysed using a Coulter laser diffraction granulometer (LS200). The variable organic content of salt-marsh sediments, as identified from LOI results, resulted in samples being pre-treated to remove unwanted organic particulates that may contaminate the minerogenic particle size results (Allen and Thornley, 2004; Gray et al., 2010). This involved sub-samples of sediment (between 0.5g and 5g depending on organic content) first being sieved through 2 mm to remove larger rootlets and stems, before being heated gently on a hot plate in a solution of 20% hydrogen peroxide (H_2O_2) and double distilled water. The reaction was continued until all organic material had been digested. Prior to inputting to the granulometer, clay-rich samples were disaggregated on a watch glass using Calgon. During the analysis, which measures particle size distributions between 4 and 2000 μm (0.004 and 2 mm), samples were sonicated to further aid even dispersion of the sediment. Finally, output data from the analyses were processed using the computer program GRADISTAT version 8 (Blott and Pye, 2001). For statistical analyses presented in chapter 4, the data were separated into the individual proportions of percentage sand, silt and clay using the size classes provided by GRADISTAT.

3.6.2.4. Dry Bulk Density

Dry bulk density (DBD) analyses were performed to complement the analysis of short-lived radionuclides, providing information regarding changes in mass accumulation rate that may also be used to identify potential sediment compaction issues, often associated with minerogenic low-energy intertidal sediments (Brain et al., 2011). At a resolution of 1 cm throughout the core material, approximately 1 cm³ of sediment was carefully cut and its dimensions recorded before being weighed wet. Each sample was frozen and then placed in a freeze-drier to remove all water content. Finally the samples were re-weighed using a high-precision analytical balance and the dry bulk density calculated using the following equation:

$$DBD = DW/V$$

Where;

DBD = Dry-bulk density (g/cm³)

DW = Dry-weight of the sample (g)

V = Volume of the sample (cm³)

Where the volume of core samples was unable to be achieved through the above procedure, due to compression (either during transportation or storage), a volume by displacement method was used following the principal that 1 mL of water has a volume of 1 cm³. An initial water level was subtracted from the final water level allowing volume to be calculated.

3.7. CORE CHRONOLOGY

The construction of a reliable, high resolution chronology is pre-requisite in sediment-based sea-level reconstructions (e.g. Marshall et al., 2007). These are usually acquired through a multi-proxy dating approach involving radiocarbon dating (¹⁴C), short-lived radionuclides and independent markers of known age (e.g. pollen chronohorizons). The organic nature of salt-marsh sediments has made ¹⁴C dating the most widely used technique in Quaternary palaeoenvironmental studies. However, limitations in the application of ¹⁴C for dating more recent or low organic sediments, often associated with UK and NW European salt-marshes, mean it is often used in conjunction with other sources of age data to construct composite chronologies which seek to link the chronological data together (Edwards, 2004).

Age determinations by ¹⁴C have the ability to extend to 9 to 10 half-lives, which equates to approximately 50,000 years (Hua, 2009). Previously these estimations were based on measurements of radioactive decay by counting ¹⁴C atoms. This method, referred to as

'conventional' radiocarbon dating, required large amounts of carbon (~100g), which often corresponded to large sample intervals and long counting times. An alternative approach to radiocarbon age determinations is through accelerator mass spectrometry (AMS). This relatively new, improved method has considerable benefits over conventional dating by counting ^{14}C atoms directly, relative to stable carbon isotopes ^{12}C and ^{13}C (Hua, 2009). Counting times are also significantly reduced, as are sample volumes of required carbon (0.1-10 mg) (Blaauw and Heegaard, 2012). Indeed developments in AMS have permitted the dating of samples containing as little as 10-20 μg of carbon (Hua et al., 2004) allowing new sources of material to be dated (e.g. pollen and foraminifera). With reference to salt-marsh environments, dating terrestrial plant macrofossils is preferable, especially those found *in situ*, to avoid contamination of 'old carbon' which is often associated with bulk date samples where carbon has been transferred into the sample from an unknown source, producing illogical age estimates (Edwards, 2004).

Whilst the application of ^{14}C dating is widespread, sediments deposited since AD ~1650 represent a significant challenge for this technique due to variations in the production of ^{14}C within the atmosphere, which have not been constant throughout time (Stuiver and Braziunas, 1998; Reimer et al., 2009). Natural fluctuations in atmospheric ^{14}C caused by changes in the Earth's magnetic field, solar activity and changes in the carbon cycle are further complicated by anthropogenic disturbances related to the combustion of fossil fuels and land-use changes (van der Plicht, 2007; Hua, 2009). More recently, atomic bomb explosions since the 1950s has created huge surges in atmospheric ^{14}C concentration which is then followed by a gradual decline to pre-bomb levels in the past few decades (Hua and Barbetti, 2004). As a result, radiocarbon years are not the same as calendar years and so need to be converted from the former to the latter using a calibration curve (e.g. McCormac et al., 2007; Reimer et al., 2009). However variations in the concentration of atmospheric ^{14}C , creating 'wiggles' and 'plateaus', mean that simply intercepting the calibration curve to acquire a calendar year is often difficult because multiple dates are possible from a single sample (Reimer and Reimer, 2007). Despite recent advances in the application of radiocarbon dating for modern deposits in salt-marsh environments by calibrating ages relative to known 'bomb spikes' since the 1950s (e.g. Marshall et al., 2007; Hua, 2009), short-lived radionuclides such as lead-210 (^{210}Pb) and caesium-137 (^{137}Cs) provide an alternative method to ^{14}C in dating sediments of more recent age (e.g. Allen et al., 1993; Plater et al., 1999; Gehrels et al., 2002; 2005; Plater and Appleby, 2004; Wang et al., 2005; Horton et al., 2006; Leorri and Cearreta, 2009; Kemp et al., 2009; 2012).

Lead-210 is a naturally occurring radionuclide formed as a decay product of the ^{238}U series. The proposal of ^{210}Pb as a dating tool by Goldberg (1963), is based on measurements of the

vertical distribution of unsupported (excess) ^{210}Pb activity which becomes integrated into sediments as a result of accumulation from atmospheric fallout. Estimations of sediment age are then calculated from measurements of the excess ^{210}Pb activity as a result of its known decay rate of approximately 22.3 years (Appleby and Oldfield, 1992). Since its first application in dating lake (Krishnaswamy et al., 1971) and marine (Koide et al., 1973) sediments, ^{210}Pb dating has become the most widely adopted technique for dating marine and lacustrine sediments deposited over the past 100-200 years (Cundy and Croudace, 1995). To further constrain the ages provided by a ^{210}Pb chronology, ^{137}Cs (half-life 30 years), an artificially produced radionuclide is often used. Its application is used to provide markers within the sediment record that can related to atmospheric fallout from peak nuclear weapons testing (1963), waste discharge from nuclear facilities and reactor accidents (e.g. Chernobyl 1986) (Haslett et al., 2003).

To construct age-depth profiles using ^{210}Pb various models have been developed. An initial Constant Flux, Constant Sedimentation (CF-CS) model, developed by Krishnaswamy et al. (1971) and Robins (1978), was based on the assumption that there was a constant rate of ^{210}Pb deposition from the atmosphere and no-post depositional disturbances or redistribution had occurred. At sites where these assumptions were unfounded, more sophisticated models were developed, including the Constant Rate of Supply (CRS) model (Appleby and Oldfield, 1978; Appleby et al., 1979) and the Constant Initial Concentration (CIC) model (Appleby and Oldfield, 1978; Appleby, 2001). The former model, whilst still assuming a constant flux of ^{210}Pb through time, was developed to compensate for changes in accumulation rate and has proved successful for environments which have obtained a steady supply of unsupported ^{210}Pb from the atmosphere (Appleby, 2001). The CIC model however was developed for environments where atmospheric fall-out was not the main source of unsupported ^{210}Pb . Like the CRS model, it too allows for variation in accumulation rate through time but assumes sediments to have an constant initial excess of ^{210}Pb (Appleby, 2001).

In addition to the above, independent age markers may provide further age constraints within the sediment record that can be related to documented evidence. These markers also possess the ability to extend the beyond the limits of ^{210}Pb dating to bridge the crucial age gap covered by short-lived radionuclide and radiocarbon chronologies (Gehrels and Woodworth, 2013). Techniques often include pollen chronohorizons, geochemical or pollution indicators, stable Pb isotopes, spheroidal carbonaceous particles (SCPs) and/or tephra (volcanic) layers. Whilst these methods may be site-specific, their use in salt-marsh based sea-level reconstructions is potentially very useful as they can provide very precise dating markers in the sedimentary record if related to documented evidence of pollution

and/or land use change (e.g. Allen et al., 1993; Cundy and Croudace, 1995; Haslett et al., 2003; Gehrels et al., 2002; Plater and Appleby, 2004; Gehrels et al., 2005; 2008; Marshall et al., 2007; Kemp et al., 2009). With reference to Croatia, the frequent application of agrichemicals is one of the major causes of trace metal accumulation in soils (Zovko and Romic, 2011) and the accumulation of Cu is often related to the long-term widespread use of copper-sulphate (Bordeaux mixture) and other copper-based fungicides in controlling vineyard mildew (Romic and Romic, 2003). The areas surrounding Adriatic Bays are influenced, to a varying extent, by human activity related to agricultural activities supplying various types of contaminants to bay environments (Miko et al., 2007). Changes in the geochemical stratigraphic record and elevated concentrations of trace elements associated with anthropogenic change (e.g. Pb, Cu and Zn) have become increasingly important as the use of peloid muds/sediments from these environments for medicinal and cosmetic purposes is currently unregulated (Mihelčić et al., 2006; Miko et al., 2007).

The Morinje Bay environment, from where cores JD1 and JD2 were retrieved, has been the focus of a number of investigations focusing on the geochemical properties of the sediment in relation to the above issue. Šparica et al. (2005a) investigated aspects of the sediment/water interface in the Morinje Bay environment concluding increased but not anomalous concentrations of Pb and Cu are a result of regional atmospheric deposition and localised vineyard activity as sediment from the surrounding catchment is transported into the bay. Mihelčić et al. (2006) investigated the vertical distribution of trace metals in the Morinje Bay focusing on the history of anthropogenic emissions into the bay environment. Whilst their analysis focused on a 55 cm core from the middle of the bay, dated by ^{137}Cs peaks, they also report concentrations in Cu, Pb and Zn from approximately the past 50 years to be related to local anthropogenic activity within a fine-grained silt sediment. They conclude leaded gasoline to be the primary source of Pb enrichment increasing up to the 1980s, and decreasing thereafter due to a reduction of traffic in the area after the construction of an alternative route in the early 1980s. The beginning of war in Croatia in 1991 also isolated the area resulting in a marked reduction in traffic (Mihelčić et al., 2006). Unlike Western Europe, however, a decrease in Pb accumulation cannot be linked with the change to unleaded fuel as high levels of leaded fuel were only phased out in 2005 (Mihelčić et al., 2006). Maximum copper concentrations occur between a depth interval of 5 and 15 cm. However, the authors were unable to differentiate the main source of Cu enrichment between an aeolian or rivulet supply of copper-based plant protection agents or copper-based antifouling paints from numerous boats moored in the Morinje Bay. The main source of Zn to the bay is attributed to tourist activities and housing infrastructure (Mihelčić et al., 2006). Similar results are also reported from Makirina Cove, approximately 7 km north of the

Morinje Bay, where elevated concentrations of Cu, Pb, Zn from sediment cores are attributed to traffic circulation and agricultural activity (Šparica et al., 2005b). Miko et al. (2007) also studied sediments from the Morinje and Makirina Bay environments. The authors analysed the influence of land-use changes on geochemical properties of peloid sediments focusing on surface deposits from the surrounding vineyards and sediment cores. Similar conclusions are drawn from the study highlighting an enrichment of Pb and Cu which are attributed to local road runoff (Pb) and vineyard activity.

To accompany the fossil foraminiferal records presented in section 5.3, composite chronologies have been established involving an array of techniques including short-lived radionuclides, AMS ^{14}C dating and X-ray fluorescence elemental concentrations as detailed below. Radiocarbon dating was restricted to core JD1 only and its combination with other age data in the construction of an age-depth model is discussed in section 3.7.4.

3.7.1. Short-Lived Radionuclides

Lightly disaggregated freeze-dried sediment samples from cores JD1, JD2 and BL were analysed for ^{210}Pb , ^{226}Ra , ^{137}Cs and ^{241}Am by direct gamma assay at the University of Liverpool Environmental Radioactivity Laboratory using Ortec HPGe GWL series well-type coaxial low background intrinsic germanium detectors (Appleby et al., 1986). Lead-210 was determined via its gamma emissions at 46.5 keV, and ^{226}Ra by the 295 keV and 352 keV γ -rays emitted by its daughter isotope ^{214}Pb following three weeks storage in sealed containers to allow radioactive equilibration. Caesium-137 and ^{241}Am were measured by their emissions at 662 keV and 59.5 keV, respectively. The absolute efficiencies of the detectors were determined using calibrated sources and sediment samples of known activity. Corrections were made for the effect of self-absorption of low energy γ -rays within the sample (Appleby et al., 1992) and ^{210}Pb dates were calculated using the CRS model (Appleby and Oldfield, 1978; Appleby et al., 1979) as described above. To further constrain ages obtained via ^{210}Pb dating, ^{137}Cs (half life of 30 years) is used as a chronological marker (Appleby, 2001).

3.7.2. Radiocarbon Dating

The age-limitations of short-lived radionuclides in dating sediments deposited longer than 100 years or so (Smith, 2001) restricted the extent of a reliable and precise radiometric chronology to the upper section of the core material due to a known ^{210}Pb half-life of approximately 22.3 years (Appleby and Oldfield, 1992). All cores were therefore investigated for suitable dating material with a goal of establishing ages for sediments below the limits of ^{210}Pb dating. When sampling for ^{14}C dating, it was important to select terrestrial plant

macrofossils, rather than randomly selected detritus, as they obtain their carbon by sub-aerial photosynthesis (Hatté and Jull, 2007). This would help minimise complications of reservoir effects and old carbon being incorporated into the sample, which could result in samples appearing older than contemporaneous terrestrial materials (Hua, 2009). However, this often proved difficult due to the inorganic nature that characterised sediments from the lower reaches of each core. Whilst organic matter is present, cores JD2 and BL were void of any ‘reliable’ material that could be dated confidently by ^{14}C . Radiocarbon dating of suitable organic derived material was therefore investigated to extend the chronological history of JD1 core only, where a varying abundance of small, black seed-like material was encountered within an otherwise organic-deprived (<10%) clay-rich sediment. First, sediment samples were dried, sieved (at 500 μm) and carefully inspected before the material was carefully extracted and washed with double distilled water. They were then oven dried over-night at 50°C to obtain dry-weights. Using a binocular microscope, the material was identified as *Scirpus holoschoenus* seeds or fruits (figure 3.8), a common salt-marsh species along the eastern Adriatic coastline (Pandža et al., 2007) and found at higher elevations on the contemporary salt-marsh surface at Jadrtovac.

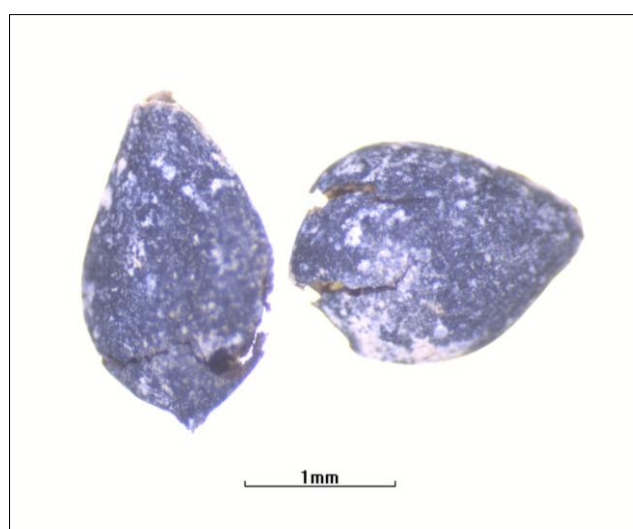


Figure 3.8. *Scirpus holoschoenus* seeds analysed for ^{14}C from JD1 core (26-27 cm).

Following this, an application for radiocarbon dating support from the Natural Environment Research Council (NERC) was sourced and successfully received (April, 2013) for three high-precision ^{14}C dates between depths of 25 cm and 30 cm (NERC Radiocarbon Analysis Allocation Number 1678.1012). Samples were prepared to graphite at the NERC Radiocarbon Facility, East Kilbride before analysis of ^{14}C at the Scottish Universities Environmental Research Centre AMS Laboratory. Prior to analysis, samples were digested in 1M HCl (80°C for 30 minutes), washed free from mineral acid with deionised water and

then digested in 0.2M KOH (80°C, for a maximum of 20 minutes). The digestion process was repeated using deionised water until no further humics were extracted. The residue was then rinsed free of alkali, digested in 1M HCl (80°C for 1 hour) and then rinsed free of acid before being transferred to an Ag cup, dried and homogenised. Total carbon in the pre-treated sample was recovered as CO₂ by heating with CuO in a sealed quartz tube and gas converted to graphite by Fe/Zn reduction. Results are reported as conventional radiocarbon years BP (relative to AD 1950) and percentage modern ¹⁴C, both expressed at the ±1σ level for overall analytical confidence. The results were corrected to δ¹³C_{V_PDB}‰ -25 using the δ¹³C values. The δ¹³C value was measured on a dual inlet stable isotope mass spectrometer (Thermo Fisher Delta V) and is representative of δ¹³C in the original, pre-treated sample material. Details regarding the calibration of ¹⁴C dates to provide calendar ages (Reimer et al., 2009) are provided in section 5.5.3.1. The radiocarbon analytical dating report for core JD1 is provided in Appendix C.

3.7.3. X-Ray Fluorescence (XRF)

Down-core changes in elemental concentrations were investigated to identify pollution signals to provide further potential chronological constraints within the sediment records to accompany radiometric analyses described above. This procedure may also be used to explore potential dissolution issues associated with calcareous foraminifera, as identified from changes in calcium carbonate (CaCO₃) from the geochemical record (e.g. Murray, 1989). XRF analyses were performed using a BRUKER S2 Ranger energy dispersive X-ray fluorescence spectrometer to obtain information on the relative abundance of elements within the core material. Elemental concentrations are assessed by photoelectric fluorescence of secondary X-rays, which measures the characteristic X-ray photons given off by various elements (Boyle, 2002). The energy of secondary X-rays generated by a sample will correspond to the characteristics of certain elements and the rate of emission is a reflection of the elemental concentration. Sub-samples of all core material were first frozen and then freeze-dried until all moisture content was removed. Samples were then lightly disaggregated using a pestle and mortar and transferred into labelled sample holders lined with spectro-certified polypropylene film and gently compacted using a brass plunger. Freeze-drying samples is a popular method for drying sediments prior to chemical analysis because of the lower risk of losing volatile elements in marine sediments (Loring and Rantala, 1992). The spectrometer was calibrated before and during usage using copper standard discs and standard samples of known elemental concentrations from different sedimentary environments (e.g. river, stream and pond). Absolute geochemical

concentrations were subsequently determined using the PASCAL program DECONV (Boyle, 2000).

3.7.4. Age-Depth Modelling

The purpose of constructing age-depth models is to present an interpolated chronological framework to provide calendar ages between a series of dated points that may be derived from a variety of sources (Blaauw, 2010). The model can then be used to give age estimates for both the dated levels and undated levels and extrapolated throughout a core sequence (Blaauw and Heegaard, 2012). A significant challenge, however, in constructing age-depth models for use in sea-level studies is the combination of different chronological methods in establishing ages for different sections of a core sequence. The analysis of short-lived radionuclides is usually utilised for establishing ages in the upper section of a core and limited to the past 100 years or so (Smith, 2001) whereas ^{14}C dating is harnessed for sediments beyond this limit where organic matter that may return reliable ^{14}C ages can still be found. The difficulty arises when combining the two chronologies together in an age-depth model as an offset (inflexion) between the two techniques is often observed (e.g. Gehrels et al., 2005; Kemp et al., 2009). Unfortunately this inflexion is often during a period crucial to the understanding of when recent sea-level rise occurred (Barlow et al., 2013). As a result, a change in sedimentation rate and/or sea-level rise will inherently be transferred into the resultant sea-level reconstruction when really it is simply an artefact of switching between sources of age data (Edwards, 2004). To constrain the crucial age gap between these radiometric chronologies, independently dated markers, such as a tephra layers or an historical pollen event can provide very useful information in age-depth models. In an ideal scenario, it is desirable to construct a chronological framework using multiple, overlapping techniques (Barlow et al., 2013) ideally incorporating intervals before and after an inflexion (Gehrels and Woodworth, 2013). Financial project constraints and the assumption that organic material exists within the desired stratigraphic intervals mean this is not always realistically achievable. However overlapping techniques offer some benefits in that they can act as a validation tool. For example the use of high precision bomb spike ^{14}C dating since ~AD 1950 can be used to assess the accuracy of a ^{210}Pb and ^{137}C chronology (e.g. Marshall et al., 2007; Kemp et al., 2009).

A proposed alternative to age-depth modelling altogether is to date key points in the stratigraphic record ('events') which would ideally incorporate dates from directly above and below the 'event' horizon (Telford et al., 2004a). In the context of sea-level studies this would allow changes in sea-level to be assessed more directly rather than using interpolated points provided by age-depth models described above (Gehrels and Woodworth, 2013). Again,

however, the limited availability of organic material, where key changes in the stratigraphic record often occur within a silt/clay substrate, hinders the application of this approach with ^{14}C dating.

Combining multiple sources of age data usually requires some form of modelling. In general, there are two main types, referred to as the classical or Bayesian approach (Hua et al., 2012). The most common and basic approach uses linear interpolation or regression techniques between dated levels, where lines are used to connect individual age estimations with no *a priori* information. Gradients between these dated intervals are then used to estimate rates of accumulation and ages are calculated for the intermediate depths (Blaauw and Heegaard, 2012). While this approach can achieve realistic results (e.g. Bennett, 1994), it is based on the unrealistic assumption that abrupt changes in sedimentation rate occurred at exactly the same depths as the dated levels (Blaauw, 2010). Similarly these models, where the line has been drawn through single-age point estimations (e.g. mean or median), do not consider the full potential age distribution of a calibrated ^{14}C date (Telford et al., 2004b). Conveniently, ecological graphic software such as *Tilia* (Grimm, 2004) offers the ability to construct such models by drawing straight or curved (e.g. polynomials and splines) lines through age data. However, external age calibration is required and nor does it consider the full age distribution or multi-modal, asymmetrical nature of calibrated ^{14}C dates. As ^{14}C age estimates rarely follow symmetrical distributions, users often require a more sophisticated approach to age-depth modelling in which the full age distribution is considered along with other potential useful information (Blaauw and Heegaard, 2012). An alternative approach to age-depth modelling adopts a Bayesian approach (e.g. Blaauw and Christen, 2005; 2011; Bronk Ramsey, 2008) which uses more advanced and flexible numerical methods and is often the preferred choice for users requiring higher precision (Blaauw, 2010). This method allows the user to incorporate additional information such as stratigraphic and chronological ordering, referred to as *a priori*, to reach a *posterior* conclusion (Blaauw and Heegaard, 2012; Hua et al., 2012).

To assess the accuracy in modelling accumulation rate through time, two models were created, adopting 'classical' (*Clam*; Blaauw, 2010) and Bayesian (*OxCal*; Bronk Ramsey, 2009) approaches for core JD1 using data from the short-lived radionuclides and AMS ^{14}C analyses. Further details and the results from both age-depth models are presented in section 5.5.3.

3.8. MULTIVARIATE STATISTICAL ANALYSES

A primary aim of Quaternary palaeoecological studies is to reconstruct features of the past environment from fossil assemblages preserved in a variety of sedimentary environments (Birks, 1995). Expressing a biological indicator (e.g. foraminifera) as a function of an environmental variable (e.g. pH), known as a transfer function (Imbrie and Kipp, 1971), first requires an understanding of the contemporary environment and how the two are related. In essence the statistical methods applied to ecological data seeks to explore and quantify what environmental factors influence the distribution of contemporary organisms (Dale and Dale, 2002). In salt-marsh foraminiferal-based sea-level reconstructions, the relationship between modern assemblages and elevation within the tidal frame must first be quantified to assess the suitability of modern foraminiferal datasets before they are used as proxies of sea-level change from fossil assemblages (Gehrels, 2002).

Prior to statistical analyses, the contemporary foraminiferal datasets were converted into percentages and screened to remove insignificant species and low counts, following Fatela and Taborda (2002). Usually, those species which do not contribute more than 5% of the total dataset are removed, however due to the low diversity of the studied salt-marsh environments, this was amended to 2% (following Horton et al., 2003; Edwards et al., 2004). Samples which contained less than 150 dead foraminiferal tests were excluded from the analyses, with exceptions made for samples containing dominant species that contributed more than 50% of the total count, following Patterson and Fishbein (1989) and Fatela and Taborda (2002).

3.8.1. Zonation

To quantify the nature of vertical distribution, two multivariate statistical techniques were employed to describe and classify the distribution of the contemporary foraminiferal datasets. First, unconstrained cluster analysis based on unweighted Euclidean distance, using no transformation or standardization, of the relative percentage 'dead' data was performed to identify faunal zones (clusters) grouping samples together based on similarities in the foraminiferal assemblages. Secondly, Detrended Correspondence Analysis (DCA) (Hill and Gauch, 1980) was utilized to represent those samples of similar characteristics close together in a multidimensional space. Conversely it would also identify those samples which are dissimilar by plotting them far apart and/or show potential outliers in the modern dataset. These techniques are considered complementary (Birks, 1986; 1992) as cluster analysis is useful in extracting faunal zones while DCA provides further information regarding the interaction within and between the faunal zones in a multidimensional space (Horton and

Edwards, 2006). While cluster analysis is useful in segregating samples and species into naturally occurring groups (Parker and Arnold, 2003), it is important that cluster analyses are unconstrained as this will identify ecological faunal zones based on similarities in the foraminiferal assemblages rather than constrained cluster analyses which will automatically be altitudinally constrained due to the nature of the data collection along a transect from high- to low-marsh. Unconstrained cluster analysis was performed using the program CONISS within Tilia View (Grimm, 2004) using the output from CONISS total sum of squares to identify faunal zones. DCA ordination was processed using CANOCO version 4.5.4 (ter Braak and Smilauer, 1997-2003). Using the zones identified from these techniques, elevation-dependent faunal zones were then created, represented through simple box plots of cluster order (faunal zone) by height relative to vertical datum (m HVR571).

3.8.2. Ordination

To further explore the nature of foraminiferal distribution, with a focus on the controls governing vertical distributions as identified from the zonation process, constrained ordination was utilised to evaluate the potential effects of the tested environmental variables (pH, salinity, LOI, grain size, distance and altitude). The aim of this process was to confirm the suitability of the foraminifera as proxies for sea-level change by quantifying elevation as an important control. It is essential to select the appropriate statistical method by determining linear or unimodal regression models to best describe the distribution of foraminifera along the environmental gradient (Birks, 1995; Gehrels, 2002). Calculations of the gradient lengths for axis 1 derived from DCA results, which are measured in standard deviation (SD) units, gives an indication about the distribution of the foraminiferal datasets allowing the appropriate ordination technique to be selected. Birks (1995) stated that if ordination axis lengths are <2 SD units, the species are linear, whereas >2 units would indicate unimodal distributions. ter Braak (1995) also reported linear distributions with gradient lengths of <2 SD units whilst unimodal distributions are associated with gradient lengths >4 SD units with SD units between 3 and 4 being ambiguous (Leps and Smilauer, 2005).

Following this, constrained ordination Canonical Correspondence Analysis (CCA) and Redundancy Analysis (RDA) were selected accordingly, to test the hypothesis that contemporary foraminifera are related to elevation. CCA is an eigenvector ordination technique that relates species composition to known variations in the environment (ter Braak, 1986; 1987; ter Braak and Verdonschot, 1995) and is suitable for unimodal distributions. RDA however is more suitable for linear species-environment relationships, where the axes are linear combinations of the environmental variables (Leyer and Wesche, 2007). For both procedures, data were processed using inter-species distances with biplot

scaling and no data transformation, and the canonical eigenvalues produced provide a measure of the total explained variance in the foraminiferal dataset by the tested environmental variables. Where DCA axis lengths varied between 2 and 3 SD units, both linear and unimodal ordination techniques were performed to assess their ability in explaining variation in the contemporary datasets. To quantify the relative importance of each environmental variable, partial CCAs/RDAs were performed following Borcard et al. (1992). This procedure would allow an assessment of the tested environmental variables outlined above in explaining the distribution of contemporary foraminifera. Following this, the statistical significance of each environmental variable in explaining variation in the datasets was then determined using Monte Carlo permutation tests (499 permutations under reduced model). All ordination techniques were performed using the software package CANOCO version 4.5.4 (ter Braak and Smilauer, 1997-2003).

For clarity and ease of understanding, the statistical methods used in the transfer function development precede the sea-level reconstruction presented in chapter 6.

RESULTS I

CONTEMPORARY SALT-MARSH DATA

4.1. INTRODUCTION

This chapter provides a detailed analysis of the contemporary salt-marsh environment at Jadrtovac and Blace focusing on the measured environmental variables (elevation, distance, pH, salinity, organic matter and grain size) and modern foraminiferal distributions. Through environmental graphs, correlations and assemblage diagrams the data are first explored in a qualitative manner, describing key trends and patterns, before a more statistical approach is adopted in order to identify vertical faunal zones and links between the modern foraminiferal assemblages and environmental parameters through clustering and multivariate statistical techniques. As the relationship between contemporary microfossil assemblages and the environmental variable to be reconstructed is fundamental to the transfer function methodology, their use as quantitative indicators of former elevation is then critically assessed in preparation for transfer function development in the sea-level reconstruction (chapter 6).

4.2. ENVIRONMENTAL VARIABLES

4.2.1. Jadrtovac Site 1 (JD1)

Spanning a total length of 122 m, 22 sample stations were established across the transect at JD1 covering an altitudinal range of 0.44 m from the upper salt-marsh limit to the seaward edge (figure 4.1a). The uppermost two samples were beyond the clearly identifiable limits of tidal inundation (HAT; 0.284 m HVR571) and indeed proved to be devoid of statistically sufficient counts to be included in the foraminiferal dataset, as discussed below. Increased sampling frequency was focused in the upper salt-marsh environment from sample station 1 to 10 where an elevation change from 0.485m to 0.095m occurs over just 13 m. From this point a small altitudinal range is observed across the remainder of the transect, with sample stations 10 to 22 all situated below present MTL at Split (0.128 m HVR571).

Salinity values show a clear increasing trend with distance towards the seaward edge, with the uppermost samples highlighting their position within and above the upper tidal range (<0.4‰) (figure 4.1b). Conversely organic matter concentrations (LOI) show an overall decreasing trend towards the low tide shoreline. Between sample stations 5 and 16, LOI values range from 65% to 21% 73 m along the transect before a steady but increasing trend is then observed to the low tide shoreline at sample station 22, 122 m along the transect (figure 4.1d). With a mean value of 7.3, pH levels are variable across the salt-marsh surface. From sample station 1 to 13 (43 m along the transect) pH decreases from 8.5 to 5.7 before rising to 7.4 towards the end of the transect at station 21 (figure 4.1c). The substrate of the salt-marsh surface is composed predominately of silt (70-82%) and clay (15-21%), as shown in figure 4.5a. A small increase in sand % is observed at sample station 4, corresponding to a brief increase in mean grain size to 15 μm , 3 m along the transect (figure 4.1e).

Pearson's correlation coefficients (r) were performed to quantify the strength of the relationship between the measured environmental variables. Significant correlations at the 95% confidence limit ($p < 0.05$) are also used to highlight their strong co-variance. Inspection of table 4.1 shows significant relationships exist between a number of the measured variables and serve as confirmation of the qualitative descriptions given above. In particular, pH and salinity show a strong positive and negative relationship with elevation, respectively, whilst distance displays a strong relationship with elevation and salinity. Silt and clay show a strong negative relationship with sand while organic matter (LOI) shows no clear correlation with any of the variables except silt.

Table 4.1. Pearson's correlation coefficients (r) for environmental variables at JD1.

	Elevation	pH	Salinity	LOI	Distance	Sand	Silt	Clay
Elevation	1							
pH	0.74936*	1						
Salinity	-0.83622*	0.77224*	1					
LOI	-0.1656	-0.33033	-0.11592	1				
Distance	0.61991*	0.32355	0.70892*	0.36449	1			
Sand	0.25468	0.56877*	-0.3959	-0.41542	0.18213	1		
Silt	-0.26017	-0.4765*	0.32837	0.46109*	-0.12268	-0.90608*	1	
Clay	-0.18828	0.54117*	0.3805	0.26474	-0.2078	-0.87262*	0.58402*	1

*Bold denotes an r value with a significant correlation at the 0.05 level.

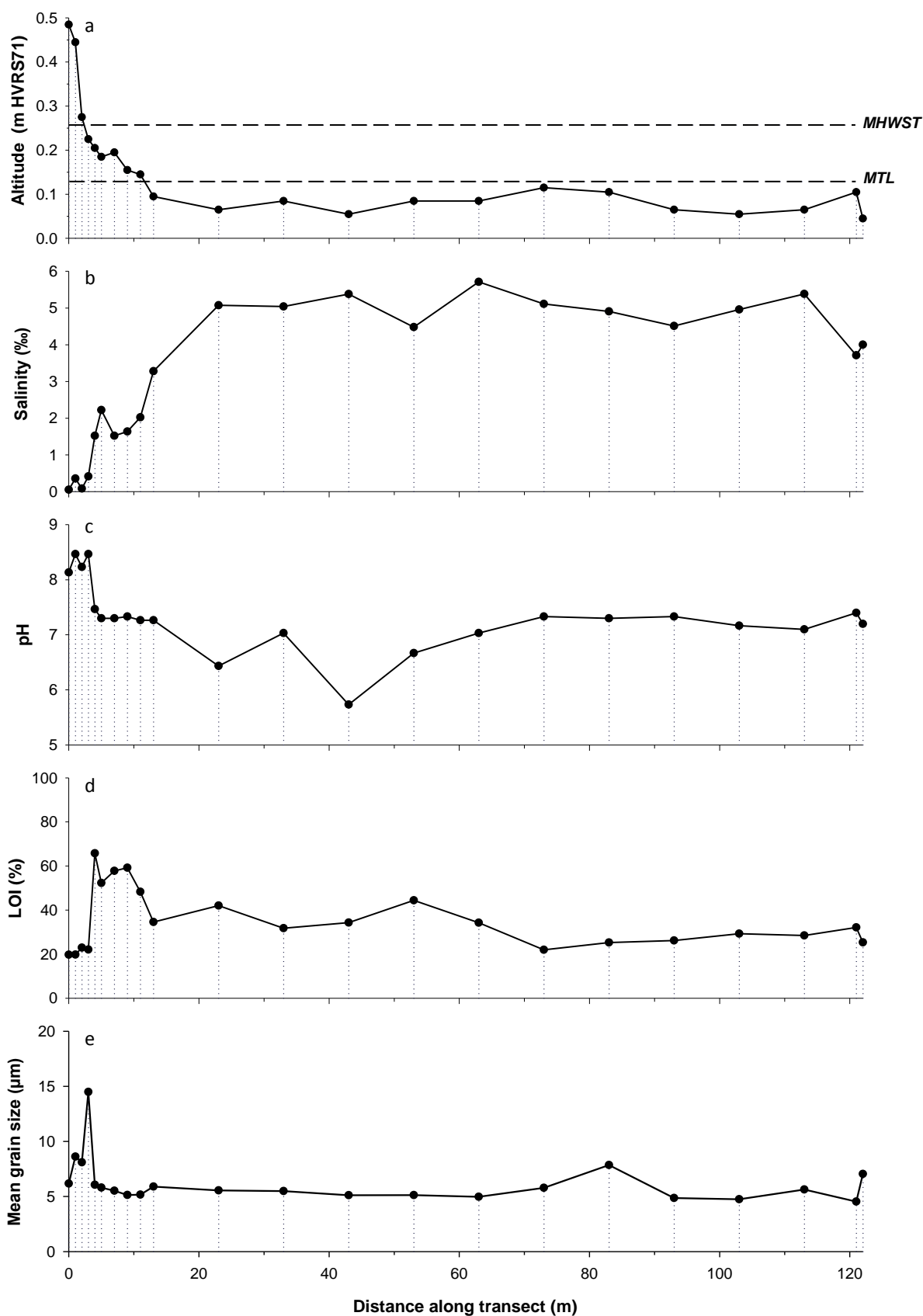


Figure 4.1. Measured environmental variables (altitude m HVR571, salinity, pH, LOI and mean grain size) across JD1 transect. Sampling locations and tidal levels (Split) also shown.

4.2.2. Jadrtovac Site 2 (JD2)

Covering an altitudinal range of 0.27 m, 10 sample stations were established across a smaller second transect at JD2 spanning a total length of 16.5 m (figure 4.2a). In contrast to JD1, a more transitional profile from the upper salt-marsh limit to the seaward edge is observed here. Sample stations 1 and 2 similarly appear above the limits of the highest astronomical tide (0.284 m HVR571) while only sample station 10 lies below MTL (0.128 m HVR571).

Excluding sample station 4, where salinity values drop to 0.3‰, an overall increasing trend is observed across the transect (figure 4.2b). However values are slightly lower when in direct comparison to JD1. While a decreasing trend is observed in the pH values, they remain relatively constant across the transect, ranging from 8.1 to 7.4 (figure 4.2c). Likewise organic matter (LOI) and mean grain size appear relatively constant across the transect. LOI levels range from 36% to 19% and shows some variability towards the edge of the salt-marsh (figure 4.2d). With a mean grain size of 5.1 μm (figure 4.2e), the substrate here is again predominantly silt (74%-81%) and clay (17%-25%) in nature with a minor addition of sand (<2%), as shown in figure 4.5b.

Pearson's correlation coefficients (r) revealed the same strong relationship between pH, salinity and elevation as found at JD1 (table 4.2). Distance shows a strong positive relationship with elevation and pH while a negative relationship with salinity is observed. In comparison with JD1, only clay and silt appear highly correlated with a strong negative relationship between the other grain size classes.

Table 4.2. Pearson's correlation coefficients (r) for environmental variables at JD2.

	Elevation	pH	Salinity	LOI	Distance	Sand	Silt	Clay
Elevation	1							
pH	0.73839*	1						
Salinity	-0.70262*	-0.95942*	1					
LOI	-0.24749	-0.61744	0.63284*	1				
Distance	0.93961*	0.82185*	-0.79235*	-0.36988	1			
Sand	0.19137	0.49425	-0.55035	-0.56879	0.26466	1		
Silt	0.61223	0.23072	-0.38398	-0.06268	0.51735	-0.02776	1	
Clay	-0.64638*	-0.39297	0.55768	0.26052	-0.58264	-0.32764	-0.93534*	1

*Bold denotes an r value with a significant correlation at the 0.05 level.

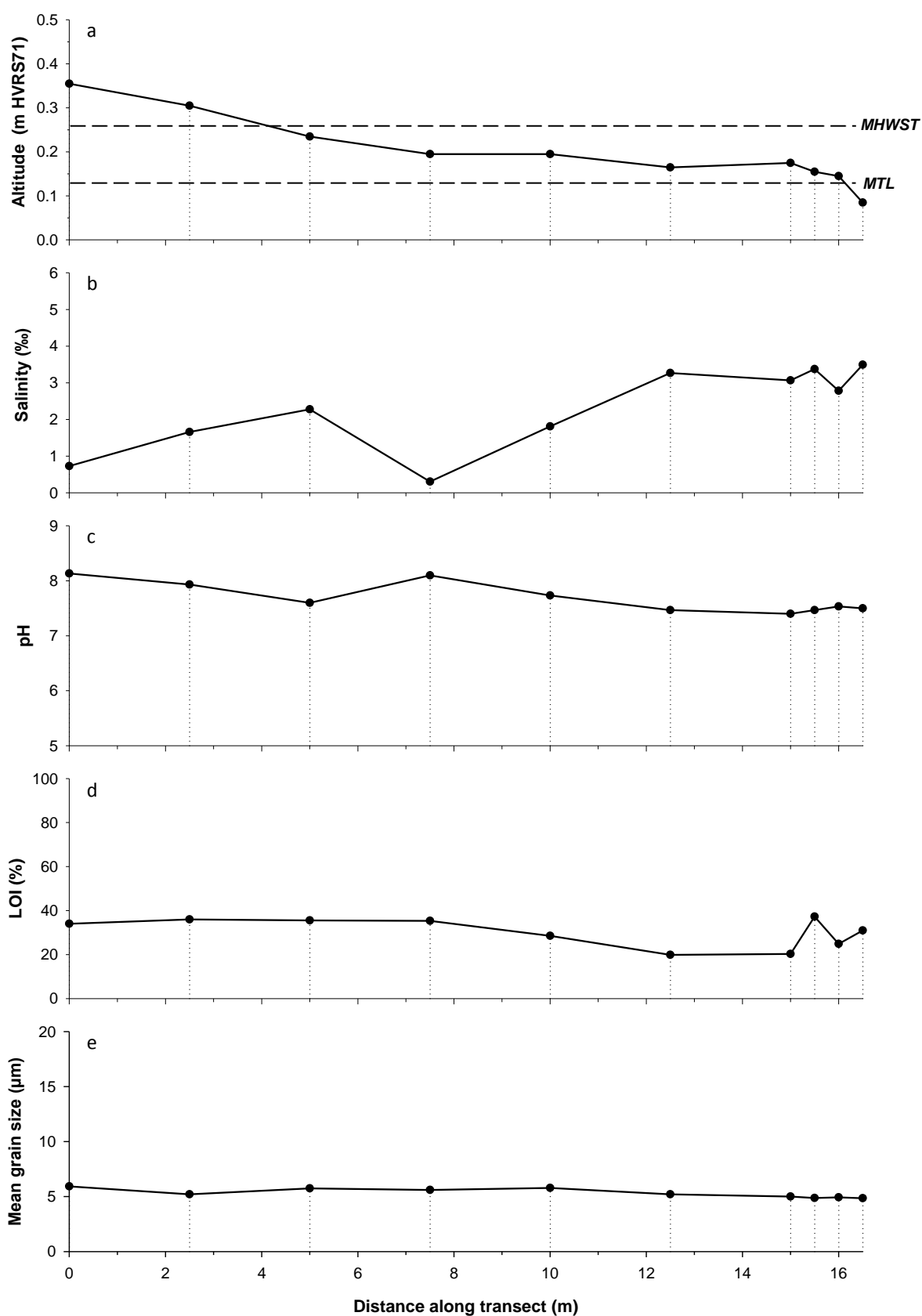


Figure 4.2. Measured environmental variables (altitude m HVR571, salinity, pH, LOI and mean grain size) across JD2 transect. Sampling locations and tidal levels (Split) also shown.

4.2.3. Blace Transect 1 (BL1)

A total of 15 sample stations were established across a 29.2 m transect at Blace incorporating all sub-environments from the high salt-marsh zone to the low salt-marsh/sea interface. Similar to JD2, a transitional profile to the lower salt-marsh limit is observed, covering an altitudinal range between 0.37 and -0.01 m HVRS71 (figure 4.3a).

Unlike at Jadrtovac, an overall increasing trend is not observed in salinity values at Blace. Salinity rises from 2.7‰ at station 1 to 5.9‰ at station 6 (3.5 m along the transect) before decreasing towards the seaward edge, dropping to 2.3‰ at sample station 13 (figure 4.3b). With a mean value of 7.3, pH levels are again relatively constant across the transect. The lowest reading occurs 5.5 m along the transect at sample station 7 (6.4) before rising to 7.9 in the lower salt-marsh environment at 29 m (figure 4.3c). A similar but more pronounced decreasing trend in organic content is observed at Blace in comparison to JD1. Figure 4.3d shows a clear distinction between upper and lower salt-marsh environments where LOI values in the upper 5 sample stations fall from >40% to <11% in the lower 4 stations. The upper 8 sample stations have a very similar substrate composition, with a mean grain size between 5-6 µm before rising to 25 µm 22.5 m along the transect at sample station 11 (figure 4.3e). This is again highlighted by the substrate composition graphs in figure 4.5c where a dominant silt fraction corresponds to an increase in coarser grained material towards the end of the transect.

The Blace data display a higher number of significant relationships between the environmental variables (table 4.3) when compared to the previous sites. However unlike at Jadrtovac, pH and salinity show no clear relationship with elevation. Distance and LOI show strong positive relationships with elevation, again confirming the descriptions above. Similar to JD1, silt and clay show a strong negative relationship with sand while silt and clay display a significant positive relationship with each other. The sediment size fractions also show a strong positive and negative correlation with organic matter across the transect.

Table 4.3. Pearson's correlation coefficients (*r*) for environmental variables at BL1.

	Elevation	pH	Salinity	LOI	Distance	Sand	Silt	Clay
Elevation	1							
pH	-0.37891	1						
Salinity	0.36522	-0.82856*	1					
LOI	0.84456*	-0.41003	0.34917	1				
Distance	0.90154*	-0.53109*	0.45616	0.95547*	1			
Sand	-0.8535*	0.52946*	0.39042	-0.84859*	-0.89481*	1		
Silt	0.82647*	-0.512	0.37301	0.78309*	0.82649*	-0.98494*	1	
Clay	0.82534*	-0.51342	0.38808	0.90143*	0.94896*	-0.93221*	0.85561*	1

*Bold denotes an *r* value with a significant correlation at the 0.05 level.

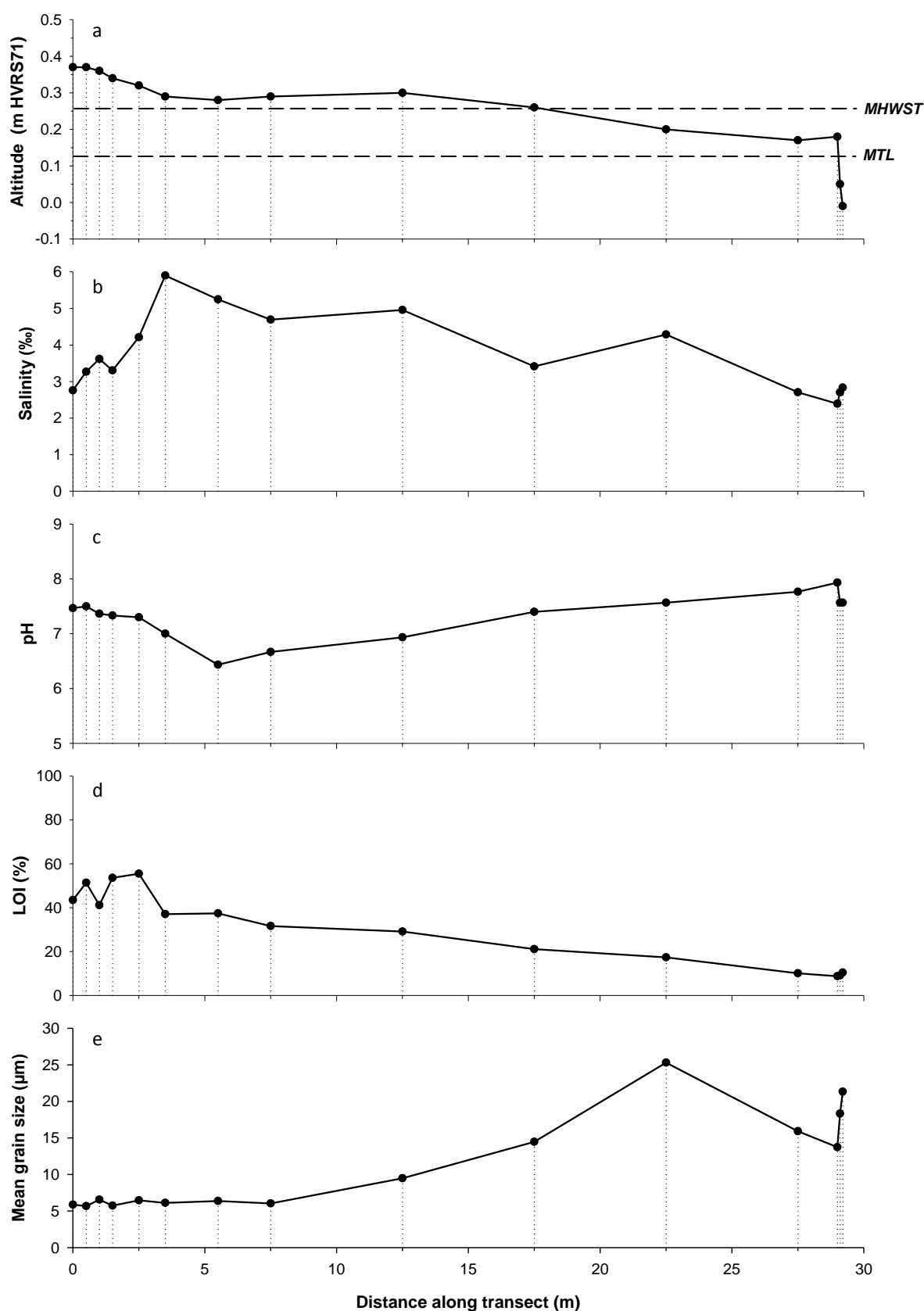


Figure 4.3. Measured environmental variables (altitude m HVR571, salinity, pH, LOI and mean grain size) across BL1 transect. Sampling locations and tidal levels (Split) also shown.

4.2.4. Blace Transect 2 (BL2)

An additional 9 surface samples were retrieved across a separate transect adjacent to transect 1 spanning 46 m from the upper salt-marsh environment towards the low tide shoreline (figure 4.4a). However, this transect proved substantially different to BL1 covering a larger altitudinal range between 0.4 m and -0.16 m HVRs71.

Unlike BL1, increasing trends in surface salinity values correspond to increases and decreases with distance and altitude. This is also highlighted by the significant negative and positive relationships observed in table 4.4. Relatively constant pH values are observed across the transect (figure 4.4c). With values ranging between 7.2 in the high salt-marsh zone (0.40 m HVRs71) to 8.0 at station 9 (-0.16 m HVRs71) pH is only correlated with distance showing a strong negative relationship. Unlike BL1, there is no clear divide between upper and lower salt-marsh environments based on the organic content which never exceed 20% (figure 4.4d). Thus the relationship between LOI with distance and elevation remains insignificant (table 4.4). The mean grain size graph for this transect shows a substantial increase in coarser grained material at sample station 6, 23 m along the transect (420 μ m) (figure 4.4e). Substrate composition results (figure 4.5d) show a clear dominant silt fraction in stations 1 to 5 before the increase at station 6 which is almost completely composed of sand. As a result of the above, significant negative correlations are observed between silt and clay with sand while silt and clay again display a strong positive relationship.

Overall there are less significant correlations between the tested environmental variables in comparison to BL1 (table 4.3). There is a strong relationship between elevation and distance but unlike BL1, a strong negative relationship exists between elevation and salinity. Distance shows a strong negative correlation with pH and salinity.

Table 4.4. Pearson's correlation coefficients (*r*) for environmental variables at BL2.

	Elevation	pH	Salinity	LOI	Distance	Sand	Silt	Clay
Elevation	1							
pH	-0.53143	1						
Salinity	-0.94662*	0.59315	1					
LOI	0.24178	0.05168	-0.25	1				
Distance	0.80734*	-0.81811*	-0.86628*	0.35329	1			
Sand	-0.53595	0.02791	0.58759	-0.51616	-0.44836	1		
Silt	0.51847	0.02409	-0.56434	0.50031	0.40705	-0.99822*	1	
Clay	0.60182	-0.37183	-0.68729*	0.57292	0.68139*	-0.91776*	0.89246*	1

*Bold denotes significant correlation at the 0.05 level.

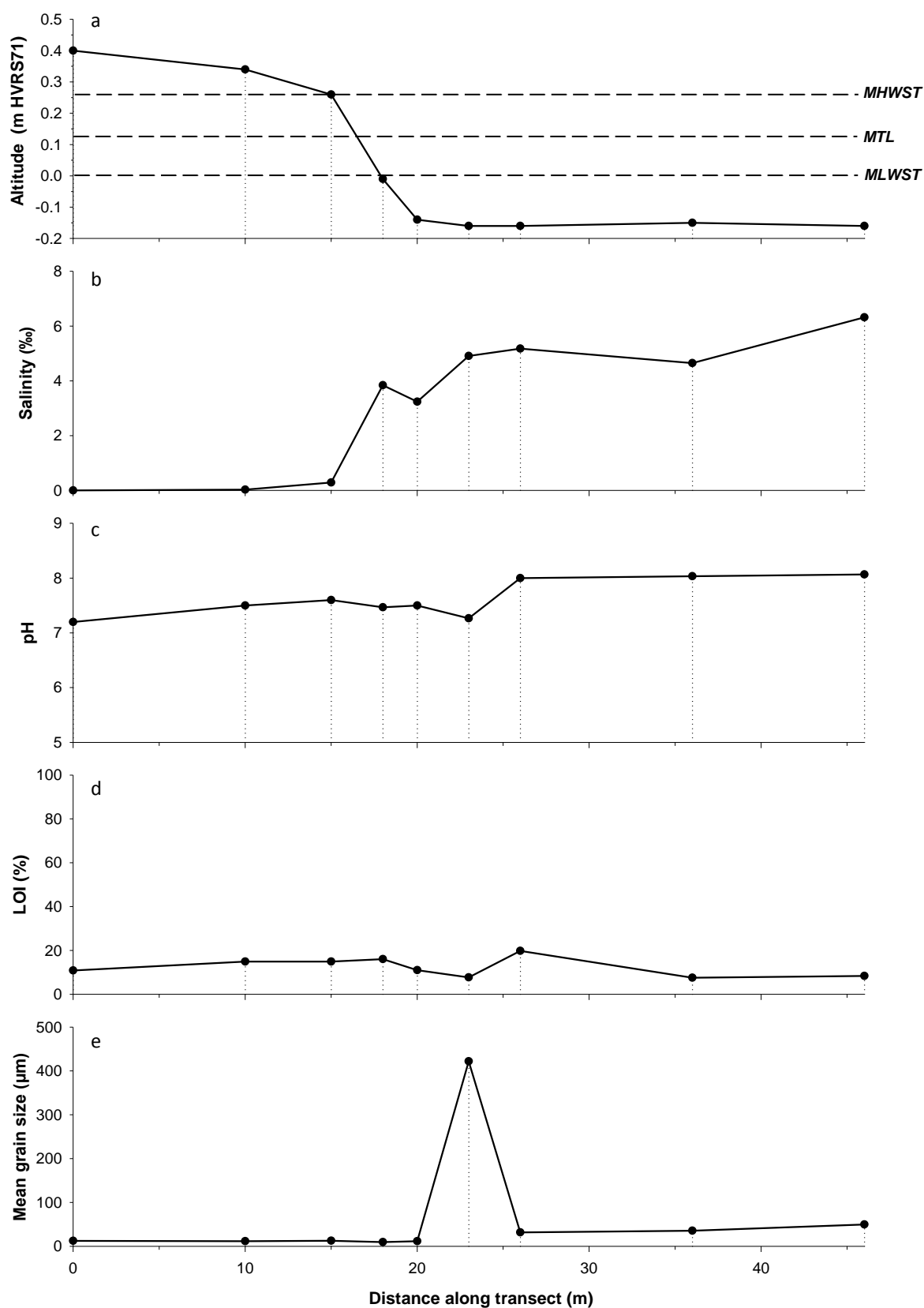


Figure 4.4. Measured environmental variables (altitude m HVR571, salinity, pH, LOI and mean grain size) across BL2 transect. Sampling locations and tidal levels (Split) also shown.

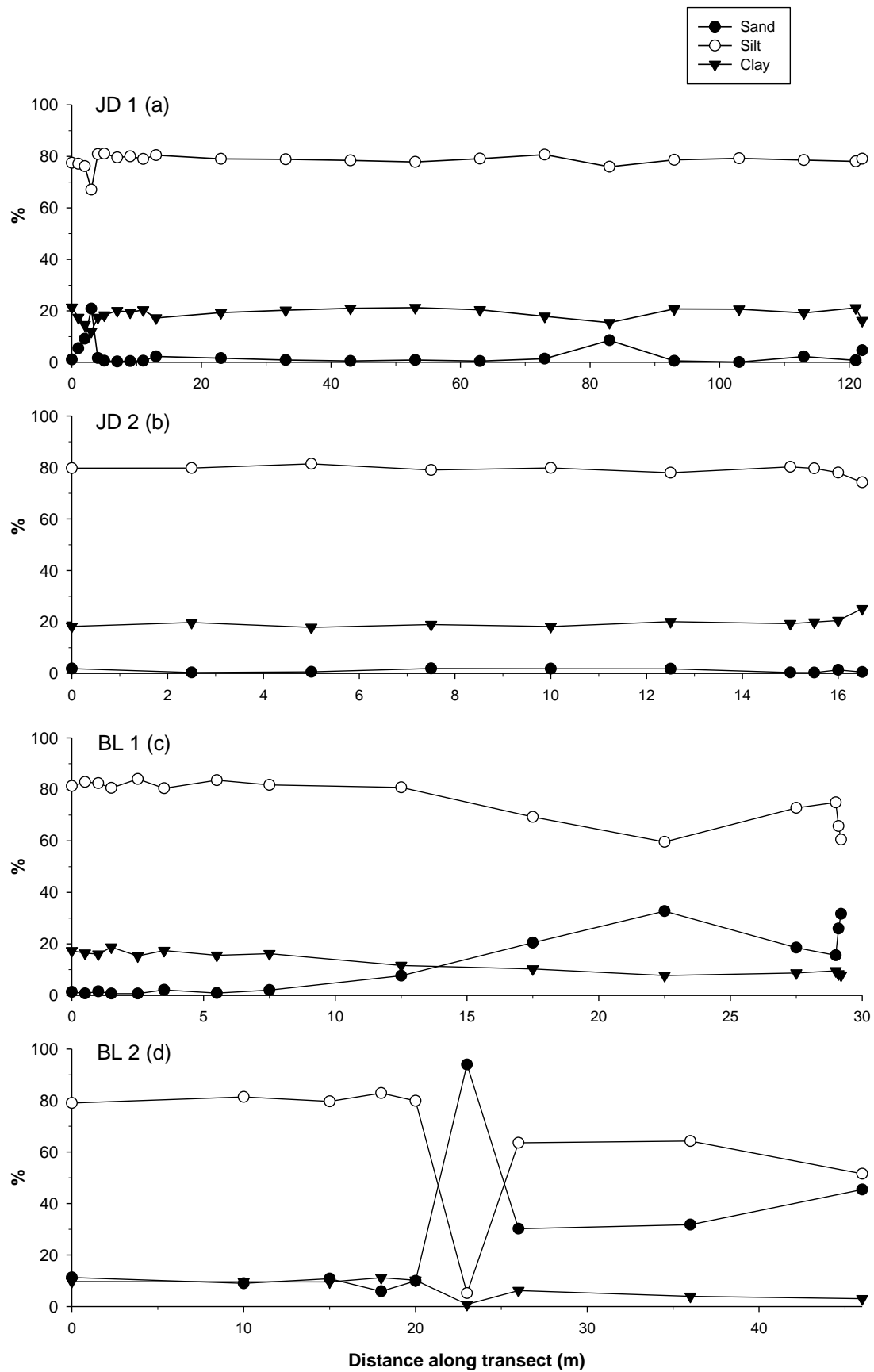


Figure 4.5. Substrate composition showing total sand, silt and clay percentage across transects (a) JD1, (b) JD2, (c) BL1 and (d) BL2. Sample locations also shown.

4.3. THE DISTRIBUTION OF CONTEMPORARY FORAMINIFERA

A total of 14 species of foraminifera in 70 surface samples were identified from the four transects and random sample collection. The concentration of dead foraminiferal tests was generally quite high at both Jadrtovac and Blace, varying between 0 and 12,954 per 5 cm³. Whilst species diversity remained reasonably low, over 49,100 dead individuals were counted in total, with the most dominant taxa remaining similar throughout the samples. These included relatively high abundances of agglutinated species *Jadammina macrescens*, *Miliammina fusca*, and *Trochammina inflata* and calcareous species *Ammonia* spp., *Elphidium* spp. and *Quinqueloculina* spp. In most instances *Trochammina inflata* was the most commonly observed species. The concentration of 'living' foraminifera at the time of collection was significantly lower than that observed for dead assemblages. A description of their distribution is provided while raw counts for both 'live' and 'dead' populations are provided in Appendix B. The relative abundance (%) of dead foraminiferal assemblages is presented in figures 4.6 - 4.10 and described below.

4.3.1. Jadrtovac Site 1 (JD1)

Dead foraminifera:

As described in section 4.2.1, 22 surface samples were collected over a 122 m transect with an elevation change of 0.44 m from high to low salt-marsh (figure 4.1). A total of 14 species were identified at this site; the most diverse of all studied transects. With a mean and maximum abundance of 2917 and 8820 individuals per 5 cm³ total concentration appears to increase at the end of the transect towards the low tide shoreline. The assemblages at this site are dominated by two agglutinated species, *Jadammina macrescens* and *Trochammina inflata*, and two calcareous species, *Ammonia* spp. and *Quinqueloculina* spp. (figure 4.6).

Sample station 1, at an altitude of 0.485 m contained no foraminifera while sample station 2 (0.44 m) contained fewer than 10 individuals. From station 3, 2 m along the transect, *J. macrescens* and *T. inflata* are present in every sample covering all of the sampled altitudinal range. The occurrence of *Elphidium* spp. in samples 3 (12%) and 4 (33%) at 2 and 3 m, respectively, is perhaps unusual, but also corresponds to a decrease in the relative abundance of *J. macrescens*. Likewise the appearance of calcareous taxa *Ammonia* spp. (29%) and *Quinqueloculina* spp. (25%) 13 m along at sample station 10 corresponds to a decrease in the relative abundance of the two dominant agglutinated species and also a fall in altitude below MSL (figure 4.1). *T. inflata* dominates from 2 to 11 m along the transect, between stations 3 and 9, exceeding 73% of the total count at station 9. Its relative

abundance then rapidly decreases a further 2 m along at sample station 10 to 7% and remains relatively low moving across the transect where *J. macrescens* becomes increasingly common, peaking at station 14 to 78% of the total count 53 m along. Whilst relatively low counts of *Miliammina fusca* were observed, its presence is limited to the upper 23 m of the salt-marsh transect, reaching 14% of the total count in station 6 at an altitude of 0.185 m. The reappearance of calcareous taxa (principally *Quinqueloculina* spp. and *Ammonia* spp.) at sample stations 16 and 17 coincides with a significant decrease in the relative abundance of *J. macrescens* 83 m along the transect. However, their presence is interrupted between stations 18 and 19 where an increase in *T. inflata* is observed, peaking at 75% of the total count 103 m along the transect. Calcareous taxa then reappear at station 20 where the highest abundance of *Quinqueloculina* spp. throughout the transect is observed (46%).

Living foraminifera:

The contemporary distribution of living foraminiferal assemblages at JD1 was significantly lower than those observed for the dead fraction as described above. A minimum count of 150 tests was achieved in only two samples at 113 m (sample station 20) and 122 m (sample station 22) along the transect and only nine sample stations contained foraminiferal taxa totalling 50 or more. The upper two samples (station 1 and 2) contained no foraminifera. Stations 3 and 4 contained just 9 and 28 live specimens compared to 748 and 931 specimens observed in the dead foraminiferal population. Species diversity was severely restricted in the living assemblage with *J. macrescens*, *T. inflata* and *Quinqueloculina* spp. being relatively common with very minor occurrences of other foraminiferal taxa (e.g. *M. fusca* and *Spirillina vivipara*). Raw counts of both live and dead foraminiferal assemblages for JD1 are provided in table A1.

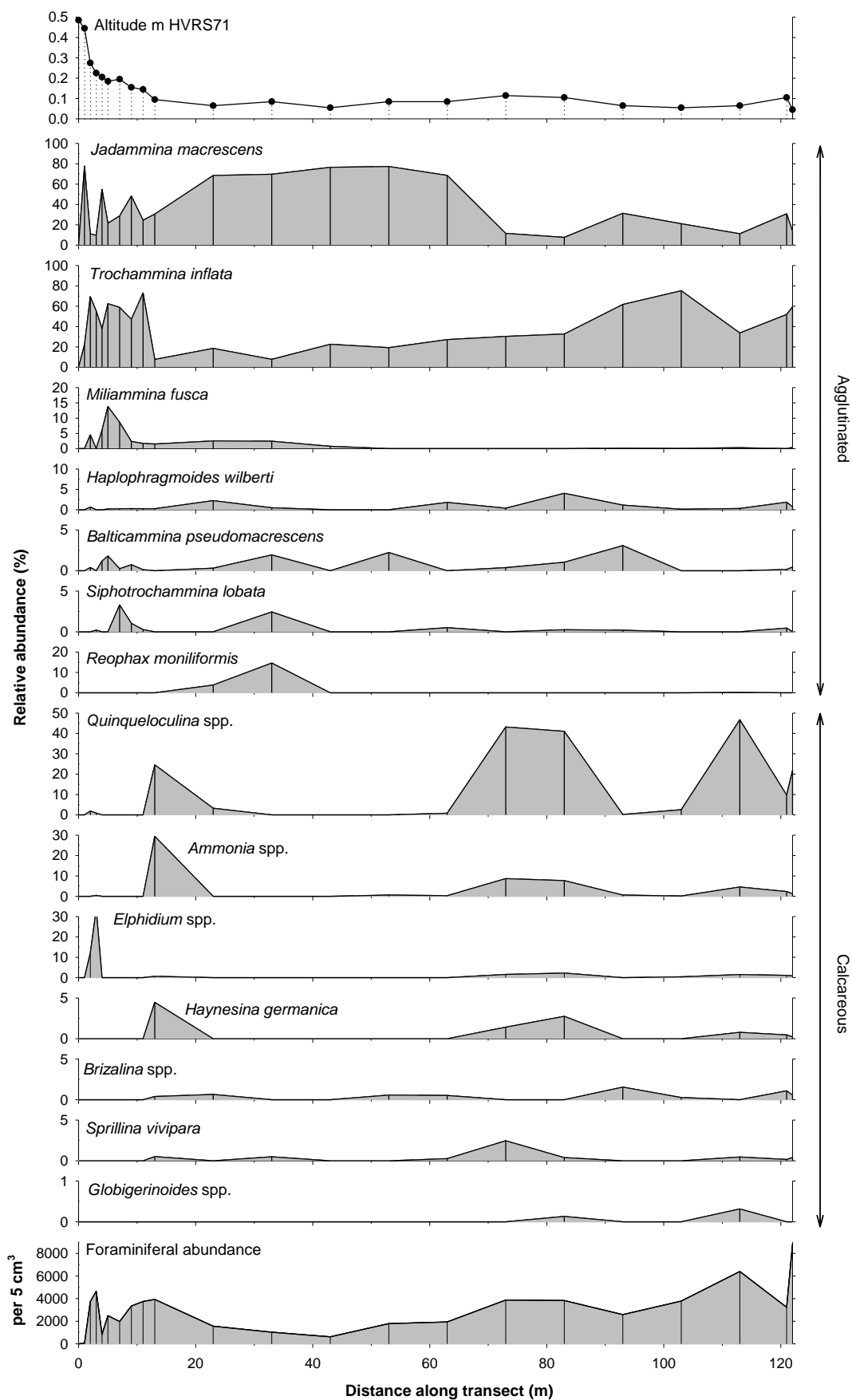


Figure 4.6. Relative abundance (%) of 'dead' foraminifera and concentration (per 5 cm³) across JD1 transect. Altitude (m HVR71) also shown.

4.3.2. Jadrtovac Site 2 (JD2)

Dead foraminifera:

Ten surface samples were collected over a small transect covering an altitudinal range of 0.53 m over 16.5 m from the high salt-marsh zone to the seaward edge (figure 4.2). Overall, species abundance was higher than at JD1, with mean and maximum concentrations of 4489 and 7850 individuals per 5 cm³, respectively. The lowest observed concentration occurred in the uppermost samples at stations 1 and 2 at altitudes of 0.355 m and 0.305 m, above the altitude of HAT. A total of 12 species were identified at this site and are dominated by three agglutinated (*J. macrescens*, *T. inflata* and *M. fusca*) and three calcareous taxa (*Ammonia* spp., *Elphidium* spp. and *Quinqueloculina* spp.), as shown in figure 4.7.

Similar to JD1, *J. macrescens* and *T. inflata* are found in abundance across the transect and span the entire sampled altitudinal range of this salt-marsh. *J. macrescens* dominates the upper two samples (82% and 69%), up to 2.5 m along, before decreasing to 14% of the total count at 5 m. This decrease corresponds to a relative increase of *T. inflata*, peaking at 59%. A similar trend to JD1 in the distribution of *Elphidium* spp. can be seen where a peak of 19% is observed at sample station 3, within a broadly similar altitude range (c. 0.20 – 0.30 m HVR571). The presence of *M. fusca* is focused in the middle section of the transect, increasing to 45% of the total count at sample station 5, 10 m across the transect. Again its altitudinal range is comparable to the same species at JD1 and appears confined to a narrow altitude window (0.185 – 0.205 m HVR571). Moving towards the seaward edge of the transect, an increase in the relative abundance of calcareous taxa is observed where *Quinqueloculina* spp. increases to a peak of 38% of the total count 15.5 m across.

Living foraminifera:

Similar to the contemporary environment at JD1, living foraminiferal assemblages occur in much lower numbers in comparison to the dead fraction described above. A minimum of 150 observations was achieved in only one sample at station 8, 15.5 m along the transect, with 172 foraminiferal tests present. Sample station 3 contained just 7 living specimens (at the time of collection) in comparison to 1570 observations made for the dead assemblages. The most common species observed in the living assemblage repeated that observed at JD1 with *J. macrescens*, *T. inflata* and *Quinqueloculina* spp. occurring in relative abundance with insignificant numbers for other foraminiferal taxa. Raw counts of both live and dead foraminiferal assemblages for JD2 are provided in table A2.

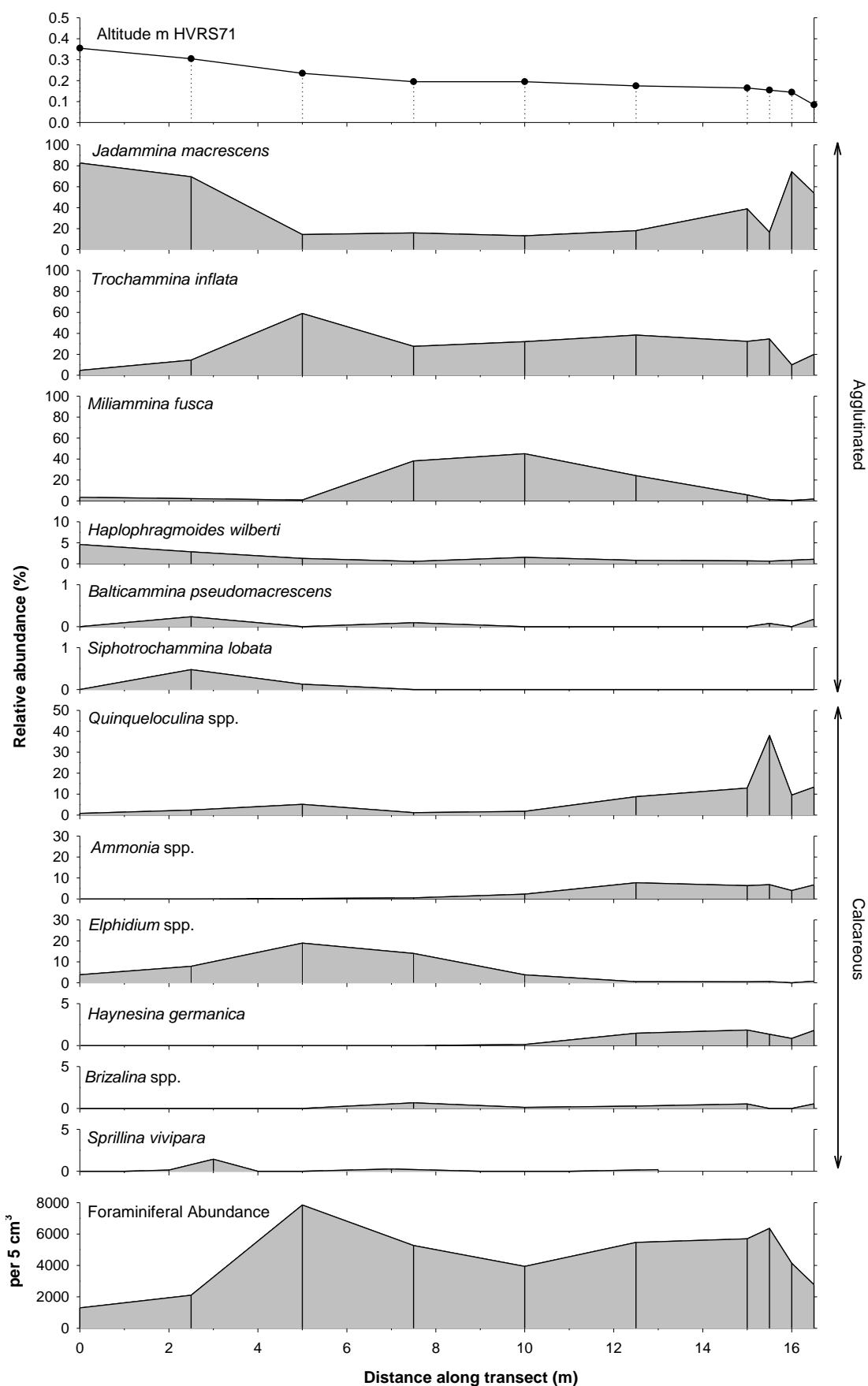


Figure 4.7. Relative abundance (%) of 'dead' foraminifera and concentration (per 5 cm³) across JD2 transect. Altitude (m HVR571) also shown.

4.3.3. Jadrtovac Random Sampling (JDR)

Dead foraminifera:

Ten additional surface stations were established at Jadrtovac site 1 covering an altitudinal range of 0.20 m following a random sampling approach. As these were not collected across a transect, they are presented below in the form of a species diagram ordered from high (1) to low (10) elevation (figure 4.8). For clarity the original sample number is also displayed and is referred to in the text. A total of 11 species were identified throughout the samples and are comparable to those observed across transect JD1 (see section 4.3.1). Species abundance, which shows an overall decreasing trend according to altitude from high to low, was generally very high, with as much as 12,945 specimens observed per 5 cm³ in sample 9 (0.185 m HVR571).

Agglutinated species are again found throughout the entire altitudinal range of the studied samples. Sample stations 10, 9, 2 and 3, found between altitudes 0.275 and 0.165 m, are characterised by an agglutinated-dominated assemblage, principally *J. macrescens* and *T. inflata* and minor occurrences of *M. fusca*. The increase in the relative abundance of calcareous taxa at stations 6, 7 and 5 occurs within a narrow altitude window between 0.115 and 0.095 m, and indeed the peak observed in *Quinqueloculina* spp. at station 5 to 47% of the total count is of a comparable altitude range (0.095 – 0.115 m) to peaks observed in samples taken across the transect at this site (JD1).

Living foraminifera:

Similar to transects 1 and 2 at Jadrtovac, living foraminiferal populations were severely restricted from a random sampling approach compared to dead foraminiferal populations. A minimum count of 150 was achieved in only 1 sample at station 5. Sample 10 contained no living specimens at the time of collection. Species diversity in the living population was again very limited with agglutinated taxa *J. macrescens* and *T. inflata* the most commonly observed species together with calcareous taxa and *Quinqueloculina* spp. and *Ammonia* spp. Raw counts of both live and dead foraminiferal assemblages for JDR are provided in table A3.

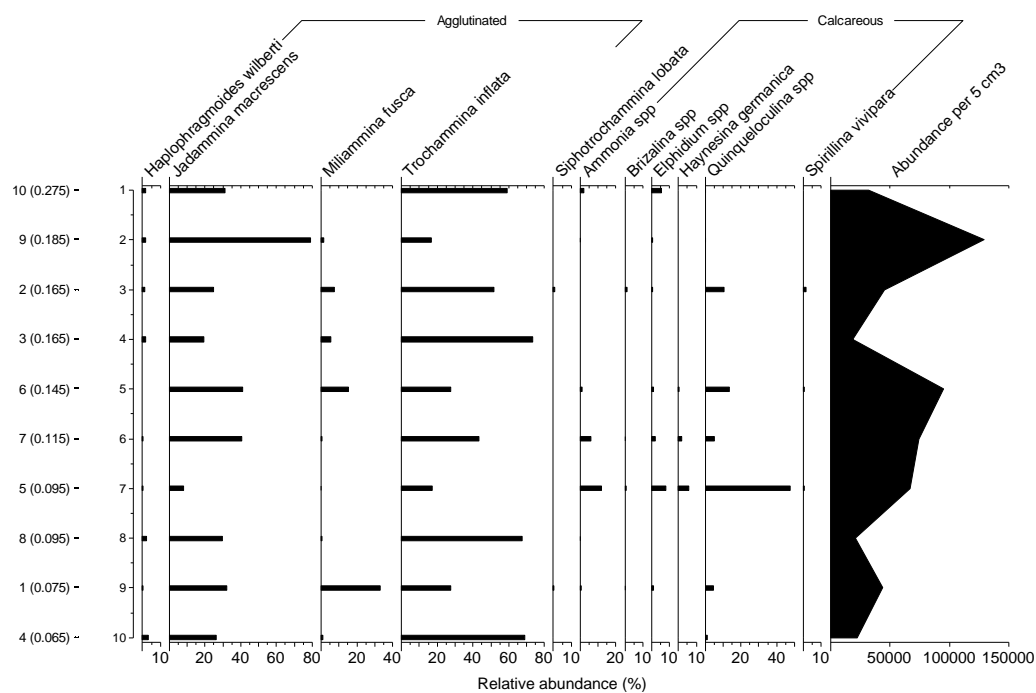


Figure 4.8. Relative abundance (%) of 'dead' foraminifera and concentration (per 5 cm³) from JDR ordered by elevation from high (1) to low (10). Original sample number also shown including altitude (m HVR571).

4.3.4. Blace Transect 1 (BL1)

Dead foraminifera:

Fifteen surface samples were collected along a transect spanning 29.2 m, with an elevation change of 0.35 m from the high salt-marsh to the seaward edge (figure 4.3). A total of 11 species were identified and are dominated by the agglutinated species *J. macrescens*, *T. inflata* and *M. fusca* and calcareous species *Quinqueloculina* spp., *Ammonia* spp., *Elphidium* spp., and *Haynesina germanica* (figure 4.9). Whilst species abundance remains high at this site, with a maximum concentration of 8210 individuals per 5 cm³ occurring at sample station 11, in contrast to JD1, foraminiferal abundance decreases in the lowermost samples (<1000 per 5 cm³).

With the exception of the occurrence of *Quinqueloculina* spp. in the upper 3 samples (up to 43% at 0 m), there appears to be a clear divide between the foraminiferal assemblages, where the transition to low salt-marsh corresponds with an increase in the relative abundance of calcareous taxa and reduction of agglutinated types. *J. macrescens* increases to a peak of 65% of the total count, 2.5 m along the transect, before gradually decreasing whilst the relative abundance of *T. inflata* increases to 66% (12.5 m across). Their dominance is then replaced by a more diverse calcareous assemblage where increases *Ammonia* spp., *Elphidium* spp., *Quinqueloculina* spp. and *Spirillina vivipara* are observed. The maximum occurrence of *Quinqueloculina* spp. occurs 22.5 m along the transect, peaking to 68% of the overall count at sample station 11. Whilst found in low abundance again, *M. fusca* appears confined to the upper reaches of the salt-marsh environment, peaking to 13% of the total count 3.5 m along the transect at an altitude of 0.29 m. The lowermost sample stations are characterised by an increase in calcareous species with *Ammonia* spp., rising to 66% of the total count at sample station 14 (29.1 m along the transect).

Living foraminifera:

A similar observation to the studied transects at Jadrtovac (section 4.3.1 and 4.3.2) is witnessed at BL1 where living foraminiferal populations are significantly smaller in comparison to dead assemblages. Across transect BL1 all analysed samples contained fewer than 100 living individuals. At station 1, 1478 specimens were observed in the dead fraction in comparison to just 31 living examples. Species diversity is similarly restricted with the main foraminifera species observed again comprising *J. macrescens*, *T. inflata* and *Quinqueloculina* spp. Raw counts of both live and dead foraminiferal assemblages for BL1 are provided in table A4.

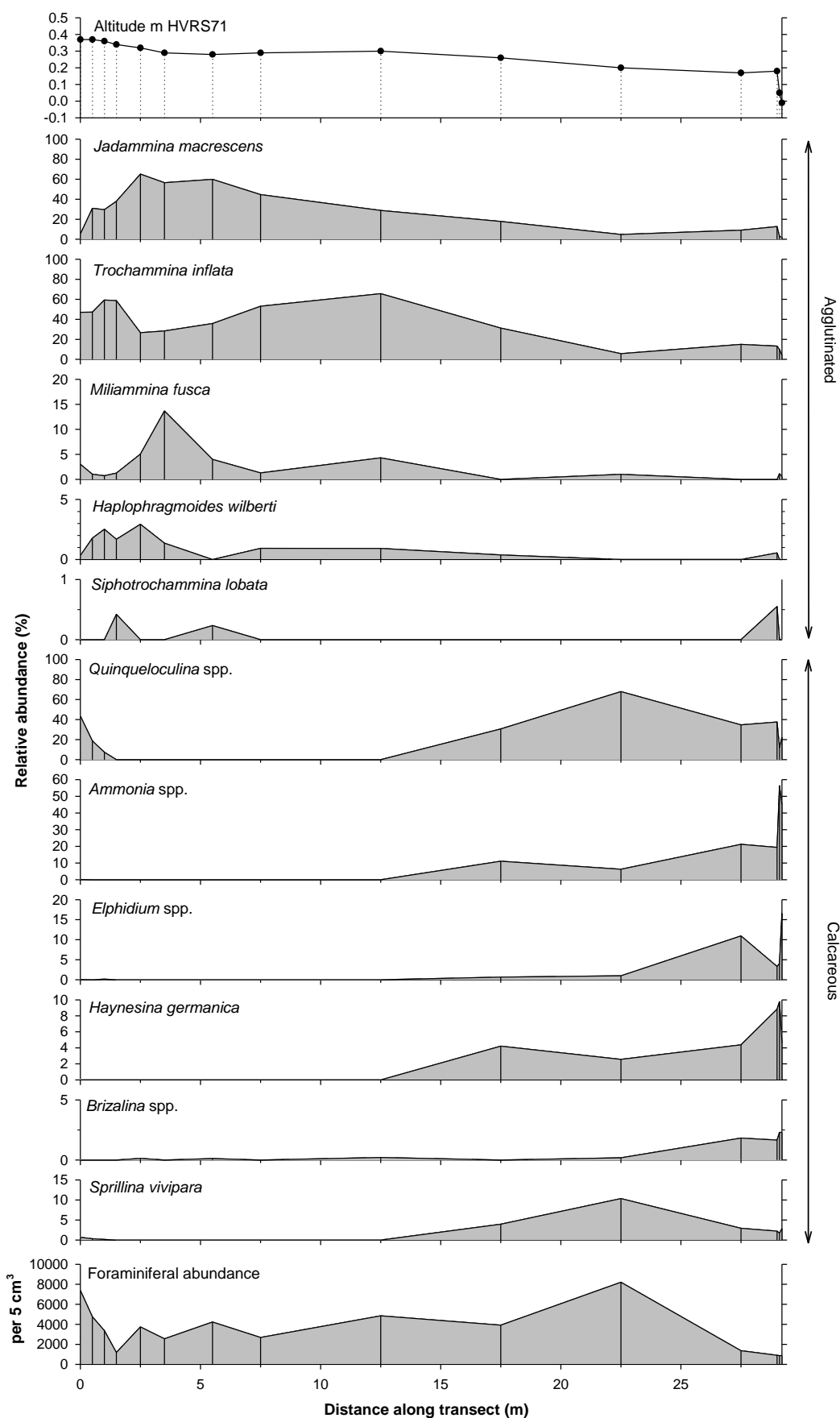


Figure 4.9. Relative abundance (%) of 'dead' foraminifera and concentration (per 5 cm³) across BL1 transect. Altitude (m HVR571) also shown.

4.3.5. Blace Transect 2 (BL2)

Dead foraminifera:

Nine surface samples were collected across a 46 m transect covering an altitudinal range of 0.56 m (figure 4.4). Ten foraminiferal species were identified and show the same species dominating the assemblage as BL1, with a similarly good divide between the dominant agglutinated and calcareous taxa (figure 4.10). Total foraminiferal abundance across transect 2 shows a substantial reduction in samples near the seaward edge. Maximum abundance occurs at sample station 5 (26 m along), where up to 4630 individuals are observed per 5 cm³. Abundance decreased towards the sea-ward edge and sample station 9 was devoid of foraminifera altogether. Again there was a substantial change in the substrate composition when analysing samples towards the sea-ward edge of the transect as highlighted in the grain size data in figure 4.5d.

Similar to BL1, *Quinqueloculina* spp. constitutes 45% of the total count at station 1. Its abundance then gradually decreases to station 7 (3% of the total count), 31 m across the transect. *J. macrescens* increases to station 3, totalling 60% of the overall count before decreasing to just 5% at 28 m in sample 6. As the agglutinated species diminish, calcareous species *Ammonia* spp. and *Elphidium* spp. increase in relative abundance. The maximum occurrence of *Ammonia* spp. occurs at station 7 (31 m), reaching 71% of the total count.

Living foraminifera:

Only sample station 1 contained a foraminiferal population of 150 or more, with 167 tests observed. Similar to the dead foraminiferal populations, stations 7, 8, 9 and 10 contained almost no living specimens. Overall, living foraminiferal assemblages mirrored that of the dead fraction, albeit in much lower concentrations. The most common species observed included *J. macrescens*, *T. inflata* and *Quinqueloculina* spp. Raw counts of both live and dead foraminiferal assemblages for BL2 are provided in table A5.

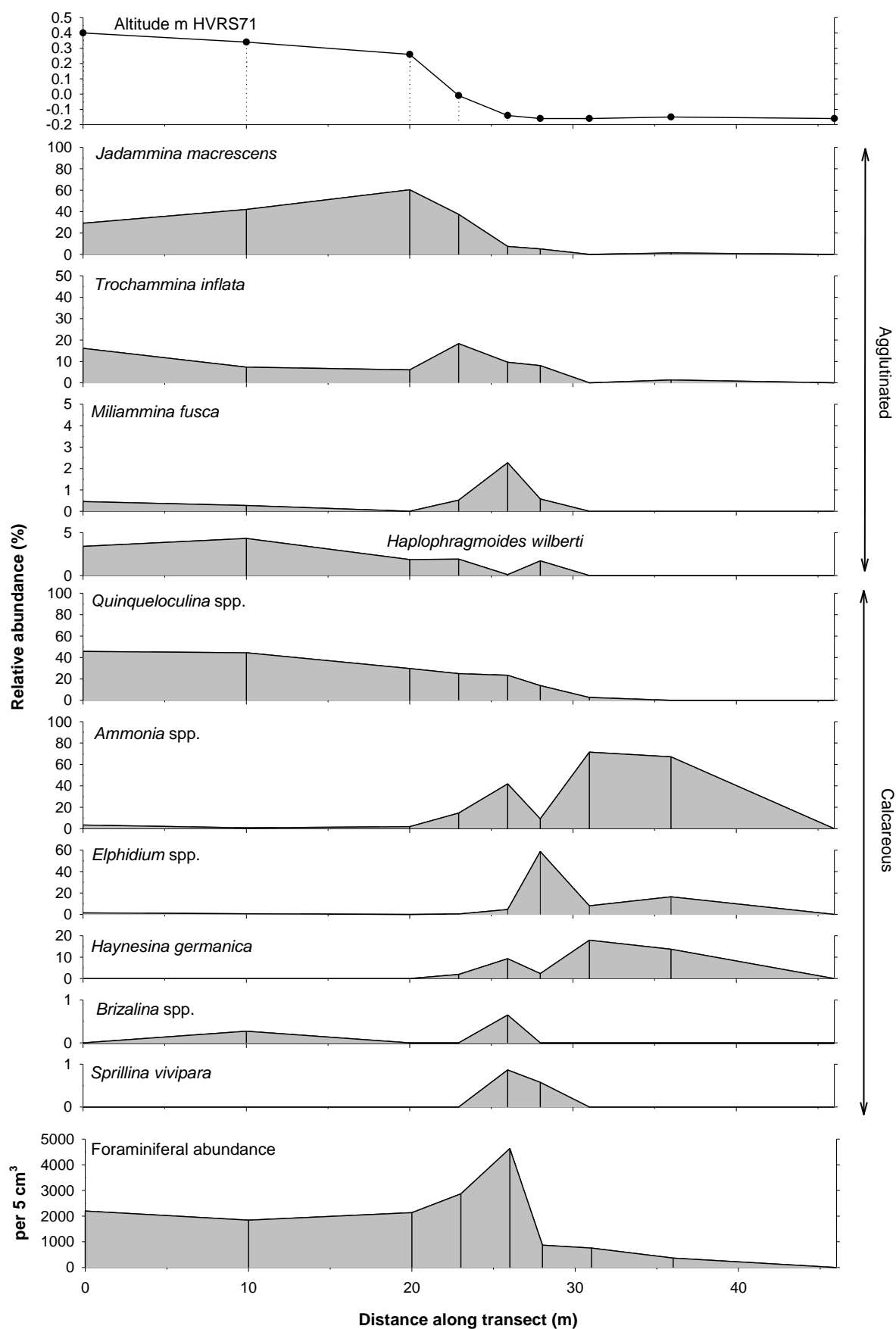


Figure 4.10. Relative abundance (%) of 'dead' foraminifera and concentration (per 5 cm³) across BL2 transect. Altitude (m HVR571) also shown.

4.4. THE VERTICAL DISTRIBUTION OF CONTEMPORARY SALT-MARSH FORAMINIFERA

From the qualitative descriptions made above, there appears to be a notable elevation-dependent zonation in which characteristic foraminiferal species are observed. To explore this relationship in more detail, the following section applies a statistical approach in order to quantify faunal zones and their associated elevational constraints before exploring how the contemporary surface distributions are influenced by the tested environmental variables in section 4.5. The analyses were applied to the 'dead' foraminiferal assemblages only due to the limited and sporadic nature of living populations across the studied salt-marsh environments. The data are first analysed individually (e.g. JD1) before collectively (e.g. JD1 and JD2) to create local training sets for each site (JDT and BLT).

Prior to the statistical analyses the data were screened, first to remove species groups which did not contribute more than 2% of the total species abundance (following Horton et al., 2003; Edwards et al., 2004) and second to exclude those samples which did not exceed the 150 minimum count required to be included in the dataset. An exception was made, however, for sample 13 at JD1 and sample 8 at BL2, where the assemblage is dominated by indicator species totalling 50% or more of the total count, according to Patterson and Fishbein (1989) and Fatela and Taborda (2002). Following these criteria, a number of insignificant species were removed and samples 1 and 2 from JD1 and samples 9 and 10 from BL2 were excluded from the subsequent analysis. Specific details regarding samples and species excluded are provided for each site as described below. For reference, out of a total seventy analysed surface samples (table 4.5), only five stations returned statistically sufficient counts (i.e. 150 or more) from living foraminiferal assemblages.

An additional three surface samples were included in the dataset for BL1. These samples were collected from very similar location and altitudes to samples 1 to 4 from BL1. For clarity these are referred to as samples 16, 17 and 18. The relative abundance of 'dead' foraminifera for these samples is provided in Appendix B. A summary of the contemporary foraminiferal (dead) assemblages for each sample site is provided in table 4.5 with the modern training set for this study totalling 66 samples.

Table 4.5. Summary table of contemporary surface samples used in the modern training set.

Name	Samples Analysed	Samples Removed	Total
JD1	22	2	20
JD2	10	-	10
JDR	10	-	10
BL1	15 + (3)	-	18
BL2	10	2	8
	70	4	66

4.4.1. Jadrtovac Site 1 (JD1)

An initial dataset containing 22 samples was reduced to twenty following the removal of samples 1 and 2 on insufficient counts. Similarly species diversity was significantly reduced once taxa contributing less than 2% of the overall assemblage were removed. Foraminiferal taxa removed included agglutinated species *Haplophragmoides wilberti*, *Balticammina pseudomacrescens* and *Siphrochammina lobata* and calcareous species *Haynesina germanica*, *Brizalina* spp. and *Spirillina vivipara*. Unconstrained cluster analysis based on unweighted Euclidean distance was used to identify three faunal zones (clusters) at JD1 which are confirmed by through DCA results as shown in figure 4.11.

Zone JD1-A is characterised by an exclusively agglutinated-dominated assemblage with high abundances of *J. macrescens* (up to 77% in sample 14), *T. inflata* (up to 47%) and minor occurrences of *M. fusca* (figure 4.11a). Inspection of the DCA biplot confirms the strong relationship between this group of samples (figure 4.11b), which differs from the other zones through the relatively high abundances of *J. macrescens*, which exceeds 48% in all samples. The altitudinal range of this zone extends from below MTL at 0.085 m to 0.205 m, with a vertical range of 0.12 m (figure 4.11c). A clear decrease in the relative abundance of *J. macrescens* and increase in *T. inflata* (up to 78%) characterises zone JD1-B while the occurrence of calcareous taxa, *Elphidium* spp. and *Quinqueloculina* spp., and peaks of *M. fusca* are also observed. Again DCA shows the strong relationship between this group of samples as well as highlighting samples 3 and 4 as potential outliers in this faunal zone due to the occurrence of *Elphidium* spp. at high elevations. As a result the vertical range of this zone extends the whole of the sampled marsh environment between altitudes 0.045 m and 0.275 m. Zone JD1-C, comprising four samples, is characterised by a clear increase in calcareous taxa (*Ammonia* spp. and *Quinqueloculina* spp.) and occupies altitudes below MTL between 0.065 m and 0.115 m with a narrow vertical range of 0.05 m.

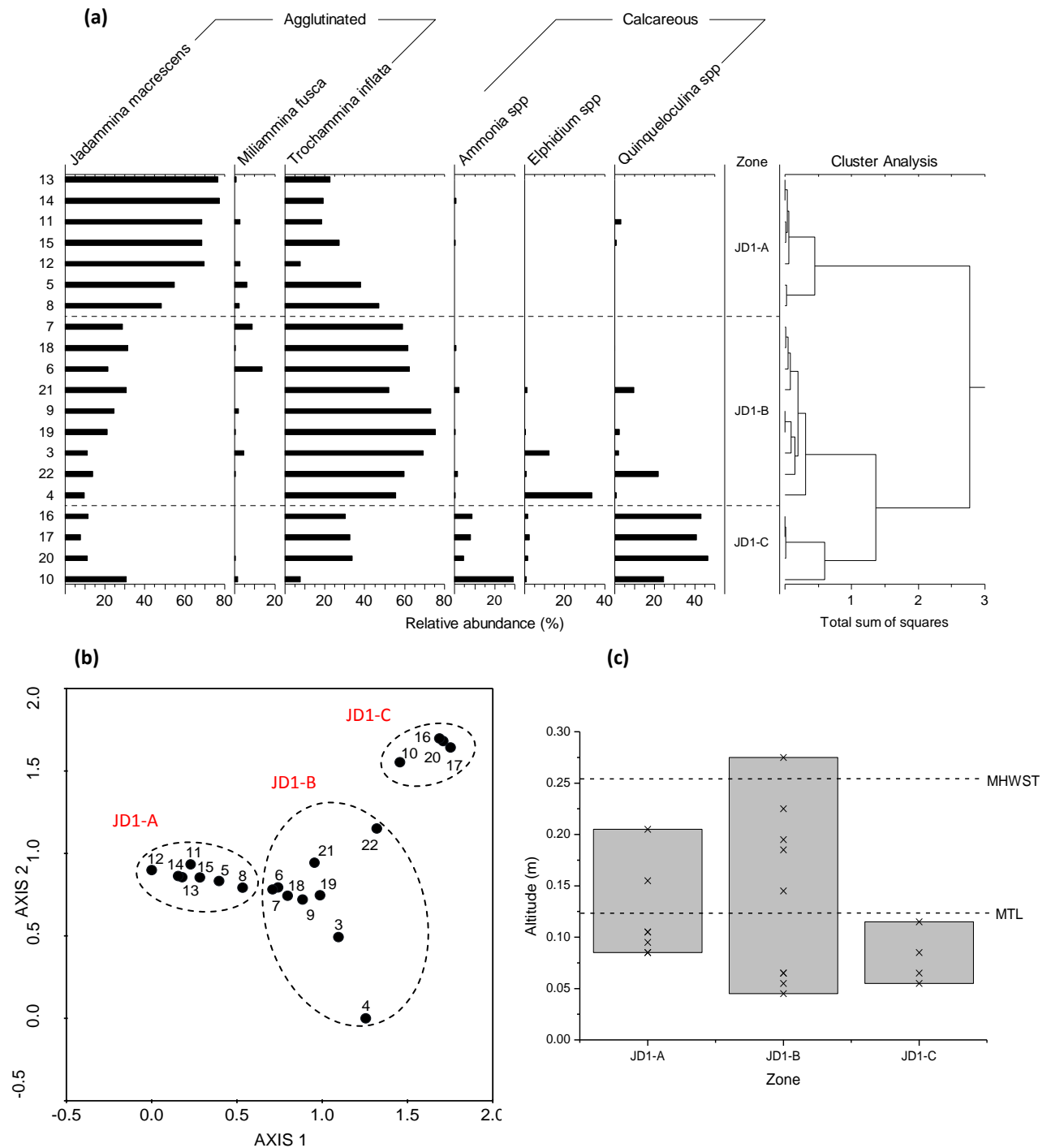


Figure 4.11. (a) Unconstrained cluster analysis based on unweighted Euclidean distance identifying faunal zones, (b) detrended correspondence analysis displaying faunal zones, and (c) altitude of faunal zones (m HVR571) based on relative percentages of 'dead' assemblages from JD1 with tidal levels superimposed.

4.4.2. Jadrtovac Site 2 (JD2)

No samples were removed from in the dataset screening for JD2. However, insignificant species including *B. pseudomacrescens*, *S. lobata* and calcareous taxa *Haynesina germanica*, *Brizalina* spp. and *Spirillina vivpara* were removed from the following quantitative analyses. Similar to JD1, multivariate statistical analyses were used to indentify three faunal zones at JD2 as shown in figure 4.12.

The first faunal zone, JD2-A, comprises 3 samples and is again characterised by an assemblage dominated by *J. macrescens* (>69%) and *T. inflata* with minor occurrences of calcareous taxa (figure 4.12a). DCA confirms the strong relationship between this group of samples (figure 4.12b) which occupy an altitudinal range stretching above MHWST between 0.145 m to 0.355 m (range 0.21 m) (figure 4.12c). Zone JD2-B shows a reduction in *J. macrescens* (<19%) with increases in the relative abundance of *M. fusca* (up to 45%) and *T. inflata* (up to 38%) and slight increases in calcareous taxa. The similarity between the assemblages is confirmed through DCA which are found within a very narrow altitudinal window between of 0.175 m and 0.195 m, above MTL. Zone JD2-C incorporates four samples, showing an increase in the relative abundance of calcareous taxa (principally *Quinqueloculina* spp.) similar to that observed at JD1. While DCA shows a strong relationship between some of the samples in this zone, it shows sample station 3 as being distinct due to the high occurrence of *T. inflata* at this station (59%). Indeed the inclusion of this sample in this zone creates an altitudinal overlap between the three zones, stretching from below MTL at 0.085 m to just below MHWST at 0.235 m.

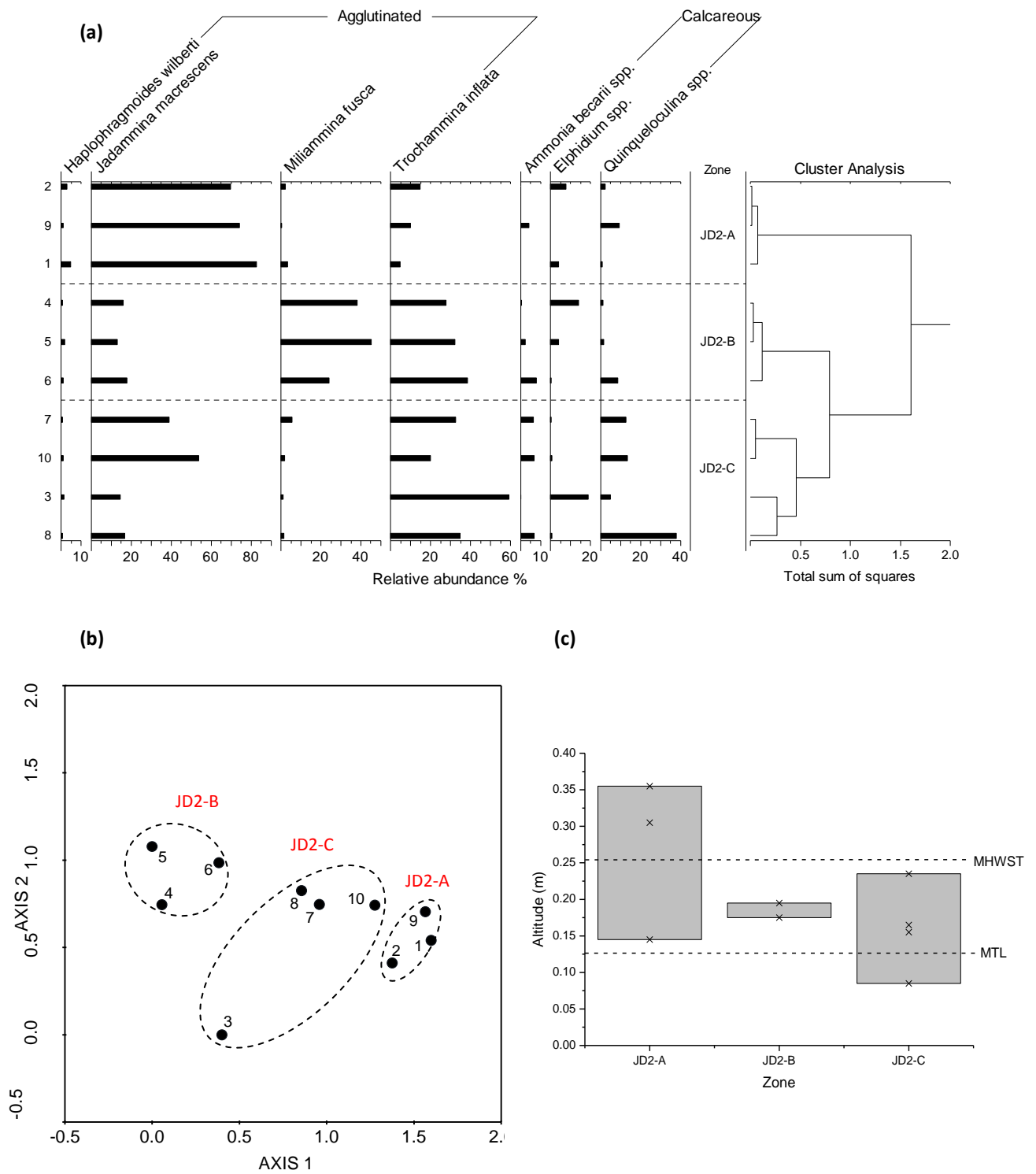


Figure 4.12. (a) Unconstrained cluster analysis based on unweighted Euclidean distance identifying faunal zones, (b) detrended correspondence analysis displaying faunal zones, and (c) altitude of faunal zones (m HVR571) based on relative percentages of 'dead' assemblage from JD2 with tidal levels superimposed.

4.4.3. Jadrtovac Random Sampling (JDR)

Similar to the transect datasets, unconstrained cluster analysis was used to identify three faunal zones from the random sampling collection at Jadrtovac (figure 4.13). No samples were removed during the data screening. However, insignificant counts of *S. lobata*, *Brizalina* spp. and *Spirillina vivipara* were excluded. Overall inspection shows the vertical zonation of foraminiferal assemblages appears weaker in comparison to foraminiferal assemblages taken along transects at Jadrtovac.

Faunal zone JDR-A is characterised by very high abundances of *T. inflata* (up to 73%) accompanied by *J. macrescens* (<45%) (figure 4.13a) and covers a large altitudinal range of 0.21 m between 0.065 m and 0.275 m above and below MTL (figure 4.13c). DCA confirms the strong relationship between this group of samples (figure 4.13b). An increase in the relative abundances of *J. macrescens*, *M. fusca* and *Quinqueloculina* spp. characterise zone JDR-C. Inspection of DCA results confirms this but suggests sample 5 to have a weaker relationship with the assemblages found in samples 1, 6 and 9 due to the significant increase in *Quinqueloculina* spp. at this sample station. Zone JDR-C has an altitudinal range between 0.075 m and 0.185 m.

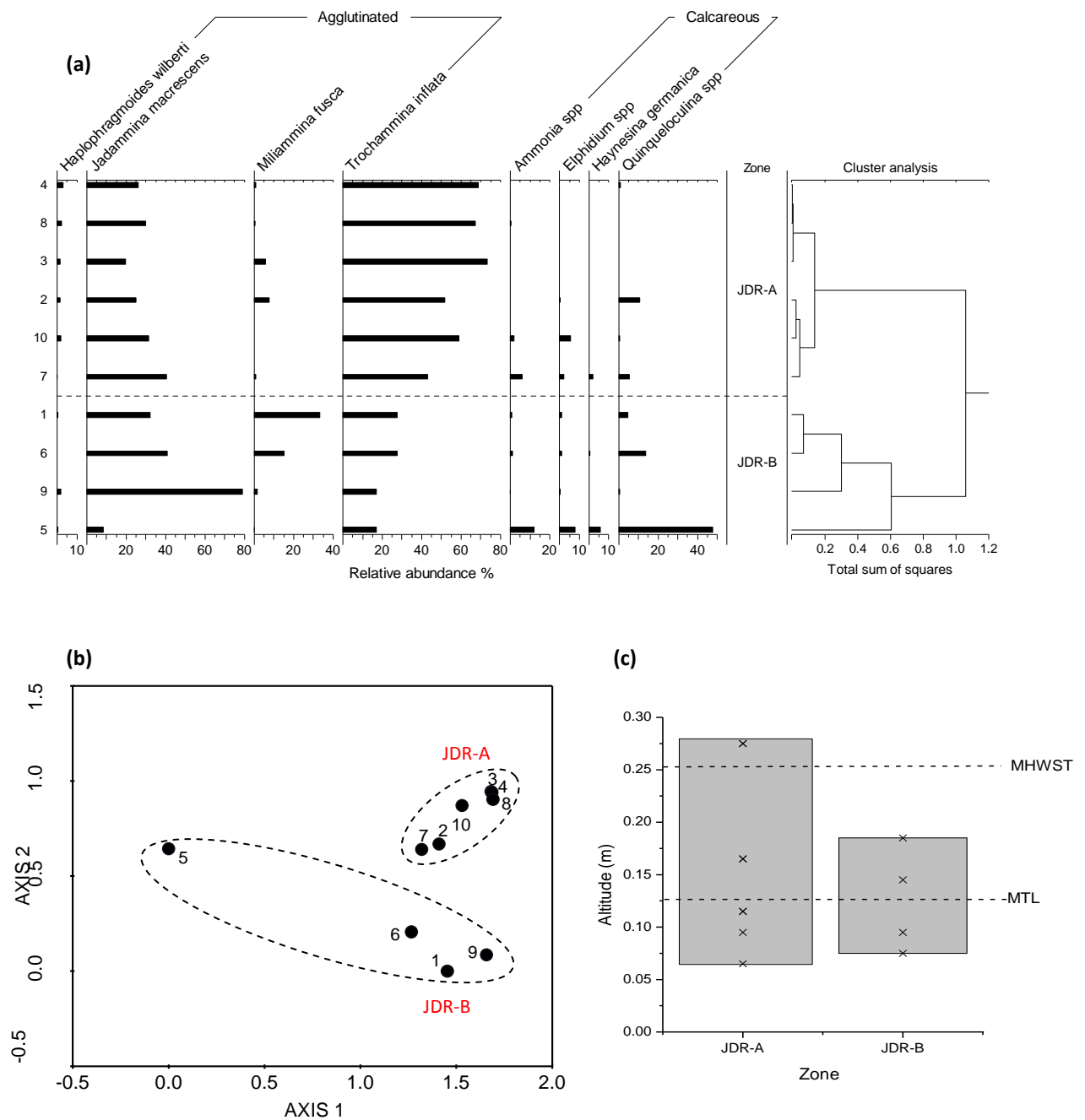


Figure 4.13. (a) Unconstrained cluster analysis based on unweighted Euclidean distance identifying faunal zones, (b) detrended correspondence analysis displaying faunal zones, and (c) altitude of faunal zones (m HVR571) based on relative percentages of 'dead' assemblage from JDR with tidal levels superimposed.

4.4.4. Blace Transect 1 (BL1)

The altitudes and distance (from the upper marsh limit) of the three additional surface samples added to this dataset are provided in table 4.6 below whilst the relative abundance of 'dead' foraminifera for these samples is plotted in figure A1 (Appendix B). No samples were excluded from the statistical analyses at BL1, however insignificant populations of *S. lobata* and *Brizalina* spp were removed. Three faunal zones have again been interpreted from the multivariate analyses where the vertical zonation appears much clearer between the high- and low-salt-marsh assemblages (figure 4.14).

Zone BL1-A (which could itself be separated into two faunal zones based on elevated frequencies of *J. macrescens* in samples 5, 6 and 7) is characterised by a high agglutinated component where high abundances of *J. macrescens* (up to 65%) and *T. inflata* (up to 65%) with minor occurrences of *M. fusca* are observed (figure 4.14a). DCA confirms the similar assemblages found throughout these samples (figure 4.14b) which have an altitudinal range covering 0.12 m above MHWST between 0.28 m and 0.40 m (figure 4.14c). Samples 14 and 15 (zone BL1-B) have a much lower altitudinal range below MTL between -0.01 m and 0.05 m and are dominated by calcareous species *Ammonia* spp. (up to 56%), *Elphidium* spp. (up to 16%), *Haynesina germanica* and *Quinqueloculina* spp. (up to 22%) with minimal frequencies of agglutinated species. Zone BL1-C is characterised by a more diverse assemblage of agglutinated and calcareous taxa. While there is a decrease in *Ammonia* spp. (< 21%), increases of *Quinqueloculina* spp. (up to 68%), *Spirillina vivpara*, *J. macrescens* and *T. inflata* are all observed. As a consequence, zone BL1-C occupies the largest vertical range between altitudes 0.17 m and 0.37 m, creating an altitudinal overlap between the zones due to the inclusion of samples 1 and 18 where relatively high abundances of *Quinqueloculina* spp. (43%) are observed at high altitudes (>0.29 m). The occurrence of *Quinqueloculina* spp. in these samples is similar to that observed from samples 2, 3 and 17 from faunal zone BL1-A which are from a similar altitude. Removal of samples 1 and 18 from BL1-C would create a vertical zonation that is much more distinct.

Table 4.6. Altitude and distance of samples 16, 17 and 18 added to the BL1 dataset.

Sample station	Altitude m HVRS71	Distance m
16	0.40	0
17	0.34	2
18	0.29	4

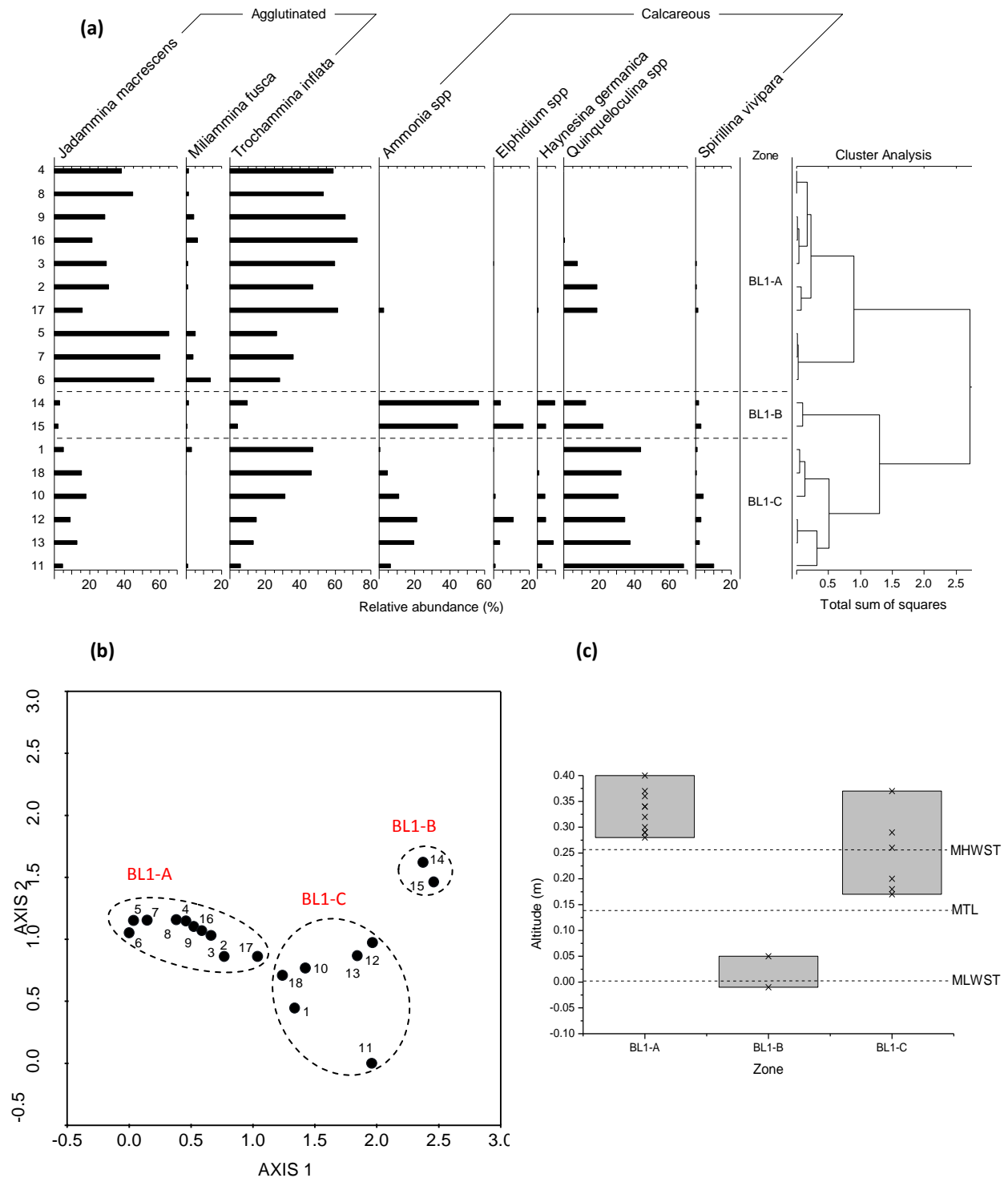


Figure 4.14. (a) Unconstrained cluster analysis based on unweighted Euclidean distance identifying faunal zones, (b) detrended correspondence analysis displaying faunal zones, and (c) altitude of faunal zones (m HVR571) based on relative percentages of 'dead' assemblage from BL1 with tidal levels superimposed.

4.4.5. Blace Transect 2 (BL2)

Insufficient counts in samples 9 and 10 and foraminiferal taxa including *M. fusca*, *Haplophragmoides wilberti*, *Brazilina* spp. and *Sprillina vivipara* were excluded from following analyses. Unconstrained cluster analysis has revealed two faunal zones across transect 2 at Blace (figure 4.15).

Faunal zone BL2-A is characterised by an almost exclusive calcareous-dominated assemblage where relatively high abundances of *Ammonia* spp. (up to 71%) and *Elphidium* spp. (up to 58%) are observed (figure 4.15a). Due to the high abundance of *Elphidium* spp. in sample 6 compared with samples 5, 7 and 8; DCA separates this out (figure 4.15b). The very narrow vertical range of zone BL2-A (0.02 m) (figure 4.15c) is comparable to the calcareous-dominated assemblage (BL1-B) observed in BL1 (figure 4.14c). Faunal zone BL2-B is characterised by an increased agglutinated component with high abundances of *J. m. acrescens* (up to 60%) but also with the addition of *Quinqueloculina* spp. (up to 45%). Minor occurrences of *T. inflata* (<19%) are also observed. DCA confirms the strong relationship between sample stations 1 to 4 which cover a broad altitudinal range between - 0.01 m and 0.40 m from above MHWST to MLWST. The occurrence of relatively high abundances of *Quinqueloculina* spp. in this zone, occupying higher altitudes, is perhaps unusual but repeats the trend observed across the first transect at Blace (samples BL1-1, 2, 3, 17 and 18).

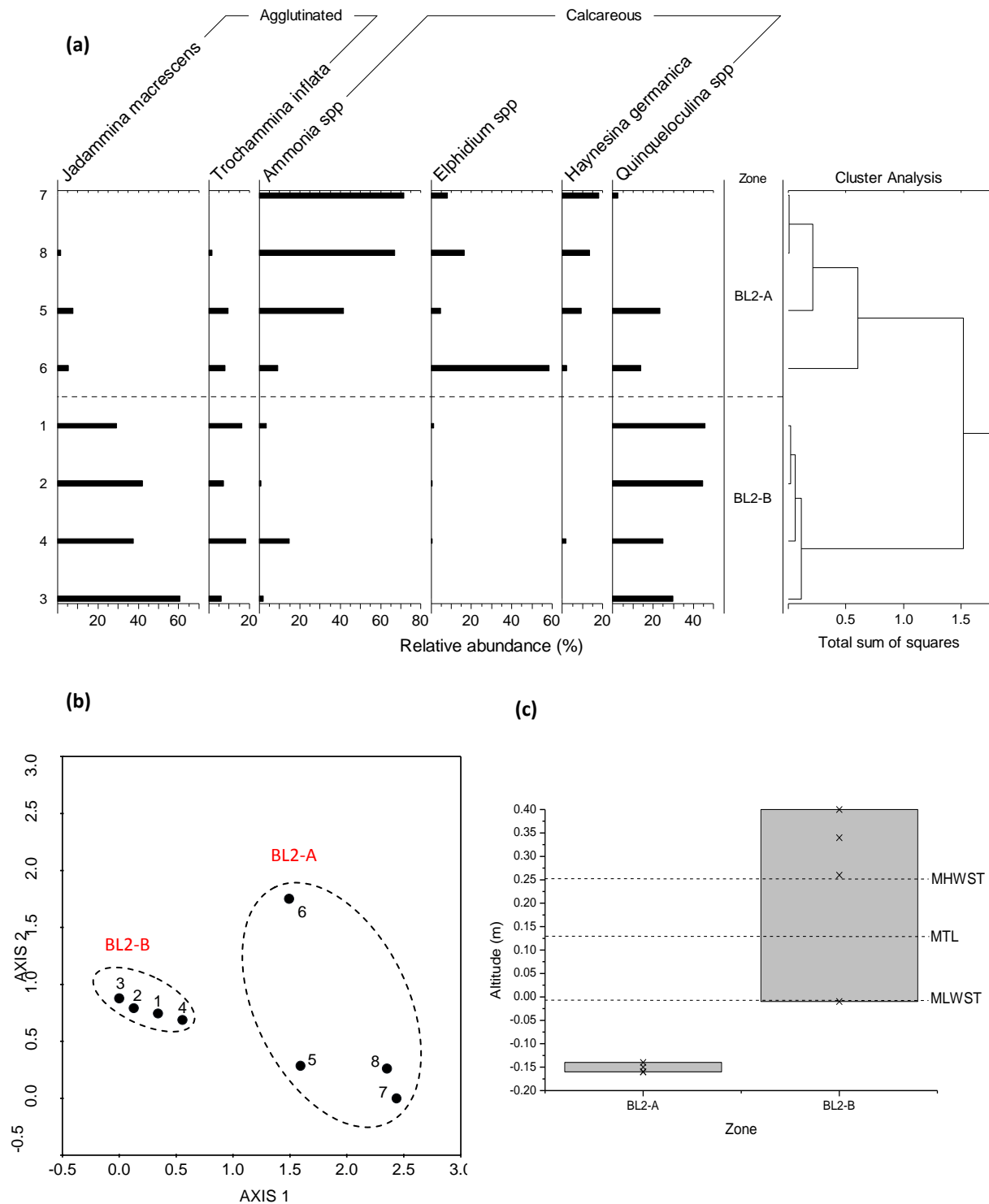


Figure 4.15. (a) Unconstrained cluster analysis based on unweighted Euclidean distance identifying faunal zones, (b) detrended correspondence analysis displaying faunal zones, and (c) altitude of faunal zones (m HVR71) based on relative percentages of 'dead' assemblage from BL2 with tidal levels superimposed.

4.4.6. Jadrtovac Transects 1 & 2 (JDT)

Transects 1 and 2 from Jadrtovac were combined to create a transect only training set for Jadrtovac (JDT) totalling 30 surface samples as shown in figure 4.16. Following the screening of the data, statistically insignificant species were removed (<2%), including *Haplophragmoides wilberti* and *Haynesina germanica*. In combining transects JD1 and JD2 together these multivariate analyses reveal five faunal zones (figure 4.16) as discussed below.

Fauna zone JDT-A is dominated by a high agglutinated component where *J. macrescens* is found in abundance (>69%) (figure 4.16a) and DCA confirms the strong correspondence across this group of samples (found to the left of the biplot; figure 4.16b). JDT-A covers a large altitudinal range (0.30 m) extending above MHWST and below MTL between 0.055 m to 0.355 m (figure 4.16c). Zone JDT-B is characterised by a decrease and increase in the relative abundance of agglutinated species *J. macrescens* and *T. inflata*, respectively, occupying an altitude between 0.085 m and 0.205 m. A substantial increase in the relative abundance of calcareous taxa *Quinqueloculina* spp. and *Ammonia* spp. and decrease in *J. macrescens* characterises zone JDT-C. DCA also confirms the strong association across this group of samples which occupies a relatively narrow altitudinal window (predominately below MTL) between 0.065 m and 0.155 m. This again emphasizes the lower altitudinal range in which a calcareous-dominated assemblage is observed at Jadrtovac and similarly the higher altitude to which an agglutinated-dominated assemblage incorporating *J. macrescens* and *T. inflata* can extend to (e.g. faunal zone JDT-A and JDT-E). The relative abundance of *J. macrescens* and *T. inflata* remains similar in zone JDT-D compared with JDT-C, however it is differentiated by an increase in *M. fusca* (up to 45%) and decrease in calcareous taxa. The separation of this faunal zone is confirmed by DCA and occupies a very narrow altitude window between 0.165 m and 0.195 m above MTL.

Faunal zone JDT-E is dominated by an agglutinated assemblage where *T. inflata* (up to 75%) is the most dominant taxa. The relative increase in *Elphidium* spp. in samples JD1-3, JD1-4 and JD2-3 occur within a broadly similar altitudinal range between the two transects (0.235 m to 0.275 m). The zone again highlights that *T. inflata* is found in abundance across much of the salt-marsh environment at Jadrtovac, hence its large altitudinal range between 0.045 m and 0.275 m creating an overlap between the faunal zones.

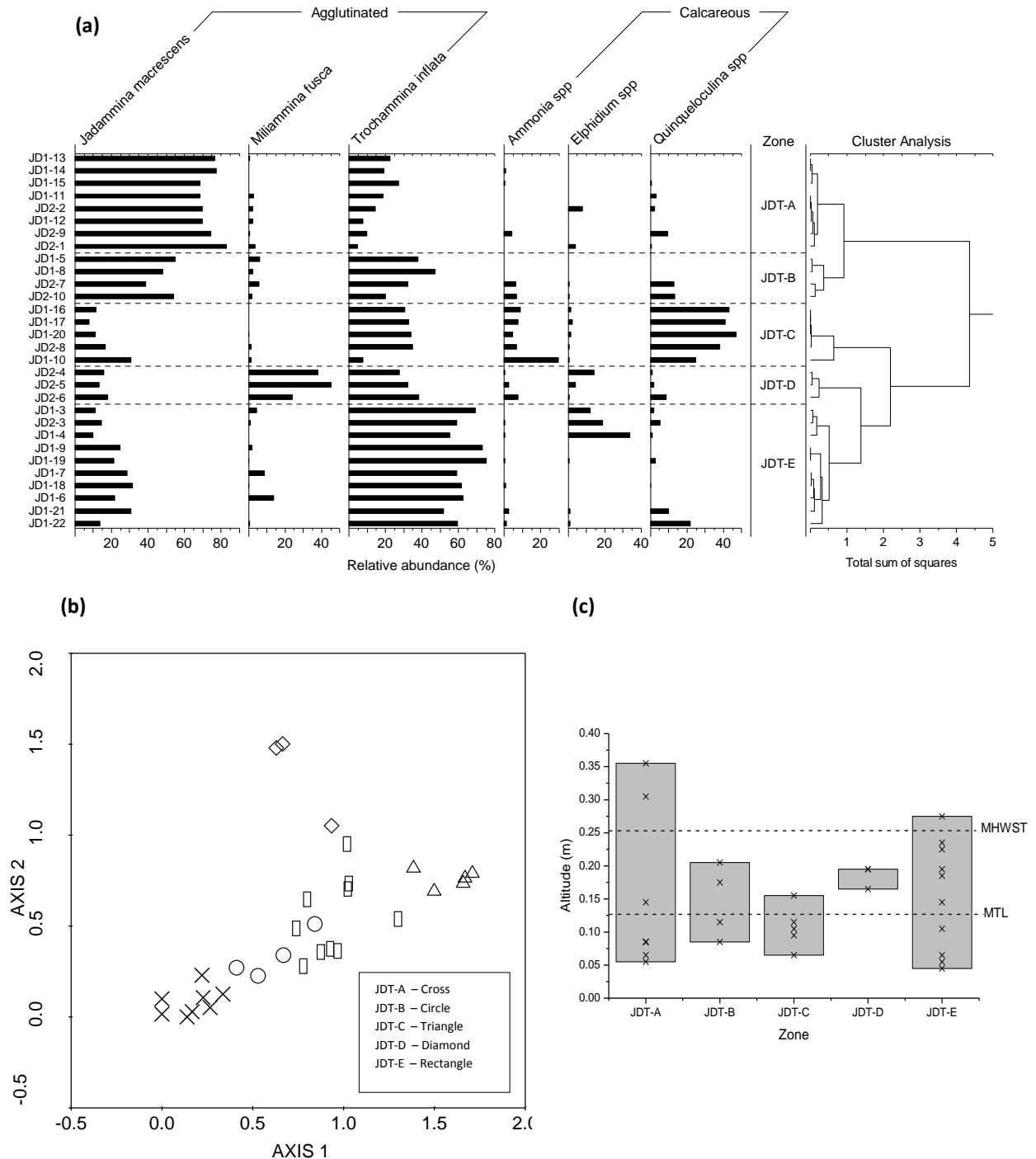


Figure 4.16. (a) Unconstrained cluster analysis based on unweighted Euclidean distance identifying faunal zones, (b) detrended correspondence analysis displaying faunal zones, and (c) altitude of faunal zones (m HVR571) based on relative percentages of 'dead' assemblage from the combined transect dataset at Jadrtovac with tidal levels superimposed.

4.4.7. Blace Transects 1 & 2 (BLT)

Transects 1 and 2 from Blace were combined to create a modern training set for this site containing a total of twenty six surface samples. Following the pre-treatment of the data before statistical analyses, species abundance was reduced to just five taxa after the exclusion of *Elphidium* spp., *Haynesina germanica* and *Sprillina vivpara* (<2%). Cluster analysis and DCA reveals three faunal zones when combining the datasets together where the zonation between the assemblages appears much stronger in comparison to Jadrtovac (figure 4.17).

A mixed foraminiferal assemblage characterises zone BLT-A where the relative abundance of agglutinated (*J. macrescens* and *T. inflata*) and calcareous (*Ammonia* spp. and *Quinqueloculina* spp.) taxa are broadly similar throughout. This zone extends over a large altitudinal range (0.56 m) between -0.16 m and 0.40 m, covering all of the sampled salt-marsh environment. Inspection of the elevation boxplot shows that while the majority of the samples included in this zone are well constrained altitudinally, an overlap is created due to the inclusion of sample BL2-4 (at 0.01 m) and sample BL2-6 (at -0.16 m). Zone BLT-B is dominated by a calcareous assemblage comprising high abundances of *Ammonia* spp. (up to 71%) and *Quinqueloculina* spp. (up to 23%) and low agglutinated types. The five samples are all taken from the lowest altitudes from their respective transects, as identified previously in figures 4.14 and 4.15. DCA again confirms the strong association across the samples which occupy an altitudinal range of 0.21 m between -0.16 m and 0.05 m. Zone BLT-C is altitudinally well-constrained, covering an elevation between 0.28 m and 0.40 m (range 0.12 m). This assemblage is dominated by agglutinated species *J. macrescens* (up to 65%) and *T. inflata* (up to 72%). The occurrence of *Quinqueloculina* spp. (18%) in samples 1 and 17 from BL1 is limited between 0.34 m and 0.37 m. DCA plots these samples to the left of the biplot and signifies the strong relationship between the agglutinated dominated assemblages. The slight separation of samples 5, 6 and 7 from the main group in this zone represents the minor increase in *J. macrescens* and *M. fusca* taxa in these samples.

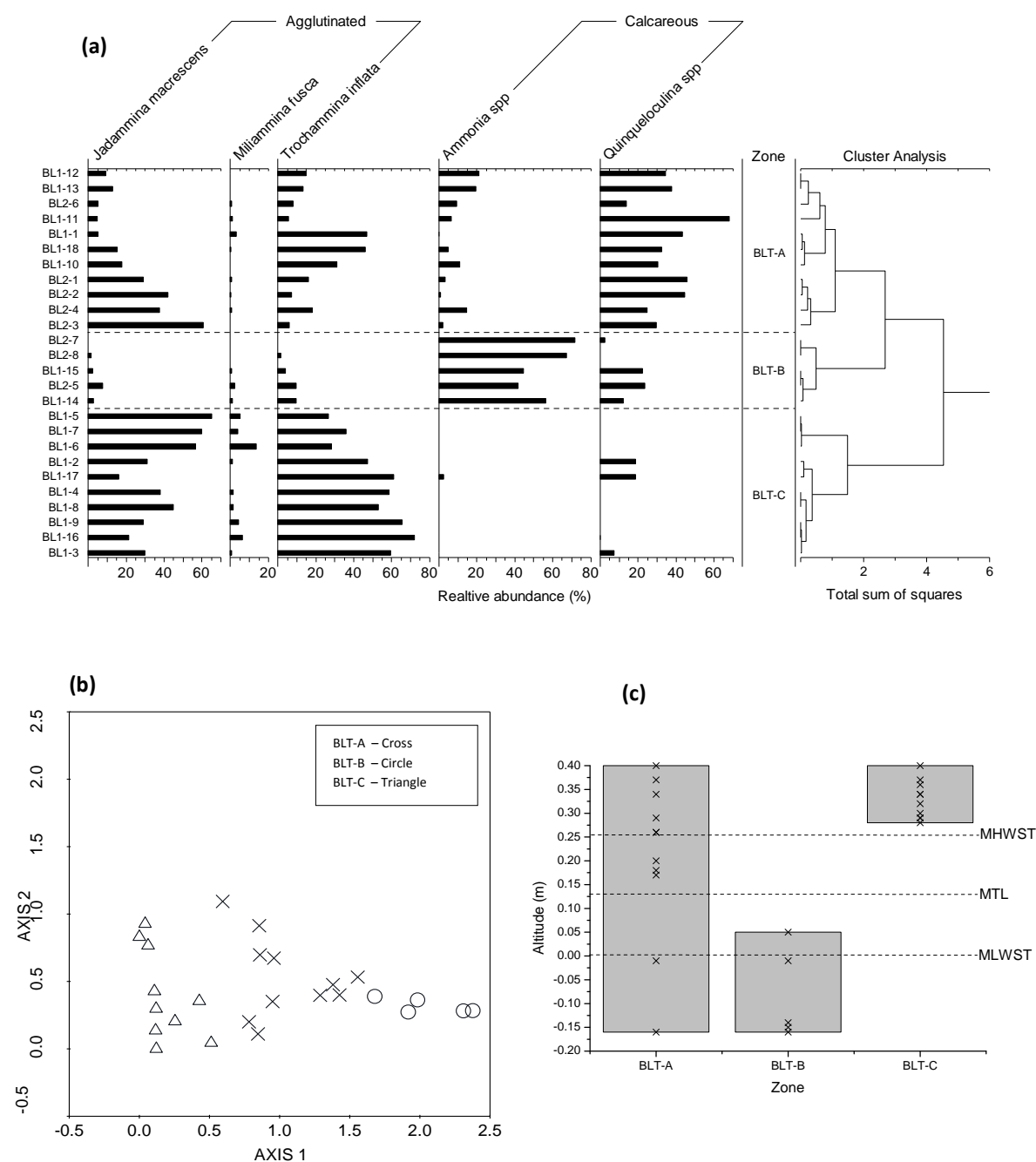


Figure 4.17. (a) Unconstrained cluster analysis based on unweighted Euclidean distance identifying faunal zones, (b) detrended correspondence analysis displaying faunal zones, and (c) altitude of faunal zones (m HVERS71) based on relative percentages of 'dead' assemblage from the combined Blace dataset with tidal levels superimposed.

4.5. CONTROLS GOVERNING CONTEMPORARY SALT-MARSH FORAMINIFERAL DISTRIBUTIONS

The vertical distribution of foraminifera from each site has revealed elevation-dependent zones in which characteristic assemblages occur in abundance. Despite variability between the study sites, unconstrained cluster analysis and DCA revealed on average three faunal zones from the studied transects which were broadly similar throughout. Results from DCA in section 4.4 provided a measure of gradient length (in SD units) allowing the appropriate constrained ordination technique to be applied based on the species' linear or unimodal distribution. To understand the environmental controls influencing vertical zonation, further quantitative measures were employed to investigate the relationship between dead foraminiferal assemblages and analysed environmental variables (altitude, pH, salinity, organic matter, grain size composition and distance) presented in section 4.2. Distance was used as a separate variable due to the non-linear relationship between increasing salt-marsh altitude and distance from the seaward edge. The ultimate aim of this procedure was to test the hypothesis that altitude is a controlling factor influencing surface foraminiferal distributions, thus confirming their suitability in transfer function reconstructions of palaeo-sea-level for the Croatian coast. For the following analyses the datasets are structured as follows; the individual transect were combined (e.g. JD1 and JD2) to create local training sets for each site (JDT and BLT). The datasets from both sites were then analysed collectively to create a regional training set (TCD). Results from the random sampling approach were not included; this is discussed further in section 4.6.

In salt-marsh foraminiferal sea-level reconstructions, the relationship between the modern assemblages and elevation within the tidal frame must first be quantified to assess their suitability as proxies for sea-level change (Gehrels, 2002). Here, the term altitude has previously been used to describe the foraminiferal assemblage zones relative to tidal levels and the Croatian vertical datum (m HVR571). Elevation in sea-level studies however is differentiated from altitude as it is often used to describe the height relative to a reference water level (e.g. MSL). The following analyses are therefore based on the height of the sample relative to MSL.

4.5.1. Jadrtovac Transects 1 & 2 (JDT)

The results from DCA revealed gradient lengths of 1.708 SD (axis one) and 1.501 SD (axis two) indicating linear species distribution (table 4.7). RDA was therefore used to evaluate environmental controls on contemporary foraminiferal distributions for a combined transect dataset at Jadrtovac. Eigenvalues for RDA axis one (eigenvalue = 0.288) and axis two (eigenvalue = 0.079) explain 36.7% of the total variance in the species dataset and 86.3% of the species-environment relationship (table 4.8). The lengths and direction of the environmental arrows give an approximation of their relative importance in explaining variance in the foraminiferal data and correlation to ordination axes one and two. Similarly they also indicate any correlation between the tested environmental variables allowing foraminiferal species indicative of particular environmental conditions to be identified (Horton and Edwards, 2006). Figure 4.18 shows the relative importance of the tested environmental variables in explaining variance in the foraminiferal dataset, which account for 42.5% of the variation in the dataset for JDT (figure 4.18c). Intra-set correlations between the variables and RDA axes one and two indicate altitude, distance and salinity to be highly correlated with axis two whilst clay and sand are correlated with axis one. Silt, LOI and pH display a joint correlation between the axes (figure 4.18a). Partial RDAs show that the total explained variance is composed of 13% altitude, 4.1% salinity, 3.6% pH, 2.9% silt, 2.5% clay, 1.9% LOI, 1.6% distance and 0.7% sand. Inter-correlation between the variables accounts for 69.7% (figure 4.18d). The associated Monte Carlo permutation tests, which assesses whether the *p*-value is significant or not, indicates that only altitude is statistically significant in explaining variance for a combined foraminiferal dataset at Jadrtovac (*p* = 0.014, 499 permutations under reduced model).

Table 4.7. Summary DCA results for dead foraminiferal assemblages for JDT.

Axes	1	2	3	4	Total inertia
Eigenvalues:	0.327	0.159	0.051	0.029	0.990
Lengths of gradient:	1.708	1.501	1.639	1.769	
Cumulative percentage variance of species data:	33.0	49.1	54.3	57.2	
Sum of all Eigenvalues:					0.990

Table 4.8. Summary RDA results from dead foraminiferal assemblages for JDT.

Axes	1	2	3	4	Total Variance
Eigenvalues	0.288	0.079	0.036	0.021	1.000
Species-Environment correlations	0.700	0.636	0.479	0.728	
Cumulative percentage variance					
of species data:	28.8	36.7	40.3	42.3	
of species-environment relation:	67.7	86.3	94.7	99.6	
Sum of all Eigenvalues					1.000
Sum of all canonical Eigenvalues					0.425

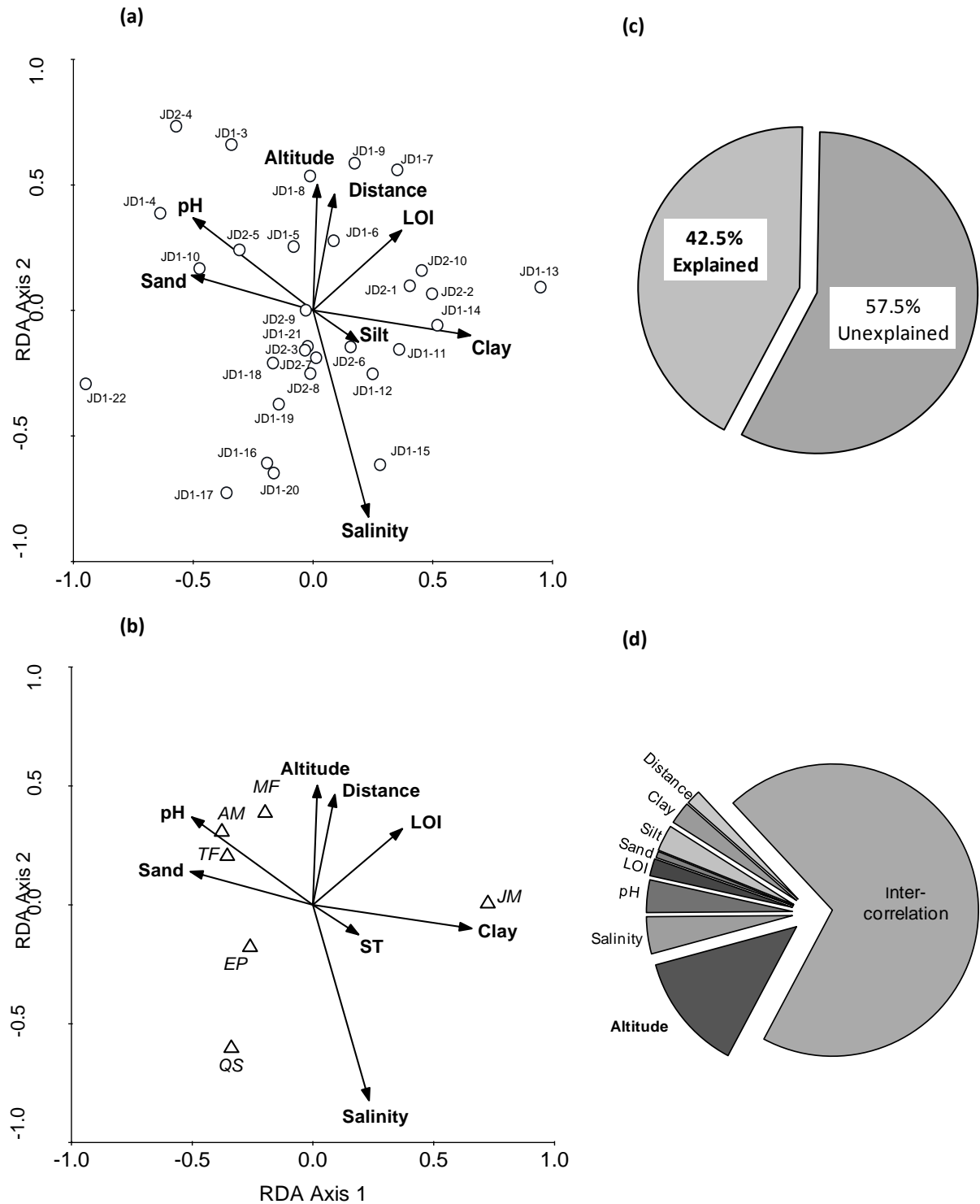


Figure 4.18. Redundancy Analysis biplots of (a) samples relative to environmental variables and (b) species relative to environmental variables from JDT. Pie charts showing (c) total explained and unexplained variance and (d) unique contributions of tested environmental variables as identified from pRDA. Species abbreviations: JM=*Jadammina macrescens*, TF=*Trochammina inflata*, MF=*Miliammina fusca*, AM=*Ammonia* spp., EP=*Elphidium* spp., QS=*Quinqueloculina* spp. Environmental abbreviation: LOI=Loss-on-ignition.

4.5.2. Blace Transects 1 & 2 (BLT)

Detrended correspondence analysis illustrates the use of a unimodal response model for a combined transect dataset at Blace as reported by a gradient length of 2.376 SD (axis one) (table 4.9). Conical correspondence analysis was therefore used to investigate the relationship between foraminiferal assemblages and tested environmental variables. Eigenvalues for CCA axis one (eigenvalue = 0.513) and axis two (eigenvalue = 0.123) explain 63% of the species data and 93.7% of the species-environment data (table 4.10). Intra-set correlations between the environmental variables and CCA ordination axes show altitude, distance, silt, clay, sand and pH to be correlated with axis one while salinity is correlated with axis two. Organic matter (LOI) displays joint correlation between the axes (figure 4.19a). CCA axis one therefore reflects the major environmental gradient with agglutinated species *J. macrescens* and *T. inflata*, positioned to the left of the biplot related to higher altitude and distance (from open water) (figure 4.19b).

The tested environmental variables account for 67% of the explained variance (figure 4.19c) and partial CCAs demonstrate that this is composed of 22.1% altitude, 11.2% LOI, 9.6% pH, 6.7% clay, 5.5% sand, 4.9% silt, 3.4% distance and 3.1% salinity. Inter-correlation between the variables represents 33.5%, as shown in figure 4.20d. Monte Carlo permutation tests indicate that altitude is again the only environmental variable that is statistically significant in explaining variance for a combined foraminiferal dataset at Blace ($p = 0.01$, 499 permutations under reduced model).

Table 4.9. Summary DCA results for dead foraminiferal assemblages for BLT.

Axes	1	2	3	4	Total inertia
Eigenvalues:	0.596	0.106	0.023	0.011	1.010
Lengths of gradient:	2.376	1.092	1.922	1.659	
Cumulative percentage variance of species data:	59.0	69.6	71.9	73.0	
Sum of all Eigenvalues:					1.010

Table 4.10. Summary CCA results from dead foraminiferal assemblages for BLT.

Axes	1	2	3	4	Total Variance
Eigenvalues	0.513	0.123	0.037	0.005	1.010
Species-Environment correlations	0.930	0.697	0.567	0.333	
Cumulative percentage variance					
of species data:	50.8	63.0	66.7	67.2	
of species-environment relation:	75.7	93.7	99.2	100.0	
Sum of all Eigenvalues					1.010
Sum of all canonical Eigenvalues					0.679

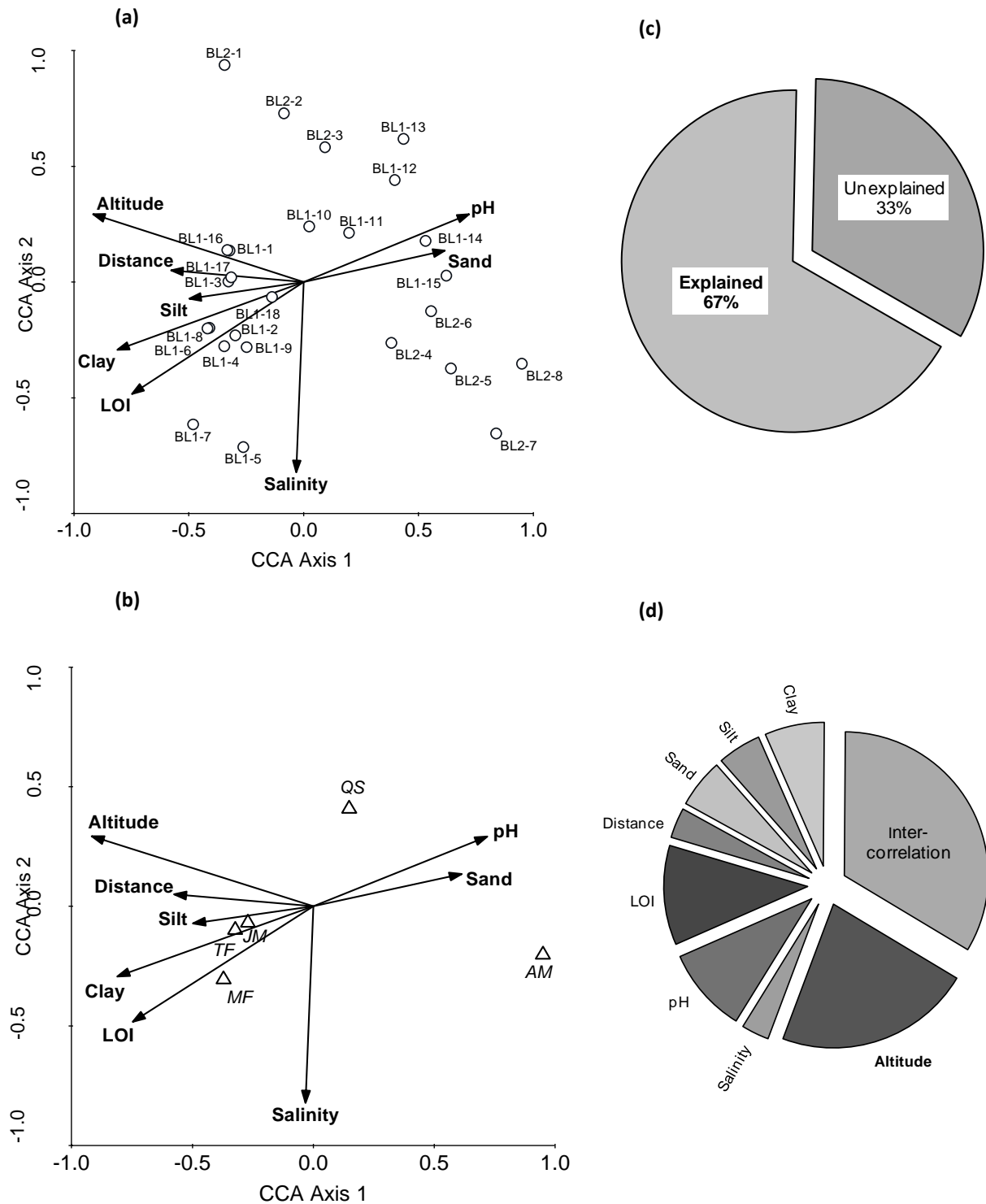


Figure 4.19. Canonical correspondence analysis biplots of (a) samples relative to environmental variables and (b) species relative to environmental variables from BLT. Pie charts showing (c) total explained and unexplained variance and (d) unique contributions of tested environmental variables as identified from pCCA. Species abbreviations: JM=*Jadammina macrescens*, TF=*Trochammina inflata*, MF=*Miliammina fusca*, AM=*Ammonia* spp., QS=*Quinqueloculina* spp. Environmental abbreviation: LOI=Loss-on-ignition.

4.5.3. Total Combined Dataset (TCD)

The results from DCA for a total combined dataset (TCD) reveals gradient lengths of 2.861 SD (axis one) and 2.051 SD (axis two) (table 4.11). A unimodal response model was therefore again used to explain variance in the foraminiferal data that can be accounted for by the analysed environmental variables. CCA axis one (eigenvalue = 0.430) and axis two (eigenvalue = 0.126) explains 41.1% of the species data and 85.3% of species-environment relationship (table 4.12). Inspection of ordination biplots shows altitude, LOI and clay to be highly correlated with axis one while salinity is well correlated with axis two. Sand, pH, silt and distance show joint correlation between the axes (figure 4.20a). CCA axis one reflects the major environmental gradient with agglutinated species *J. macrescens*, *T. inflata* and *M. fusca* positioned to the left of the biplot related to higher altitude and distance (from open water) (figure 4.20b).

Of the explained variance, the environmental variables account for 48.2% (figure 4.20c) and partial CCAs demonstrate that this is composed of 13.5% altitude, 5% pH, 3% LOI, 2% distance, 1.6% salinity, 1.5% clay, 1.2% sand and 1% silt. Inter-correlation between the environmental variables again remains very high and accounts for 71.8% (figure 4.20d). When assessing the significance of the environmental variables, Monte Carlo permutation tests indicates that only altitude and pH are statistically significant in explaining variance in a combined Jadrtovac and Blace transect dataset (p value= 0.002 - 0.04, 499 permutations under reduced model).

Table 4.11. Summary DCA results for dead foraminiferal assemblages for TCD

Axes	1	2	3	4	Total inertia
Eigenvalues:	0.520	0.199	0.105	0.043	1.351
Lengths of gradient:	2.861	2.051	1.769	1.711	
Cumulative percentage variance of species data:	38.5	53.2	61.0	64.2	
Sum of all Eigenvalues:					1.351

Table 4.12. Summary CCA results for dead foraminiferal assemblages for TCD.

Axes	1	2	3	4	Total Variance
Eigenvalues	0.430	0.126	0.053	0.024	1.351
Species-Environment correlations	0.913	0.739	0.498	0.350	
Cumulative percentage variance					
of species data:	31.8	41.1	45.1	46.8	
of species-environment relation:	65.9	85.3	93.5	97.1	
Sum of all Eigenvalues					1.351
Sum of all canonical Eigenvalues					0.652

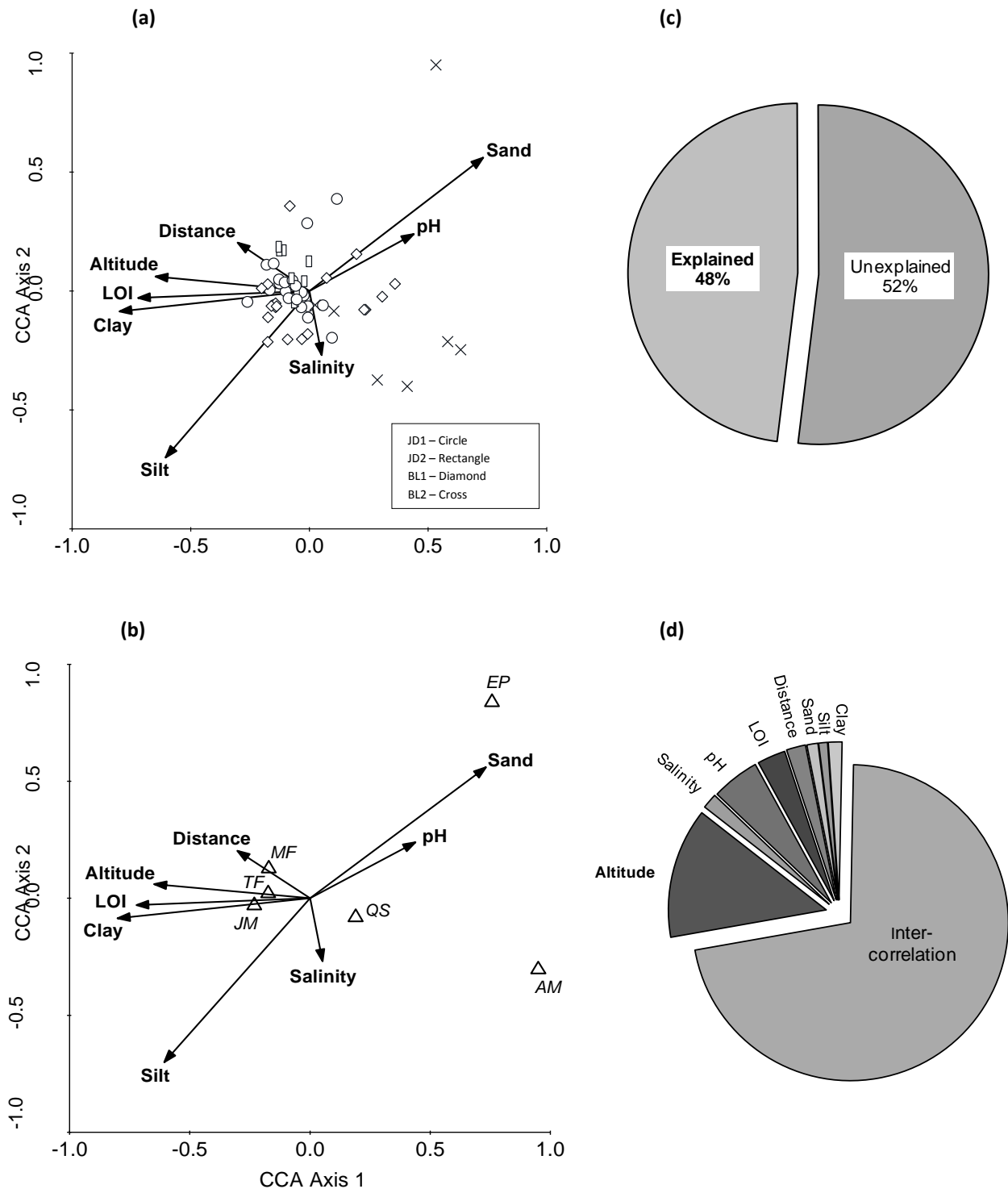


Figure 4.20. Canonical correspondence analysis biplots of (a) samples relative to environmental variables and (b) species relative to environmental variables from a total combined transect dataset. Pie charts showing (c) total explained and unexplained variance and (d) unique contributions of tested environmental variables as identified from pCCA.

Species abbreviations: JM=*Jadammina macrescens*, TF=*Trochammina inflata*, MF=*Miliammina fusca*, EP=*Elphidium* spp., AM=*Ammonia* spp., QS=*Quinqueloculina* spp.

Environmental abbreviation: LOI=Loss-on-ignition.

4.6. SUMMARY OF CONTEMPORAY SALT-MARSH DATA

This chapter has provided an overview of the studied salt-marsh environments at Jadrtovac and Blace in an attempt to establish a modern training set suitable for use in foraminiferal based transfer function sea-level reconstructions. A total of 70 surface samples were collected across four transects and from a random sampling approach from two salt-marsh sites, Jadrtovac and Blace (table 4.5). These samples were analysed for both 'live' and 'dead' foraminiferal assemblages together with environmental variables including pH, salinity, organic matter (LOI) and grain size characteristics. The altitude of each sample relative to vertical datum (m HVRS71) and distance from open water was also documented. The concentration of foraminiferal tests was generally very high despite the relatively low species diversity. The main foraminiferal taxa encountered included agglutinated species *J. macrescens*, *T. inflata*, *M. fusca*, and calcareous species *Elphidium* spp., *Ammonia* spp., *Haynesina germanica* and *Quinqueloculina* spp. Similarly the concentration of dead foraminiferal tests was significantly higher in comparison to living specimens and all subsequent analyses focused on dead assemblages only. Following the initial pre-treatment of data, a number of insignificant species were removed (<2% of the total) including samples where insufficient counts were obtained. The remaining modern training set comprised 66 samples.

Unconstrained cluster analysis and DCA reveal that the individual transect datasets can be divided into a maximum of three faunal zones. The altitudinal extent of these zones differs between Jadrtovac and Blace, however the foraminiferal assemblages observed are broadly similar throughout. The sequence of vertical zonation from a random sampling approach is however much less defined, and also when datasets are combined to create local training sets for each site, an altitudinal overlap occurs between the faunal zones identified. Despite this, an overall pattern of intertidal vertical zonation is observed, supporting their potential as proxies in paleo sea-level reconstructions.

Both transect datasets at Jadrtovac and Blace can be divided into agglutinated-dominated assemblages, which extend to a higher altitude on the salt-marsh environment, and a calcareous-dominated assemblage which is observed at a lower altitudinal level towards the salt-marsh sea interface. Excluding BL2, a third zone also exists where a mixed agglutinated and calcareous assemblage occupies a vertical range creating an altitudinal overlap between the other faunal zones. The vertical zonation of surface foraminifera at Blace is much easier to differentiate when compared to modern assemblages at Jadrtovac. Faunal zone 1 (BL1-A) shows that an agglutinated dominated assemblage, comprised of relatively high abundances of *J. macrescens*, *T. inflata* and *M. fusca*, occupies the highest vertical

level reaching above MHSWT from 0.28 m to 0.40 m. In contrast, faunal zone 2 at this site (BL1-B) shows that a calcareous dominated assemblage, where increases in the relative abundance of *Ammonia* spp. and *Elphidium* spp. are observed, occupies a much lower altitudinal level below MTL between -0.01 m and 0.05 m. The mixed foraminiferal assemblage observed at this site, faunal zone BL1-C, covers a larger altitudinal range (0.20 m) compared to BL1-A and BL1-B. The vertical overlap can be explained due to the inclusion of surface samples 1 and 18 in this zone which are above MHWST (at altitudes of 0.29 m and 0.37 m, respectively) where the relative increase of *Quinqueloculina* spp. and thus associated fall in agglutinated taxa is observed. The occurrence of this taxon found at high altitudes is similar to samples 2 and 17 from zone BL1-A. Indeed, if samples 1 and 18 were removed from zone BL1-C, the altitudinal overlap ceases to exist and the vertical zonation becomes even more defined (figure 4.14c).

A broadly similar trend is observed from the second transect at Blace where two faunal zones are identified (figure 4.15). Faunal zone BL2-A is comparable to faunal zone BL1-B at this site where a calcareous dominated assemblage, comprised of *Ammonia* spp., *Elphidium* spp., *Haynesina germanica* and *Quinqueloculina* spp. occupies a much lower altitude below MTL. Faunal zone BL2-B is also comparable to faunal zone BL1-C where a mixed assemblage covers a larger vertical range. Whilst this site is lacking a solely agglutinated dominated assemblage as observed at BL1, it is useful in confirming the higher altitude in which increased relative abundances of agglutinated taxa *J. macrescens* and *T. inflata* are observed. The reduced number of faunal zones identified across BL2 in comparison to BL1 is perhaps related to the limited number and altitudinal position of the surface samples analysed. The inclusion of surface sample 4 in BL2-B creates the large vertical range observed for this faunal zone.

Analysis of the transect datasets from Jadrtovac shows less defined vertical niches of the assemblage zones again illustrating that agglutinated and calcareous species are found across the entire vertical range of the marsh environment. Comparisons can however be made to BL1. Three faunal zones are again identified at JD1 which are also comparable in terms of their species composition (figure 4.11). Faunal zone JD1-A shows an agglutinated dominated assemblage where relatively high abundances of *J. macrescens* and *T. inflata* are observed within a vertical range spanning 0.12 m. While this agglutinated assemblage is similar to that observed in BL1, it is found at a lower altitude at Jadrtovac between 0.085 m and 0.205 m HVR571. Similar to the mixed foraminiferal assemblage observed at BL1 (faunal zone BL1-C), a reduction in *J. macrescens* and relative increase in *T. inflata* and calcareous taxa (*Elphidium* spp. and *Quinqueloculina* spp.) characterises faunal zone JD1-B. This mixed zone again has the largest vertical range (0.23 m) creating a large altitudinal

overlap. An increase in the relative abundance of calcareous taxa (*Ammonia* spp. and *Quinqueloculina* spp.) and reduction in agglutinated species *J. macrescens* and *T. inflata* characterises faunal zone JD1-C and is similar to the calcareous dominated assemblage observed at BL1 (BL1-B). At Jadrtovac, this faunal zone occupies a similarly narrow (0.06 m) and low vertical window between 0.055 m and 0.115 m below MTL. Despite the larger altitudinal overlaps between the faunal zones identified at JD1 compared to Blace datasets, it confirms the higher vertical extent to which an agglutinated-dominated assemblage is found (e.g. between MTL and MHWST) and conversely the lower altitudinal range in which calcareous species dominate (e.g. below MTL).

The vertical extent of the faunal zones identified at JD2 (figure 4.12) illustrates intra-site variability between the sampled transects at Jadrtovac. The transect established at JD2 covered 16.5 m over an altitudinal change of 0.27 m compared to JD1 which spans 122 m with an altitudinal change of 0.23 m. Faunal zone JD2-A again highlights the upper vertical extent to which an agglutinated assemblage, which is primarily dominated by *J. macrescens*, extends too (above MTL). The inclusion of sample station 9 in this faunal zone, which is due to the relatively high abundances of *J. macrescens* observed at lower altitudes, causes JD2-A to cover a larger altitudinal range (0.21 m) between 0.145 m and 0.355 m when compared to the similar faunal zone at JD1 (JD1-A). Faunal zone JD2-B is differentiated by the occurrence of *M. fusca* in abundance and decrease in *J. macrescens* creating a very narrow vertical window between 0.175 m and 0.195 m HVR571.

Transect datasets from Jadrtovac and Blace were combined to create local training sets for each site (JDT and BLT) before combining all transect samples together to form a total combined training set (TCD). Constrained ordination techniques were used to assess the degree to which the environmental variables could explain variance in the modern training sets after exploring their unimodal or linear distribution so that the appropriate statistical technique could be applied. Gradient lengths varied between 1.7 and 2.8 SD units suggesting the use of both unimodal and linear ordination techniques were suitable. The explained variance ranged from 42.5% to 67% for JDT and BLT and 48% for a total combined dataset.

Partial ordination (pCCA and pRDA) was performed to test the hypothesis that foraminifera show a statistically significant relationship with altitude. The extent explained by altitude again varied between datasets ranging from 13% to 22.1% (of the explained variance) and Monte Carlo permutation tests suggested it was statistically significant in explaining variance in the species data ($p = <0.05$). Whilst other the environmental variables did not appear significant in explaining variance in the foraminiferal assemblages ($p = >0.05$), altitude

cannot be considered totally independent of the other environmental variables due to the large intercorrelations observed (up to 71%). Despite this, the amount of explained variance and that explained by altitude observed in this study is comparable to previous studies (see table 7.1) and confirms their suitability as proxies for sea-level change in transfer function reconstructions.

RESULTS II

FOSSIL SALT-MARSH DATA AND CHRONOLOGY

5.1. INTRODUCTION

The sedimentary history of Jadrtovac and Blace was investigated using a variety of lithological, biostratigraphic, geochemical and chronological techniques. First an overview of the salt-marsh stratigraphy is provided through detailed descriptions and simplified diagrams to illustrate the nature of sediment deposition across the studied salt-marsh environments. The results from the fossil foraminiferal record for the ‘type’ cores selected for analysis are followed by analysed environmental variables: organic matter, dry bulk-density and particle size. Core chronologies are established using a variety of methods including short-lived radionuclides, radiocarbon dating and potential geochemical pollution markers provided by XRF. Radiocarbon dating is restricted to core JD1 where three AMS ^{14}C dates were obtained. The results of this are used in the construction of age-depth models adopting both classical and Bayesian approaches.

5.2. SEDIMENT STRATIGRAPHY

The sediment stratigraphy of the Jadrtovac and Blace salt-marshes was investigated to explore their accumulation history. This approach is essential in sea-level studies as a consistent record of sediment deposition throughout a salt-marsh environment is preferable when conducting sea-level reconstructions (Horton and Edwards, 2006). It is also important to understand the sedimentary nature of the investigated cores, especially in the context of quantifying former sea level due to the associated problems of autocompaction, i.e. thick sequences of organic sediments, in the lowering of sea-level index points from their original depositional altitude (Allen, 2000; Brain et al., 2011). Based on their lithological composition, ‘type’ cores were then sampled for further analysis (e.g. biostratigraphy). A simplified form of the salt-marsh stratigraphy at Jadrtovac and Blace is presented in figures 5.1 and 5.3 below, while full Troëls-Smith (1955) descriptions are provided in Appendix A.

5.2.1. Jadrtovac Site 1 (JD1)

Twelve sediment cores were analysed across a transect spanning 110 m at JD1; following a similar strategy to the contemporary surface transect incorporating all sub-environments from high to low salt-marsh. All cores were drilled to the underlying bedrock, in which sediment depth generally increased with distance towards the open sea. Although variable, five stratigraphic units were identified, as shown in figure 5.1, where sediment accumulation appears to have been fairly uniform across the site. An unrecoverable/saturated unit was found between cores 8 and 12, 40 to 110 m along the transect. Overlying this, approximately 70 m along the transect and extending to the open sea, was a dark coarse silt with abundant (broken and whole) shell fragments. This unit is then overlain by variable silty clay and clayey silt units, which are occasionally mottled and become increasingly saturated with depth. Above this, a grey/brown organic clay unit which extends to the surface 20 m along and to the end of the transect is then observed. A highly organic peat layer was restricted to the landward 20 m of the transect and varied in thickness between 8–11 cm. Following the survey, a 42 cm ‘type’ core (JD1) was collected from the upper salt-marsh at an altitude of 0.165 m (figure 5.2). A full description of JD1 core 4 is provided in table 5.1, which comprised a silty clay bottom section overlain by an increasingly organic clay and a 10 cm-thick humified peat deposit towards the surface.

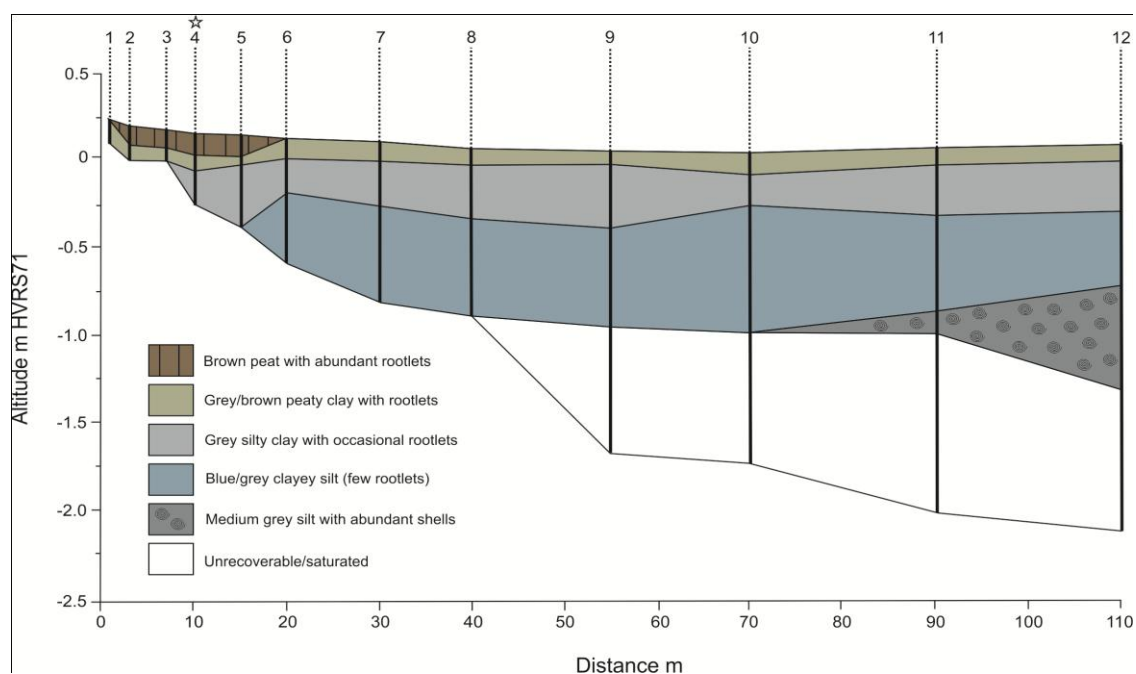


Figure 5.1. Simplified sediment stratigraphy at JD1, plotted relative to altitude (m HVR571) from high (1) to low (12) marsh. ‘Type’ core JD1 also highlighted (4).



Figure 5.2. Photograph of JD1 42 cm ‘type’ core illustrating the up-core transition of basal minerogenic silts and clays (right) to highly organic peat sediments (left) towards the surface.

Table 5.1. Lithology of JD1 ‘type’ core following the Troëls-Smith (1955) classification.

Depth (cm)	Altitude m HVR571	Sediment description (after Troels-smith, 1955)	Nig	Strf	Elas	Sicc	Lim Sup
0-11	0.165 – 0.055	Dark brown peat with abundant roots. Th ⁰ 3, Sh1, As+, Th ² +	3+	0	0	2+	-
11-20	0.055 – -0.035	Grey brown peaty clay with abundant roots. As2, Th ¹ 2, Sh+.	3	0	0	2+	0
20-42	-0.035 – -0.255	Blue grey slightly mottled silty clay with some rootlets. As2+, Ag1, Th ¹ ++, Lf+, Sh+.	2	0	0	2	0
42	-0.255	Bedrock.	-	-	-	-	-

5.2.2. Jadrtovac Site 2 (JD2)

An additional ‘type’ core was retrieved at Jadrtovac (JD2) near to the second contemporary transect established at this site (figure 3.5). A 56 cm core was sampled at an altitude of 0.245 m and was again drilled to bedrock. Five stratigraphic units were identified in this core, which similar to JD1, briefly comprised variable lower minerogenic sediments characterised by high silt and clay content, becoming increasingly more organic moving up through the core. A full Troëls-Smith (1955) description of JD2 core is provided in table 5.2 below.

Table 5.2. Lithology of JD2 ‘type’ core following Troëls-Smith (1955) classification.

Depth (cm)	Altitude m HVR571	Sediment description (after Troels-smith, 1955)	Nig	Strf	Elas	Sicc	Lim Sup
0-6	0.245 – 0.185	Dark brown, organic clay with abundant modern roots. As2, Sh1+, Th ⁰ 1.	3+	0	0	2+	-
6-19	0.185 – 0.055	Brown, light grey clay with abundant roots and organic detritus. As3, Th ⁰ 1, Sh+, Dh+.	2+	0	0	2+	0
19-56	0.055 – -0.315	Mottled grey orange brown clay with trace of silt and rootlets (slightly less rootlets and organic than above unit). As4, Ag+, Lf+, Th ¹ ++.	2+	0	0	2+	0
56	-0.315	Bedrock.	-	-	-	-	-

5.2.3. Blace (BL)

Similar to the location of the surface sediment transect BL1 at this site (figure 3.6), seven cores were drilled across a 20 m transect, extending from the high to low salt-marsh. All cores were again drilled to the underlying bedrock, and similarly increased in depth with distance towards the open sea with four main stratigraphic units identified (figure 5.3). Sediment accumulation was observed to be consistent across the salt-marsh at BL. The overall pattern of sedimentation is similar to JD1, where basal minerogenic silts and clays are overlain by increasingly organic sediments with humified peat-like deposits restricted to the upper salt-marsh. Between cores 5 and 7 (10–20 m along the transect) a basal coarse silt was again observed, which becomes saturated with depth, containing variable amounts of broken and whole shell fragments. Following the survey, a 32 cm ‘type’ core (BL) was collected from the upper salt-marsh environment at an altitude of 0.30 m (figure 5.4). A full description of BL core 2 is provided in table 5.3, comprising an organic silty clay bottom section overlain by a dark brown 9 cm-thick humified peat deposit towards the surface.

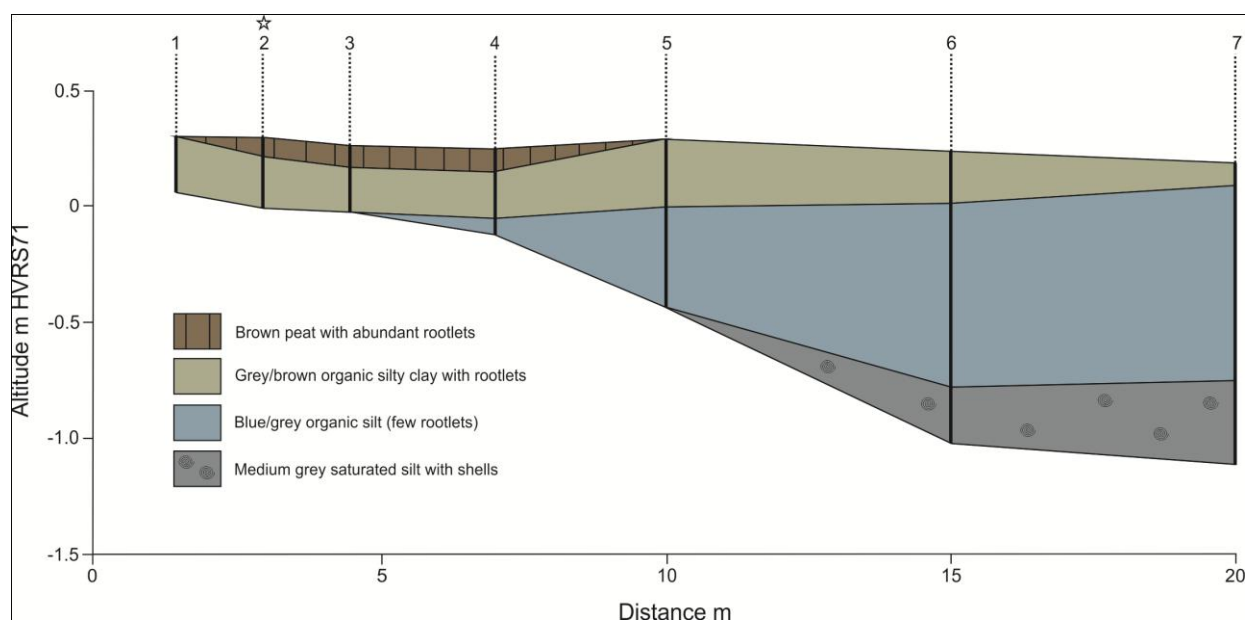


Figure 5.3. Simplified sediment stratigraphy at BL, plotted relative to altitude (m HVR71) from high (1) to low (7) salt-marsh. ‘Type’ core BL also highlighted (2).



Figure 5.4. Photograph of BL 32 cm ‘type’ core.

Table 5.3. Lithology of BL ‘type’ core following Troëls-Smith (1955) classification.

Depth (cm)	Altitude m HVR571	Sediment description (after Troëls-smith, 1955)	Nig	Strf	Elas	Sicc	Lim Sup
0-9	0.30-0.21	Dark brown peat with abundant rootlets and some clay. Th ¹ 3, As1, Sh+.	3+	0	0	3	-
9-28	0.21-0.02	Grey brown organic silty clay with abundant rootlets and occasional mottles. As2, Ag2, Th ¹ ++, Sh+, Lf+.	2+	0	0	3	0
28-32	0.02- -0.02	Dark brown organic peaty clay with abundant detrital stems and rootlets. Th ² 1, As1, Dh1, Ag1, Sh+.	3	0	0	2+	0
32	-0.02	Bedrock	-	-	-	-	-

5.3. FOSSIL FORAMINIFERA

5.3.1. Jadrtovac Site 1 (JD1)

Foraminifera are preserved throughout the entire 42 cm core at JD1, showing similar assemblages dominating the core sediments as those observed on the contemporary salt-marsh surface (figure 5.5). The major exception to this is the almost complete absence of *Quinqueloculina* spp. from the fossil record, which is found in abundance at the surface (figure 4.6). In total 15,733 individuals were counted and eleven species identified. The fossil foraminiferal record shows a clear up-core transition from a calcareous-dominated assemblage in the lower half of the core becoming replaced by agglutinated types at approximately 27 cm depth where a change from basal minerogenic clays and silts to increasingly organic sediments is observed. With a mean and maximum abundance of 1310 and 5510 individuals per 5 cm³, total concentration is significantly higher in the upper half of the core, with the lowest abundance occurring between depths 29 cm and 22 cm. A minimum count of 150 tests was achieved in all samples in this zone, apart from depths of 24-25 cm, 26-27 cm and 27-28 cm. The increase in foraminiferal abundance also corresponds to an increase in organic matter at a broadly similar depth, as illustrated by LOI values (see figure 5.8a).

Between depths 42 cm and 28 cm high abundances of *Ammonia* spp., *Elphidium* spp. and *Haynesina germanica* are observed before agglutinated types *J. macrescens* and *M. fusca* increase in relative abundance. The transition to agglutinated dominated assemblages at 27 cm is characterised by an increase in the relative abundance of *J. macrescens* to 76% and significant reduction in calcareous species *Ammonia* spp. and *Haynesina germanica* to 2% and 12%, respectively. Moving up through the core, agglutinated species dominate the remainder of the record. An increase in the relative abundance of *M. fusca* to 70% at 19 cm

corresponds to a decrease in *J. macrescens* (7%). Above this, an increase in *T. inflata* and *J. macrescens* towards the present-day surface is observed within an organic peat deposit. Indeed the present-day environment from which the core was retrieved shows similar species dominating the record (see figure 4.6).

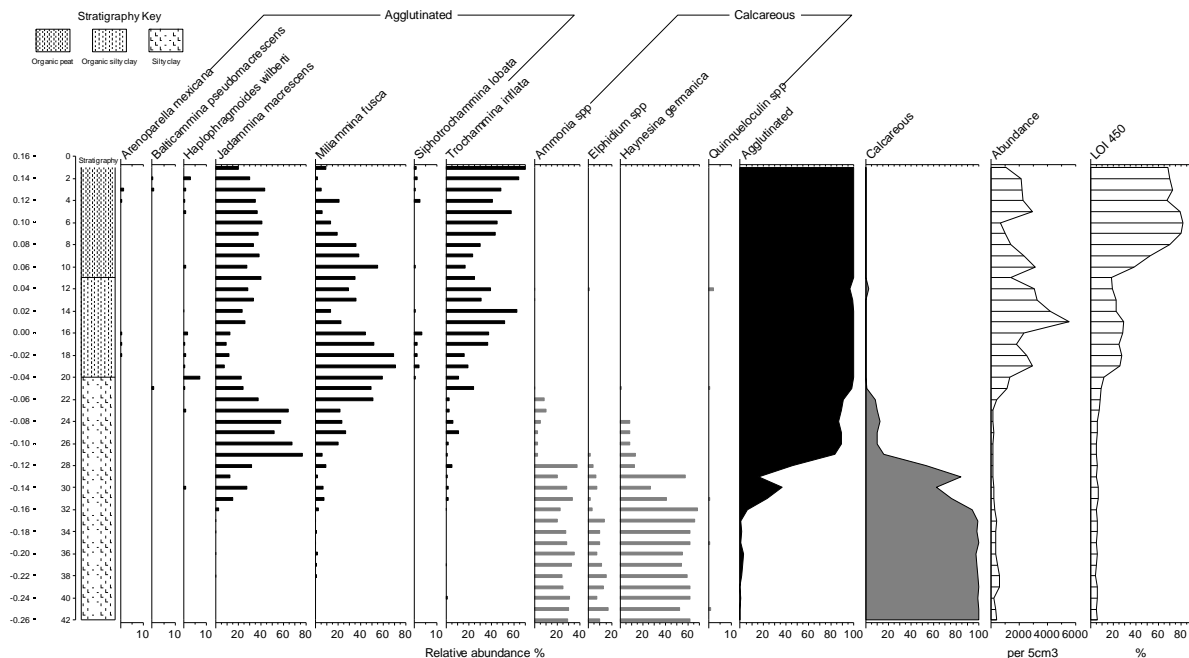


Figure 5.5. Fossil foraminiferal stratigraphy from core JD1 expressed as a percentage, ordered by depth (cm) and altitude (m HRS71). Simplified sediment stratigraphy, foraminiferal abundance (per 5 cm³) and LOI_{450°C} are also displayed.

5.3.2. Jadrtovac Site 2 (JD2)

Preservation of foraminifera extends the whole length (56 cm) of core JD2. Similar to JD1 core, species diversity was relatively low but again reflected that observed from the contemporary environment at Jadrtovac. The biostratigraphic record shows a very similar trend to JD1, with a change from calcareous types dominating the lower core sediments to agglutinated types moving up through the core, between approximately ~44 cm and ~25 cm, as shown in figure 5.6. Excluding the upper 1 cm, *Quinqueloculina* spp. is again absent from the fossil record, which again is common in the contemporary surface samples at this site (figure 4.7). In total, 38,823 individuals were counted, with 10 species identified. With a mean foraminiferal abundance of 2313 per 5 cm³, higher numbers were observed in the upper 30 cm of the record, peaking at 10,560 individuals per 5 cm³ at 5-6 cm depth. Below 30 cm the relative abundance decreases, with a mean abundance of 448 per 5 cm³. The lowest count observed was at 42-43 cm with 146 individuals per 5 cm³. The sample is

however included due to indicator species (*Ammonia* spp.) totalling more than 50% of the total count (63%).

Between 56 cm and 44 cm, the fossil record is composed almost entirely of calcareous species *Ammonia* spp., *Elphidium* spp. and *Haynesina germanica* within a basal silty/clay stratigraphic unit. A mixed foraminiferal assemblage between depths of 44 cm and 25 cm is observed where the relative increase in agglutinated species (*J. macrescens*, *M. fusca* and *T. inflata*) corresponds to a decrease in calcareous taxa (*Ammonia* spp., *Elphidium* spp. and *Haynesina germanica*). Above 25 cm, *T. inflata* dominates the record, peaking at 76% at 13-14 cm depth. *M. fusca* becomes increasingly common above 11 cm, increasing to 51 % of the overall count also corresponding to increasing LOI values.

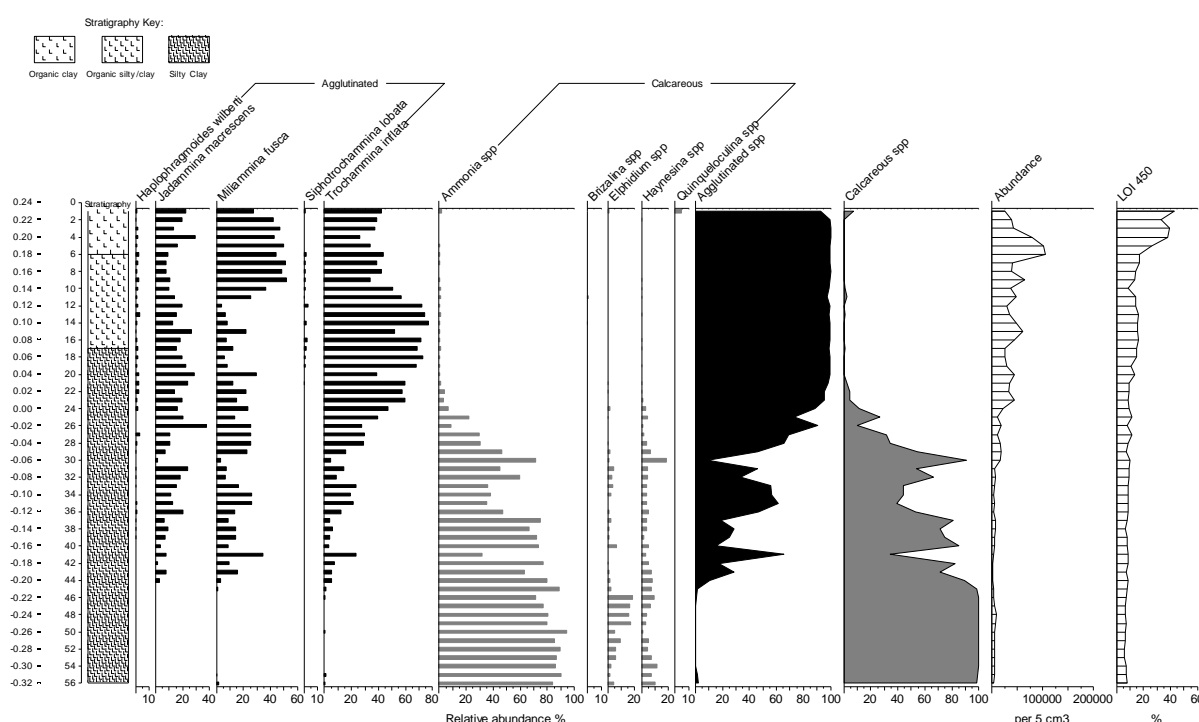


Figure 5.6. Fossil foraminiferal stratigraphy from core JD2 expressed as a percentage, ordered by depth (cm) and altitude (m HVR571). Simplified sediment stratigraphy, foraminiferal abundance (per 5 cm³) and LOI_{450°C} are also displayed.

5.3.3. Blace (BL)

Foraminifera were also well preserved throughout the 32 cm core at Blace where a total of 17,127 individuals were counted, with ten species identified (figure 5.7). Similar to JD1 and JD2, *Quinqueloculina* spp. is restricted to the upper 1 cm of the core. With a mean foraminiferal abundance of 1878 per 5 cm³, abundance is greater in the upper 12 cm of the core, peaking at 6315 per 5 cm³ at 6-7 cm depth. A minimum count was achieved in all

samples, except 26-27 cm where only 116 tests were observed. However no individual species totalled 50% or more, potentially making this sample obsolete in the sea-level reconstruction. This is unfortunate considering the key location of this depth in foraminiferal changes observed in the core. Calcareous foraminifera dominate the lower 4 cm of the core where *Ammonia* spp. is found in abundance, reaching 79% of the total count at 28-29 cm depth. The transition to agglutinated types (*J. macrescens*, *M. fusca* and *T. inflata*) occurs between 29 cm and 27 cm within silty clay stratigraphic unit. Above 26 cm agglutinated foraminifera dominate the record to the surface. *M. fusca* appears in abundance between 28 cm and 5 cm, peaking to 86 % of the total count at 18 cm. *T. inflata* shows a steady increase up-core, reaching 59% of the total count at 3-4 cm and 5-6 cm depth. *J. macrescens* is also found in abundance towards the top of the core, reaching 76% of the overall count at 2-3 cm depth also corresponding with elevated LOI values.

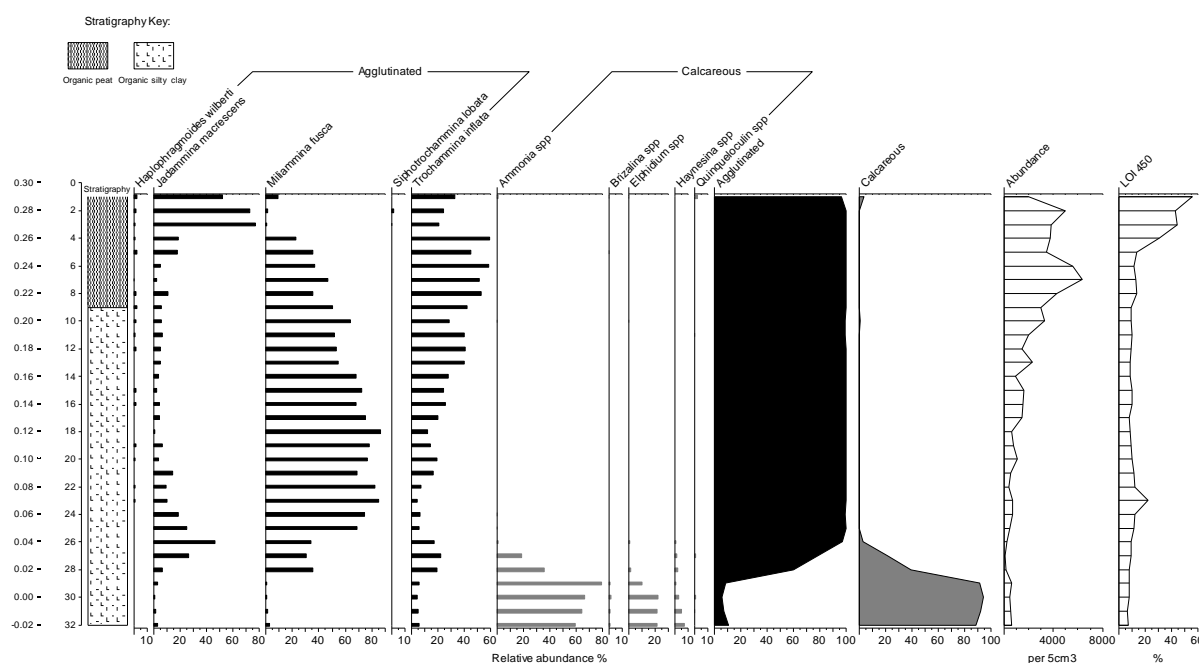


Figure 5.7. Fossil foraminiferal stratigraphy from core BL expressed as a percentage, ordered by depth (cm) and altitude (m HVR571). Simplified sediment stratigraphy, foraminiferal abundance (per 5 cm³) and LOI_{450°C} are also displayed.

5.4. ENVIRONMENTAL VARIABLES

5.4.1. Organic matter (LOI)

A clear increasing up-core trend in LOI is observed in core JD1 (figure 5.8a). The organic content from the bottom of the core remains very consistent up to approximately 20 cm,

rarely exceeding 8%. Between 19 cm and 12 cm LOI values then increase, peaking at 29% at a depth of 15 cm before rapidly increasing to 81% at 6 cm. The organic content then remains high to the top of the core, varying between 67% and 72%. A similar increasing up-core trend in organic matter is observed in core JD2 (figure 5.8b), albeit at lower values at depths compared to core JD1 and thus illustrating intra-site variability at Jadrtovac. Moving up through the core, organic content remains very similar up to a depth of 20 cm varying between 6% and 8%. A very minor increase in LOI values to 14% between 20 cm to 11 cm is then observed before values increase to the top of the core, varying between 37% and 42%. The organic content of the BL core again shows an increasing up-core trend as shown in figure 5.8c. From the base of the core, LOI values remain low (<10%) up to a depth of ~10 cm, despite a minor increase at 23 cm where the organic content rises to 22%. This ‘event’ in the record is also repeated in the down-core changes in particle size characteristics (figure 5.10c). Above 10 cm, LOI values then increase to the top of the core, ranging between 30% and 55%.

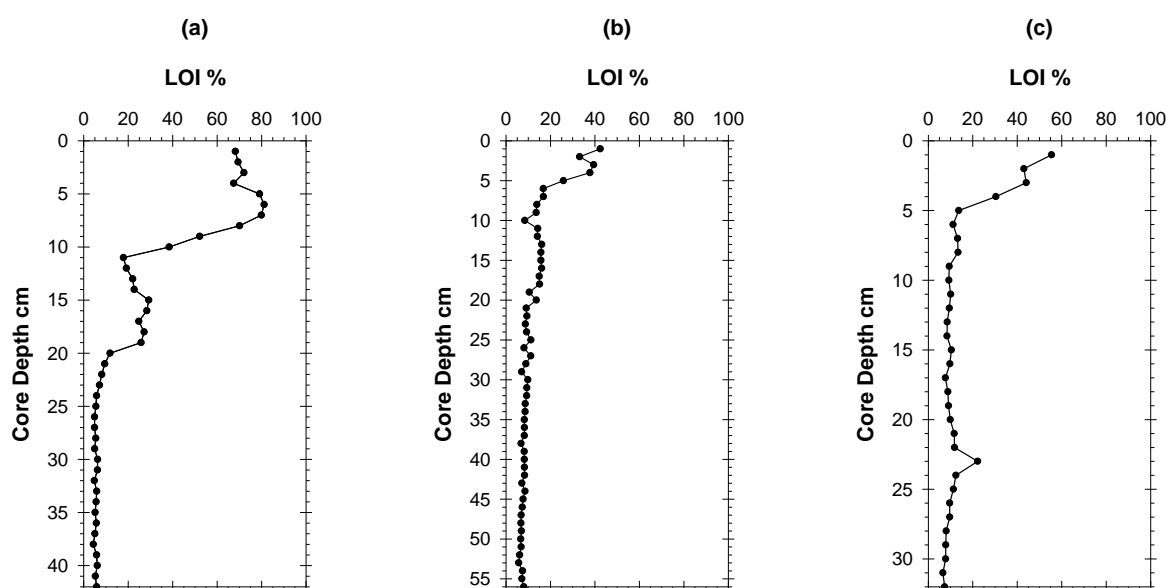


Figure 5.8. Down-core trends of LOI (%) for cores (a) JD1, (b) JD2 and (c) BL.

5.4.2. Dry Bulk-Density (DBD)

Moving up through core JD1, DBD shows a general decreasing trend towards the surface and can be divided into two sections (figure 5.9a). Below ~24 cm, DBD is relatively uniform; varying between 1.5 g/cm³ and 0.8 g/cm³. Above 24 cm, however, a decreasing trend from around 0.7 g/cm³ to 0.08 g/cm³ is observed. Similar to JD1, DBD in core JD2 decreases towards the surface, showing a divide at approximately 11 cm (figure 5.9b). Below 11 cm, DBD is relatively consistent, excluding depths 43, 45, 48, 49 and 54 cm. These samples

correspond to depths where a displacement method was used to achieve volume weights (see section 3.6). Excluding these depths, DBD varies between 1.7 g/cm³ and 1.2 g/cm³ (between 56 cm and 34 cm). Above 34 cm, a decreasing trend continues to approximately 11 cm (1.2-0.9 g/cm³) where DBD drops below 0.5 g/cm³. An overall up-core decreasing trend is also observed in core BL, as shown in figure 5.9c. The decreases in DBD at depths of 14, 18 and 23 cm and increases at 16, 19 and 27 cm are again an artefact of the displacement method used to achieve volumes. Excluding these samples, DBD is relatively uniform, ranging from 2.0 to 1.3 g/cm³ (between 32 and 10 cm). Above 10 cm DBD decreases to below 1.0 g/cm³ towards the top of the core (0.17 g/cm³ at 1 cm). All cores show the onset of decreasing DBD values that broadly correspond with notable increases in organic matter, as shown in figure 5.8.

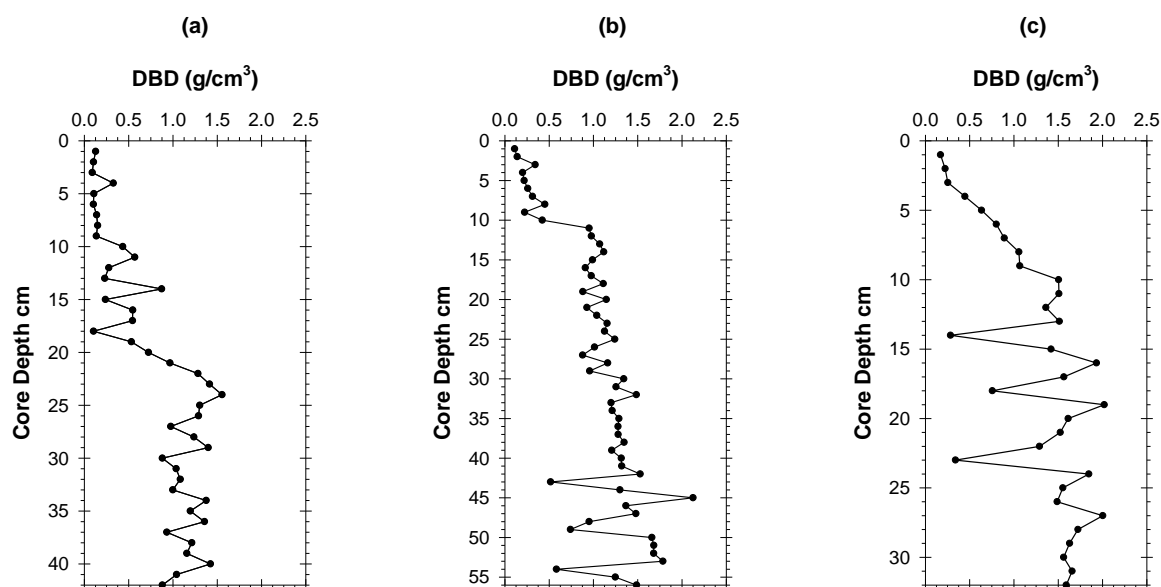


Figure 5.9. Down-core trends of DBD (g/cm³) for cores (a) JD1, (b) JD2 and (c) BL.

5.4.3. Particle Size Analysis (PSA)

Figure 5.10 shows down-core profiles of particle size characteristics for core JD1, JD2 and BL. The dominant size fraction throughout JD1 core is silt (figure 5.10a), accounting for over 72% in all samples, with the remaining component predominantly clay. The sand fraction remains insignificant throughout the core, with a minor peak at 5-6 cm to 2.6% corresponding to an increase in the mean grain size of the core to 9.6 μ m. Excluding this sample, the mean grain size for the core varies between 4 and 7 μ m (fine silt). A very uniform pattern of deposition is observed throughout core JD2 (figure 5.10b), where silt accounts for up to 81%. The remaining grain size fraction is almost exclusively clay, varying between 18% and 28%, with sand contributing very little (<0.1%) to the record. The mean

grain size for the core varies between 3 and 5 μm (very fine-fine silt). Both cores at Jadrtovac display symmetrical distributions which are poorly sorted. A notable feature of the particle size characteristics for core BL (figure 5.10c) is that whilst silt is again the overall dominant grain size fraction, the mean grain size is greater in comparison to cores JD1 and JD2. It also shows two distinct periods in the record in which the depositional environmental is interrupted by distinct increases in sand content. At depths 21 cm and 18 cm, sand content increases to 38% and 29%, corresponding to an increase in mean grain size for the core to 27 μm and 25 μm respectively. Clay content throughout the core varies between 8% and 19%. The more variable grain size fractions observed in core BL results in very poorly sorted and symmetrical to finely-skewed distributions.

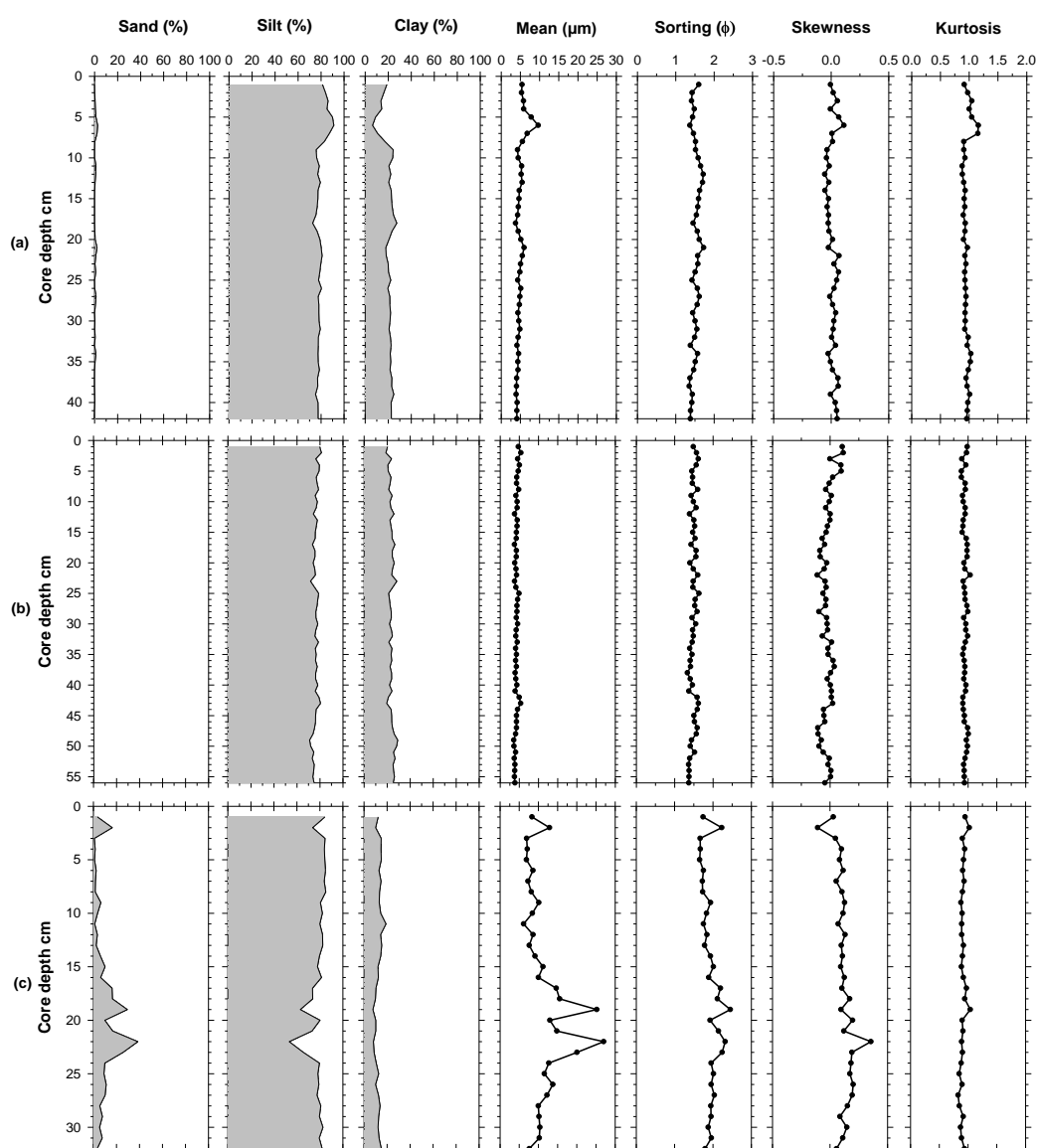


Figure 5.10. Down-core particle size data for cores (a) JD1, (b) JD2 and (c) BL showing percentage sand, silt, clay, mean grain size (μm), sorting (ϕ), skewness and kurtosis.

5.5. CORE CHRONOLOGY

To establish sediment chronologies for the analysed salt-marsh cores, a multi-proxy approach was employed to establish an age-depth relationship in sedimentation rate including short-lived radionuclides (^{210}Pb , ^{137}Cs and ^{241}Am), high-precision AMS ^{14}C dating (JD1) and potential pollution signals from geochemical evidence (XRF).

5.5.1. Short-lived Radionuclides

Figure 5.11 and table 5.4 show the results of the radiometric analyses for core JD1 where total ^{210}Pb activity reaches equilibrium with the supporting ^{226}Ra at a depth of approximately 20 cm. Unsupported ^{210}Pb concentrations, calculated by subtracting ^{226}Ra concentrations from the total ^{210}Pb concentrations, shows a declining trend with depth and records a discontinuity of some kind between 10-13 cm. Below 13 cm, concentrations decline more or less exponentially with depth, suggesting relatively uniform accumulation in the deeper sections of the core. The down-core profile of ^{137}Cs activity (figure 5.11c) shows a relatively well-defined maximum, peaking at 69.9 Bq kg^{-1} between 9-12 cm, that would appear to record the 1963 fallout peak from the atmospheric testing of nuclear weapons. Its presence as a double peak appears to be the consequence of the same event that affected the ^{210}Pb concentrations in this part of the core. As a result, the $^{137}\text{Cs}/^{210}\text{Pb}$ activity ratio (figure 5.11d) is sometimes a better guide (e.g. Plater and Appleby, 2004) to the fallout record where a clear defined peak between 10-12 cm is observed. A second, more recent ^{137}Cs peak of 57.1 Bq kg^{-1} at 5-6 cm is interpreted as fallout from the 1986 Chernobyl accident. Peaks in ^{137}Cs broadly correspond to those found from previous research in the Morinje Bay environment by Mihelčič et al. (2006) where maximum ^{137}Cs activity occurs within the upper 20 cm, albeit in lower concentrations.

Figure 5.12 and table 5.5 show the results of the radiometric analyses for core JD2 where total ^{210}Pb activity appears to reach equilibrium with the supporting ^{226}Ra at a depth of 7-8 cm, which was significantly shallower compared to JD1. An abrupt decline in unsupported ^{210}Pb concentrations below 5 cm (figure 5.12b) suggests a possible hiatus in the sediment record where concentrations fall below the level of detection in all sediments below 8 cm. Down-core profile of ^{137}Cs activity (figure 5.12c) shows a relatively well defined maximum to 81.9 Bq kg^{-1} between 5-6 cm that again presumably records the 1963 fallout peak from the atmospheric testing of nuclear weapons. Unlike JD1, a second peak recording fallout from the 1986 Chernobyl accident is not obvious, apart from perhaps occurring between 2-5 cm where ^{137}Cs activities remain high ($57\text{-}63 \text{ Bq kg}^{-1}$).

Figure 5.13 and table 5.6 show the results of the radiometric analyses for core BL where total ^{210}Pb activity appears to reach equilibrium with the supporting ^{226}Ra at a depth of around 13 cm. Activities of unsupported ^{210}Pb decline more or less exponentially with depth and indicate a relatively uniform sedimentation rate over the past 100 years or so. The down-core profile of ^{137}Cs activity (figure 5.13c) shows a relatively well-defined maximum value of 109.5 Bq kg^{-1} at 6-7 cm depth. This also corresponds to a similar but smaller peak in ^{241}Am activities (4.7 Bq kg^{-1}) at the same depth, which almost certainly records the 1963 fallout peak from weapons testing. A smaller and more recent ^{137}Cs peak (94.0 Bq kg^{-1}) at 4-5 cm is again interpreted as fallout from the 1986 Chernobyl accident.

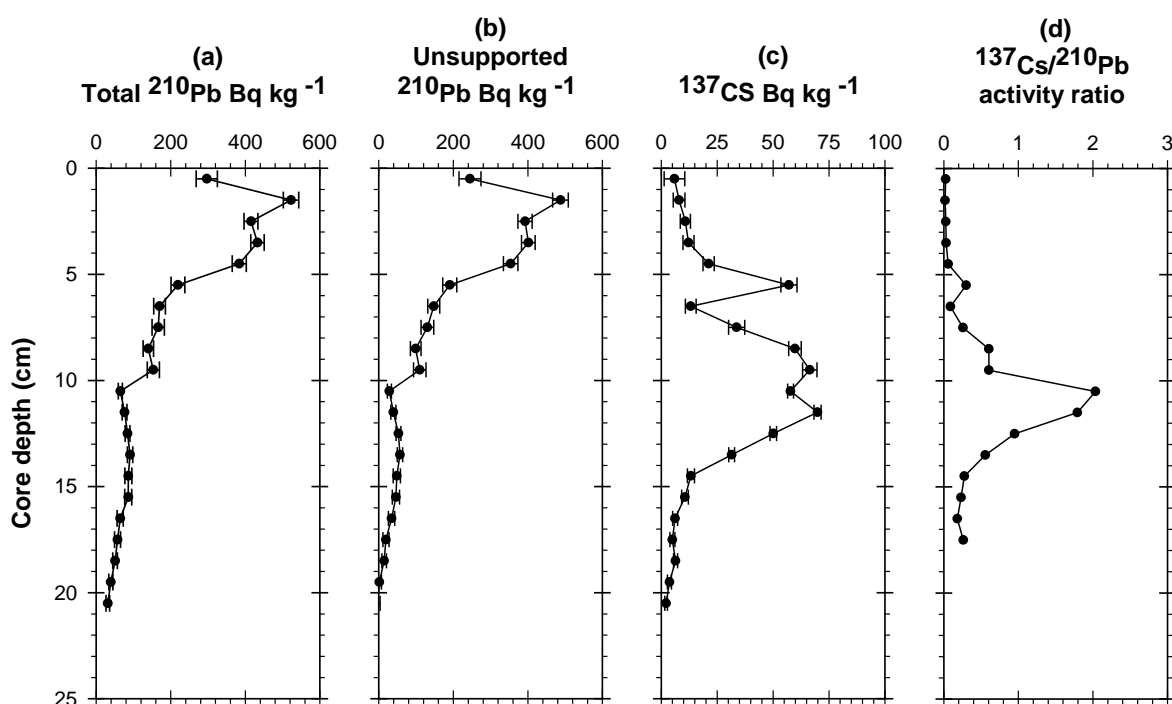


Figure 5.11. Fallout radionuclides of the JD1 core showing (a) total ^{210}Pb , (b) unsupported ^{210}Pb , (c) ^{137}Cs concentrations and (d) $^{137}\text{Cs}/^{210}\text{Pb}$ activity ratio versus depth.

Table 5.4. Fallout radionuclide activities of the JD1 core.

Depth cm	g cm ⁻²	²¹⁰ Pb						¹³⁷ Cs	
		Total Bq kg ⁻¹	±	Unsupported Bq kg ⁻¹	±	Supported Bq kg ⁻¹	±	Bq kg ⁻¹	±
0.5	0.06	296.7	28.4	244.6	29.5	52.0	7.8	5.9	4.6
1.5	0.18	522.5	20.7	487.4	21.1	35.1	4.1	8.0	2.6
2.5	0.27	415.2	18.7	392.3	19.0	22.9	3.4	10.8	2.3
3.5	0.48	432.5	18.0	401.2	18.3	31.3	3.6	12.2	2.5
4.5	0.70	383.6	18.9	353.7	19.3	29.9	3.7	21.2	2.5
5.5	0.80	219.2	18.4	190.3	18.9	28.9	4.4	57.1	3.6
6.5	0.92	169.8	15.6	147.3	16.0	22.5	3.4	13.2	2.4
7.5	1.06	166.4	16.4	130.3	16.9	36.1	4.0	33.7	3.6
8.5	1.20	139.8	13.9	99.0	14.3	40.7	3.5	59.8	2.8
9.5	1.49	153.2	16.2	109.8	16.6	43.5	3.8	66.4	3.2
10.5	1.99	64.7	5.4	28.4	5.5	36.3	1.2	57.8	1.3
11.5	2.41	76.0	6.6	39.0	6.8	37.0	1.6	69.9	1.6
12.5	2.66	84.1	6.4	52.8	6.5	31.2	1.3	50.1	1.5
13.5	3.21	90.7	7.2	56.7	7.3	34.1	1.5	31.5	1.3
14.5	3.77	86.2	9.3	48.2	9.6	38.0	2.4	13.3	1.6
15.5	4.16	85.9	9.5	45.9	9.8	40.0	2.3	10.6	1.5
16.5	4.70	64.3	8.2	34.3	8.4	30.0	1.8	6.2	1.1
17.5	5.02	57.0	8.0	19.1	8.2	37.9	1.8	5.0	1.1
18.5	5.34	50.7	6.2	14.4	6.3	36.3	1.5	6.4	0.9
19.5	5.96	39.3	5.3	1.4	5.5	38.0	1.3	3.7	0.9
20.5	6.81	31.1	4.7	-1.4	4.8	32.5	0.8	2.2	0.6

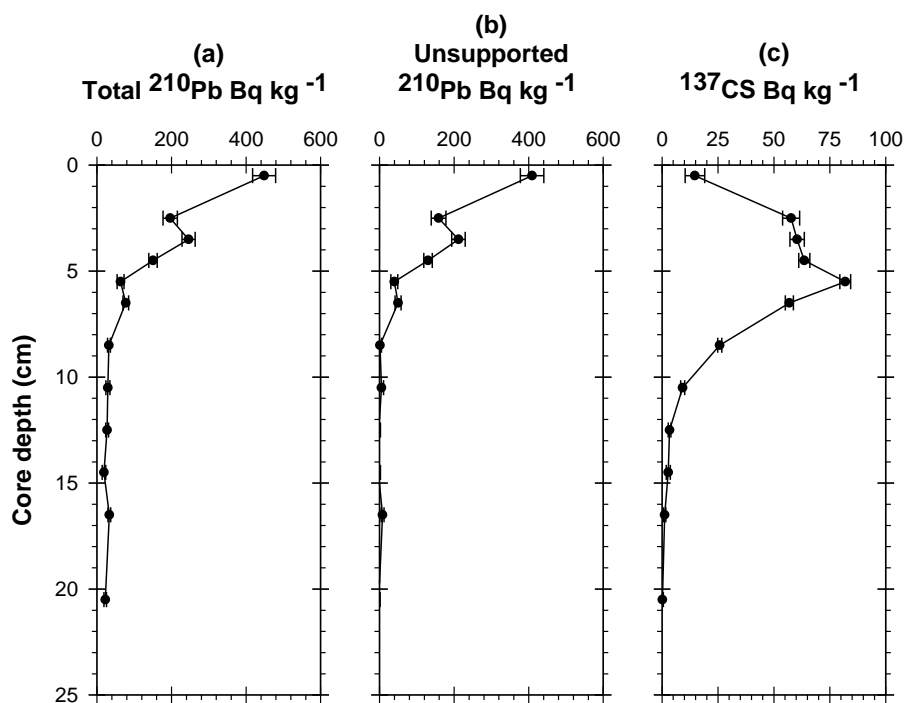
**Figure 5.12.** Fallout radionuclides of the JD2 core showing (a) total ²¹⁰Pb, (b) unsupported ²¹⁰Pb and (c) ¹³⁷Cs concentrations versus depth.

Table 5.5. Fallout radionuclide activities of the JD2 core.

Depth cm	$g\ cm^{-2}$	^{210}Pb						^{137}Cs	
		Total $Bq\ kg^{-1}$	\pm	Unsupported $Bq\ kg^{-1}$	\pm	Supported $Bq\ kg^{-1}$	\pm	$Bq\ kg^{-1}$	\pm
0.5	0.05	448.2	30.8	409.0	31.5	39.2	6.6	14.7	4.4
2.5	0.42	196.2	19.2	158.2	19.7	37.9	4.5	57.7	3.8
3.5	0.69	245.8	17.6	211.7	18.0	34.1	3.5	60.4	3.2
4.5	0.89	150.2	11.2	129.9	11.4	20.3	2.0	63.6	2.5
5.5	1.13	63.1	9.1	39.5	9.4	23.6	2.1	81.9	2.4
6.5	1.41	77.1	7.7	49.5	7.9	27.6	1.8	56.9	1.8
8.5	2.13	32.0	3.7	1.1	3.9	30.9	1.1	25.8	0.9
10.5	3.14	29.2	5.5	5.0	5.7	24.1	1.3	9.2	0.9
12.5	5.14	27.2	3.8	-1.7	3.9	28.9	1.0	3.4	0.6
14.5	7.28	18.7	4.9	-2.9	5.0	21.6	1.1	2.8	0.9
16.5	9.17	33.2	3.6	8.0	3.7	25.2	0.8	1.2	0.5
20.5	13.25	22.2	3.4	-1.9	3.5	24.2	0.8	0.2	0.4

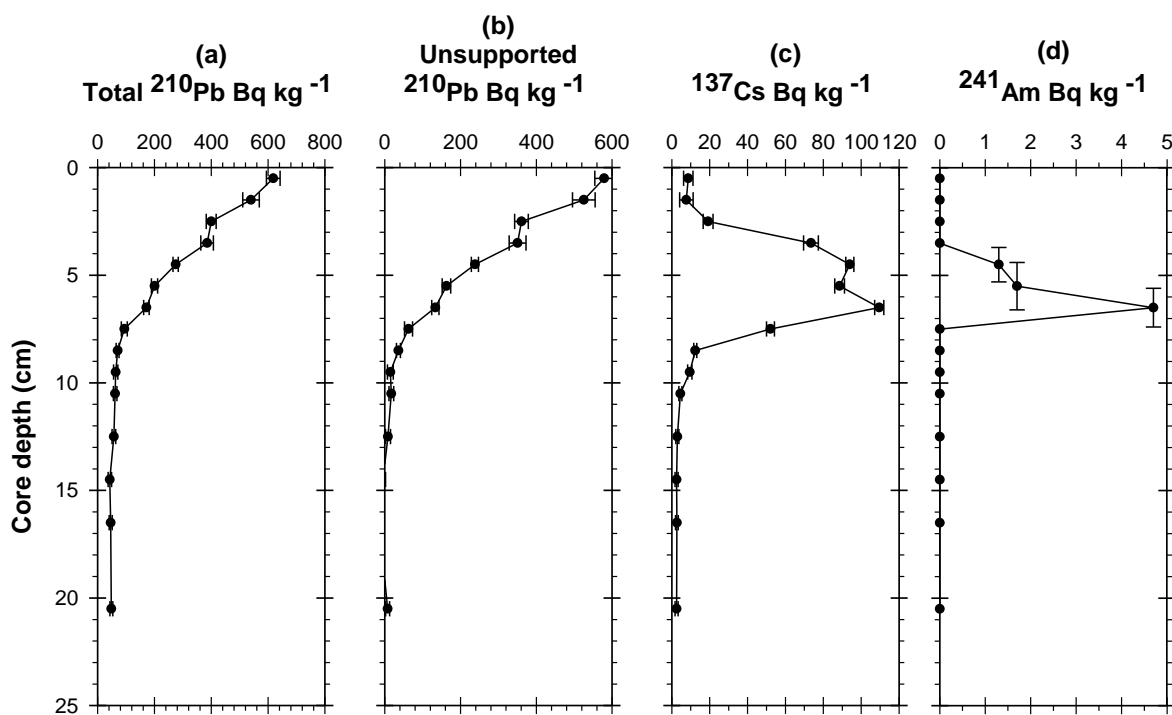
**Figure 5.13.** Fallout radionuclides of the BL core showing (a) total ^{210}Pb , (b) unsupported ^{210}Pb , (c) ^{137}Cs and (d) ^{241}Am concentrations versus depth.

Table 5.6. Fallout radionuclide activities of the BL core.

Depth		²¹⁰ Pb						¹³⁷ Cs		²⁴¹ Am	
		Total		Unsupported		Supported		Bq kg ⁻¹	±	Bq kg ⁻¹	±
		Bq kg ⁻¹	±	Bq kg ⁻¹	±	Bq kg ⁻¹	±				
0.5	0.1	618.1	24.1	579.1	24.5	39.0	4.4	8.7	2.5	0.0	0.0
1.5	0.3	539.5	29.3	525.3	29.9	14.2	6.0	7.7	3.6	0.0	0.0
2.5	0.5	399.5	17.6	360.8	18.0	38.7	3.7	19.2	2.6	0.0	0.0
3.5	0.9	385.1	22.1	350.5	22.4	34.6	3.7	73.5	3.9	0.0	0.0
4.5	1.4	274.5	9.4	237.9	9.5	36.5	1.5	94.0	2.1	1.3	0.8
5.5	2.1	200.1	11.0	162.7	11.2	37.3	2.2	88.6	2.6	1.7	1.1
6.5	3.0	171.4	9.5	133.3	9.7	38.0	2.0	109.5	2.4	4.7	0.9
7.5	3.9	93.7	10.3	62.5	10.5	31.2	2.0	52.1	2.1	0.0	0.0
8.5	5.0	70.2	5.2	35.9	5.4	34.3	1.2	12.4	0.8	0.0	0.0
9.5	6.3	63.3	7.4	14.6	7.6	48.7	1.8	9.5	1.1	0.0	0.0
10.5	7.8	61.4	6.0	17.2	6.2	44.1	1.4	4.5	0.8	0.0	0.0
12.5	10.7	56.9	6.4	8.3	6.6	48.6	1.6	2.9	0.8	0.0	0.0
14.5	13.6	42.6	6.1	-4.6	6.3	47.2	1.7	2.5	0.8	0.0	0.0
16.5	17.0	45.7	5.4	-14.5	5.6	60.2	1.5	2.7	0.7	0.0	0.0
20.5	24.0	47.9	5.1	7.4	5.2	40.5	1.2	2.5	0.8	0.0	0.0

5.5.2. X-ray fluorescence (XRF)

Down-core changes in element concentrations were investigated to identify pollution signals from which to provide further potential chronological constraints within the sediment records. Figure 5.14 shows down-core profiles of heavy metal concentrations (Cu, Pb and Zn) for cores JD1, JD2 and BL as a comparison to previous work investigating anthropogenic signals in the geochemical record. Section 3.7 discussed the use of agrichemicals and in particular copper sulphate in reducing vineyard mildew. Moving up through the core, an increasing trend in Cu concentrations is observed in JD1 (figure 5.14a), peaking to 94 ppm at 12 cm. Indeed elevated levels of Cu occur between approximately 5 cm and 15 cm and is similar to that observed by Mihelčič et al. (2006). JD2 also shows an up-core increasing trend in Cu (figure 5.14b), increasing from approximately 20 cm to a peak of 118 ppm at 5 cm. The elevated and sustained concentrations of Cu to the surface, compared to JD1, probably reflect this site's close proximity to vineyards in the northern part of the region which are extremely close to the edge of the salt-marsh environment.

The record at BL (figure 5.14c) shows a very uniform accumulation of Cu with no distinct peak observed. No agricultural activities are practised in the immediate vicinity to Blace and the lack of available documented history surrounding the sample site limits the utility of XRF in providing independent age markers. Background levels of Cu are very similar throughout all the studied cores, suggesting the increased but not especially high levels of Cu in cores JD1 and JD2 reflect localised vineyard activity. A decrease in Pb is observed towards the

surface of all cores, reflecting a trend observed by Mihelčič et al. (2006) and Šparica et al. (2005a: b) who attributed the decrease to anthropogenic influences. Whilst concentrations in Cu might reflect agricultural activity in the surrounding environment, similar to that observed by Šparica et al. (2005a: b), Mihelčič et al. (2006) and Miko et al. (2007), no specific date is provided by the authors from documented evidence of land-use change. Based on their ^{137}Cs profile, Mihelčič et al. (2006) date a decrease in Pb concentration to approximately 1980 whilst no satisfactory evidence was found to describe a peak in Cu concentration other than it is simply a reflection of localised anthropogenic land-use activity over the past 50 years.

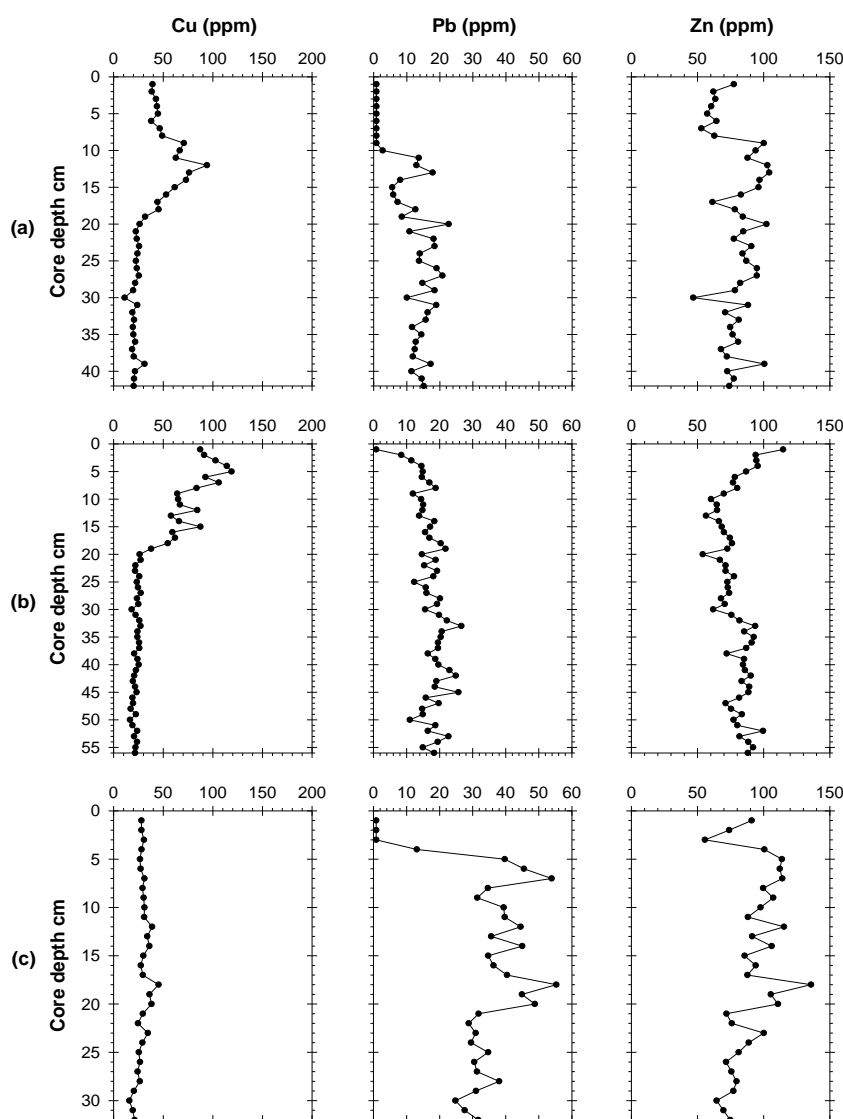


Figure 5.14. Cu, Pb and Zn profiles for (a) JD1, (b) JD2 and (c) BL cores.

5.5.3. Jadrtovac Site (JD1) Chronology

Figure 5.15 and table 5.7 shows the chronology for core JD1 based on the radiometric analyses presented in section 5.5.1. Lead-210 dates calculated using the CRS dating model (Appleby and Oldfield, 1978) place 1963 at a depth of 11.5 cm and 1986 at a depth of 5.5 cm, evidently in good agreement with the depths suggested by the ^{137}Cs record. With a mean volumetric accumulation rate of 0.25 cm y^{-1} , post-1960 sedimentation is fairly uniform, showing a mean dry mass sedimentation rate of around $0.032 \text{ g cm}^{-2} \text{ y}^{-1}$. The reduction in the ^{210}Pb and ^{137}Cs concentrations between 10-12 cm is attributed to a brief episode of increased sedimentation dated to the mid- to late 1960s, possibly caused by the remobilisation and deposition of a layer of older material. Prior to 1960, dates become more problematic. An increase in dry bulk density below 19 cm (figure 5.9a) in combination with the disappearance of unsupported ^{210}Pb (figure 5.11b) suggests a hiatus in the sediment record. Calculations of the mean pre-1960 accumulation using the gradient of the unsupported ^{210}Pb activity versus depth profile between 13-19 cm date this interruption to the late 19th century. Pre-1960 dates were calculated using this and the 1963 ^{137}Cs date as reference points (Appleby, 2002). The results are relatively unambiguous down to a depth of 16 cm, dated to 1920. The uncertainty of age estimates increases below this depth and are regarded with caution unless supported by other evidence.

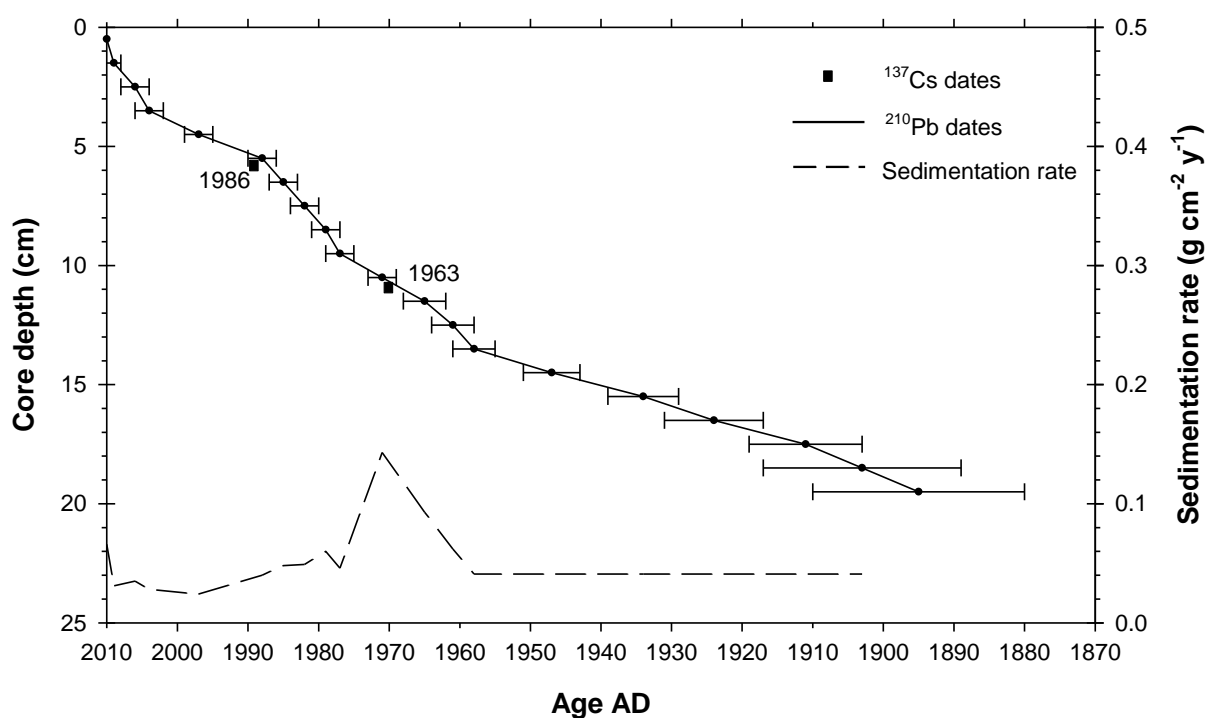


Figure 5.15. Radiometric chronology for JD1 showing CRS model ^{210}Pb dates, sedimentation rate ($\text{g cm}^{-2} \text{ y}^{-1}$) and the 1963 and 1986 depths suggested by ^{137}Cs record.

Table 5.7. Combined ^{210}Pb (CRS) and ^{137}Cs chronology of the JD1 core.

Depth		Chronology			Sedimentation rate		
Cm	g cm ⁻²	Date	Age		g cm ⁻²	cm y ⁻¹	± (%)
		AD	y	±			
0.0	0.00	2010	0	0			
0.5	0.06	2009	1	1	0.066	0.38	12.5
1.5	0.18	2006	4	2	0.031	0.40	5.6
2.5	0.27	2004	6	2	0.035	0.22	6.1
3.5	0.48	1997	13	2	0.028	0.13	6.3
4.5	0.70	1988	22	2	0.024	0.17	7.6
5.5	0.80	1985	25	2	0.040	0.33	11.4
6.5	0.92	1982	28	2	0.048	0.33	12.4
7.5	1.06	1979	31	2	0.049	0.40	14.5
8.5	1.20	1977	33	2	0.060	0.25	16.0
9.5	1.49	1971	39	2	0.046	0.17	16.7
10.5	1.99	1965	45	3	0.143	0.20	21.1
11.5	2.41	1961	49	3	0.093	0.29	19.6
12.5	2.66	1958	52	3	0.062	0.15	15.7
13.5	3.21	1947	63	4	0.041	0.09	
14.5	3.77	1934	76	5	0.041	0.09	
15.5	4.16	1924	86	7	0.041	0.09	
16.5	4.70	1911	99	8	0.041	0.09	
17.5	5.02	1903	107	14	0.041	0.09	
18.5	5.34	1895	115	15	0.041	0.09	

5.5.3.1. Radiocarbon Dating

Between depths 18 cm and 33 cm, a varying abundance of *Scirpus holoschoenus* seeds (figure 3.8), a common salt-marsh plant of the eastern Adriatic coast (Pandža et al., 2007), was found in core JD1. Depths and dry weights of these seeds are shown in table 5.8. These intervals, whilst not extending the full 42 cm length of the core, would potentially provide ages for sediments beyond the limits of the current radiometric chronology which was restricted to the upper ~20 cm as described above. As radiocarbon years are generally longer than calendar years, due to variations in the production of atmospheric ^{14}C , reported conventional ^{14}C dates need to be calibrated using a calibration curve (e.g. McCormac et al., 2007; Reimer et al., 2009). Differences in the natural concentration of ^{14}C between the northern and southern hemispheres, referred to as inter-hemispheric ^{14}C offsets, mean different calibration curves are available depending on the site's location (Hua, 2009). The current internationally accepted calibration curve for the southern hemisphere is SHCal04 (McCormac et al., 2007) whilst in the northern hemisphere, IntCal09 (Reimer et al., 2009) is used. The IntCal09 calibration curve is based on a large-number of ^{14}C dates obtained from dendro-dated tree rings and is used for age determinations over the past 12,550 cal BP (Blaauw and Heegaard, 2012).

Table 5.8.

Depths and dry weights (mg) at which *Scirpus holoschoenus* seeds were found in core JD1.

Depth (cm)	Material to date	Dry weight (mg)
18-19 cm	<i>Scirpus holoschoenus</i> seeds	0.2
21-22 cm	<i>Scirpus holoschoenus</i> seeds	0.8
25-26 cm	<i>Scirpus holoschoenus</i> seeds	4.1
26-27 cm	<i>Scirpus holoschoenus</i> seeds	10.5
27-28 cm	<i>Scirpus holoschoenus</i> seeds	1
28-29 cm	<i>Scirpus holoschoenus</i> seeds	1.2
29-30 cm	<i>Scirpus holoschoenus</i> seeds	3.8
30-31 cm	<i>Scirpus holoschoenus</i> seeds	0.8
31-32 cm	<i>Scirpus holoschoenus</i> seeds	0.1
32-33 cm	<i>Scirpus holoschoenus</i> seeds	0.3

*Bold font denotes depth intervals dated by AMS ^{14}C . Samples between 28-30 cm were combined to achieve sufficient dry weight needed for analysis.

Fluctuations (i.e. wiggles) in the concentration of atmospheric ^{14}C between AD 1650 to AD 1950 hinder the application of ^{14}C dating for the recent past as several calendar age ranges are theoretically plausible for a single ^{14}C age. In this case, using the ‘intercept method’ to simply interpret the radiocarbon age is therefore not recommended (Telford et al., 2004b). If however, dates are acquired from a sequence of sediments spaced close together, we can adopt a Bayesian approach (e.g. Buck et al., 1991; Buck et al., 1992; Bronk Ramsey, 2001; Blaauw and Christen, 2005) and use additional information such as chronological and stratigraphic ordering (referred to as *a priori* knowledge) and assume the logical principal that the lowermost sample to have been deposited first, thus producing the oldest age (Reimer and Reimer, 2007; Bronk Ramsey, 2008). Following Stuiver and Polach (1977) conventional radiocarbon ages are first reported in uncalibrated form and shown in table 5.9 below.

Table 5.9. AMS ^{14}C results for core JD1 (NERC allocation number 1678.1012).

Publication no.	Sample Identifier (depth cm)	^{14}C Enrichment (% modern $\pm 1\sigma$)	Conventional ^{14}C Age (years BP $\pm 1\sigma$)	$\delta^{13}\text{C}_{\text{VPDB}}\text{‰}$ ± 0.1
SUERC45020	(1) JD1 25-26	96.86 \pm 0.44	256 \pm 37	-25.3
SUERC45021	(2) JD1 26-27	97.38 \pm 0.45	213 \pm 37	-26.2
SUERC45022	(3) JD1 28-30	98.61 \pm 0.45	112 \pm 37	-26.8

Sample 1 (JD1 25-26) has a reported (uncalibrated) ^{14}C age of 256 (± 37) years BP, whilst sample 2 (JD1 26-27) and 3 (JD1 28-30) have reported (uncalibrated) ^{14}C ages of 213 (± 37) and 112 (± 37) years BP, respectively. At first glance, it would appear the results obtained from AMS ^{14}C dating to be counterintuitive, with the oldest age reported for the uppermost (theoretically youngest) sample. However, using *a priori* knowledge of stratigraphic position

and chronological ordering, we would assume date 3 to be older than date 2, and date 2 to be older than date 1. It can also be assumed that all dates reported probably originate from before the period ~AD 1900 as the sediments analysed should pre-date the limits of the ^{210}Pb and ^{137}Cs chronology, which extends to a depth of approximately 20 cm (see section 5.5.3).

Due to the non-linear relationship between radiocarbon and calendar years, the above results highlight the importance of conventional radiocarbon age calibration (Reimer et al., 2009). This is especially true where the data are to be incorporated into an age-depth model, as uncalibrated (raw) ^{14}C ages will often result in multi-peaked calendar age uncertainties (Telford et al., 2004a; Blaauw, 2010; Blaauw and Heegaard, 2012). Calibration can be performed using an array of dedicated calibration packages as well as being integrated into many age-depth modelling software (e.g. *Clam*; Blaauw, 2010). In this instance, conventional radiocarbon dates are calibrated using *OxCal* version 4.2 (Bronk Ramsey, 2009a) using the *IntCal09* calibration curve (Reimer et al., 2009). *OxCal* offers a Bayesian approach to deposition models in which *a priori* information (e.g. stratigraphic position) can be utilized to constrain the ages of ^{14}C dates (Bronk Ramsey, 2008). Using *a priori* knowledge of chronological and stratigraphic ordering, calibrated ^{14}C age distributions now appear in correct chronological order as shown in figure 5.16 below.

While it is often desirable to reduce calibrated ^{14}C ages to single calibrated year point estimates, especially in the context micropalaeontological studies, the asymmetric nature of calibrated ^{14}C distributions means reducing them to single-ages poses significant risks (Telford et al., 2004b). Indeed this is amplified when drawing a curve through single year point estimates in age-depth models because it does not consider the full potential of the calibrated ^{14}C age distribution. Following Blaauw (2010), calibrated ^{14}C ages are therefore reported as age distributions to 2 standard deviations (σ) (c. 95% probability) rather than 1σ (68% probability), as the probability of the 'true' calendar date falling outside 1σ range (c. 32%) cannot be overlooked. As ^{14}C dates were acquired from a stratigraphic position below the limits of an independently dated (^{210}Pb) layer at 20 cm (~AD 1900), interceptions with the calibration curve post ~AD 1900 can safely be neglected. Calibrated distributions of ^{14}C date SUERC45020 (JD1 25-26; 256 ± 37) shows highest *posterior* density ranges between cal. AD 1764-1805 (95.4% probability). Calibrated distributions of ^{14}C date SUERC45021 (JD1 26-27; 213 ± 37) shows highest *posterior* density ranges between cal. AD 1742-1800 (95.4% probability) while calibrated distributions of ^{14}C date SUERC45022 (JD1 28-30; 112 ± 37) ranges between cal. AD 1692-1784 (95.4% probability). Median dates are also provided for reference (see figure 5.16). Reported agreement level indexes are all above the accepted

limit of 60% (Bronk Ramsey, 2008) necessitating the need for outlier analysis (e.g. Bronk Ramsey, 2009b).

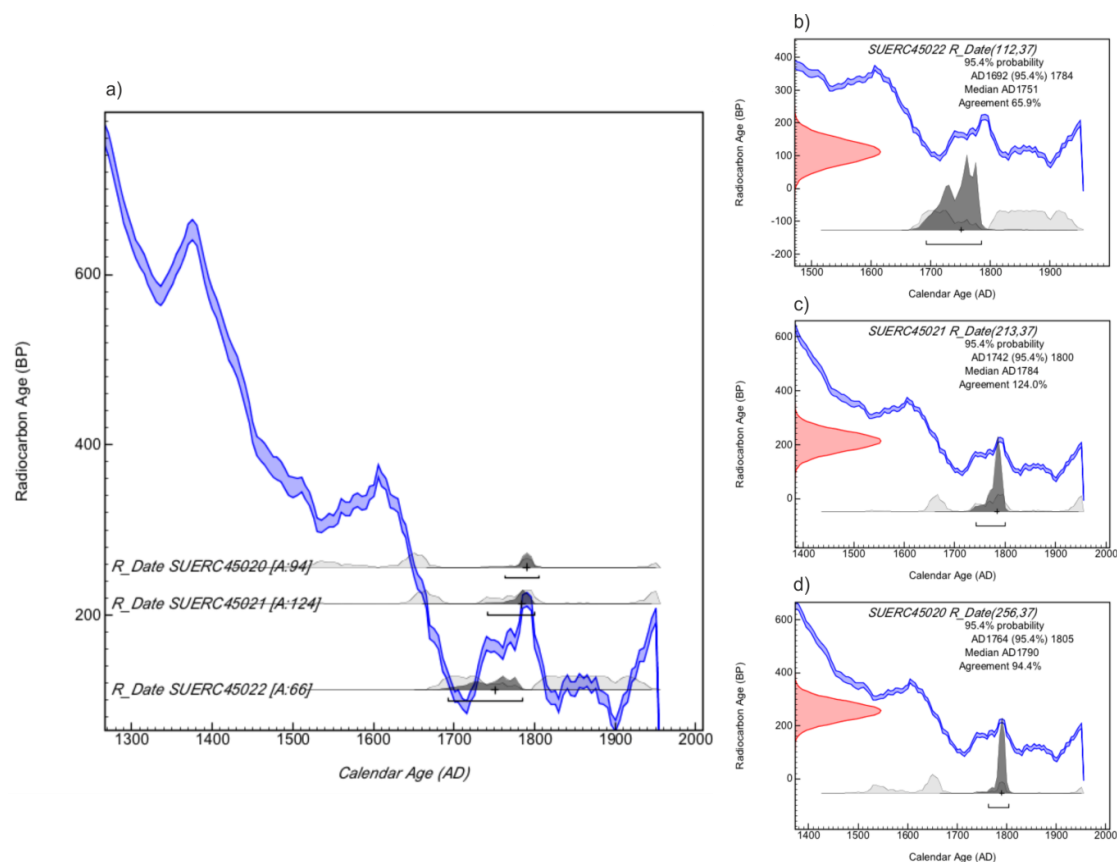


Figure 5.16. OxCal (Bronk Ramsey, 2009a) calibration of ^{14}C ages showing (a) ^{14}C ages intercepting IntCal 09 calibration curve (Reimer et al., 2009) and (b, c and d) individual calibration plots displaying Gaussian distribution of uncalibrated ^{14}C ages (red curve), IntCal 09 calibration curve (blue curve) (Reimer et al., 2009) and highest *posterior* density ranges (2σ c. 95% probability) of calibrated ages (dark grey curve). Median age (AD) and agreement level indexes are also provided.

Following the above, age-depth models were created combining the short-lived radionuclide data with calibrated ^{14}C age distributions to further extend the record at JD1. The purpose of constructing age-depth models is to present an interpolated chronological framework to provide ages between a series of dated points that may be derived from a variety of sources (Blaauw, 2010). The model can then be used to give age estimates for both the dated levels and undated levels and extrapolated throughout a core sequence (Blaauw and Heegaard, 2012). To assess the accuracy in modelling accumulation rate through time, two models were created, adopting ‘classical’ and Bayesian approaches. The use of geochemical markers is not included due to their inability to provide accurate independently dated depths.

5.5.3.2. *Clam* Age-Depth Model

Clam (version 2.1; Blaauw, 2010) is an open source environmental statistics package used within the *R* framework (R Development Core Team, 2013). It offers a rapid, non-Bayesian ‘classical’ approach to age-depth modelling and is useful before Bayesian techniques are explored (e.g. Hua et al., 2012). Prior to modelling, calibration of single ^{14}C dates within the software using the IntCal09 calibration curve (Reimer et al., 2009) are performed in a similar way to that offered by *OxCal* (Bronk Ramsey, 2009a) (e.g. 2σ c. 95% probability) presented above. *Clam* offers the user various different modelling approaches to estimate the ages of non-dated points. These are selected based on the user’s requirements and type depositional environment and include linear interpolation, linear or polynomial regression and various types of spline approaches (e.g. smooth or locally weighted). Monte Carlo sampling selects ages from each of the calibrated age distributions to produce an age-depth model through the sampled dates (Blaauw, 2010). An adjustable ‘smoothing’ parameter allows further adaptations in the rigidity/flexibility of the age model. Other features such as the top of a core sequence (e.g. year of sampling) can provide an additional anchor points (Blaauw, 2010).

Following the above, various age-depth models were created and their performance was assessed in constructing an accurate model through the dated levels. The output from *Clam* provides the user with various information about the model runs including model settings, age estimations and graphs. Of particular interest though is the “goodness-of-fit” value which provides a measure of the probabilities of the modelled ages of the dated depths and in general, the lower this value, the better the age-model performance (Blaauw, 2010). Figure 5.17 shows the results of the smooth spline age-depth model with a ‘smoothing’ of 0.6. This type of model assumes relatively stable accumulation rates throughout the depositional history of a core sequence. Extrapolation beyond the dated levels has not been performed, following Blaauw (2010), and is restricted to the upper 28 cm of the core. Calendar ^{14}C age distributions are shown in blue and the ^{210}Pb and ^{137}Cs chronology in green. The solid black line depicts the ‘best’ age-depth model within a 2σ age uncertainty range (shaded grey area) and calendar age estimations are provided for all depths (to 2σ) based on weighted average of all depth curves. The smooth spline model returns a “goodness-of-fit” value of 22.97. A calculated mean sedimentation rate of 0.13 cm yr^{-1} is reported for the core (to 28 cm). Moving up through the core, sedimentation rates are relatively stable between depths 28 cm and 14 cm, ranging from 0.06 to 0.09 cm yr^{-1} . Above 13 cm (~1950), sedimentation rates begin to increase to a maximum of 0.27 cm yr^{-1} at 7 cm before decreasing slightly to 0.21 cm yr^{-1} at 3 cm.

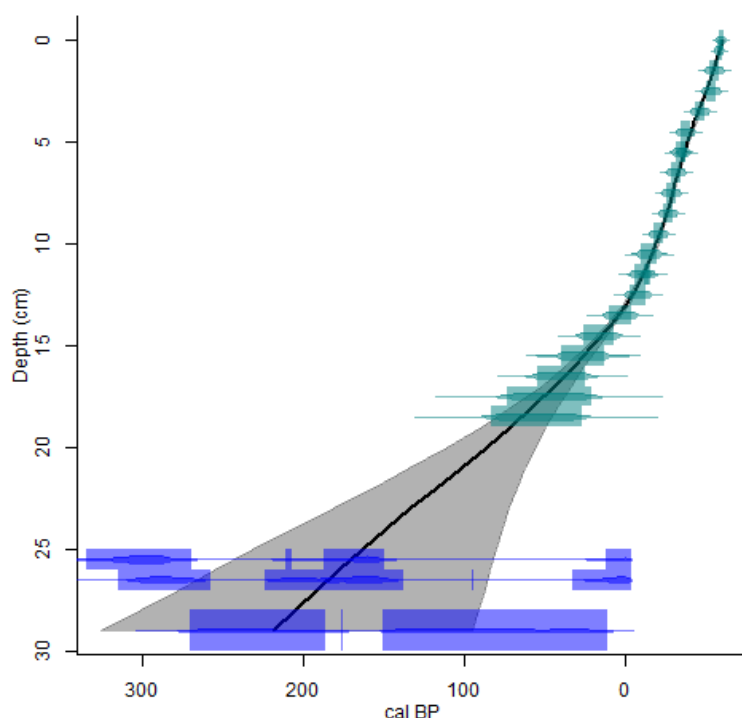


Figure 5.17. Smooth spline (smoothing=0.6) age-depth model produced by *Clam* (Blaauw, 2010) for core JD1 combining ^{210}Pb and ^{137}Cs analyses and calibrated ^{14}C age distributions.

5.5.3.3. *OxCal* Age-Depth Model

OxCal (version 4.2; Bronk Ramsey, 2009a) adopts a Bayesian approach to age-depth modelling and allows for *a priori* information to be utilized, such as stratigraphic and chronostratigraphic ordering. In a similar way to *Clam*, it offers various depositional models (known as ‘sequences’) based on the accumulation history of the investigated environment. For example, if the age intervals between a series of points are precisely known, as is the case for tree rings or varved sediments, then a D_Sequence age-model would be appropriate for selection (Bronk Ramsey, 2008). Figure 5.18 shows the results of a P_Sequence (*Poisson*) model (Bronk Ramsey, 2008) constructed in *OxCal* (Bronk Ramsey, 2009a) which allows for variations in the rate of sediment accumulation (*Poisson* process) and is suitable for fine-grained sediments (Bronk Ramsey, 2008). An adjustable k parameter within the model allows for variation in the size of the deposition events and gives the number of accumulation events per unit depth. A high k value (small increments) reduces flexibility in the model whereas a low k value (large increments) provides more flexibility (Hua et al., 2012). A variety of models were therefore run, each with a differing k parameter value to assess the age-depth models performance. Following this trial and error procedure, a k parameter value of 0.5 mm^{-1} was selected which provided sufficient flexibility in the age-depth model to incorporate all calibrated age distributions. Figure 5.18 shows calendar age

distributions in grey within a blue curve which represents the model uncertainty to 2σ . The overall agreement level index for the age-depth model (A_{model}) was excellent at 123.1% and well above the accepted limit of 60% (Bronk Ramsey, 2008). The agreement level index reported for all ^{210}Pb and ^{137}Cs (C_Date) dates was similarly high (>97%) as were the returned index levels for the three ^{14}C dates (R_Date) (>65%). The modelling data suggest median dates for R_Date SUERC45020 (JD1 25-26) and R_Date SUERC45021 (JD1 26-27) of AD 1790 and AD 1784, respectively. The median date reported for the lowermost dated sample (R_Date SUERC45022; JD1 28-30) is AD 1751. Extrapolation beyond the dated levels has not been performed. The model calculates a mean sedimentation rate of 0.136 cm yr^{-1} for the core from 28 cm. Moving up through the core, sedimentation rates are stable between depths 28 and 14 cm, ranging from 0.05 to 0.10 cm yr^{-1} . A substantial increase in sedimentation rate is then observed above 13 cm (~1950), increasing to a maximum of 0.33 cm yr^{-1} at 7 cm before decreasing slightly to 0.20 cm yr^{-1} above 3 cm.

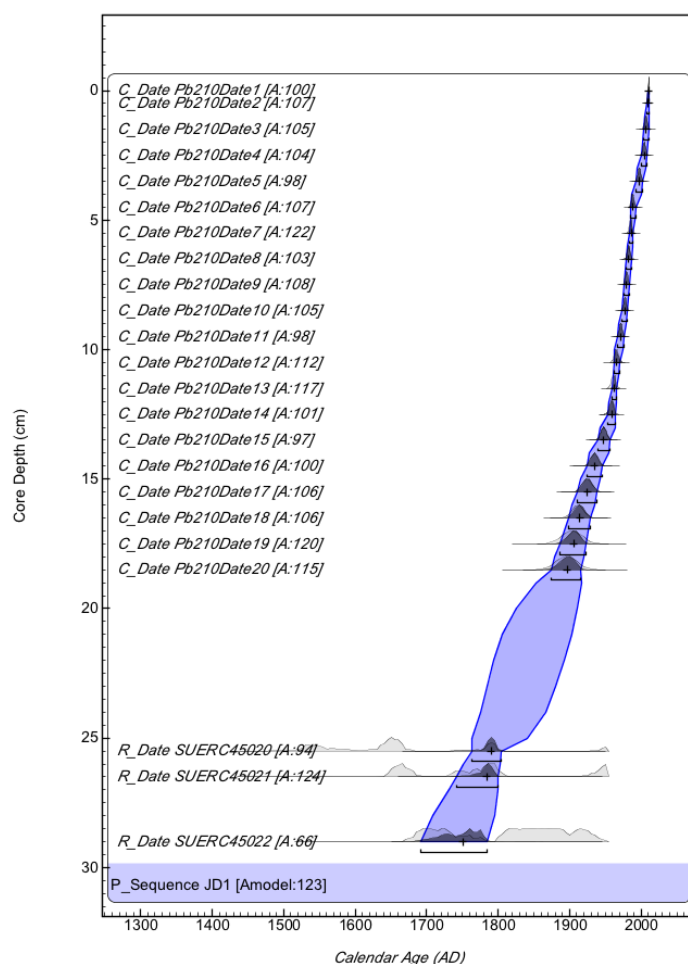


Figure 5.18. P_Sequence age-depth model with $k = 0.5 \text{ mm}^{-1}$ produced by OxCal (Bronk Ramsey, 2009a) for core JD1 combining ^{210}Pb and ^{137}Cs analyses and calibrated ^{14}C age distributions to 2σ (95% confidence level). Agreement indexes [A: #] and median ages also highlighted (crosshair).

5.5.4. Jadrtovac Site 2 (JD2) Chronology

The chronology for core JD2 is based on ^{210}Pb and ^{137}Cs analyses only and is presented in figure 5.19 and table 5.10. The ^{210}Pb dates, calculated using the CRS dating model (Appleby and Oldfield, 1978) places 1963 at a depth of 4.4 cm. Unlike at JD1, this is significantly above the depth as suggested by the ^{137}Cs record shown in figure 5.12. The most likely cause of this discrepancy would appear to be loss of part of the ^{210}Pb due to a hiatus at 8 cm. Revised CRS model dates calculated using the 1963 ^{137}Cs date as a reference point (Appleby, 2002) dates the hiatus to the mid-1950s. The results of these calculations plotted in figure 5.19 and given in detail in table 5.10, place 1986 at a depth of 3 cm, supporting the suggestion that the high ^{137}Cs activity 'shoulder' between 2-5 cm records fallout from the 1986 Chernobyl accident. Sedimentation rates following the hiatus appear to have been relatively uniform, with a mean value of $0.025 \pm 0.003 \text{ g cm}^{-2} \text{ y}^{-1}$ (0.12 cm y^{-1}) apart from a brief episode of more rapid accumulation in the mid-1960s. The chronology based on ^{210}Pb and ^{137}Cs analyses alone limits the sea-level reconstruction for this core to the mid-1950s to a depth of ~9 cm.

5.5.5. Blace (BL) Chronology

The chronology for core BL is also based on ^{210}Pb and ^{137}Cs analyses only and presented in figure 5.20 and table 5.11. The record shows a coherent record to the reliable limits of the dating technique (e.g. ~100 years). The ^{210}Pb dates calculated using the CRS dating model (Appleby and Oldfield, 1978) place 1963 at a depth of 6.5 cm and 1986 at a depth of 4.5 cm, which is in good agreement with the depths suggested by the ^{137}Cs activities. The results of the ^{210}Pb calculations imply a relatively uniform dry mass sedimentation rate over the past century; the mean value during this period was calculated to be $0.065 \pm 0.008 \text{ g cm}^{-2} \text{ y}^{-1}$. Due to compaction accumulation rate declines from 0.30 cm y^{-1} in the most recent sediments to 0.05 cm y^{-1} in the deeper parts of the core. This chronology extends to a depth of approximately 11 cm, dated to the late 19th century, equating to a potential sea-level reconstruction for core BL spanning the past 100 years or so.

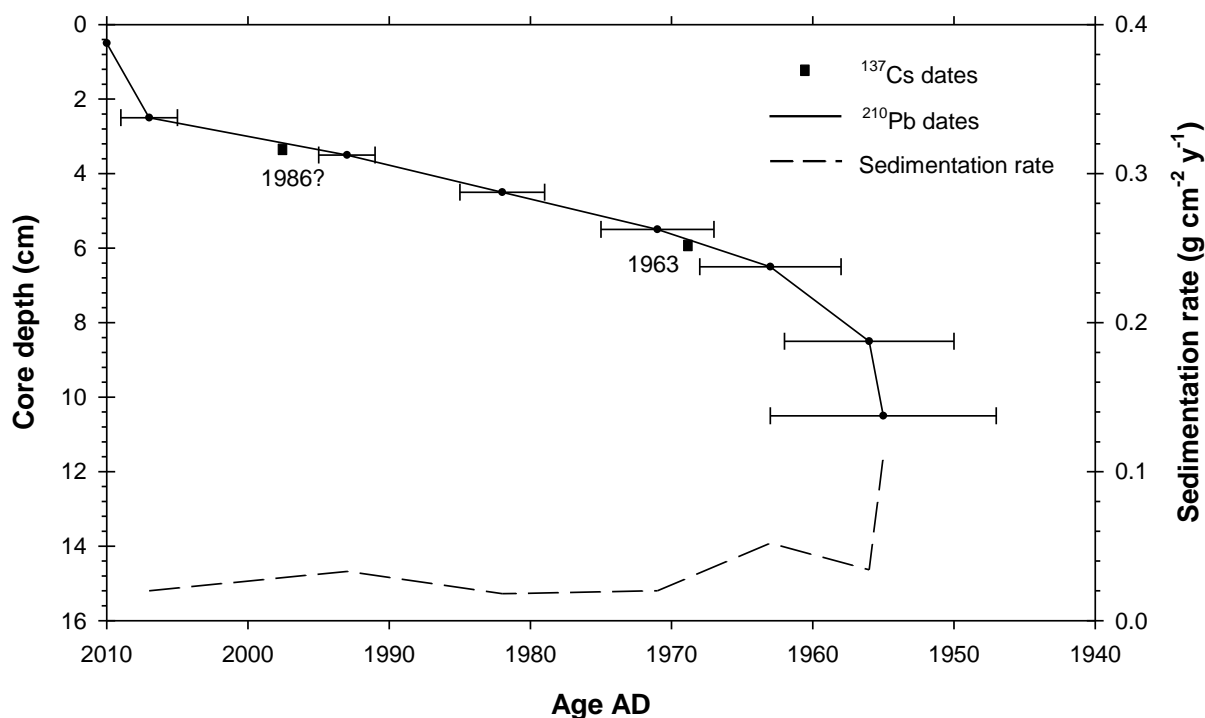


Figure 5.19. Radiometric chronology of the JD2 core showing the 1963 and possible 1986 depths suggested by the ^{137}Cs stratigraphy and also the CRS model ^{210}Pb dates and sedimentation rates calculated using the 1963 ^{137}Cs date as a reference point.

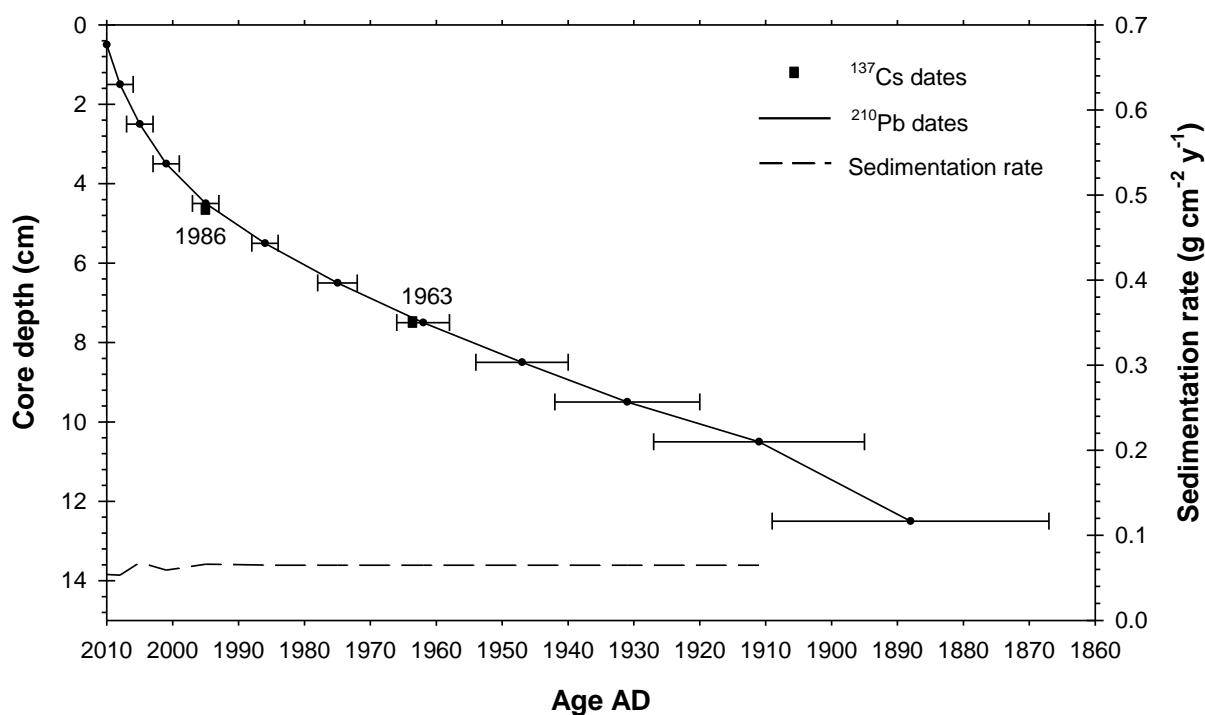


Figure 5.20. Radiometric chronology of the BL core showing CRS model ^{210}Pb dates, sedimentation rate ($\text{g cm}^{-2} \text{y}^{-1}$) and the 1963 and 1986 depths suggested by the ^{137}Cs stratigraphy.

Table 5.10. Revised ^{210}Pb chronology of the JD2 core.

Depth		Chronology			Sedimentation rate		
		Date	Age				
cm	g cm ⁻²	AD	y	±	g cm ⁻²	cm y ⁻¹	± (%)
0.0	0.00	2010	0	0			
0.5	0.05	2007	3	2	0.020	0.15	9.5
2.5	0.42	1993	17	2	0.033	0.12	14.2
3.5	0.69	1982	28	3	0.018	0.09	12.3
4.5	0.89	1971	39	4	0.020	0.11	14.9
5.5	1.13	1963	47	5	0.052	0.13	28.0
6.5	1.41	1956	54	6	0.034	0.38	24.5
8.5	21.3	1955	55	8	0.594	0.12	38.8

Table 5.11. Combined ^{210}Pb (CRS) and ^{137}Cs chronology of the BL core.

Depth		Chronology			Sedimentation rate		
		Date	Age				
cm	g cm ⁻²	AD	Y	±	g cm ⁻²	cm y ⁻¹	± (%)
0.0	0.00	2010	0	0			
0.5	0.09	2008	2	2	0.054	0.30	6.2
1.5	0.28	2005	5	2	0.053	0.29	7.5
2.5	0.52	2001	9	2	0.068	0.20	7.5
3.5	0.87	1995	15	2	0.059	0.13	9.0
4.5	1.41	1986	24	2	0.066	0.10	9.0
5.5	2.13	1975	35	3	0.065	0.08	12.2
6.5	2.97	1962	48	4	0.065	0.07	12.2
7.5	3.95	1947	63	7	0.065	0.06	12.2
8.5	5.01	1931	79	11	0.065	0.06	12.2
9.5	6.29	1911	99	16	0.065	0.05	12.2
10.5	7.80	1888	122	21	0.065	0.04	12.2

5.6. SUMMARY OF FOSSIL SALT-MARSH DATA

This chapter has provided an overview of the fossil environments at Jadrtovac and Blace through a combination of litho-, bio- and chronostratigraphic data. An investigation into the sediment stratigraphy revealed a relatively uniform pattern of sedimentation throughout the study sites where basal minerogenic silts and clays were overlain by increasingly organic deposits. A humified peat horizon was limited to the upper reaches of both environments and was variable in depth. Following this survey, ‘type’ cores were selected based on their stratigraphic characteristics incorporating the transition from highly organic peat deposits to basal silts and clays. These cores formed the basis from which all subsequent analyses were applied.

The ‘Type’ cores were collected, dissected and analysed for fossil foraminiferal and environmental data at a 1 cm resolution. Analysis of foraminiferal assemblage’s revealed

good preservation and similarly low biodiversity, generally reflecting that observed in the contemporary environment. A relatively uniform pattern of change was observed in all cores showing a transition from calcareous taxa, principally comprising high abundances of *Ammonia* spp., *Elphidium* spp. and *Haynesina germanica* dominating the lower organic deprived (<10%) minerogenic sediments to agglutinated species moving up through the core. The main agglutinated taxa encountered were *J. macrescens*, *T. inflata* and *M. fusca*. Analysis of environmental data (LOI and DBD) reflected the stratigraphic survey, highlighting the change from basal minerogenic sediments to increasingly organic deposits moving up through the cores. Particle size characterises revealed minor changes in grain size within each core which were composed primarily of silts and clays.

An array of techniques was used to establish a chronology (^{210}Pb and ^{137}Cs , XRF, AMS ^{14}C dating). Clear peaks in ^{137}Cs in core JD1 were assigned to peak weapons testing (1963) and Chernobyl reactor accident (1986). Using the CRS model, cores JD1 and BL provided favourable results, allowing the extension of the record almost to the limits of the technique (e.g. 100 years or so). For core JD2 however, a hiatus in the record restricted its application to the upper 9 cm of the core extending back to AD 1955. To further extend the chronologies, three levels in JD1 were selected for dating between 25 cm and 30 cm. The lowermost sample (JD1 28-30) suggested a reconstruction possible dating back to AD 1751 ($\pm 2\sigma$). The dates obtained by ^{14}C were then combined with ages produced by short-lived radionuclides and incorporated into an age-depth model using classical and Bayesian approaches. This allowed estimations of age (and uncertainty) for both the dated and undated levels. Modelled sedimentation rates using *Clam* suggested relative stable rates of $0.06 - 0.09 \text{ cm yr}^{-1}$ between 29 and 14 cm. Mean sedimentation rate for the core was 0.13 cm yr^{-1} . Above 13 cm (~ 1950) sedimentation increases to a maximum of 0.27 cm yr^{-1} before decreasing slightly to 0.21 cm yr^{-1} at 3 cm depth. Modelled sedimentation rates using Bayesian approach (*OxCal*) also suggested a mean sedimentation rate 0.13 cm yr^{-1} and stable rates in the lower section of the dated core ranging from $0.05 - 0.1 \text{ cm yr}^{-1}$. An increase from 13 cm is again observed albeit at slightly higher rate peaking at 7 cm to 0.33 cm yr^{-1} before decreasing to 0.20 cm yr^{-1} above 3 cm. Both models appear to capture the increase sedimentation rates observed above ~13 cm.

RESULTS III

TRANSFER FUNCTION ANALYSIS AND SEA-LEVEL RECONSTRUCTION

6.1. INTRODUCTION

The analysis of contemporary foraminiferal data demonstrated altitude as having a statistically significant control on their distribution and confirmed their suitability as proxy indicators of tidal level for use in a transfer function-based reconstruction of sea level. This chapter begins with an overview of the statistical methods involved in developing transfer function models, particularly an analysis of the species' unimodal or linear distribution in relation to altitude. Following this, the various transfer function models are outlined before details regarding how their performance is assessed are provided. In a similar structure to section 4.5, transfer functions are first developed for the dead foraminiferal assemblages for training sets established at Jadrtovac (JDT) and Blace (BLT) before collating them together in a total combined training set (TCD). The reconstructive ability of these models in reconstructing sea level is assessed before a final model is chosen for further screenings.

The second iteration transfer function is then applied to calibrate fossil samples to produce estimates of palaeo-marsh altitude for cores JD1, JD2 and BL. Results produced by PLS and WA-PLS models are compared with 'Maximum Likelihood' results as an independent assessment of model performance. Following this, fossil samples which display a poor relationship with samples in the modern training set are explored using the modern analogue technique to highlight levels where reconstructed values may be considered unreliable. Finally sea-level trends are created where the data are converted and plotted against core depth (cm) and then modelled sample age.

6.2. TRANSFER FUNCTION METHODOLOGY

6.2.1. Species-Environment Response Model

After compiling a modern training set, the next stage in developing a transfer function requires an understanding of the species response (i.e. distribution) in relationship to the environmental variable of interest (Birks, 1995; Leps and Smilauer, 2005) so to derive 'ecological response functions' (Horton and Edwards, 2006). Determining this allows the selection of the most appropriate regression model based on the modern training sets linear or unimodal distribution along the environmental gradient. Foraminiferal taxa that respond in unimodal fashion suggest taxa peak in abundance at an optimal elevation and display a Gaussian distribution (Gauch and Whittaker, 1972). Foraminifera taxa that are linear in relationship with the environmental gradient however suggest abundance increases or decreases in line with the environmental variable (e.g. altitude) (Birks, 1995; Horton and Edwards, 2006). To determine this, detrended canonical correspondence analysis (DCCA) (ter Braak, 1986), an extension of DCA presented in chapter 4, was performed using altitude (m HVSR71) as the only constraining variable. Detrending by segments and with non-linear rescaling, gradient lengths were assessed using CANOCO (version 4.5; ter Braak and Smilauer, 1997-2003; Leps and Smilauer, 2005) providing a measure in SD units. The analysis was performed for both the local (JDT and BLT) and regional (total combined) training sets, as shown in tables 6.2 to 6.4, so that the appropriate regression model could be selected. In general, where the lengths of gradient are short, reporting 2 SD units or less, linear regression and calibration models are most appropriate (ter Braak and Juggins, 1993). Where gradient lengths are greater than 2 SD units however, the use of unimodal methods may be more suitable to express the species data as a function of an environmental variable (ter Braak and Prentice, 1988; Birks, 1995; 2010). Table 6.1 shows the number of surface samples included for each training set used in developing first iteration transfer functions.

Table 6.1. Summary of the number of surface samples included in each training set.

Training Set Name (abbreviation)	Total
Jadrtovac Transects 1 & 2 (JDT)	30
Blace Transects 1 & 2 (BLT)	26
Total Combined Dataset (TCD)	56

6.2.2. Model Selection

Following the analysis of a modern training sets' species-response along the environmental gradient, various transfer function models are available to express an environmental variable

(e.g. altitude) as a function of biological data (e.g. foraminifera). Where the statistical analyses indicate strong unimodal distributions, regression and calibration techniques such as Weighted Averaging (WA) and Weighted Averaging-Partial Least Squares (WA-PLS) are suitable and should be applied. If the foraminiferal data, however, display linear distributions with respect to elevation, regression and calibration methods such as PLS are more appropriate. Further detail regarding these transfer function models was provided in section 2.3.4. Whilst unimodal methods are undoubtedly more common in paleo-sea-level reconstructions from salt-marsh environments and are considered robust and reliable reconstruction techniques (ter Braak and Juggins, 1993; Telford et al., 2004; Telford and Birks, 2005), linear regression and calibration methods have also been successfully applied, particularly where foraminiferal assemblages are derived from short vertical ranges (e.g. Leorri et al., 2010; Rossi et al., 2011).

Despite the short gradient lengths indicated by DCCA for both local and regional training sets (tables 6.2 to 6.4), the transfer function methods utilized in this study included linear PLS, unimodal WA-PLS and the Maximum Likelihood (ML) approach. The analogue-based method, MAT (modern analogue technique), was also applied as described below. Transfer function regression and calibration procedures were processed using the programme C² (version 1.7.4; Juggins, 2003-2011), which provides a tool for developing and applying palaeoecological transfer functions (Juggins, 2007). All analyses were based on relative percentage species data, following Leorri et al. (2010) who observed insignificant differences when using concentration data on transfer function model performance. Output from the statistical models was compared and assessed using the statistical parameters described below.

6.2.3. Assessing Model Performance

Quantitative reconstructions will produce a result regardless of the data used. Whilst there is no simple way to directly evaluate transfer function performance (Imbrie and Webb, 1981), statistical parameters produced from the model output provide a measure of the training sets predictive ability and associated error. This is useful not only as a comparative tool between the various regression techniques applied, allowing the selection of the best model, but permits comparisons with other published work. The regression statistics provided by the software include the coefficient of determination (r^2), the standard error or root mean square error (RMSE) and the maximum bias. The RMSE measures the predictive ability of the training set assessing prediction errors while r^2 measures the strength of the relationship between observed and predicted values (Birks, 1995). The maximum bias provides a measure of the mean difference between observed and predicted values (Birks, 1998).

Whilst these parameters are useful for comparing transfer function models they are ‘apparent’ measures which use the whole training set to test transfer function performance (Edwards and Horton, 2000; Horton and Edwards, 2006). Birks (1995) notes however that RMSE and r^2 are consistently underestimated and overestimated, respectively, when based on the training set alone and so more realistic and reliable estimates of prediction error and ability are needed through split-sampling or cross-validation processes (ter Braak and Juggins, 1993).

A simple cross-validation approach commonly practised in quantitative paleoecological studies is known as jack-knifing, commonly referred to as or “leave-one-out” (ter Braak and Juggins, 1993). In this procedure, the prediction errors form a “jack-knifed” root mean square error of prediction ($RMSEP_{jack}$) where the reconstruction is applied n times using a training set ($n - 1$) (Birks, 1995). $RMSEP$ is calculated when each sample is, in turn, eliminated from the training set, and computations are then made on the remaining samples. This process produces a predicted value and by subtracting this from the observed value, a prediction error for the sample is formed ($RMSEP_{jack}$) (Birks, 1995). In comparison to RMSE, jack-knifed $RMSEP$, and additionally r^2_{jack} measures, offer a more robust and reliable assessment of the training sets predictive ability and error (Gehrels, 2000) and so are used to assess model performance in this study. The cross-validation method jack-knifing does not however provide errors for the individual fossil samples from within the core as the observed errors here are not known (Birks, 1995). Thus, in addition to the procedures described above, another cross-validation technique termed ‘bootstrapping’ was also used to also provide an assessment of the modern training set (r^2_{boot} and $RMSEP_{boot}$) and also sample-specific root mean squared errors of prediction (SE_{pred}) for individual fossil samples (Birks et al., 1990; Birks, 1995).

6.2.4. Data Screening

Due to the influence of additional environmental variables (e.g. salinity) exerting a control to contemporary foraminiferal distributions, inevitably some samples (and similarly species) within the dataset may show a weaker relationship with elevation, displaying a high residual distance from the first ordination axis constrained by the environmental variable of interest (e.g. altitude) (Birks, 1995; Horton and Edwards, 2006). Ultimately these may degrade the transfer function reconstruction so it is often useful to re-assess the modern training set prior to calibration (Birks et al., 1990). Some studies attempt to improve model performance by removing training set samples that are from low elevations or those that fall below a standardized water level index due to the weaker relationship with elevation that exists here (e.g. Edwards and Horton, 2000; Hamilton and Shennan, 2005; Kemp et al., 2009a; Leorri et

al., 2011). These samples may contain an allochthonous component where species are transported into the lower salt-marsh tidal-flat environment (Horton and Edwards, 2006). Whilst these taxa usually appear in low concentrations, and are therefore removed from the training set during the initial data treatment process (e.g. Fatela and Taborda, 2002), they can impact upon the reconstructive ability of a training set. Horton and Edwards (2006) approach to this issue is to group a number of in-washed species together into an ‘exotics’ species component which ultimately improve their transfer function performance. Mills et al. (2013) also highlight the potential benefits in screening modern training sets in which an assessment of an ‘agglutinates only’ transfer function reveals an improvement in statistical parameters r^2_{jack} from 0.52 to 0.79 and RMSEP_{jack} from 0.24 m to 0.13 m. However, in doing so this screening impacted on the proportion explained by elevation and overall explained variance, so caution is required when adopting this approach.

To assess whether improvements in reconstruction performance and their associated errors could be enhanced, the TCD training set was ‘screened’ to remove sample outliers that have a detrimental effect in order to increase the overall model performance (e.g. Gasse et al., 1997). There are various procedures from which sample outliers are removed from modern training set data. Alternatively however it can be argued that all sample data should be included because this most accurately represents the modern sampling environment (e.g. Callard et al., 2011; Barlow et al., 2013). The approach adopted in this study involved the removal of surface samples with an absolute residual (observed minus predicted) greater than the standard deviation (SD) of the environmental gradient (e.g. altitude) following Jones and Juggins (1995); Edwards et al. (2004); Gehrels et al. (2005); Horton and Edwards (2006); Leorri et al. (2008).

6.2.5. Component Selection

Each regression model produces multiple components and choosing the appropriate one is based on their predictive ability and associated errors. Selecting the best component, however, is an important decision as it has consequences for the elevation reconstruction and its associated error (Barlow et al., 2013). Simply assessing the model performance based on the RMSEP alone is not recommended and other statistical parameters should be considered before selecting the final component from which to base the reconstruction (Telford et al., 2004). Therefore the choice of component followed the ‘principle of parsimony’ (Horton et al., 2003) where the lowest component that gave acceptable results based on statistical parameters displaying low RMSEP under cross-validation and high r^2 values (following Birks, 1995) was chosen. If possible an independent control should also be used to assess the reconstructive ability of the transfer function.

As is the goal of many foraminiferal-based studies from salt-marsh environments, instrumental records from nearby tide-gauge stations provide a validation tool from which the transfer function reconstructed model can be compared with (e.g. Gehrels, 2000; Donnelly et al., 2004; Gehrels et al., 2005). In this study, instrumental data from tide-gauge observations at Split, Croatia are similarly used to assess the accuracy of the transfer function-based sea-level reconstruction. This is discussed further in chapter 7.

6.2.6. Modern Analogue Technique

The purpose of the MAT is to quantitatively compare differences and similarities of the biological taxa from a fossil core sample with the biological taxa that comprise the modern training set together with their associated environmental data (Birks, 1995). Essentially it assesses whether or not fossil samples have good modern analogies in the contemporary training set. Non-analogue situations may arise if within a fossil sequence an environment is not sampled in the assemblages that comprise the modern training set. The MAT looks for closest 'modern' analogues from a contemporary training set in fossil assemblages by calculating dissimilarity coefficients (Birks, 1998). Predictions of past sea-level will perform best when they are inferred from fossil samples similar in composition to modern assemblages that comprise the modern training set (Edwards et al., 2004). The MAT is differentiated from the above regression models (e.g. WA-PLS) as it is not based on a species-response model (Birks, 1995). It has, however, been criticised for the over-optimistic estimations it produces (Telford and Birks, 2005). Whilst the technique can be used to infer palaeo-sea-levels, in this instance the MAT was adopted to assess the reliability of the reconstruction by identifying fossil samples in the core sequences which did not possess modern equivalents, following Edwards and Horton (2000). In this way it provides an independent assessment of the regression models (PLS and WA-PLS) applied.

Similarities and dissimilarities between the fossil core samples and assemblages in the modern training set are quantified using a squared chord dissimilarity measure (Prentice, 1980; Overpeck et al., 1985; Birks, 1995). Statistical parameters from the MAT provide a minimum dissimilarity coefficient (minDC) for each fossil sample based on the modern training set. A minDC value of zero would indicate perfect similarity whilst increasing minDC values indicate increasing dissimilarity (Jackson and Williams, 2004). Percentiles produced by the dissimilarity coefficient are used to determine which fossil samples have "good" or "poor" modern analogues. However selecting the appropriate value can be an arbitrary process and indeed varies between authors. For example Woodroffe (2009) used the largest dissimilarity coefficient calculated between the modern training set as a threshold to determine "good" or "poor" analogues. Other authors use a more constrained approach such

as the fifth percentile to determine “good” modern analogues (e.g. Barlow et al., 2013; Watcham et al., 2013). Here the approach of Horton and Edwards (2006) and Kemp et al. (2009a) was followed by assigning core samples below the tenth percentile to have good matching analogues, therefore providing a reliable reconstruction (Birks et al., 1990). Samples below the twentieth percentile, however, are deemed poor or have no matching analogues and so reconstructions from these samples are considered unreliable. Those samples that fall between these cut-off points are considered fair or “close”. The number of possible modern analogues was limited to 5 following Southall et al. (2006), who suggest using a lower number of analogues for smaller training sets due to the increased likelihood of estimates appearing similar when a larger number of analogues are used (e.g. 10). Statistical parameters for MAT were calculated using the final screened transfer function and applied to cores JD1, JD2 and BL using the programme C2 (version 1.7.4; Juggins, 2003-2011).

6.2.7. Transfer Function Application

Following the construction of the transfer function model and identifying fossil samples with poor modern analogues, calibration was then performed where the ecological response functions were applied to fossil samples to produce estimates of palaeo-marsh altitude (PMA) relative to MSL. Standard errors of prediction (SE_{pred}) were calculated for all fossil samples using the cross-validation procedure bootstrapping, to assess errors for all reconstructed values (Birks et al., 1990). As an additional test of reliability, a second transfer function was created using ML approach. Following the same methodology described for PLS and WA-PLS, the ML transfer function was used to demonstrate that the statistical technique used does not significantly affect the outcome of the reconstruction following Horton and Edwards (2006). All calibration procedures were processed using C2 (version 1.7.4; Juggins, 2003-2011).

After establishing heights of palaeo-marsh altitude, RSL changes can then be inferred when combined with chronostratigraphic data (Horton and Edwards, 2006). Sea-level trends were created by plotting a series of sea-level index points (SLIPs) on a time-altitude diagram including both fossil sample prediction errors (SE_{pred}) and chronological errors (cal. AD) described in chapter 5. Inferring sea-level changes was restricted to the extent of the chronologies beyond which no age control exists. However the reconstructions were applied to the whole length of each core sequence. In this study mean sea-level (MSL) will be reconstructed (following Hill et al., 2007; Kemp et al., 2011) and its former position calculated using following equation:

$$\text{MSL} = (S_D - \text{PMA})$$

where S_D is the fossil sample depth (m HVR571), PMA is the estimated palaeo-marsh altitude.

6.3. TRANSFER FUNCTION RESULTS

The following analyses are based on unscreened training sets including all samples and foraminiferal taxa after the removal of insignificant species following the same procedure outlined in chapter 4. The results of model performance for unscreened training sets are summarised in tables 6.3, 6.5 and 6.7 and figures 6.1 to 6.3. The potential improvements to transfer function model performance through data screening processes are explored further in section 6.3.5.

6.3.1. Jadrtovac Transects 1 & 2 (JDT)

Detrended canonical correspondence analysis (DCCA) reveals a gradient length of 0.775 SD units for axis 1 when using altitude as the only constraining environmental variable (table 6.2). Whilst the lengths of gradient are greater for axes 2, 3 and 4, only axis 1 is canonical as only one independent constraint can be formed from the environmental variable. The results therefore suggest the modern training set is strongly linear and, thus, the use of a linear-based PLS regression and calibration model for the 30 samples and 6 species that comprise the JDT training set.

Table 6.2. Summary DCCA results for JDT training set. Length of gradient is in SD units.

Axes	1	2	3	4	Total inertia
Eigenvalues:	0.077	0.233	0.051	0.038	0.990
Lengths of gradient:	0.775	1.664	1.869	1.899	
Sum of all Eigenvalues:					0.990
Sum of all Canonical Eigenvalues:					0.077

Table 6.3 and figure 6.1 show the results of apparent measures and cross-validation statistical parameters using PLS regression for the JDT training set. The transfer function produces five components, which become progressively more complex (number 5 being the most complex). Apparent measures (r^2 and RMSE) are often prone to over- and under-estimations (Birks, 1995) and so jack-knifed parameters are used to provide a better assessment of model performance. Overall, all components of the PLS model reveal relatively weak correlations between observed and predicted values, with highest values observed in components two, four and five ($r^2_{\text{jack}} = 0.11$). In this instance, RMSEP may provide a better guide to model performance as the low r^2_{jack} values are strongly dependent

on the very short gradient length shown in table 6.2; axis one (Gehrels et al., 2001; Leorri et al., 2010). These values provide a measure of the precision (or error) of the regression model and therefore indicate precise reconstructions of former sea-level are possible where $RMSEP_{jack}$ values range from 0.07 m for components two and three to 0.09 m for component one. Cross-validation results from bootstrapping also produce similar prediction errors ranging from 0.08 to 0.11 m ($RMSEP_{boot}$). Maximum bias values remain very similar for all components ranging from 0.26 to 0.21. Following the assessment criteria described above (i.e. principle of parsimony; high r^2_{jack} and low $RMSEP_{jack}$), component two was selected as this illustrated precise reconstructions of former sea-level are possible ($RMSEP_{jack} = 0.07$ m) despite the weak correlation ($r^2_{jack} = 0.11$). Inspection of scatter plots for observed versus predicted altitude and residuals (for component two) in figure 6.1 also highlight this relatively weak relationship in the JDT training set. These plots indicate the potential benefits of a data screening process to improve model performance by removing outliers in the dataset as described in section 6.3.5 below.

Table 6.3. Statistical summary of PLS transfer function performance from modern dead foraminiferal assemblages using the JDT training set. C = Component.

TF Model	Statistical Parameter	C1	C2	C3	C4	C5
PLS	r^2	0.22	0.28	0.30	0.33	0.34
	RMSE (m)	0.06	0.06	0.06	0.06	0.06
	Max_bias	0.19	0.20	0.18	0.17	0.17
	r^2_{jack}	0.02	0.11	0.08	0.11	0.11
	$RMSEP_{jack}$ (m)	0.09	0.07	0.07	0.08	0.08
	Max_bias _{jack}	0.26	0.22	0.22	0.21	0.21
	r^2_{boot}	0.01	0.08	0.12	0.14	0.13
	$RMSEP_{boot}$ (m)	0.08	0.08	0.08	0.10	0.11
	Max_bias _{boot}	0.25	0.22	0.22	0.21	0.21

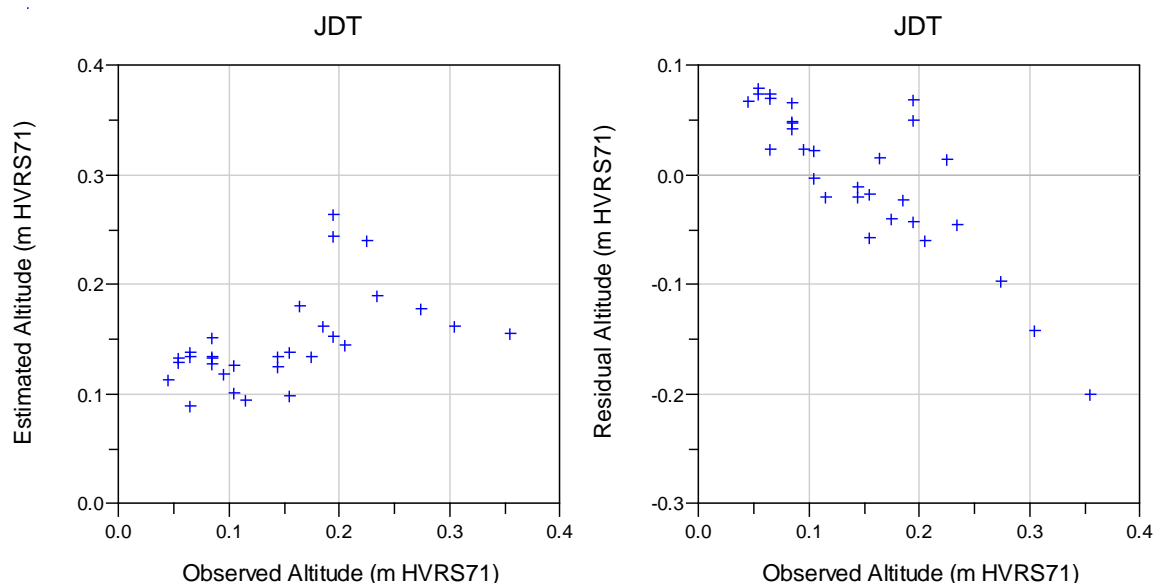


Figure 6.1. Transfer function (PLS) observed versus predicted altitude (m HVR571) and residual values for JDT training set (component 2; jack-knife measures).

6.3.2. Blace Transects 1 & 2 (BLT)

Using altitude as the only constraining environmental variable, DCCA again indicates linear species distribution as revealed by a length of gradient for axis one of 1.536 SD units (table 6.4). Again only axis one can only be used to infer species-response as this is the only canonical axis. Whilst greater in comparison to JDT, DCCA also indicates a relatively strong linear relationship with altitude and suggests the use of linear-based regression models (e.g. PLS) for the 26 samples and 5 species in the BLT training set. In this instance, however, unimodal WA-PLS was also performed as a comparative tool to assess reconstructive ability between the two regression models.

Table 6.4. Summary DCCA results for BLT training set. Length of gradient is in SD units.

Axes	1	2	3	4	Total inertia
Eigenvalues:	0.443	0.149	0.088	0.039	1.010
Lengths of gradient:	1.536	1.683	1.746	2.364	
Sum of all Eigenvalues:					1.010
Sum of all Canonical Eigenvalues:					0.443

A statistical summary of PLS and WA-PLS transfer function models is shown in table 6.5 and figure 6.2. Analysis of model performance parameter r^2_{jack} reveals much stronger correlations between observed and predicted altitude in comparison to the training set at Jadrtovac. When comparing results from the two regression models, PLS marginally

outperforms WA-PLS, which only produces 4 components. However, given the short gradient length (table 6.4), this is expected. The strength of relationship was strongest for component two ($r^2_{\text{jack}} = 0.71$) and weakest for component five ($r^2_{\text{jack}} = 0.56$) for the PLS model, demonstrating robust transfer function performance. Inspection of prediction errors for the training set ($\text{RMSEP}_{\text{jack}}$) shows very similar values for all model components. However, component two also produced the most favourable results, suggesting precise sea-level reconstructions are possible ($\text{RMSEP}_{\text{jack}} = 0.09$ m). Boot-strapped performance (r^2_{boot}) and prediction errors ($\text{RMSEP}_{\text{boot}}$) are again very of similar magnitude to jack-knifed cross-validation. The relationship between observed versus predicted foraminiferal altitude shown in figure 6.2 for component two demonstrates the stronger relationship observed in the BLT training in comparison to JDT. However, it also highlights the potential sample outliers that exist in the training set which are potentially detrimental to the overall transfer function model performance. Similarly the BLT training set would therefore benefit from data screening processes.

Table 6.5. Statistical summary of PLS and WA-PLS transfer function performance for dead foraminiferal assemblages using the BLT training set. C = Component.

TF Model	Statistical Parameter	C1	C2	C3	C4	C5
PLS	r^2	0.73	0.78	0.81	0.84	0.84
	RMSE (m)	0.09	0.08	0.07	0.07	0.07
	Max_bias	0.11	0.13	0.10	0.10	0.10
	r^2_{jack}	0.68	0.71	0.69	0.64	0.56
	$\text{RMSEP}_{\text{jack}}$ (m)	0.10	0.09	0.10	0.11	0.12
	Max_bias _{jack}	0.12	0.16	0.12	0.13	0.15
	r^2_{boot}	0.66	0.70	0.69	0.63	0.57
	$\text{RMSEP}_{\text{boot}}$ (m)	0.11	0.11	0.11	0.13	0.15
	Max_bias _{boot}	0.14	0.18	0.16	0.15	0.16
WA-PLS	r^2	0.72	0.73	0.73	0.73	-
	RMSE (m)	0.09	0.09	0.09	0.09	-
	Max_bias	0.10	0.10	0.10	0.10	-
	r^2_{jack}	0.68	0.67	0.68	0.67	-
	$\text{RMSEP}_{\text{jack}}$ (m)	0.10	0.10	0.10	0.10	-
	Max_bias _{jack}	0.12	0.12	0.12	0.12	-
	r^2_{boot}	0.68	0.67	0.66	0.66	-
	$\text{RMSEP}_{\text{boot}}$ (m)	0.11	0.12	0.12	0.12	-
	Max_bias _{boot}	0.12	0.14	0.14	0.14	-

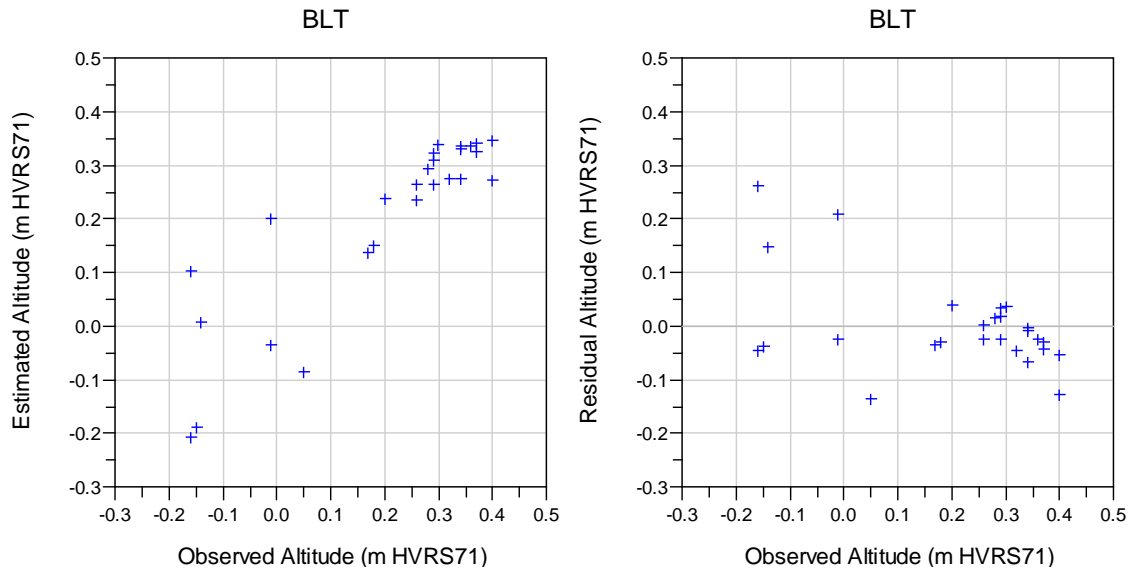


Figure 6.2. Transfer function (PLS) observed versus predicted altitude (m HVR571) and residual values for BLT training set (component 2; jack-knife measures).

6.3.3. Total Combined Dataset (TCD)

Inspection of table 6.6 again shows a short gradient length for axis one (1.173 SD units) as revealed by DCCA (table 6.6). This also illustrates linear-species response in relation to altitude, suggesting linear-based PLS is again most appropriate for a total combined training set comprising 56 samples and 6 species. As a comparison, WA-PLS was again performed to assess transfer function model performance.

Table 6.6. Summary DCCA results for TCD training set. Length of gradient is in SD units.

Axes	1	2	3	4	Total inertia
Eigenvalues:	0.198	0.307	0.128	0.093	1.351
Lengths of gradient:	1.173	2.134	1.831	1.571	
Sum of all Eigenvalues:					1.351
Sum of all Canonical Eigenvalues:					0.198

Table 6.7 and figure 6.3 provide a statistical summary of PLS and WA-PLS transfer function performance for dead foraminiferal assemblages in the total combined training set. Linear (PLS) and unimodal (WA-PLS) regression models revealed five components. Overall PLS appears to marginally outperform WA-PLS although the results are very similar for both regression models. Inspection of model performance parameter r^2_{jack} reveals components two and three to demonstrate robust transfer function performance ($r^2_{\text{jack}} = 0.32$). Analysis of prediction errors are similar for all components displayed where $\text{RMSEP}_{\text{jack}}$ ranges from 0.11 to 0.12 m suggesting precise sea-level reconstructions are possible using a total

training set which is comparable to that of previous studies (table 7.2). Figure 6.3 shows the relationship between observed and foraminiferal estimated altitude using component 2 and illustrates strong performance but a bias towards the upper part of the altitudinal gradient. Sample outliers in the dataset are also observed which would benefit from data screening.

Table 6.7. Statistical summary of PLS and WA-PLS transfer function performance for dead foraminiferal assemblages using a total combined transect training set. C = Component.

TF Model	Statistical Parameter	C1	C2	C3	C4	C5
PLS	r^2	0.37	0.44	0.44	0.45	0.45
	RMSE (m)	0.11	0.10	0.10	0.10	0.10
	Max_bias	0.16	0.14	0.14	0.14	0.14
	r^2_{jack}	0.27	0.32	0.32	0.28	0.25
	RMSEP _{jack} (m)	0.12	0.11	0.11	0.12	0.12
	Max_bias _{jack}	0.17	0.16	0.16	0.16	0.16
	r^2_{boot}	0.26	0.30	0.29	0.25	0.20
	RMSEP _{boot} (m)	0.12	0.12	0.12	0.13	0.14
	Max_bias _{boot}	0.18	0.16	0.16	0.17	0.17
WA-PLS	r^2	0.41	0.44	0.44	0.44	0.44
	RMSE (m)	0.10	0.10	0.10	0.10	0.10
	Max_bias	0.16	0.15	0.15	0.15	0.15
	r^2_{jack}	0.33	0.29	0.25	0.25	0.25
	RMSEP _{jack} (m)	0.11	0.11	0.12	0.12	0.12
	Max_bias _{jack}	0.16	0.16	0.16	0.16	0.16
	r^2_{boot}	0.33	0.30	0.26	0.25	0.25
	RMSEP _{boot} (m)	0.11	0.12	0.13	0.13	0.13
	Max_bias _{boot}	0.16	0.16	0.16	0.16	0.16

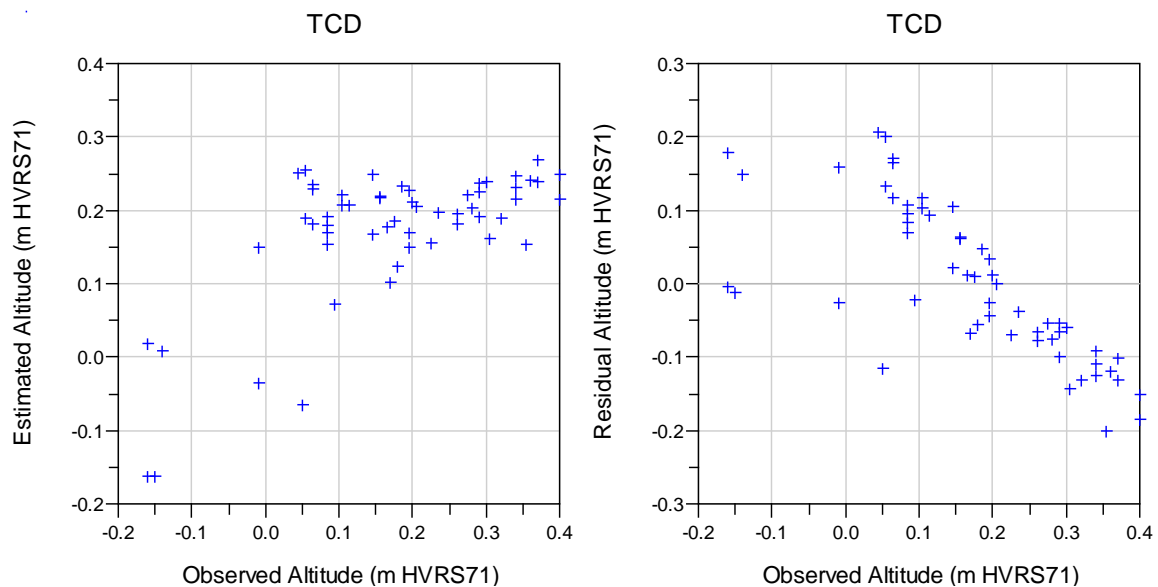


Figure 6.3. Transfer function (PLS) observed versus predicted altitude (m HVR571) and residual values for TCD training set (component 2; jack-knife measures).

6.3.4. Local Versus Regional Training Set

The spatial scale from which foraminiferal training sets are derived can have important consequences for transfer function performance (e.g. Watcham et al., 2013). Local training sets may be collected from sites within close proximity to the fossil core (e.g. Woodroffe and Long, 2010) whilst regional datasets may comprise multiple training sets spanning multiple countries (e.g. Horton and Edwards, 2006). A problem arises where the contemporary training set is limited or does not capture the full range of environments recorded in the fossil sequence. Small training sets are inherently under-representative of the modern environment containing fewer modern analogues and, therefore, are more prone to errors (Horton and Edwards, 2006). The training sets from Jadrtovac and Blace showed site-specific transfer function performance varied from r^2_{jack} 0.11 and $\text{RMSEP}_{\text{jack}}$ 0.07 m for JDT to r^2_{jack} 0.71 and $\text{RMSEP}_{\text{jack}}$ 0.09 m for BLT. The number of surface samples included for each training set was limited to between 26 and 30 surface samples (table 6.1). Indeed even the total transect training set was relatively small but comparable to previous studies comprising 56 (unscreened) surface samples (table 6.8). Given the strong similarity in the tidal regimes at Jadrtovac and Blace, a combined training in this instance may still be considered as being ‘local’. The statistical analyses gave a strength of relationship of $r^2_{\text{jack}} = 0.32$ with a reconstruction error of $\text{RMSEP}_{\text{jack}} = 0.11$ m for an unscreened total training dataset transfer function. In an attempt to improve model performance, the combined training set was explored further through data screening, as described below. By using the TCD training set, more modern analogues are available from which the fossil samples can be compared with.

Table 6.8. Comparison of training set size and salt-marshes studied with published literature

Location	Training Set Size	Salt-Marshes Studied	Reference
Central Croatia	56 (unscreened)	2	This study
UK (multiple sites)	88	6	Zong and Horton (1999)
UK (multiple sites)	200	13	Edwards and Horton (2006)
Pounawea, New Zealand	31	1	Southall et al. (2006)
Sulawesi, Indonesia	63	3	Engelhart et al. (2007)
North Carolina, USA	47	3	Horton and Culver (2008)
Bay of Biscay, Spain	46	4	Leorri et al. (2008)
North Carolina, USA	184	10	Kemp et al. (2009b)
Oregon, USA	85	5	Hawkes et al. (2010)
West Greenland	64	3	Woodroffe and Long (2010)
Tasmania, Australia	43	2	Callard et al. (2011)
Brittany, France	36	2	Rossi et al. (2011)
New Jersey, USA	62	3	Kemp et al. (2012)
Liverpool, UK	80	2	Mills et al. (2013)

6.3.5. Training Set Screening

The TCD training set was examined to remove sample outliers that degrade the overall predictive ability of the training set. Following this, a second iteration of a screened total combined training set was constructed and the results are given in table 6.11 and figure 6.4 below. The standard deviation for altitude was 0.141 m and the screening processes removed all surface samples with an absolute residual (observed minus predicted) greater than this value. This resulted in the exclusion of 13 surface samples, including seven from Jadrtovac and six from Blace, as summarised in table 6.9 below. The final transfer function model is based on the remaining 43 surface samples and in comparison to previous studies; is still an acceptable and statistically robust number (table 6.8). The removal of these samples is due to their poor relationship with altitude, and failing to do so only decreases the overall ability of the transfer function model (Jones and Juggins, 1995; Gasse et al., 1997).

Table 6.9. Summary of surface samples removed through screening process. The standard deviation of altitude for unscreened TCD training set was 0.141.

Site	Surface sample number	Absolute residual (observed versus predicted)
Jadrtovac	JD1-13	0.150
	JD1-18	0.176
	JD1-19	0.222
	JD1-20	0.187
	JD1-22	0.219
	JD2-1	-0.225
	JD2-2	-0.154
Blace	BL1-16	-0.163
	BL2-1	-0.204
	BL2-2	-0.144
	BL2-4	0.165
	BL2-5	0.164
	BL2-6	0.262

Detrended canonical correspondence analysis was performed on the new training set so that the appropriate statistical model could again be applied. Axis one revealed a longer gradient length of 1.594 SD units (table 6.10). As this value was closer to 2, following Callard et al. (2011) both linear PLS and unimodal WA-PLS regression models were applied so that the statistical parameters between the two techniques could be compared. The performance of the initial unscreened PLS regression model was moderate ($r^2_{\text{jack}} = 0.32$) but suggested precise sea-level reconstructions were possible ($\text{RMSEP}_{\text{jack}} = 0.11$ m). Updated transfer function statistical parameters from the screening training set and shown in table 6.11 results in a significant improvement to model performance as described below.

Table 6.10. Summary DCCA results for a screened TCD training set.

Axes	1	2	3	4	Total inertia
Eigenvalues:	0.264	0.315	0.107	0.045	1.280
Lengths of gradient:	1.594	2.220	1.635	1.790	
Sum of all Eigenvalues:					1.280
Sum of all Canonical Eigenvalues:					0.264

Inspection of statistical parameters reveals a screened transfer function considerably improves model performance for r^2_{jack} from 0.32 to 0.56 and $\text{RMSEP}_{\text{jack}}$ from 0.11 m to 0.07 m for component three using linear PLS regression (table 6.11). Alternatively, it can be argued that removing outliers, limits the number of modern analogues that accurately reflect the modern environment. Results produced using unimodal regression (WA-PLS) show almost identical performance (for component two) compared to linear regression (PLS), with an r^2_{jack} value of 0.55 and prediction error of 0.08 m ($\text{RMSEP}_{\text{jack}}$). The maximum bias in jack-knifed residuals also remains very similar for both models ($\text{max_bias}_{\text{jack}}$; 0.10–0.11 m). This would suggest that despite the short gradient lengths provided by DCCA (1.594; axis one) both regression models are capable of robust and precise sea-level reconstructions.

Weighted average results from MAT were also used to assess the performance of the modern training set, displaying comparable quantitative performance. The utility of MAT output helps to assess the modern training sets reconstructive potential. It is also a useful procedure as it provides percentile values which are used as thresholds to identify ‘good’ or ‘poor’ fossil samples in relationship to the modern training set (see section 6.3.6 below). It is difficult to justify the use of unimodal regression and calibration procedures due to the short-environmental gradients involved. However, both methods produced almost identical relationship coefficients (r^2_{jack}) and prediction errors ($\text{RMSEP}_{\text{jack}}$) and as a result both methods will be explored further in estimating palaeo-marsh altitude following Callard et al. (2011). Inspection of figure 6.4 shows that both models over-estimate most sample altitudes in the lower section of the height gradient and under-estimate altitudes of many samples in the higher upper salt-marsh environment. It is also clear that the training set is biased towards samples from the upper envelope of the height gradient with a limited number of samples below 0.0 m HVR571.

As a comparison to the results produced by screening the training set an additional transfer function was created incorporating all surface samples in the training set (see section 6.3.8).

Table 6.11. Statistical summary of transfer function performance for screened dead foraminiferal assemblages from a total combined training set. C = component.

TF Model	Statistical Parameter	C1	C2	C3	C4	C5
PLS	r^2	0.56	0.62	0.63	0.63	0.63
	RMSE (m)	0.08	0.07	0.07	0.07	0.07
	Max_bias	0.10	0.09	0.09	0.10	0.09
	r^2_{jack}	0.47	0.54	0.56	0.55	0.54
	RMSEP _{jack} (m)	0.08	0.08	0.07	0.08	0.08
	Max_bias _{jack}	0.11	0.10	0.10	0.10	0.12
	r^2_{boot}	0.47	0.54	0.55	0.54	0.54
	RMSEP _{boot} (m)	0.09	0.08	0.08	0.08	0.08
	Max_bias _{boot}	0.13	0.10	0.10	0.10	0.10
WA-PLS	r^2	0.55	0.62	0.62	0.62	0.62
	RMSE (m)	0.08	0.07	0.07	0.07	0.07
	Max_bias	0.11	0.10	0.10	0.10	0.10
	r^2_{jack}	0.49	0.55	0.54	0.54	0.54
	RMSEP _{jack} (m)	0.08	0.08	0.08	0.08	0.08
	Max_bias _{jack}	0.12	0.11	0.11	0.11	0.11
	r^2_{boot}	0.50	0.54	0.54	0.53	0.53
	RMSEP _{boot} (m)	0.08	0.08	0.08	0.08	0.08
	Max_bias _{boot}	0.12	0.11	0.11	0.11	0.11
MAT	r^2	0.34	-	-	-	-
	RMSE (m)	0.10	-	-	-	-
	Max_bias	0.25	-	-	-	-
WMAT	r^2	0.52	-	-	-	-
	RMSE (m)	0.08	-	-	-	-
	Max_bias	0.13	-	-	-	-

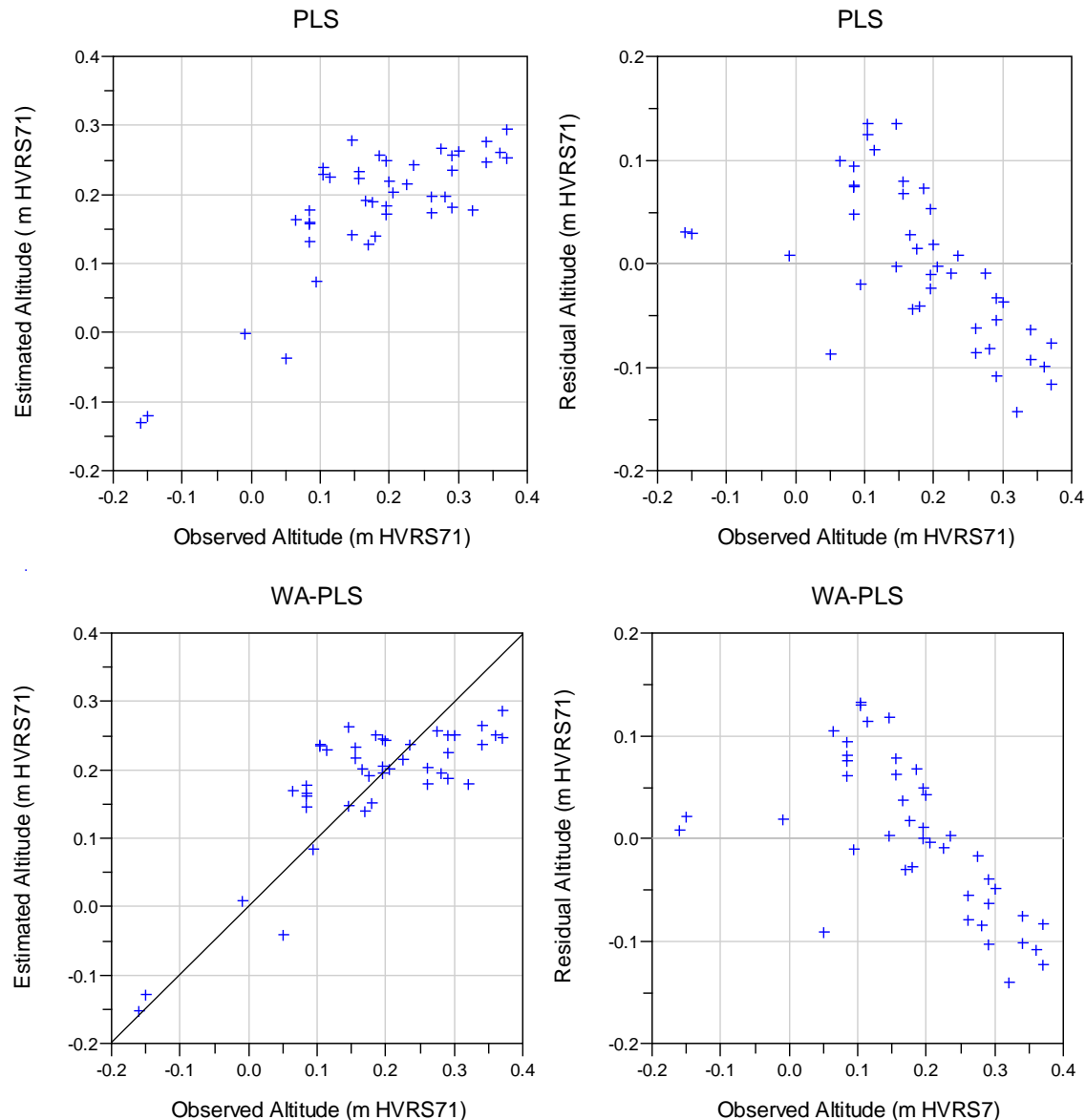


Figure 6.4. Transfer function PLS (component 2) and WA-PLS (component 2) observed versus predicted altitude (m HVRs71) and residual values for the screened TCD training set.

Following Edwards and Horton (2000); Mills et al. (2013) additional regression models (PLS and WA-PLS) were also constructed using an “agglutinated species only” training set. However, output from the analyses suggests excluding calcareous taxa (*Quinqueloculina* spp., *Ammonia* spp. and *Elphidium* spp.) does not significantly improve model performance, producing very similar coefficient (r^2_{jack}) values and prediction errors ($\text{RMSEP}_{\text{jack}}$) for component three (PLS) and component two (WA-PLS) respectively (table 6.12 and figure 6.5). The preference here is, therefore, to include all agglutinated and calcareous species in the transfer function model to provide a more accurate representation of the modern

environment and similarly more modern analogues from which the fossil samples can be compared with.

Table 6.12. Statistical summary of PLS and WA-PLS transfer function performance for screened dead agglutinated species only foraminiferal assemblages from a total combined transect training set. C = component.

TF Model	Statistical Parameter	C1	C2	C3	C4	C5
PLS	r^2	0.56	0.62	0.63	0.63	0.63
	RMSE (m)	0.08	0.07	0.07	0.07	0.07
	Max_bias	0.10	0.09	0.09	0.10	0.09
	r^2_{jack}	0.47	0.54	0.55	0.55	0.54
	RMSEP _{jack} (m)	0.08	0.08	0.08	0.08	0.08
	Max_bias _{jack}	0.11	0.10	0.10	0.10	0.12
	r^2_{boot}	0.29	0.31	0.31	-	-
	RMSEP _{boot} (m)	0.10	0.10	0.10	-	-
	Max_bias _{boot}	0.23	0.20	0.20	-	-
WA-PLS	r^2	0.55	0.62	0.62	0.62	0.62
	RMSE (m)	0.07	0.07	0.07	0.07	0.07
	Max_bias	0.11	0.10	0.10	0.10	0.10
	r^2_{jack}	0.49	0.54	0.54	0.54	0.54
	RMSEP _{jack} (m)	0.08	0.08	0.08	0.08	0.08
	Max_bias _{jack}	0.12	0.11	0.11	0.11	0.11
	r^2_{boot}	0.02	0.02	-	-	-
	RMSEP _{boot} (m)	0.11	0.11	-	-	-
	Max_bias _{boot}	0.36	0.36	-	-	-

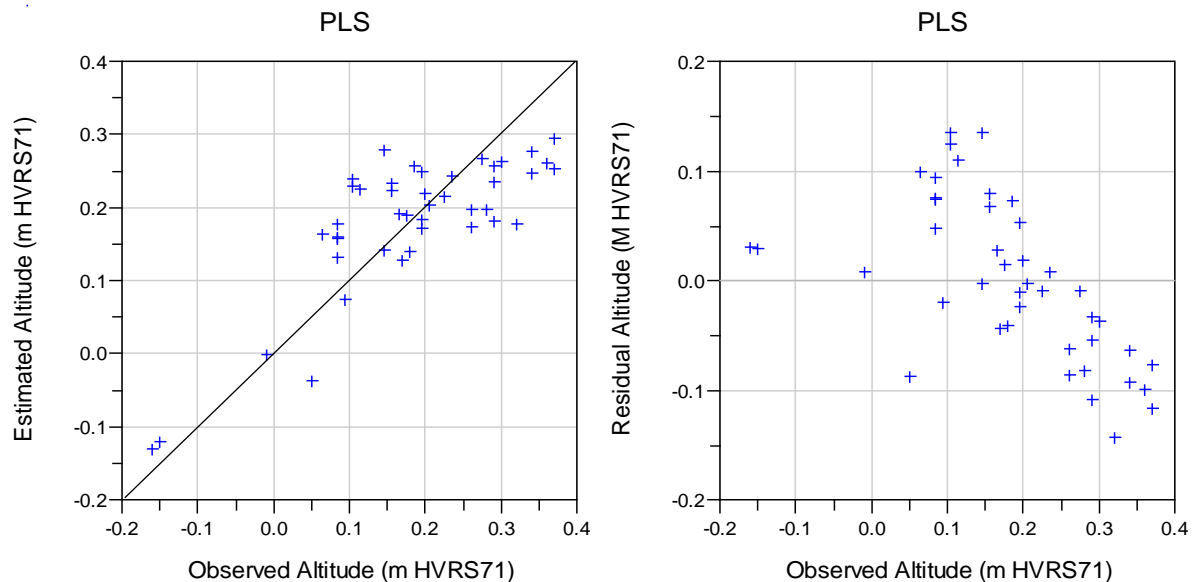


Figure 6.5. Transfer function (PLS) observed versus predicted altitude (m HVR71) and residual values for agglutinated only TCD training set (component 2; jack-knife measures).

6.3.6. Modern Analogues

The next stage assessed the degree to which fossil samples possessed reliable modern analogues (Birks et al., 1990; Birks, 1995). Table 6.13 provides a summary of the percentiles produced by dissimilarities in the TCD training set using MAT. In this study the tenth and twentieth percentiles were used (following Horton and Edwards, 2006) as thresholds to distinguish between “good”, “poor” and “close” analogues for those that fell between these thresholds. Using this information, the MAT was applied to fossil samples from each core and the results displayed in figure 6.6. Raw values of minDC are provided in Appendix D.

Table 6.13. Summary of MAT percentiles using dissimilarities in the TCD training set.

Percentile	Value
1 st	2.80863
2 nd	4.39595
5 th	7.96043
10 th	14.7963
20 th	26.4921

Based on the percentile thresholds above, the TCD training set identifies a number of samples within all cores that have good, close and poor modern analogues. In core JD1 (figure 6.6a), the lower 21 cm contains only two fossil samples (at 25 cm and 27 cm) with ‘close’ modern analogues whilst all other samples display a poor relationship as indicated by minDC values exceeding the 20th percentile (26.4921). Indeed this is particularly pronounced for fossil samples towards the bottom of the sequence, suggesting that any palaeo-marsh altitude reconstruction from this section of the core may be unreliable. In the upper 21 cm of the core, however, all fossil samples fall below the 20th percentile, suggesting they have good or close modern analogues. Fourteen fossil samples display a strong similarity with samples from the modern environment as reported by minDC values all below the 10th percentile (<14.7963). Reconstructions for this section of the core may therefore be considered statistically robust and reliable.

Core JD2 (figure 6.6b) shows a strong analogy with fossil samples from the lower 12 cm of the core where 9 samples fall below the 10th percentile between 56 cm and 44 cm. Moving up through the sequence, the relationship between fossil samples and modern analogues in the training set dramatically decreases, with 18 fossil samples reporting minDC values above the 20th percentile between 43 and 27 cm. This would suggest reconstruction values based on fossil samples from this section of the core may be unreliable. Above 25 cm, however, all fossil samples suggest a strong similarity with the modern training set, with minDC values all below the 10th percentile illustrating reliable palaeo-marsh altitude reconstructions are possible from this part of the core.

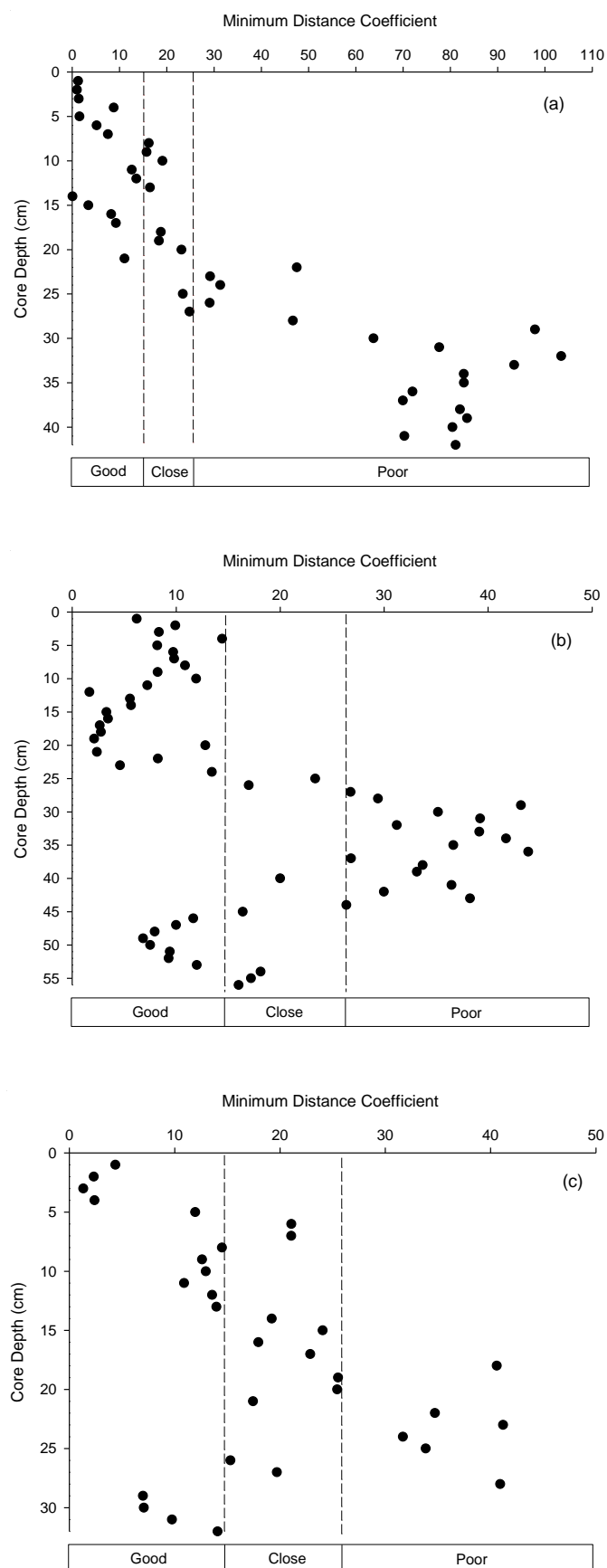


Figure 6.6. Summary MAT results showing 'good', 'close' and 'poor' analogues in cores (a) JD1, (b) JD2 and (c) BL. See table 6.13 for threshold values for 10th and 20th percentiles.

Inspection of minDC values for core BL (figure 6.6c) shows much fewer fossil samples that are without modern analogues in comparison to fossil samples in cores JD1 and JD2. The lowermost samples between 32 cm and 29 cm have good modern analogues in the TCD training set, as shown by minDC values below the 10th percentile. In total, six fossil samples in core BL have poor modern analogues, with minDC values above the 20th percentile, primarily between 25 and 18 cm. Moving up through the core sequence, reliable reconstructions are possible in all samples above 17 cm where 13 fossil samples have good analogues (below 10th percentile) and 3 close analogues (between 10th and 20th percentile).

6.3.7. Palaeo-Marsh Altitude Reconstruction

The screened TCD transfer function was used to calibrate fossil assemblages in cores JD1, JD2 and BL to provide estimates of palaeo-marsh altitude (PMA). Results for both PLS and WA-PLS calibrations are plotted against core depth (cm) and displayed in figures 6.7, 6.8 and 6.9, whilst raw values of bootstrapped predictions and standard deviation errors (SE_{pred}) are provided in Appendix D. Fossil analogues that do not possess modern equivalents, as identified by the MAT presented above, are also highlighted since inferring reconstructions from these horizons is considered unreliable. To assess the reliability of the transfer function and to determine if model selection has an important consequence for the reconstruction, transfer functions using the ML approach were also constructed and plotted as a comparative tool. Table 6.14 displays statistical parameters produced using ML and shows a comparable statistical relationship ($r^2_{jack} = 0.52$) and prediction error ($RMSEP_{jack} = 0.10$ m) to PLS and WA-PLS regression.

Table 6.14. Statistical summary of ML transfer function performance for screened dead foraminiferal assemblages from a total combined training set. C = component.

TF Model	Statistical Parameter	Performance
ML	r^2	0.57
	RMSE (m)	0.09
	Max_bias	0.11
	r^2_{jack}	0.52
	RMSEP _{jack} (m)	0.10
	Max_bias _{jack}	0.13
	r^2_{boot}	0.52
	RMSEP _{boot} (m)	0.10
	Max_bias _{boot}	0.13

Figure 6.7 shows reconstructed PMAs for PLS (component 3) and WA-PLS (component 2) transfer functions for core JD1. Estimated PMAs by PLS transfer functions range from 0.359 to 0.036 m (mean = 0.204 m). The average error for each fossil sample (SE_{pred}) is 0.085 m (table 6.15). In comparison, estimated PMAs by WA-PLS range from 0.263 m to -0.127 m (mean = 0.095 m). The average error for each fossil sample (SE_{pred}) using unimodal calibration is similar at 0.085 m. Both transfer function models show an overall increasing trend in PMA towards the modern surface. Between 42 cm and 28 cm, both models are consistent, suggesting PMA remained relatively stable (although it must be noted that no modern analogues exist in this section). Above 28 cm, PMA begins to increase to the top of the core, displaying a period of decreasing PMA between 14 cm and 10 cm. Whilst the trends and prediction errors produced by both transfer function models are similar, PMAs predicted by WA-PLS are lower in altitude in comparison to PLS transfer function estimations. Overall the results from ML regression and calibration show a similar trend in PMA when compared with PLS and WA-PLS results. An increasing trend towards the surface is again observed and estimates produced fall within the boundaries of both linear and unimodal calibrations. Towards the bottom of the core, however, prediction errors produced by ML increase dramatically, highlighting the absence or poor quality of modern analogues that exist here due to limitations in the sampled altitude range of the modern training set.

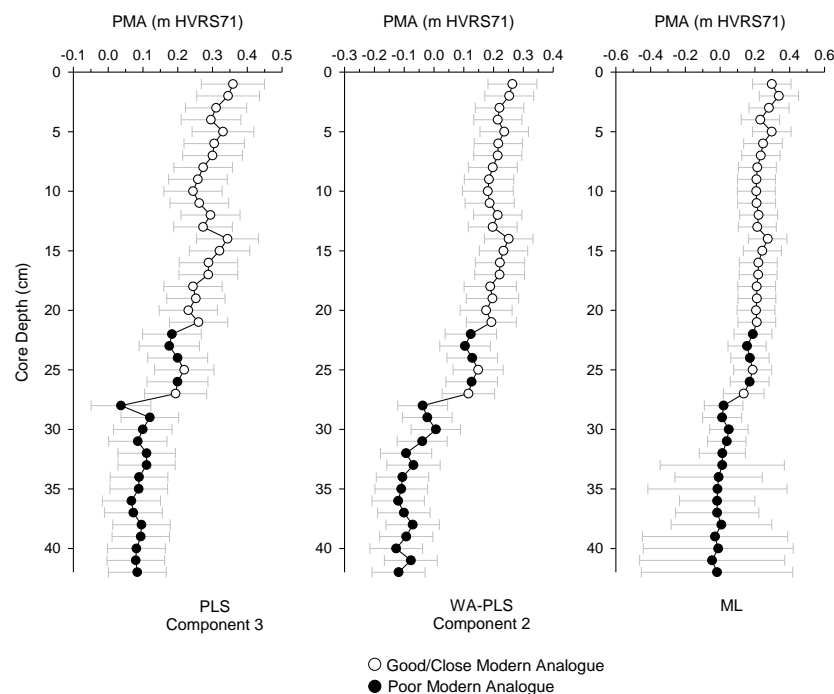


Figure 6.7. Palaeo-marsh altitude (m HVR571) estimated using PLS (component 3), WA-PLS (component 2) and ML transfer functions for core JD1 including sample specific errors estimated by bootstrapping. Good/close and poor modern analogues also displayed.

Table 6.15. Summary of palaeo-marsh altitude and average errors for core JD1.

Model		Value
PLS (C3)	Maximum PMA (m HVRS71)	0.359
	Minimum PMA (m HVRS71)	0.036
	Range of PMA (m)	0.322
	Average PMA (m HVRS71)	0.204
	Average error (m)	0.0850
WA-PLS (C2)	Maximum PMA (m HVRS71)	0.263
	Minimum PMA (m HVRS71)	-0.127
	Range of PMA (m)	0.390
	Average PMA (m HVRS71)	0.0957
	Average error (m)	0.0848
ML	Maximum PMA (m HVRS71)	0.338
	Minimum PMA (m HVRS71)	-0.046
	Range of PMA (m)	0.384
	Average PMA (m HVRS71)	0.143
	Average error (m)	0.167

Figure 6.8 shows reconstructed PMAs for PLS (component 3) and WA-PLS (component 2) transfer functions for core JD2. Linear calibration PLS shows estimated PMAs range from 0.380 m to -0.109 m (mean = 0.145 m) with an average error (SE_{pred}) of 0.091 m (table 6.16). The reconstructed values by WA-PLS transfer functions are again lower in comparison to PLS. Estimated PMAs range from 0.279 m to -0.183 m. The average error (SE_{pred}) for each fossil sample is slightly lower at 0.090 m. Both transfer functions produce similar trends, with stable PMAs observed between 56 and 44 cm above which poor analogues suggest fluctuating increases in PME. Between 25 and 12 cm PMA continues to rise before a period of decreasing PMA to approximately 4 cm and then gradually increasing again to the modern surface. In comparison to calibration by ML, prediction of PMA displays a similar increasing trend with the similar fluctuations observed between 43 and 27 cm, where poor analogues exist. Again larger prediction errors are observed towards the bottom of the core (also at 30 cm) reflecting the limitations of the modern training set in accurately predicting heights for these levels which are composed predominately of calcareous taxa.

Figure 6.9 shows reconstructed PMAs for PLS (component 3) and WA-PLS (component 2) transfer functions for core BL. Estimated PMA by PLS range from 0.328m to -0.06 m (mean = 0.221 m) with an average error of 0.086 m (table 6.17). Estimates of PMA by WA-PLS are again lower in magnitude ranging from 0.262 m to -0.124 m (mean = 0.168 m). The average error for WA-PLS is 0.088 m. Between 32 and 28 cm both transfer function indicate a decrease in PMA before rapidly increasing to 26 cm. Despite the lack of modern analogues in the fossil samples between 25 and 22 cm, the record shows a gradually increasing trend in PMA to 4 cm. A slight decrease in PMA is then observed up to 3 cm before rising towards

the modern surface. Maximum Likelihood predictions are again comparable to PLS and WA-PLS, mirroring the increasing trend towards the modern surface. Larger errors are again associated with assemblages at the bottom of the core where calcareous taxa are found in abundance.

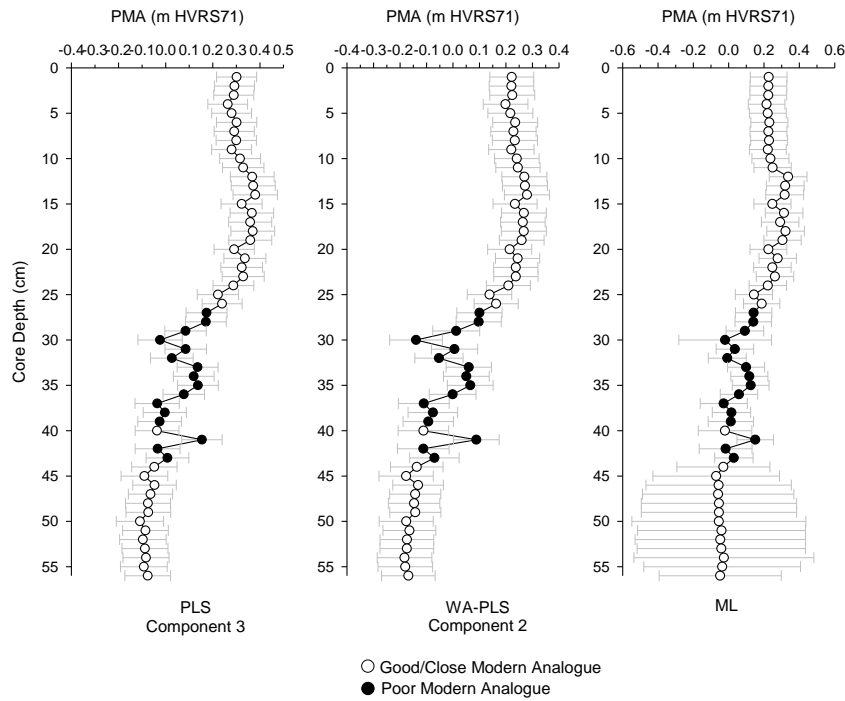


Figure 6.8. Palaeo-marsh altitude (m HVRs71) estimated using PLS (component 3), WA-PLS (component 2) and ML transfer functions for core JD2 including sample specific errors estimated by bootstrapping. Good/close and poor modern analogues also displayed.

Table 6.16. Summary of palaeo-marsh altitude and average errors for core JD2.

Model		
PLS (C3)	Maximum PMA (m HVRs71)	0.380
	Minimum PMA (m HVRs71)	-0.109
	Range of PMA (m)	0.489
	Average PMA (m HVRs71)	0.145
	Average error (m)	0.0905
WA-PLS (C2)	Maximum PMA (m HVRs71)	0.279
	Minimum PMA (m HVRs71)	-0.183
	Range of PMA (m)	0.462
	Average PMA (m HVRs71)	0.0652
	Average error (m)	0.0898
ML	Maximum PMA (m HVRs71)	0.336
	Minimum PMA (m HVRs71)	-0.071
	Range of PMA (m)	0.407
	Average PMA (m HVRs71)	0.122
	Average error (m)	0.186

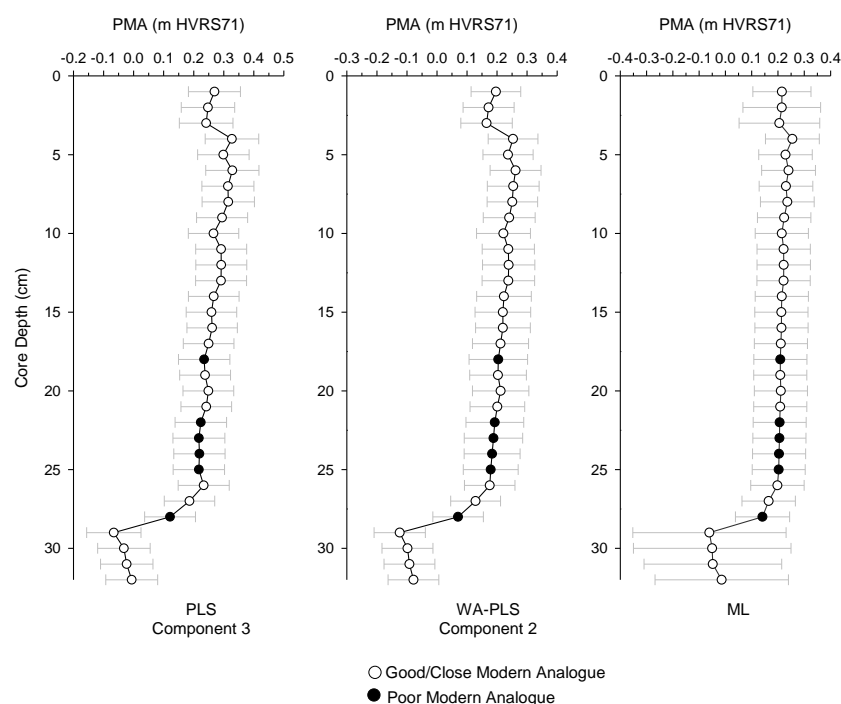


Figure 6.9. Palaeo-marsh altitude (m HVRs71) estimated using PLS (component 3), WA-PLS (component 2) and ML transfer functions for core BL including sample specific errors estimated by bootstrapping. Good/close and poor modern analogues also displayed.

Table 6.17. Summary of palaeo-marsh altitude and average errors for core BL.

Model		Value
PLS (C3)	Maximum PMA (m HVRs71)	0.328
	Minimum PMA (m HVRs71)	-0.06
	Range of PMA (m)	0.394
	Average PMA (m HVRs71)	0.221
	Average error (m)	0.0859
WA-PLS (C2)	Maximum PMA (m HVRs71)	0.262
	Minimum PMA (m HVRs71)	-0.124
	Range of PMA (m)	0.386
	Average PMA (m HVRs71)	0.168
	Average error (m)	0.0883
ML	Maximum PMA (m HVRs71)	0.255
	Minimum PMA (m HVRs71)	-0.607
	Range of PMA (m)	0.316
	Average PMA (m HVRs71)	0.180
	Average error (m)	0.127

6.3.8. Unscreened total dataset comparison

Screening ecological trainings sets to remove modern samples in order to improve the predictive ability of the transfer function is well practised in ecological sea-level studies (e.g. Edwards et al. 2004a; Gehrels et al. 2005). However an alternative approach is to include all modern samples in the training set as this is a more accurate reflection of the sampled

environment (e.g. Barlow et al. 2013). As a comparison to the training set screening presented in section 6.3.5, below are the results of a new transfer function created whereby all samples are included, including those from JDR, increasing the modern training set size to 66. Inspection of PLS model parameters in table 6.18 below reveals components two and three to demonstrate weaker transfer function performance when compared to the screened dataset presented in table 6.12 ($r^2_{\text{jack}} = 0.28$; component 2). Prediction errors produced through jack-knifing ($\text{RMSEP}_{\text{jack}}$) are also slightly larger ranging from 0.11 to 0.12m.

Table 6.18. Statistical summary of PLS transfer function performance for an unscreened total training set including samples from JDR. C = component.

TF Model	Statistical Parameter	C1	C2	C3	C4	C5
PLS	r^2	0.31	0.39	0.40	0.40	0.40
	RMSEP (m)	0.10	0.10	0.10	0.10	0.10
	Max_bias	0.17	0.15	0.16	0.16	0.16
	r^2_{jack}	0.22	0.28	0.28	0.24	0.20
	RMSEP _{jack} (m)	0.11	0.11	0.11	0.11	0.12
	Max_bias _{jack}	0.19	0.17	0.17	0.17	0.17

The unscreened total transfer function was then applied to calibrate fossil samples to provide estimates of palaeo-marsh altitude allowing a direct comparison with the results presented in section 6.3.7 above. Fossil analogues that did not possess modern equivalents as identified by the MAT in section 6.3.6 were again highlighted.

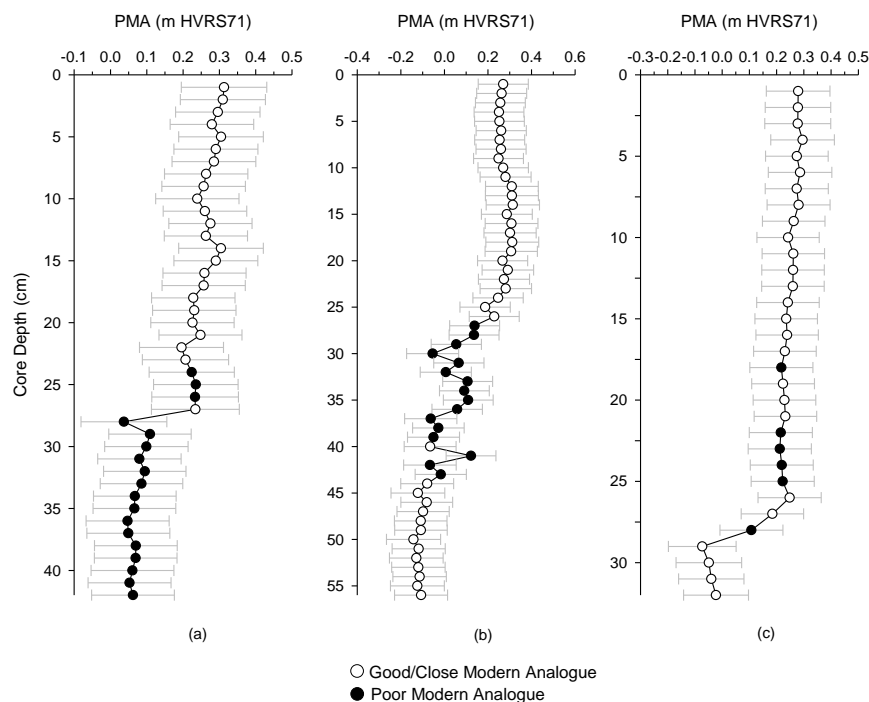


Figure 6.10. Palaeo-marsh altitude (m HVR71) for cores (a) JD1, (b) JD2 and (c) BL estimated using PLS (C2), including sample specific errors estimated by bootstrapping.

Figure 6.10 shows reconstructed palaeo-marsh altitudes for PLS (component 2) transfer functions for cores JD1, JD2 and BL using an unscreened transfer function. Whilst the trends and prediction errors produced by transfer function models are similar, PMAs predicted for JD1 core are marginally lower when compared to PMAs using the screened TCD training set (figure 6.7), however still overestimating surface altitude. Reconstructed values for cores JD2 and BL however remain very similar throughout.

Whilst the unscreened transfer function revealed a weaker strength of relationship and marginally higher prediction errors when compared to the screened transfer function, when applied to calibrate fossil samples and produce estimates of PMA, the reconstructed values and trends remain very similar throughout all cores. This process is useful to identify possible issues in removing modern samples from training sets simply based on threshold values produced by the C2 software. Ultimately this procedure identified that using a screened transfer function had no adverse effect when compared to a transfer function incorporating all modern surface samples in the training set.

6.4. SEA-LEVEL RECONSTRUCTION

Transfer function-based palaeo-marsh altitude reconstructions for cores JD1, JD2 and BL were converted to MSL and plotted against the established chronologies presented in chapter 5. Since this was restricted to the upper sections of each core, reconstructed values of MSL were also applied to the entire fossil sequences and plotted against depth. Whilst inferring sea-level changes from sections that cannot be chronologically constrained is unreliable, the procedure was useful to explore the nature of MSL change over the full depositional history of the core sequence. Fossil samples that displayed poor modern analogues are again highlighted since reconstructions based on these horizons are also considered unreliable. Estimates of palaeo-marsh altitude demonstrated WA-PLS transfer function models produced estimations that were comparable to PLS, albeit at lower altitudes. The reconstruction estimates, including ML approach, fell within the error margins of each technique and suggested that the selection of transfer function model did not significantly impact on the reconstructed trends. However, it is again difficult to justify the application of unimodal regression and calibration given the strong linear relationship of the training set as demonstrated by gradient lengths shorter than 2 SD units. As a result, the following sea-level reconstructions are constructed using the PLS (component 2) TCD screened transfer function to analyse fossil samples and produce estimates of palaeo-MSL as described below. This is also justified by the slightly improved statistical performance of PLS compared to WA-PLS in the regression stage of transfer function development (table 6.11).

6.4.1. Jadrtovac Site 1 (JD1)

Figure 6.11a shows reconstructed MSL for core JD1 plotted against depth (cm) and shows an overall increasing trend in MSL to the surface. However, inferring MSL changes from sediments below 28 cm is considered unreliable due to fossil samples displaying a poor relationship with modern analogues in the TCD training set. Thus, the sharp drop in MSL witnessed between 28-27 cm is very poorly constrained and indeed corresponds to a section of the core where insufficient counts were observed (<150; figure 5.5). Moving up through the core, MSL fluctuates to 14 cm depth but again estimates from this section of the core contain a number of poor modern analogues. By comparison, the record produced from 'good' fossil analogues appears much more stable and consistent. Above 14 cm, the sea-level reconstruction suggests a pronounced increase in MSL up to 10 cm where MSL then fluctuates towards the modern salt-marsh surface.

Figure 6.11b shows reconstructed MSL against the OxCal age-depth model (chapter 5). The extent of dating for core JD1 limits the sea-level reconstruction to the upper 28 cm of the core extending back to c. AD 1751 \pm 43 (median age) and incorporating the transition stage between agglutinated and calcareous taxa (figure 5.5). This transition also includes 6 fossil samples above 28 cm which display a poor relationship with assemblages in the modern training set. Nonetheless, the record contains useful information in resolving sea-level trends for the past 250 years or so. Disregarding the poor fossil samples, the record from AD 1765 suggests of a relatively stable MSL trend up until the early 20th century where a small decrease is observed before MSL begins to rise notably from approximately AD 1940 (\pm 13 yrs) onwards. Mean sea-level continues to rise up to AD 1968 before a period of decreasing MSL is observed to AD 1987. An increase in MSL is then observed before MSL decreases towards the surface (figure 6.10b).

6.4.2. Jadrtovac Site 2 (JD2)

Reconstructed MSL for core JD2 plotted against depth shows a more variable record in comparison to core JD1, as shown in figure 6.12a. The lowermost samples between 56 and 44 cm suggest an increasing trend in MSL before large fluctuations in the record are observed to 27 cm. Again this section of the core contains a number of fossil samples which display a poor relationship with the contemporary data and represents part of the up-core transition between agglutinated and calcareous taxa (figure 5.6). Above 24 cm, fossil samples with good modern analogues suggest an overall increase in MSL, which is amplified above 14 cm towards the present surface. Unfortunately, a hiatus in the record limited the confidence in the chronology established for core JD2 to the upper 8 cm of the

record, dating back to approximately AD 1955 (± 8 yrs). The reconstruction is therefore limited to sparse data points during the past 60 years or so (figure 6.12b) and shows an increase in MSL from AD 1955 to AD 1971. Reconstructed MSL then stabilises, displaying little change towards the surface (AD 2010).

6.4.3. Blace (BL)

Figure 6.13a plots the reconstruction of MSL against depth for core BL. It shows an increasing trend in MSL for the lowermost samples between 32 and 29 cm. These samples are composed almost exclusively of calcareous taxa (principally *Ammonia* spp. figure 5.7) and so it would appear the transfer function is over-estimating their altitude. Disregarding the fossil samples which display a poor relationship with modern assemblages, an overall increasing trend in MSL is observed from 26 cm depth upwards. A distinct increase in MSL occurs at 4 cm, corresponding to an increase in the relative abundance of *J. macrescens* (figure 5.7). Using the short-lived radionuclide chronology established for this core, the reconstruction is limited to the upper 11 cm of the core permitting sea-level inferences to be made with confidence back to AD 1888, as shown in figure 6.13b. The record shows an increase in MSL to AD 1911 (± 16 years) after which MSL appears relatively stable. The reconstruction suggests an increase in MSL from 1962 (± 4 years) at 6 cm depth before a more distinct rise is observed at 4 cm (AD 1986 ± 2 years).

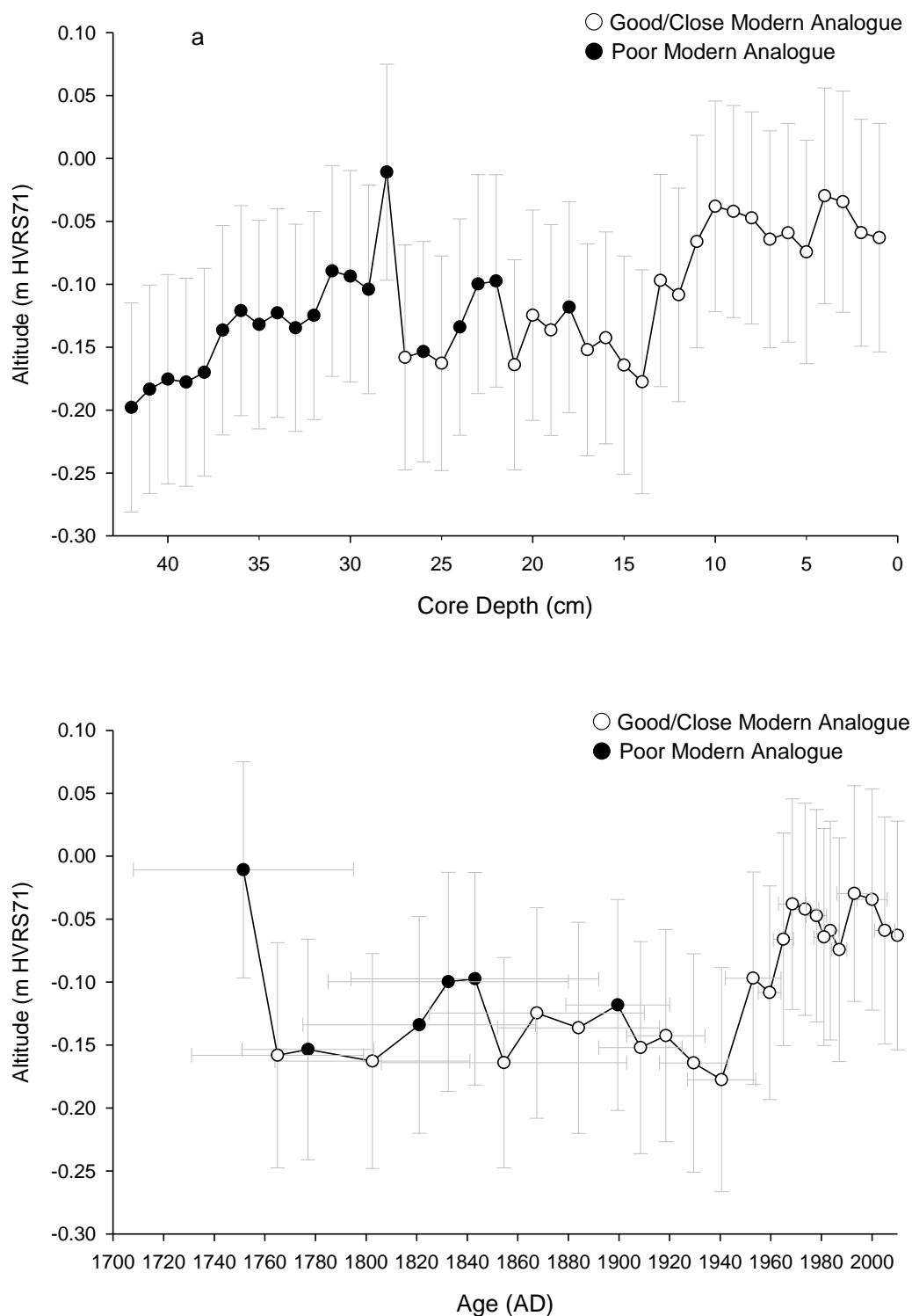


Figure 6.11. PLS transfer function reconstruction of MSL using the TCD screened training set plotted against (a) core depth (cm) and (b) OxCal age-depth model (AD) for core JD1 including bootstrap prediction errors (m) and model uncertainties (2σ). Good/close and poor modern analogues also displayed.

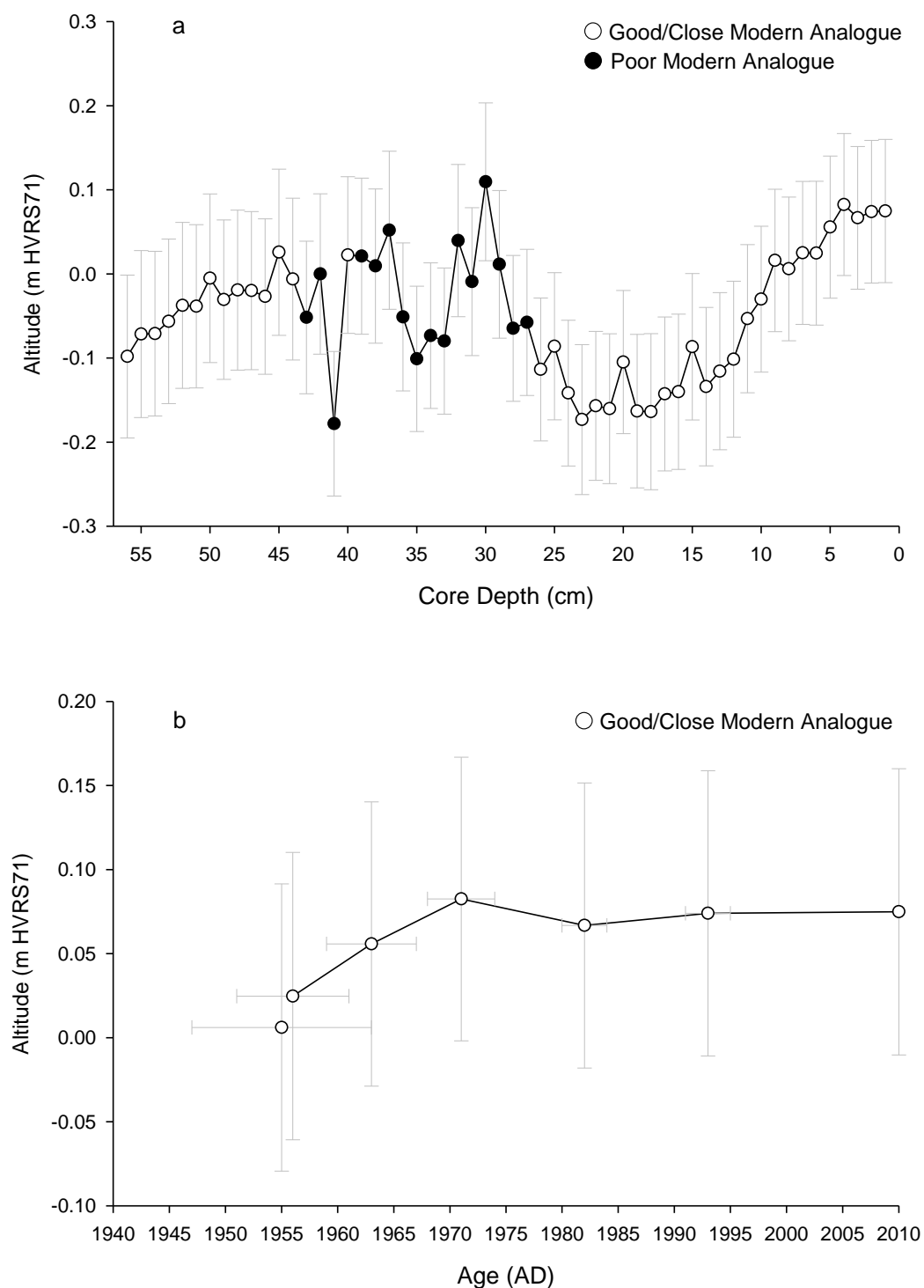


Figure 6.12. PLS transfer function reconstruction of MSL using the TCD screened training set plotted against (a) core depth (cm) and (b) chronology (AD) for core JD2 including bootstrap prediction errors (m) and age uncertainties (AD). Good/close and poor modern analogues also displayed.

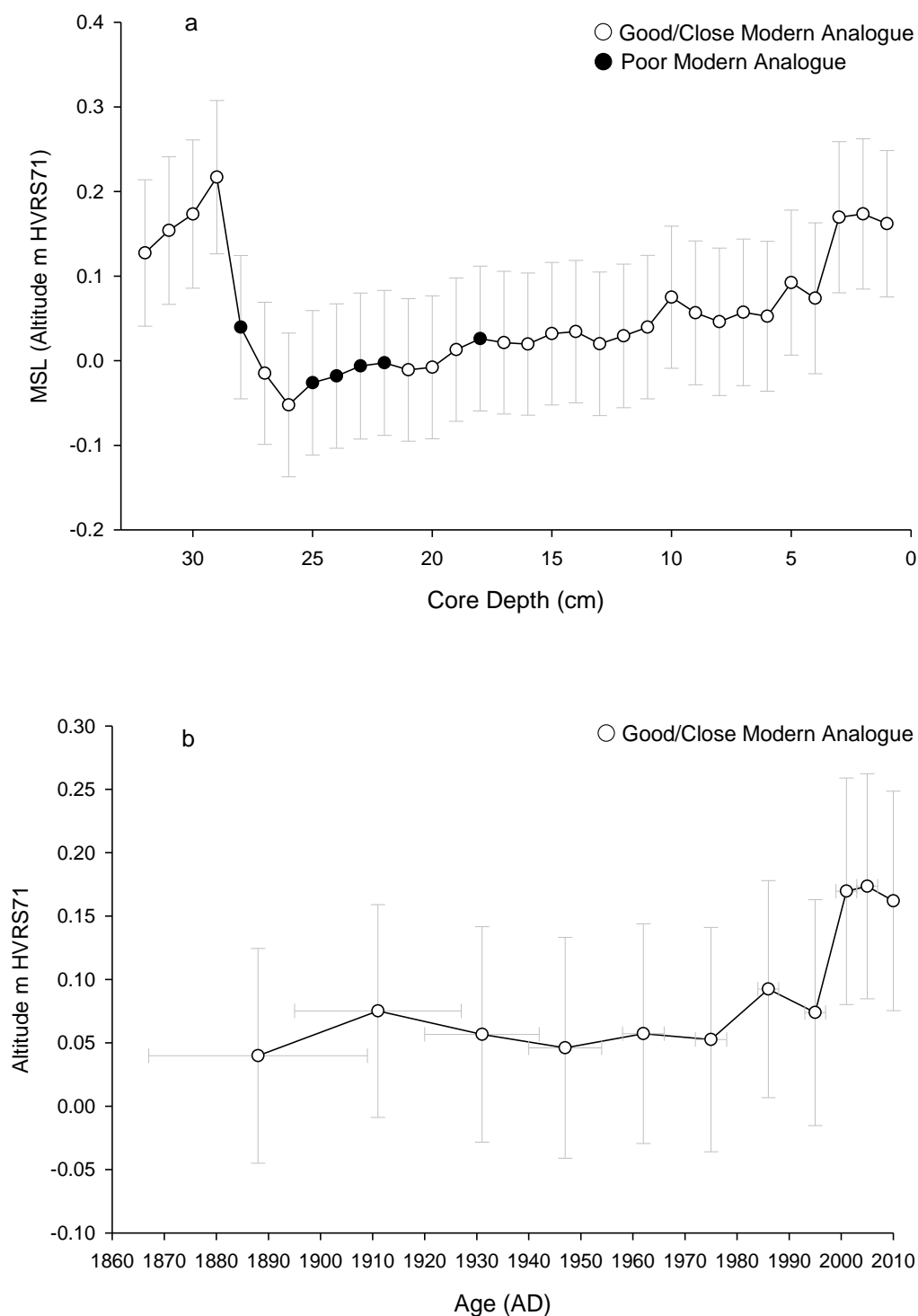


Figure 6.13. PLS transfer function reconstruction of MSL using the TCD screened training set plotted against (a) core depth (cm) and (b) chronology (AD) for core BL including bootstrap prediction errors (m) and age uncertainties (AD). Good/close and poor modern analogues also displayed.

6.5. SUMMARY OF TRANSFER FUNCTION RECONSTRUCTION

This chapter has presented the methods used in developing transfer function models for three training sets comprising site specific assemblages (JDT and BLT) and a total combined dataset (TCD). The results from unscreened analyses were variable and largely reflected the short environmental gradients of each training set. Detrended canonical correspondence analysis was used to assess the relationship between the foraminiferal assemblages in the training sets and altitude. This showed a strongly linear response along the environmental gradient with gradient lengths varying between 0.775 and 1.536 SD units. As a result linear regression models (PLS) were developed to assess the individual training sets reconstructive ability. In addition, unimodal regression (WA-PLS) was also investigated as a comparative tool for the BLT and TCD training sets which displayed longer gradient lengths in comparison to JDT.

The performance of each regression model was assessed using cross-validation results produced by jack-knifing the data. These statistical measures provided an evaluation of strength of relationship between observed and predicted values (r^2_{jack}) and associated errors of prediction ($\text{RMSEP}_{\text{jack}}$). Again results were variable, with small r^2_{jack} values reflecting the short environmental gradients, especially for JDT ($r^2_{\text{jack}} = 0.11$), despite prediction errors remaining small ($\text{RMSEP}_{\text{jack}} = 0.07$). The low strengths of relationship at this site perhaps reflect the influence of other environmental variables effecting the distribution of foraminiferal assemblages. Indeed inter-correlations between the variables were high for the JDT training set (69.7%), as shown in chapter 4. In comparison, inter-correlation between the variables for BLT training set was significantly lower (33.5%) which is reflected in a higher strength of relationship for this training set ($r^2_{\text{jack}} = 0.71$). Prediction errors remained relatively low for the BLT training set ($\text{RMSEP}_{\text{jack}} = 0.09$). When combining both training sets to create a total combined dataset (comprising 56 samples), the strength of relationship deteriorated and prediction errors increased ($r^2_{\text{jack}} = 0.32$; $\text{RMSEP}_{\text{jack}} = 0.11$).

The TCD training set was further investigated to remove sample outliers with a goal of improving model performance. This was achieved by removing all surface samples with an absolute residual greater than the standard deviation of altitude (0.141 SD units). Statistical parameters showed this procedure was useful in improving model performance with an increased strength of relationship ($r^2_{\text{jack}} = 0.54$) and lower prediction errors ($\text{RMSEP}_{\text{jack}} = 0.08$) for component three using linear regression (table 6.11). Unimodal regression (WA-PLS) showed similar performance. Component two was chosen to calibrate fossil samples as it performed better than components one and two but degraded thereafter. Similarly PLS

regression and calibration was selected as it was difficult to justify the use of unimodal techniques given the short-gradient lengths involved.

The MAT was used to assess similarities and dissimilarities of fossil samples in cores JD1, JD2 and BL with assemblages from the modern environment. Percentiles produced by dissimilarity measures in the TCD training set were used to define thresholds allowing to distinguish between good, close and poor modern analogues. The number of fossil samples with poor modern analogues varied between the cores and largely reflected the limited number of modern analogues in the contemporary training set which was biased towards the upper part of the environmental gradient. Clearly the range of environments observed in the fossil sequences was greater than that sampled in the modern environment with many lower core fossil samples lacking modern equivalents.

Changes in palaeo-marsh altitude were investigated highlighting those levels where reconstructed values were considered unreliable. Overall the cores showed a variable, but increasing trend in palaeo-marsh altitude towards the surface. To determine if the selection of transfer function model had a significant impact on the reconstruction, an additional transfer function using the ML approach was developed. Results were comparable where reconstructed values fell within the error margins of each technique. However it also highlighted the uncertainty of reconstruction for fossil samples which contained an almost exclusive calcareous component towards the bottom of each core.

Reconstructed palaeo-marsh altitudes were converted to produce estimates of MSL, first plotted against depth and then age. A high-resolution record is observed for core JD1 where age-depth modelling suggests a record dating back to AD 1751. The record here suggests relatively stable MSL observations up until the early 20th century where fossil samples with good modern analogues suggest a sharp increase in MSL around AD 1940. Mean sea-level continues to rise up to AD 1968 and then a fall to AD 1987. A fluctuating record is then observed to the present day. In contrast, core JD2 demonstrates a relatively poor resolution record when plotted against age due to the limited number of samples included in the reconstruction which dates back to AD 1955. Nonetheless the record is based on fossil samples which display a good relationship with modern assemblages and suggests an increase in MSL up until AD 1971 with stable observations of MSL recorded thereafter. Reconstructed MSL for core BL allows sea-level inferences to be made dating back to AD 1888. The record indicates increasing trends in MSL to AD 1911 after which MSL stabilises up until AD 1962. An increasing trend in MSL is observed thereafter before faster rates of MSL rise are observed from 4 cm depth (AD 1986).

INTERPRETATIONS AND DISCUSSION

7.1. INTRODUCTION

The following chapter brings the findings of the preceding results chapters together to first interpret and then consider the significance of the main outcomes of the research. First the fossil environments at Jadrtovac and Blace are discussed, focusing on site evolution through an interpretation of the sediment stratigraphy and fossil foraminiferal record. Following this, an assessment of the contemporary foraminiferal distributions is provided, including their utility as proxies for sea level using a transfer function approach. The developed PLS transfer function model is then critically examined in comparison to previous work where reconstructions have been performed in microtidal environmental and from short environmental gradients. As a final assessment of the sea-level reconstruction, tide-gauge data are used to validate the salt-marsh records by comparing them with instrumental data from Split and Trieste. The observed trends are discussed and compared before extrapolation over the period prior to the instrumental record is explored. Finally the limitations of the study are addressed with recommendations for further work.

7.2. FOSSIL ENVIRONMENTS AND SITE EVOLUTION

The investigation into the sediment stratigraphy at Jadrtovac and Blace salt-marshes presented in chapter 5 revealed an overall pattern of sedimentation that was broadly similar throughout. Both sites showed a variable thickness of minerogenic clays and silts above limestone bedrock, the depths of which generally increased towards the open sea (figures 5.1 and 5.3). Within these units there was also a variable abundance of broken and whole shell fragments. Up-core transitions show an increase in the proportion of organic matter to the present day surface where a more humified peat-like layer was restricted to the upper reaches of the salt-marsh environments. Indeed, sediment cores were much shallower here in comparison to those from the lower salt-marsh environment.

It would appear that the salt-marsh environments have undergone a transition stage, as interpreted from a change in sedimentation from deposits more characteristic of subtidal and lower intertidal mudflat conditions (e.g. fine silts and clays with low organics) to increasingly organic sediments more characteristic of vegetated, upper intertidal to supratidal environments. The deposition of sediments over time has raised the surface of the salt-marsh environments within the tidal frame which, in turn, has decreased tidal inundation frequency and duration (hydroperiod). A direct result of this sedimentation decrease has allowed halophytic vegetation to develop further to colonise much of the salt-marsh environment (e.g. Pethick, 1981). Fluctuating trends in mean sea level and also tidal range impact on salt-marsh environments by creating (or similarly removing) accommodation space which has a direct impact on vertical sedimentation rates (Allen, 2000). As silt and clay deposits are often difficult to interpret based solely on their appearance and grain size, further environmental parameters in combination with microfossil analyses provide supplementary evidence from which to interpret changes in the depositional environment (Allen, 2000).

Particle size characteristics (figure 5.10) revealed minor changes in grain size and composition within each core, where silts and clays dominate the record. The mean grain size for cores JD1 and JD2 were very similar ($\sim 5 \mu\text{m}$). By comparison, the mean grain size for core BL was slightly larger at $\sim 10 \mu\text{m}$, with a notably increase in sand content. This may reflect the locations of the study sites in relation to the open sea, where Blace lies directly adjacent to the Adriatic Sea while the salt-marshes at Jadrtovac are situated at the end of a narrow 2.5 km-long channel (section 3.3). The up-core transition from sub- and intertidal mudflat sediments to an upper intertidal environment is confirmed through the analysis of environmental variables LOI and DBD (section 5.4). Analyses show an up-core transition from basal minerogenic sediments to increasingly organic deposits matched by increasing and decreasing measurements of LOI and DBD, respectively (figures 5.8 and 5.9).

Further to this are changes in the biostratigraphic record that also show a change in the depositional environment through the up-core transition from foraminiferal taxa more characteristic of open marine and subtidal environments to foraminiferal taxa more indicative of an environment above or around MSL (section 5.3). Interestingly it would appear that changes in biostratigraphic record have responded faster in comparison to their lithogenic counterparts. This transitional zone typically shows calcareous foraminifera (*Ammonia* spp., *Elphidium* spp. and *Haynesina germanica*) replaced by agglutinated types (*J. macrescens*, *T. inflata* and *M. fusca*) moving up through the core, pre-dating the onset of increasing organic matter levels (e.g. core JD1; figure 5.5).

Inspection of the biostratigraphy shows similar species colonising the present-day environment to those observed in the fossil sequences, suggesting that the depositional environments preserved in fossil samples are largely similar to that observed today. An exception to this was the almost complete omission of *Quinqueloculina* spp. from the lower section of the fossil records where other calcareous taxa flourish. Indeed *Quinqueloculina* spp. were found in abundance on the contemporary salt-marsh surface at both sites, in conjunction with the other main calcareous taxa. Therefore, it seems odd that only this species is absent from the fossil record. Calcareous foraminifera are notoriously susceptible to post-depositional dissolution processes where the test linings are destroyed (e.g. Murray, 1989). In a study of core material from Poole Harbour, southern England, (Edwards and Horton, 2000) observed a significant destruction of calcareous tests due to post-depositional dissolution. The absence of *Quinqueloculina* spp. does not appear to be site-specific, as its exclusion from the fossil record is repeated in all analysed cores.

7.3. CONTEMPORARY FORAMINIFERAL DISTRIBUTIONS

7.3.1. Foraminiferal assemblages

In foraminiferal-based transfer function sea-level reconstructions, the relationships between modern assemblages and environmental controls are often varied. The dynamic environments that characterise salt-marshes mean that a global model for palaeoenvironmental reconstructions is not applicable and thus the transfer functions are generally site specific. Differences in tidal range create faunal zones in which characteristic species occur which are altitudinally constrained in relation to tidal level. Indeed environmental conditions that effect foraminiferal distributions at one site may be negligible at another. Despite this, there is much consistency regarding the vertical zonation of intertidal foraminifera with respect to the tidal level from salt-marsh and mangrove environments around the world (Scott and Medioli, 1978).

Typically agglutinated forms are usually found in abundance within upper intertidal vegetated high salt-marsh elevations whereas calcareous tests tend to dominate lower intertidal and subtidal unvegetated levels (Berkeley et al., 2007). The most common agglutinated species, *J. macrescens* and *T. inflata*, are consistently found in abundance to dominate areas around MHWST in salt-marsh environments (Horton et al., 1999b; de Rijk and Troelstra, 1997; Edwards et al., 2004b). Whilst other agglutinated taxa such as *M. fusca* are typically more constrained in mid salt-marsh settings between MTL and MHWST (de Rijk and Troelstra, 1997; Edwards et al., 2004b). Calcareous foraminifera such as *Ammonia* spp., *Elphidium*

spp and *Quinqueloculina* spp. on the other hand are more indicative of low vegetated elevations in low salt-marsh and mudflat environments (Woodroffe et al., 2005; de Rijk and Troelstra, 1997; Horton et al., 1999b).

The analysis of contemporary foraminiferal distributions in this study has shown that whilst agglutinated and calcareous species are found throughout the entire sampled range, solely agglutinated or calcareous assemblages are altitudinally constrained and support the theory of vertical foraminiferal zonation. Indeed, the observations made are comparable with other studies of foraminifera within intertidal salt-marsh and mangrove environments. Despite inter-site variability, multivariate analyses revealed a broadly similar faunal zonation between the Jadrtovac and Blace datasets. This consisted of a faunal zone dominated by an agglutinated assemblages, where high abundances of *J. macrescens* and *T. inflata* were observed with minimal calcareous taxa. This faunal zone typically extended from around MTL to above MHWST. A second faunal zone was also observed which was characterised by high abundances of *J. macrescens* and *T. inflata* with increased calcareous numbers. This mixed assemblage zone spanned the largest large vertical range ranging from around MHWST to below MTL. A third faunal zone was also observed, where calcareous taxa were substantially more abundant. Whilst agglutinated forms are often present, they typically are in low abundance. This faunal zone was also altitudinally constrained below MTL.

The lack of comparable studies concerning the vertical zonation of foraminifera for sea-level studies along the eastern Adriatic coastline hinders comparisons with more localised work. However, similarities with studies in the northern Adriatic and other temperate salt-marshes are possible, displaying similar characteristics to the assemblages observed in this study. For example, in an investigation of foraminiferal distributions from a mangrove environment in the Great Barrier Reef, Horton et al. (2003) observed an abundance of agglutinated taxa, with high occurrences of *T. inflata* (up to 46%) to dominate the zone between MSL and MHWST. This is comparable contemporary distributions at Jadrtovac and Blace where *T. inflata* is found in abundance between MTL and MHWST. Similarly high occurrences of *T. inflata* have also been reported from studies in the northern Adriatic region, where foraminiferal distributions have been used to identify biotopes that characterise the different environments of the Venice Lagoon (e.g. Serandrei-Barbero et al., 1999; Albani et al., 2007; Serandrei-Barbero et al., 2011). In these studies, the genus *Trochammina* characterises two altimetric zones between MSL and mean high water level (MHWL) (Petrucci et al., 1983; Serandrei-Barbero et al., 1997; Serandrei-Barbero et al., 1999) and also the zone above MHWL (Albani et al., 1984). Indeed Petrucci et al. (1983) showed a *T. inflata* dominated assemblage to indicate a ground height of about 15 cm above the local MSL in the Venice Lagoon area. This is comparable to heights observed in this study where an agglutinated

assemblage with high abundances of *T. inflata* extends up to and above >0.30 m HVRS71 (MSL is 0.131 m). In a study utilising foraminiferal distributions as ecological indicators, Albani et al. (2007) also observed a foraminiferal assemblage composed of *T. inflata* with an abundance greater than 60% that was typical of an environment above MSL. The authors also demonstrate high abundances of calcareous species *Ammonia* spp. and *Haynesina germanica* characterising the inner areas of the lagoon environment which are affected more marine waters.

7.3.2. Dead versus Living Assemblages

The quantitative analyses presented in this study focused on dead foraminiferal assemblages only. The selection of the most appropriate foraminiferal assemblage can have important effects on the transfer function performance and the choice to which assemblage should be used (e.g. Jorissen and Wittling, 1999) remains a discussion topic in foraminiferal based sea-level reconstructions from salt-marsh environments. The studied environments of Jadrtovac and Blace salt-marshes displayed considerably fewer living populations in comparison to dead, with only five out of the seventy analysed surface samples sustaining statistically sufficient counts of 150 or more. Many of the surface samples were void of living foraminifera altogether. The stark contrast between the concentration of living and dead foraminiferal assemblages at Jadrtovac and Blace is a common feature characterising low sedimentation environments (Murray, 1976) and this observation confirms previous studies analysing foraminiferal assemblages along the Adriatic coast of Croatia. Cosovic et al. (2006) collected sediments from several stations along a transect extending from the coast out towards the open sea down to a depth of 55 m. Analysis of modern assemblages revealed dead foraminiferal tests to be much more abundant compared to living assemblages regardless of the sampling season. Other studies near the Gulf of Venice, northern Adriatic have also shown dead populations to be more abundant but also more diverse (Serandrei-Barbero et al., 2003).

Several authors have argued that total (i.e. living and dead) assemblages are an accurate representation of the modern environment and so offer a more reliable model in palaeoenvironmental reconstructions (e.g. Scott and Medioli, 1980; Gehrels, 1994; Hayward et al., 1999; Tobin et al., 2005). However, incorporating living assemblages into a training set includes foraminifera which are suited to the environmental conditions at the time of sampling (Callard et al., 2011). As this will fluctuate in line with seasonal changes, species diversity and abundance can change over time (Murray, 1991; 2000; Horton et al., 1999a). Murray (1991) also states that a total assemblage including living populations does not consider the post-mortem changes that have yet to take place.

In a comprehensive study of foraminiferal assemblages from Cowpen Marsh, Great Britain, Horton (1999) concluded dead foraminiferal populations are a better analogue for sub-surface samples in sea-level reconstructions. Using dead foraminiferal assemblages takes into account both live and dead populations over a greater time-average and so species diversity is generally greater (Murray, 1982; 2003). Dead foraminiferal assemblages also do not suffer from seasonal fluctuations observed in living populations (Horton and Edwards, 2006) and where living populations are spatially variable, including them into a total assemblage dataset may even degrade the quality of data from the dead assemblage (Horton and Murray, 2006). As a result and due to their sparse distribution at Jadrtovac and Blace, only dead foraminiferal populations were employed in the statistical analyses (following Horton, 1999; Gehrels et al., 2001; Horton and Edwards, 2003; Leorri et al., 2010; Rossi et al., 2011; Kemp et al., 2013).

7.3.3. Foraminifera and Environmental Controls

Whilst the relationship between foraminiferal assemblages and height within the tidal frame is well documented around the world, the significance of elevation (acting as a proxy for tidal flooding) in explaining this relationship is less clear and much more spatially variable. Quantifying elevation as an important control governing contemporary distributions is fundamentally prerequisite in transfer function-based sea-level reconstructions using microfossils. In order to justify the reconstruction, one has to demonstrate elevation as a statistically significant control in explaining variance in the modern dataset. Indeed, one of the main assumptions with the transfer function technique is that the environmental variable of interest (e.g. elevation), has remained an important control over the entire depositional history of the sediment sequence (Birks, 1995). Therefore, collecting various other environmental variables, such as salinity, pH and organic matter for example, offers some sort of independent assessment of this hypothesis.

Many investigations have observed elevation explaining a statically significant proportion of the explained variance within species data distributions (e.g. Horton et al., 1999b; Hill et al., 2007; Horton and Culver, 2008; Hawkes et al., 2010). One notable example by Horton and Edwards (2006) showed elevation that explains 42% of the explained variance when compared with other environmental variables, using foraminiferal data from sites around the UK (table 7.1). In comparison, other environmental parameters can often exert a greater control. For example, in a study of foraminiferal distributions from the Great Marshes in Massachusetts, de Rijk and Troelstra (1997) demonstrated that elevation was in part only equal or inferior to other environmental controls where salinity was more influential. The underlying response of foraminiferal distributions in relation to the environmental gradient is

important as it provides a foundation from which transfer function models are based. Selection of the appropriate statistical technique is underpinned by the species' linear or unimodal distribution (Birks, 1995).

Kemp et al. (2012a) present an alternative method to quantify the distribution of foraminiferal assemblages using partitioning around medoids (PAM) in combination with linear discriminant functions (LDFs). In this approach, the underlying distributions and response of foraminiferal distributions is not as fundamental by comparison to transfer function technique, providing probability estimates of fossil core samples based on similarities between the modern and fossil assemblages. The authors show that whilst transfer functions provide smaller error terms and have the ability to reconstruct smaller changes in sea-level, LDFs provide a robust alternative approach. In this way, it offers an additional approach to reconstructing sea-level changes but also as an independent assessment between the techniques. LDFs, however, are more suited to larger scale changes in sea-level using a varied modern assemblage. Whilst this may not be suitable for the datasets presented in this thesis, due to the low diversity observed, it is acknowledged that it may provide additional support to the reconstructions constructed in chapter 6.

Ordination and partial ordination techniques were used to investigate the relationship between foraminiferal assemblages and environmental variables for datasets at Jadrtovac (JDT), Blace (BLT) and a total combined dataset. One notable feature of the constrained ordination approach in analysing foraminiferal and associated environmental datasets is the often large unexplained variance that cannot be accounted for with the included environmental data. The unexplained proportion observed in this study ranged from 33% to 58% (table 7.1). This may reflect other environmental conditions or factors not recorded at the time of sampling such as seasonal fluctuations (Horton and Edwards, 2003), temperature, dissolved oxygen and microtopography. The explained percentage observed in this study is comparable to studies utilising intertidal microfossil for sea-level studies ranging from 42% to 67%. When analysing the individual contributions of the tested environmental variables, a weaker relationship with elevation is relatively common in microfossil-based transfer function reconstructions where multiple datasets are investigated (e.g. Sawai et al., 2004; Horton and Culver, 2008). However, the analysis of foraminiferal distributions and associated environmental controls in this thesis suggested altitude was still significant in explaining variance in combined foraminiferal datasets ranging from 13% to 22% and is comparable to other studies as shown in table 7.1. Indeed Monte Carlo permutation tests further confirmed this relationship ($p = <0.05$), illustrating statistically robust transfer functions could be developed.

Table 7.1. Summary table highlighting the amount *height accounts for in the explained variance for microfossil distributions from salt-marsh environments.

Microfossil	Study/Reference	Explained (%)	Unexplained (%)	*Height (%)
Foraminifera	JDT	42	58	13
	BLT	67	33	22.1
	Total Combined Dataset	48	52	13.5
	Horton and Edwards (2005)	52	48	23
	Horton and Edwards (2006)	76	24	42
	Horton and Culver (2008)	57	43	16
	Hawkes et al. (2010)	78	22	39
	Mills et al. (2013)	52	48	4
	Zong and Horton (1999)	22	78	23
Diatoms	Sawai et al. (2004)	20	80	15
	Hill et al. (2007)	25	75	27
Pollen	Engelhart et al. (2007)	26	74	14

*e.g. Elevation/SWLI/Altitude

Inter-correlation between the environmental variables examined on Jadrtovac and Blace salt-marshes was large, ranging from 33% to 71%. This may suggest that altitude cannot be considered independent of the other variables. Additionally it must also be assumed that the joint correlation observed in the modern datasets also applies to fossil samples in sediment cores (Birks, 1995). The joint correlation can be anticipated due to other environmental variables (e.g. salinity) also being highly correlated with tidal flooding duration and frequency (Horton and Edwards, 2006). High inter-correlations between environmental variables is a common feature of most quantitative studies using microfossil assemblages from intertidal environments. In a study of foraminiferal distributions on the Outer Banks, North Carolina, Horton and Culver (2008) show inter-correlations to be greatest contributor to the explained variance of 37%. Similarly in a study of foraminifera to reconstruct past subsidence in Oregon, USA, Hawkes et al. (2010) illustrates 29% of the variability in the explained variance is due to inter-correlations between the variables. Using mangrove pollen as sea-level indicators in Indonesia, Engelhart et al. (2007) also report large inter-correlations, up to 59% of the explained variance.

Whilst altitude remains a statistically significant control, and in some instances the only significant control, the observed intercorrelations between the environmental variables may in part reflect the limited tidal range at the study sites. A distinct advantage of developing transfer function models from microtidal environments is that the vertical errors associated with the technique are minimised and in theory transfer functions from these environments should produce the most precise sea-level reconstructions (Southall et al., 2006; Callard et al., 2011; Barlow et al., 2013). Theoretically the errors associated with reconstructions from micro-tidal salt-marshes should be proportional to the tidal range (as discussed below). Indeed Kemp et al. (2009a) observed small vertical errors ($RMSEP_{jack}$) of just 0.04 to 0.05 m

in a study using foraminifera and diatoms from microtidal salt-marshes in Northern Carolina where the difference between MLLW and MHHW was around 0.4 m. Decreasing microtidal regimes, however, can have important and significant consequences in limiting the vertical zonation of foraminiferal species and changes in other environmental parameters, such as salinity, can become more important in comparison to macro- or meso-tidal sites (Barlow et al., 2013). The effect of other individual environmental variables (e.g. salinity and LOI) observed in this study was limited with permutation tests confirming their insignificant contribution. However, collectively they contribute a significant proportion of the explained variance in the training sets used to develop transfer functions. The mean tidal range at study sites Jadrtovac and Blace was just ~23 cm. Nonetheless, altitude was still found to be a significant environmental component dictating foraminiferal distributions (up to 22%) and confirmed their suitability as proxy indicators of sea-level for use in transfer function reconstructions.

7.4. TRANSFER FUNCTION PERFORMANCE

Using altitude as the only constraining environmental variable, DCCA revealed gradient lengths that indicated strongly linear species distributions along the environmental gradient ranging from between 0.775 and 1.536 SD units for site specific training sets JDT and BLT. In combining datasets together (TCD), the gradient length was still strongly linear at 1.173 SD units. As a result, PLS linear regression models suggested the strength of relationship (r^2_{jack}) was relatively weak for an unscreened training set (0.32; component 3). Whilst this may appear poor, it is directly related to the short environmental gradient of the contemporary training set. Indeed, in combining local training sets to create a single combined training set, the strength of correlation between foraminiferal assemblages and the environmental variable (e.g. elevation) is reduced. Whilst this may seem counterintuitive to do so, a regional combined dataset provides an increased range of modern environments from which the fossil assemblages can be compared with, as discussed below (Gehrels et al., 2001).

The sampled vertical range of the contemporary training set has a strong impact on model predictive ability (Barlow et al., 2013). The small r^2_{jack} values in this study therefore reflect the bias in sampling towards in the upper part of the elevational gradient. In such cases, RMSEP_{jack} may offer a more realistic assessment of the model performance (Gehrels et al., 2001; Leorri et al., 2010). This suggested model predictions of sea-level to within 0.11 m for an unscreened training set. In order to improve model performance, sample outliers in modern training sets are often excluded on the basis of their poor relationship with elevation (Edwards et al., 2004a; Gehrels et al., 2005; Horton and Edwards, 2006; Leorri et al., 2008;

Rossi et al., 2011). The performance of transfer function models are sensitive to such 'tuning' processes (Woodroffe, 2009). However, tuning helps by improving the predictive ability of the training set whilst increasing the strength of relationship. In this study, by removing all samples with an absolute residual (observed minus predicted) greater than the standard deviation of altitude, the strength of relationship improved to $r^2_{\text{jack}} = 0.54$ whilst prediction errors (RMSEP_{jack}) decreased to 0.08 m.

Linear regression and calibration methods are less common in quantitative sea-level reconstructions due to the often observed unimodal distribution of species in response to elevation. However, the results of this study are comparable to other research where PLS transfer functions have been applied. For example, in a study of foraminiferal distributions from Brittany, France, Rossi et al. (2011) also observed short environmental gradients (0.67 SD units). Based on a modern training set comprising 36 samples, the authors demonstrated robust transfer function performance ($r^2_{\text{jack}} = 0.70$; RMSEP_{jack} = 0.07 m) and applied the model to reconstruct relative sea-level changes back to AD 1850 showing comparable rates of change to direct observations from the Brest tide-gauge. Callard et al. (2011) also used PLS regression to construct a transfer model for sea-level studies in Tasmania. Their results showed that whilst PLS produced good statistical parameters, comparable to unimodal regression WA-PLS, when the model was applied to core sediments but was unreliable when used for predictions due to estimates larger than the modern sampling range and also exceeding the tidal range.

As discussed, the strength of relationship of foraminiferal assemblages from microtidal environments is typically weaker by comparison to macrotidal settings and can be directly related to the small vertical range of the samples studied (Horton and Edwards, 2006). Counter to this however are the small vertical prediction errors associated with microtidal settings. As such, microtidal environments are regarded as ideal settings for quantitative sea-level reconstructions based on microfossils (Callard et al., 2011). In a theoretical scenario, a tidal range of 20 cm should provide prediction errors of approximately 10% of the tidal range (i.e. 2 cm) (Barlow et al., 2013). Whilst this is achievable (e.g. Kemp et al., 2009a), if the vertical relationship between foraminiferal assemblages and elevation is less defined, a microtidal environment may offer little benefit in terms of prediction errors. Inspection of model prediction errors for a screened TCD training set in this study revealed precise sea-level reconstructions were possible to within 0.07 m. At first, while these results may seem promising, when taken as a percentage of the mean tidal range, prediction errors are actually greater by comparison to those studies conducted in larger tidal ranges (table 7.2). In this study the mean tidal range at the samples sites was 0.23 m equating to prediction error of almost a third of the mean tidal range (30%). Nonetheless the data can

still be used to interpret trends of past sea level providing the record is independently assessed (i.e. tide gauge records).

Table 7.2. Comparison table of microfossil transfer function prediction errors ($RMSEP_{jack}$) and as a percentage of the tidal range with published studies.

Location	Model	RMESP (m)	RMESP (m) % tidal range	Reference
Central Croatia	PLS	0.07	30	This study
New Zealand	WA-Tol	0.05	3.3	Southall et al. (2006)
Maine, USA	WA-PLS	0.25	8	Gehrels (2000)
Western Denmark	WA-Tol	0.16	10.7	Gehrels and Newman (2004)
Nova Scotia, Canada	WA-Tol	0.06	3.7	Gehrels et al. (2005)
Biscay, Spain	WA-PLS	0.19	7.6	Leorri et al. (2008)
Tasmania	WA-PLS	0.10	16.7	Callard et al. (2011)
Brittany, France	PLS	0.07	2.3	Rossi et al. (2011)
Southern Portugal	PLS	0.10	4.8	Leorri et al. (2010)
Brittany, France	PLS	0.13	4.9	Leorri et al. (2010)
North Carolina, USA	WA-PLS	0.04	14.8	Kemp et al. (2009b)
Hokkaido, Japan	WA-PLS	0.29	27.6	Sawai et al. (2004)
North Carolina, USA	WA-PLS	0.08	22.9	Horton et al. (2006)

7.5. COMPARISON WITH INSTRUMENTAL RECORDS

As a final independent assessment of the transfer function sea-level reconstructions presented in chapter 6, instrumental tide gauge records were used to assess the validity of the reconstructed sea-level trends (following Gehrels et al., 2005; Kemp et al., 2009a; Rossi et al., 2011). Annual averaged MSL data with benchmark datum history were extracted from the PSMSL database (Holgate et al., 2013) for the Split tide gauge. This provides the longest time-series along the Croatian coast of the Adriatic Sea and is in close proximity to the study sites presented. To provide a longer time-series, annual MSL values were also extracted from Trieste tide gauge in northern Adriatic. A summary for both tide gauges is presented in table 7.3 below whilst annual mean sea-level trends for Split and Trieste are plotted in figures 7.1 and 7.2, respectively. In order to construct a time-series for each tide-gauge station, the PSMSL converts raw metric data from each station to a common global datum referred to as the revised local reference (RLR). This datum is defined to be approximately 7000 mm below mean sea-level at each station. To allow direct comparison of trends, the RLR data were converted to plot directly with the reconstructed values of mean sea-level. This was achieved by ‘tuning’ the RLR data to match the reconstruction centred around the year AD 2010 (time of sampling).

Table 7.2. Summary information for Split and Trieste tide-gauge stations (Holgate et al., 2013).

Name	PSMSL Station ID	Latitude	Longitude	Time span	Data Coverage (%)
Split	352	43.5067	16.4417	1954-2011	100
Trieste	154	45.6473	13.7584	1875-2012	86

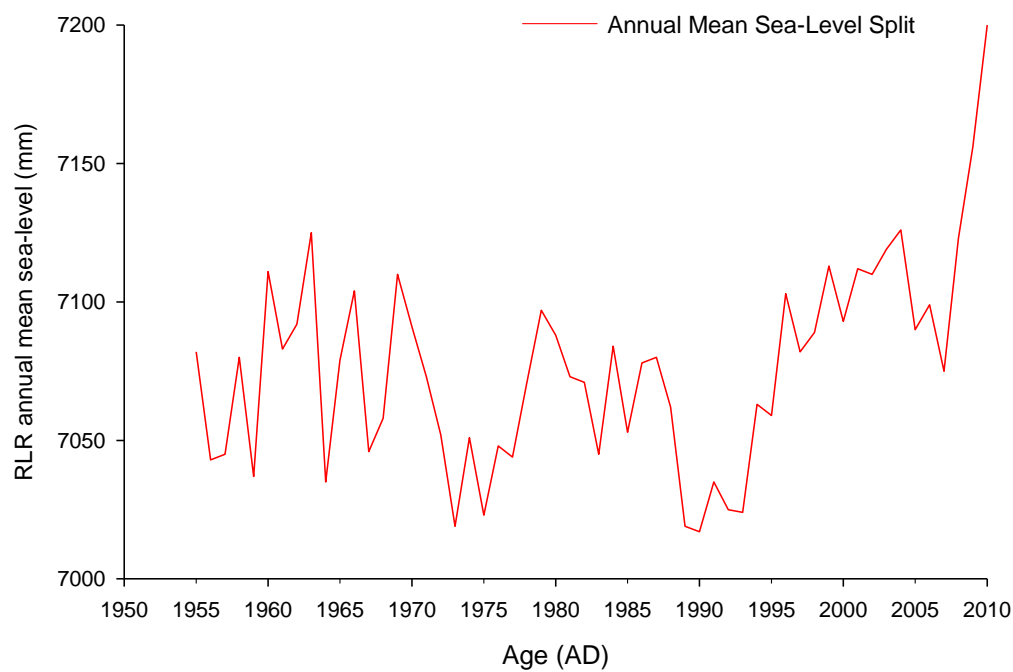


Figure 7.1. Yearly average mean sea-level from Split tide-gauge (Holgate et al., 2013).

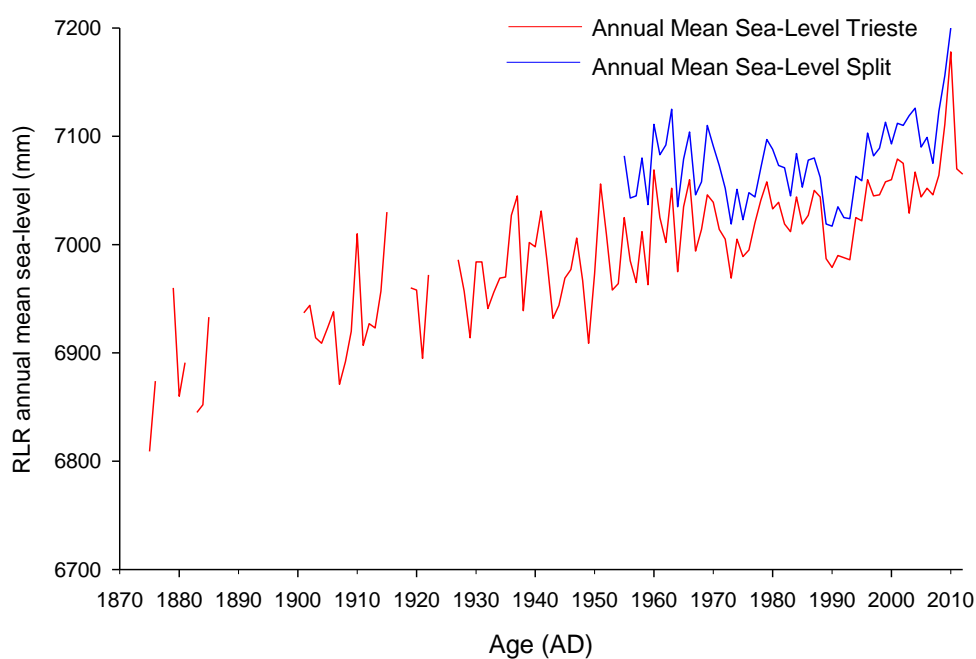


Figure 7.2. Yearly average mean sea-level from Trieste tide-gauge (Holgate et al., 2013).

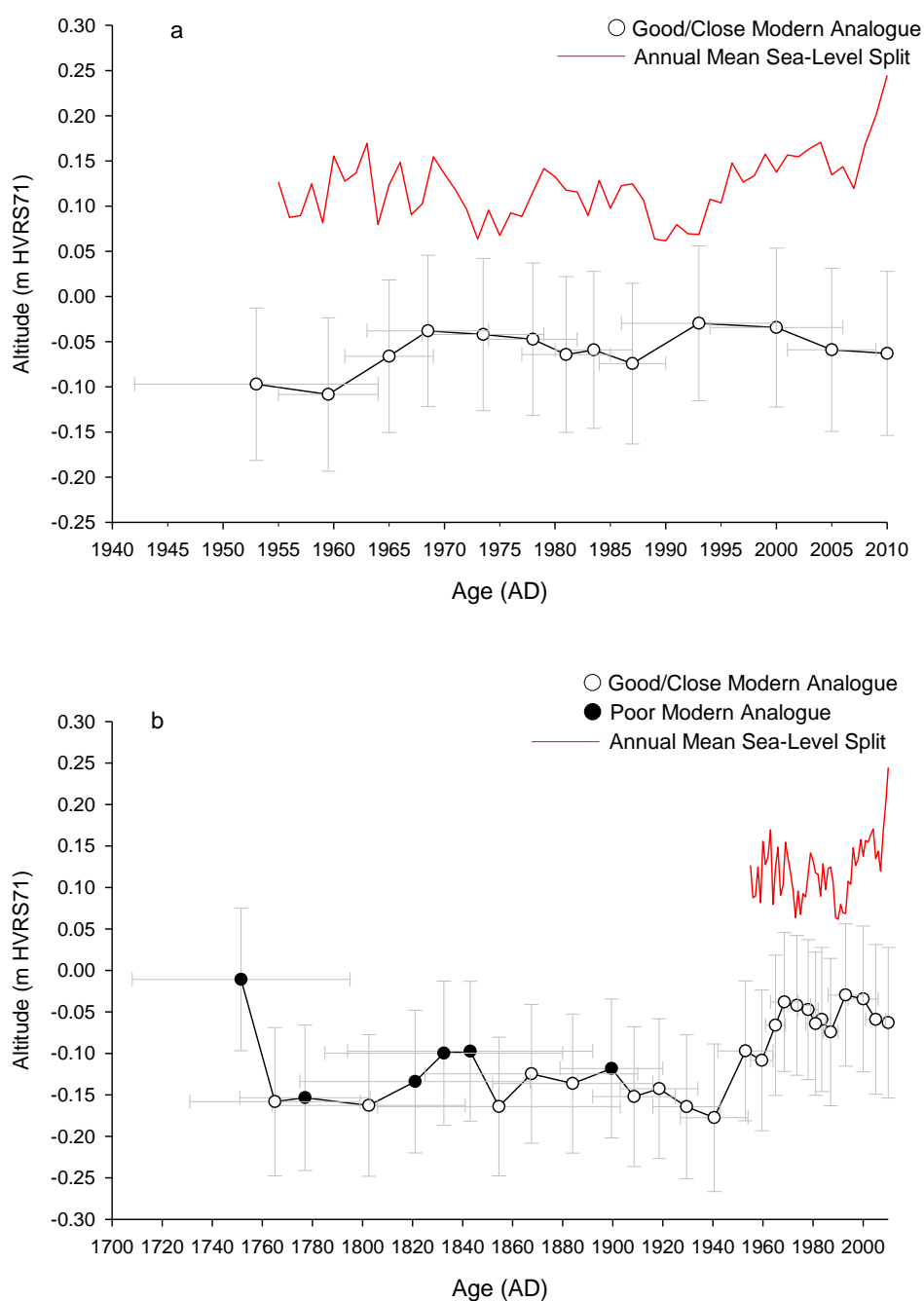


Figure 7.3 Transfer function reconstruction of MSL for core JD1 compared with (a) Split tide-gauge data from AD 1955 and (b) extrapolated back through time including bootstrap prediction errors (m) and model uncertainties (2σ). Good/close and poor modern analogues also displayed.

Figure 7.3a shows the transfer function reconstruction of MSL for core JD1 plotted with mean sea-level records from the Split tide gauge dating back to AD 1955. Figure 7.3b shows the same data, but the record has been extended beyond the instrumental record using the developed age-depth model for core JD1. Tide gauge data are offset from the reconstruction

due to the low altitude of the sample core at JD1. Indeed this salt-marsh surface altitude was significantly low compared with the cores from JD2 and BL (table 3.5). Palaeo marsh altitudes however suggested similar altitude predictions for core JD1 compared with JD2 and BL further supporting the core altitude for JD1 is anomalous. To allow a more direct comparison of sea-level trends, an estimated 14 cm was added to the altitude of each fossil sample enabling direct correspondence with the instrumental record as shown in figures 7.6a and b. Nonetheless, the reconstruction shows some striking similarities with the tide-gauge record. Most notably the minor, but constant, sea-level drop between ~AD 1970 and 1985 after which both records similarly record an increase in MSL. When extended back in time, the reconstructed MSL trend fluctuates between 1765 and 1908 (although this section of the record also contains a number of poor analogues). Sea-level rise from AD 1940 suggests an increase of 2 mm/yr. Between AD 1913 and 1940, the reconstruction suggests a fall in mean sea-level of up to 1 mm/yr. After AD 1940, the record shows a substantial increase in the rate of MSL, peaking at 8 mm-yr between AD 1959 and 1973. A drop in MSL is observed between AD 1973 and 1987 before rapidly rising by up to 7 mm/yr to AD 1993. The instrumental record shows a substantial increase in MSL in more recent times which is not repeated in the fossil record.

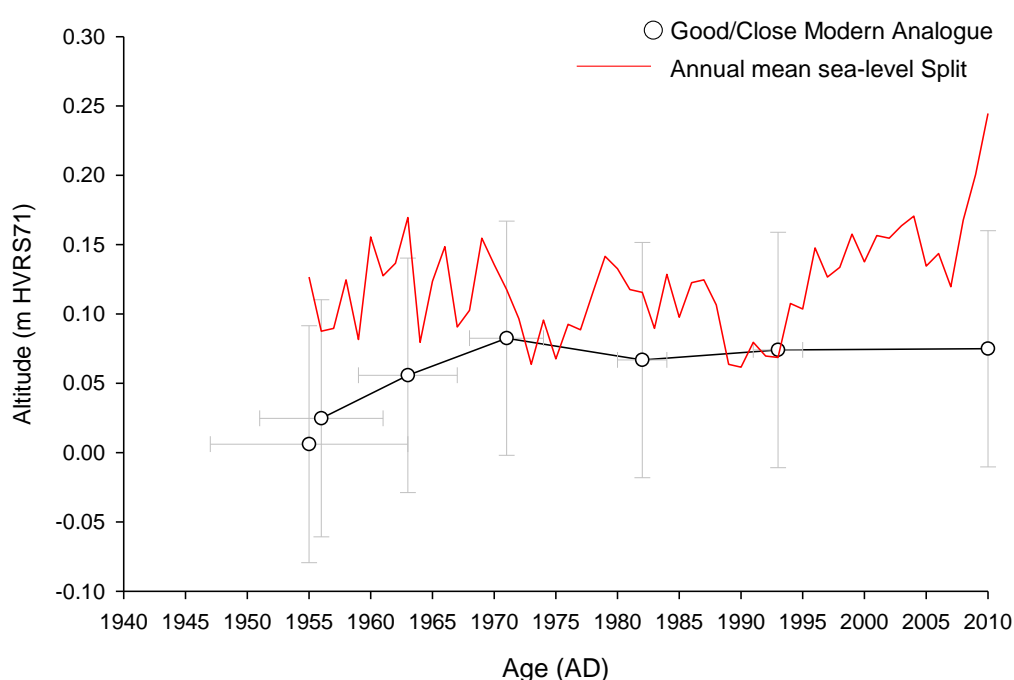


Figure 7.4. Transfer function reconstruction of MSL for core JD2 compared with Split tide-gauge data from AD 1955 including bootstrap prediction errors (m) and age uncertainties.

Figure 7.4 shows the transfer function estimates of mean sea-level for core JD2 plotted with MSL records from the Split tide gauge dating back to AD 1955. Extending the record beyond

this depth is not possible since the chronology coincidentally is also restricted to ~AD 1955. By comparison, core JD2 shows little resemblance to the trends observed in core JD1 or the tide-gauge data. From AD 1970 to the present, MSL shows insignificant changes. The lack of trend may in part reflect the relatively low resolution of this record which contains a limited number of fossil samples (8).

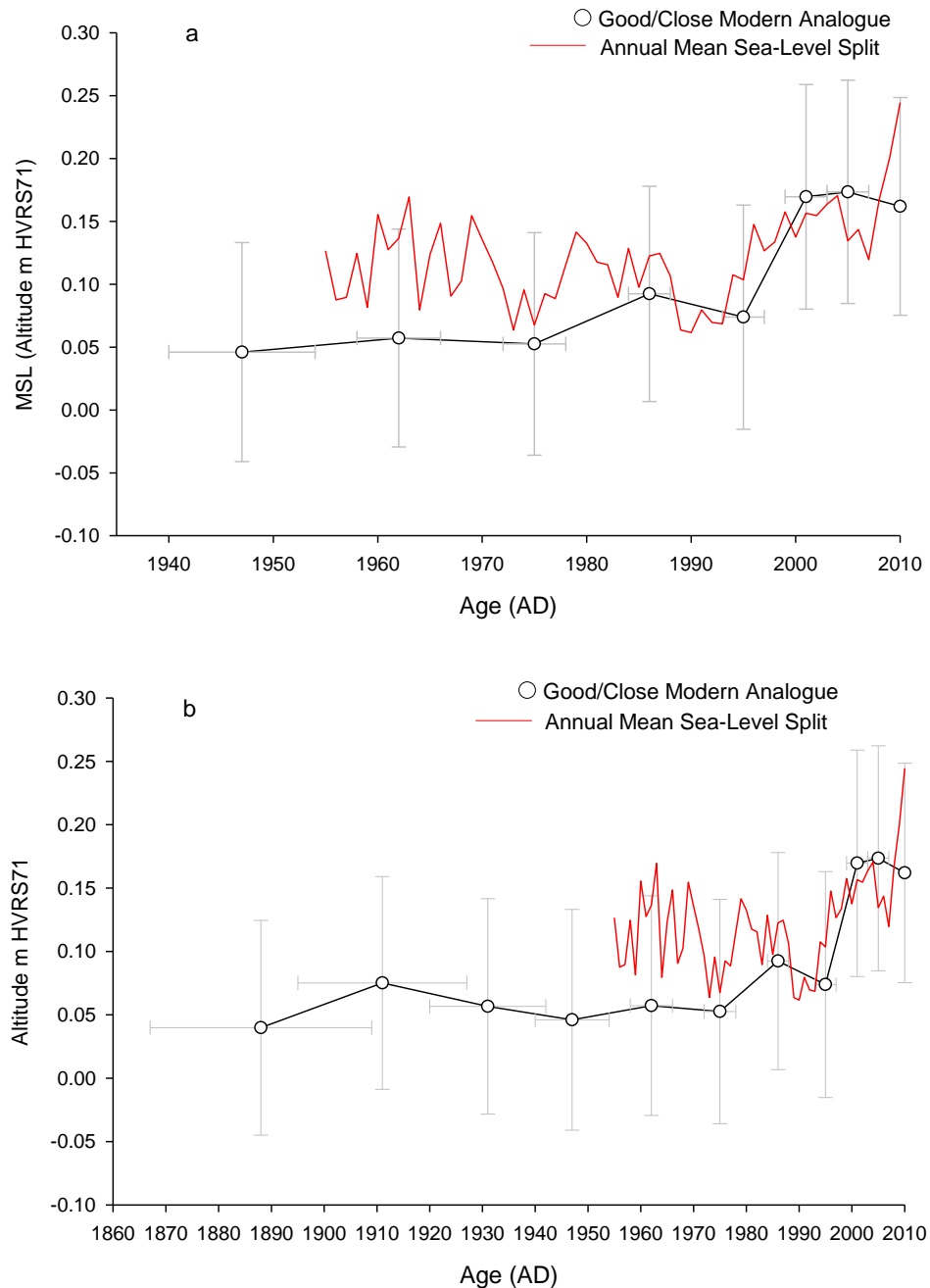


Figure 7.5 Transfer function reconstruction of MSL for core BL compared with (a) Split tide-gauge data from AD 1955 and (b) extrapolated back through time including bootstrap prediction errors (m) and model uncertainties (AD). Good modern analogues also shown.

Figure 7.5a shows the transfer function estimates of MSL for core BL plotted with MSL records from the Split tide gauge dating back to AD 1955 while figure 7.3b shows the same data, but extended beyond the instrumental record, i.e. back to AD 1888, using the chronology developed for core BL. In comparison to core JD2, the record from Blace shows significant similarities with trends observed in the tide-gauge data. The reconstruction shows a significant increase in MSL (3.6 mm/yr) between AD 1975 and 1986 before a brief period of decreasing MSL to 1995. This trend is also observed in the tide-gauge record. Similarly the substantial increase after AD 1995 is matched by both records. The transfer function sea-level reconstruction suggests an increase of up to 16 mm/yr between 1995 and 2001.

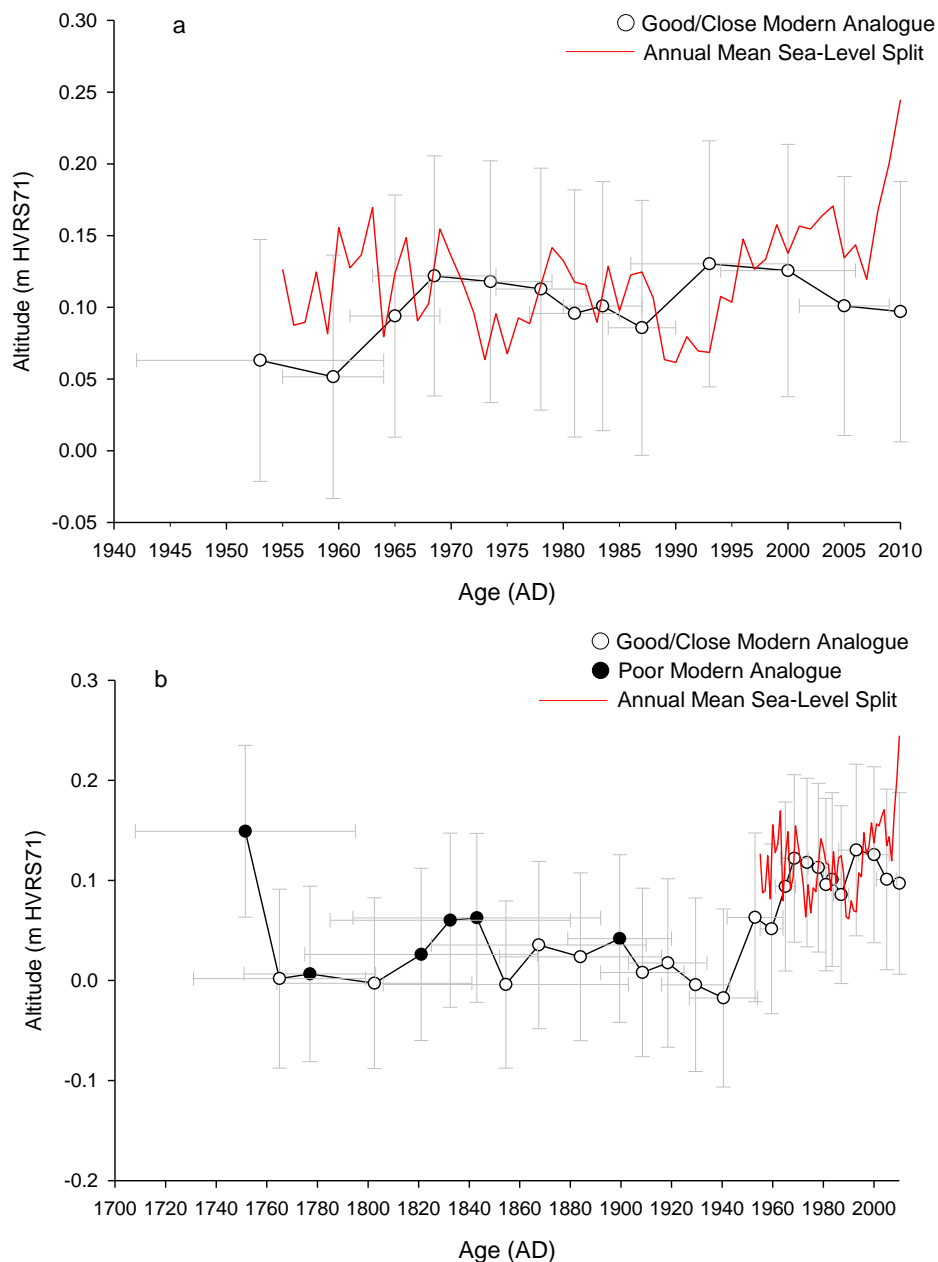


Figure 7.6 Transfer function reconstruction of MSL for core JD1. Altitudes of fossil samples were increased in line with tide-gauge where the altitude was raised 14 cm.

Further to the reconstructions above, tide-gauge data from Trieste were used to provide a longer comparative time-series. Figure 7.7 shows the transfer function reconstruction of MSL during the twentieth century to be very similar to that observed in the instrumental record. Both record a rise in MSL during the 20th Century, most notably around the period AD 1940. The records also show similar periods of decreasing MSL changes (~AD 1980).

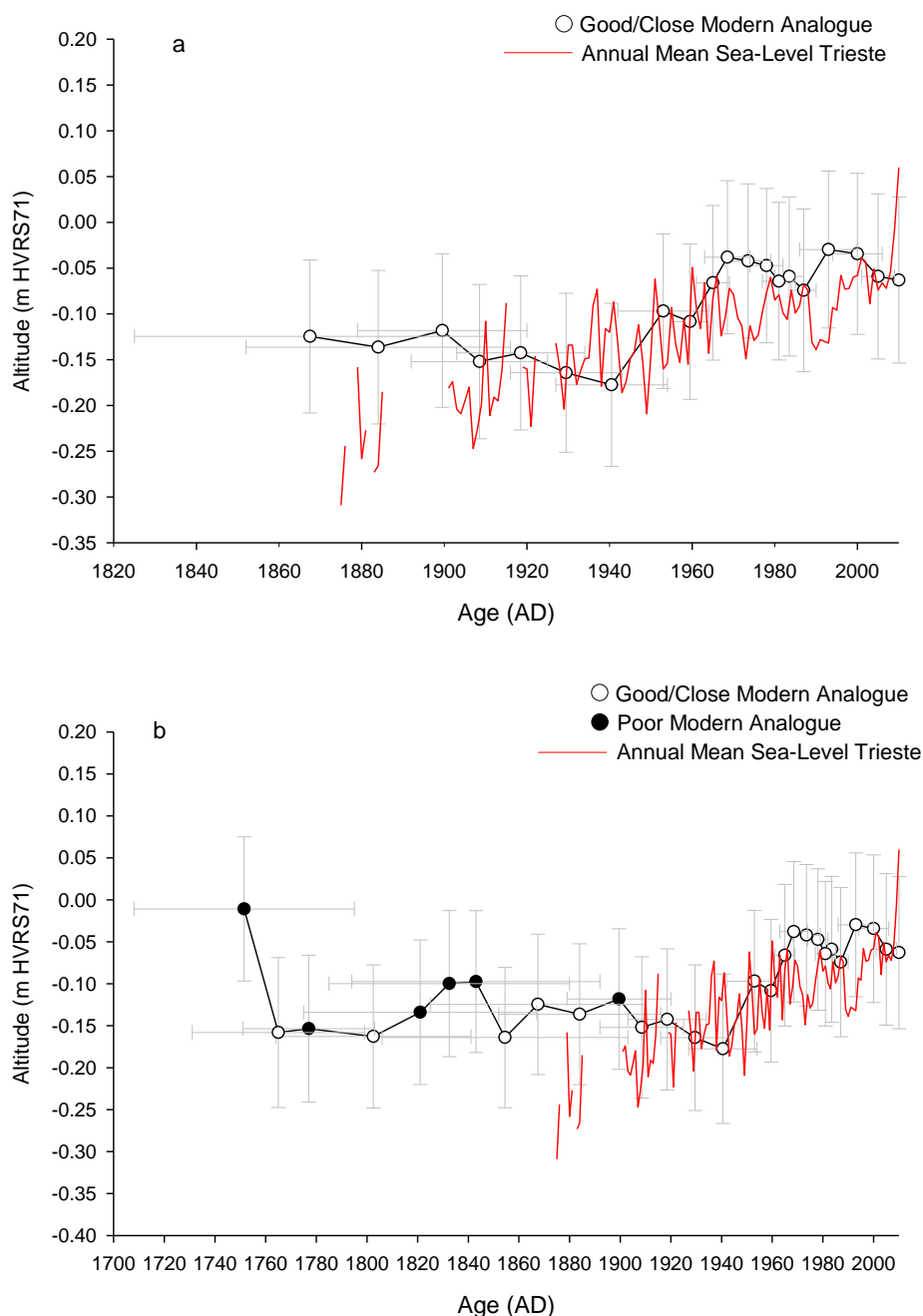


Figure 7.7. Transfer function reconstruction of MSL for core JD1 compared with (a) Trieste tide-gauge data from AD 1875 and (b) extrapolated back through time including bootstrap prediction errors (m) and model uncertainties (2σ). Good/close and poor modern analogues also displayed.

Figure 7.8 also plots instrumental records from the Trieste tide-gauge against the transfer function reconstruction for BL. The records are remarkably similar, showing an increase in MSL throughout the 20th century and again highlighting the increased rates observed from AD 1990 onwards demonstrating a substantial increase in MSL towards the end of the 20th Century.

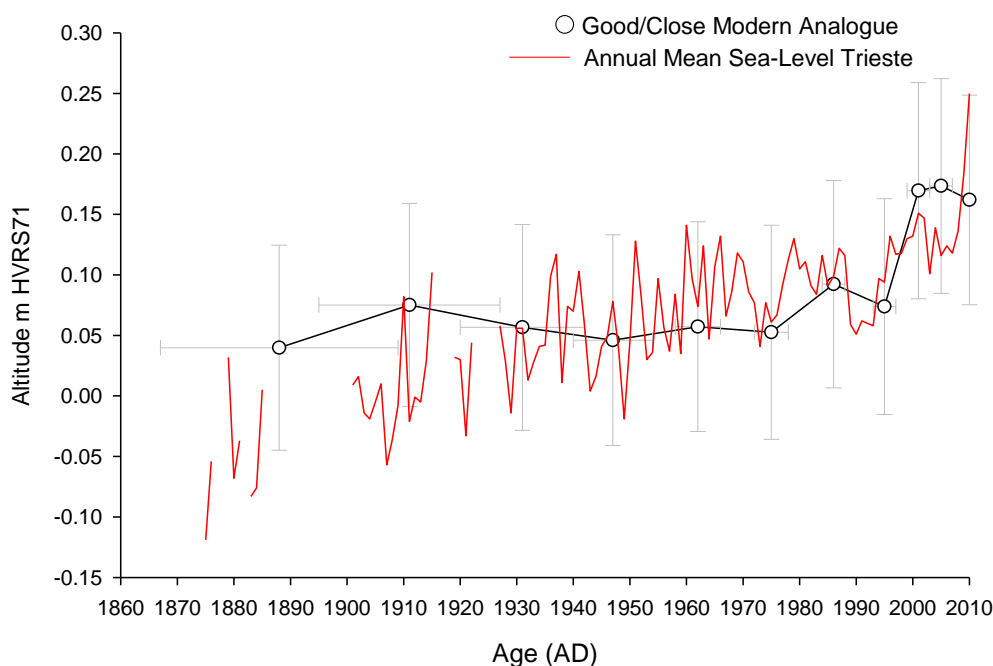


Figure 7.8 Transfer function reconstruction of MSL for core BL compared with Trieste tide-gauge data from AD 1875 including bootstrap prediction errors (m) and model uncertainties (AD). Good/close and poor modern analogues also displayed.

Sea-level trends, as observed from the longest records in the Mediterranean, have shown sea-level increases of around 1.1-1.3 mm/yr during the 20th century (Tsimplis and Baker, 2000; Raicich, 2007; Marcos et al., 2011). In the Adriatic Sea, the long-term RSL rise from these records varies from 0.5 ± 0.2 to 1.2 ± 0.1 mm/yr (Marcos and Tsimplis, 2008). Between AD 1960-2000 however, a period of decreasing sea-level is observed. Rates of change during this period vary with values ranging from -0.4 ± 0.4 to 0.3 ± 0.4 mm/yr (Marcos and Tsimplis, 2008; Tsimplis et al., 2012). The fall in sea-level has been attributed to an increase in the average atmospheric pressure over the basin (Tsimplis and Baker, 2000; Tsimplis and Josey, 2001). When analysing sea-level trends for the Adriatic, there is good consistency between the records (see figure 2.2) (Tsimplis et al., 2012). Indeed all records show a notable increase in RSL rise at approximately AD 1990. These observations are also confirmed through satellite altimetry measurements which show increases in RSL towards the end of the 20th century with sea-level increasing at a rate of 10 to 15 mm/yr between 1993 and 1999 (Cazenave et al., 2001).

These observations appear to have been readily recorded in the biostratigraphic record where transfer function reconstructions display comparable trends. Core JD1 shows a subtle but noticeable decrease in MSL at around AD 1967. This trend continues to decrease in line with tide gauge measurements up to approximately AD 1987 before rising, also in sync with instrumental observations (figure 7.3a). This trend is not repeated in the record for core JD2 however. Reconstructed values for the core are of comparatively low resolution. Indeed the record shows little variation in MSL after ~AD 1970 (figure 7.4). Core BL shows a subtle decrease in MSL at around 1986 (figure 7.5a). After this period however, the record at Blace is excellent, almost offering a mirror image of the tide-gauge trends for both Split (figure 7.6a) and Trieste (figure 7.8). Prior to this period, it would appear that the salt-marsh at Blace has recorded a steady increase in MSL rise for most of the 20th century. By comparison, core JD1 clearly shows an inflexion in the record centred around AD 1940 ± 13.5 with MSL showing a distinct increase. The onset of modern sea-level rise shown by proxy reconstructions is not globally consistent. Gehrels and Woodworth (2013) conclude that modern sea-level around the world began to display an increased rate above background Holocene trends for the year centred around 1925 (± 20 years). The reconstruction for core JD1 fits this claim, suggesting modern sea-level rise in the Adriatic to have increased around the same period. Further increases in sea-level during the later stages of the 20th century, as recorded in cores JD1 and BL are similar to other proxy reconstructions. For example, Rossi et al. (2011) (who also used PLS transfer function), showed a substantial increases in RSL from 1.6 mm/yr between AD 1890 to 1980 rising to 4.7 mm/yr from AD 1980 to 2004. The increased rates of change observed since the 1990s have also been confirmed through satellite altimetry observations (e.g. Cazenave and Nerem, 2004; Cazenave and Llovel, 2010) further implying the proxy reconstruction is reflecting real changes in sea-level over the past two decades or so. Indeed the reconstructions for cores JD1 and BL show strong relationships with trends observed in the tide-gauge data. Extrapolation beyond the limit of tide-gauge records is therefore possible. However this is limited to the extent of a reliable chronology. Further improving and extending this would allow sea-level inferences over much greater timescales.

7.6. FURTHER WORK

7.6.1. Improving Chronological Constraints

Robust chronologies comprise a significant component of transfer function studies to accurately depict changes in sedimentation that may reflect sea-level trends (e.g. Marshall et al., 2007). The chronologies established for cores in this study were restricted in terms of their depth due to limitations in dating techniques and the lack of organic material suitable for radiocarbon dating. The reconstruction for Blace could only be chronologically constrained to AD 1888 which equated to the upper 11 cm of the core. Whilst radiocarbon dates were obtained for core JD1, this too was restricted to the upper 30 cm of the core. As a result, the dates obtained do not capture the full biostratigraphic record, including the calcareous to agglutinated up-core transition. The lack of organic material that can be reliably dated by C^{14} is common in most European salt-marshes in comparison to north Atlantic sites along the coast of America (Edwards, 2004). The salt-marsh cores typically displayed increasingly low LOI values (<10%) moving down through the cores. Whilst ^{137}Cs peaks were relatively well defined in the upper sections of the cores, an independent age source was also sought to using pollution peaks identified through XRF analysis. However this proved unsuccessful as increased concentrations in Cu and decreased levels of Pb could not be assigned to specific ages through documentary evidence or published work.

An alternative approach to improve and extend the chronology would involve the use of stable Pb isotopes (e.g. Kemp et al., 2012b). Stable Pb isotopes can extend chronologies developed via ^{210}Pb and ^{137}Cs and also provide a chronological marker between these radionuclides and ^{14}C dating. Bridging this gap may help constrain the often observed inflexions observed in sea-level studies that may reflect dating limitations rather than actual sea-level trends. In addition, where the lack of organic material within minerogenic sections limits the application of ^{14}C dating, luminescence dating may provide an alternative means of establishing ages for these coastal sediments (Edwards, 2004). However there are problems associated with this technique, especially in the context of marine water-lain environments where sample grains are poorly bleached (Edwards, 2004).

7.6.2. Increasing Modern Analogues

Transfer function performance is ultimately based on the modern training set and the sampled environmental range (Barlow et al., 2013). It is preferable therefore to capture as much of the modern environment as possible. More importantly however is the need to sample environmental conditions similar to that observed in fossil sequences (Horton and

Edwards, 2006). Doing so allows for more modern equivalents from which the fossil samples will be compared with resulting in fewer poor modern analogues. The number of fossil samples with a poor analogy with the TCD training set varied between the sediment cores. Typically they were constrained to the lower section of the fossil sequences where calcareous foraminifera (*Ammonia* spp., *Elphidium* spp. and *Haynesina germanica*) flourish. These levels were clearly below the limits of the sampled environmental gradient. Also whilst screening modern training sets to remove sample outliers often results in improved correlations and predictions, it reduces the number of modern analogues from which the fossil samples are compared with. A screened transfer function in this study contained 43 samples.

To circumvent this problem, increasing the training set size and similarly sampling a greater range of the modern environmental conditions may help to improve both the strength of relationship observed, by increasing the range of the environmental gradient, but also the number of modern analogues. The eastern Adriatic however is notoriously sparse of vegetated intertidal environments due to the karstic nature of the coastline. Pandža et al. (2007) identified eight ecologically important sites in central and south-eastern Adriatic, and two of the sites presented, Jadrtovac and Blace, were the focus of this study. Further afield sites should be investigated to complement the training sets already established here. Indeed the limited tidal range in the whole of the Mediterranean would allow a wide sampling environment whilst maintaining small prediction errors associated with transfer function reconstructions from these settings.

CONCLUSIONS

This study has analysed contemporary foraminiferal distributions from two microtidal salt-marsh sites along the Croatian coastline in an attempt to reconstruct historical sea-level trends for the Adriatic Sea. In total 70 surface samples were analysed together with environmental data including salinity, pH, LOI and grain size. The altitude and distance from open water were also recorded. The analysis of contemporary foraminiferal distributions showed agglutinated and calcareous species are found throughout the entire sampled range of the salt-marsh environments. Unconstrained cluster analyses were used to classify the modern assemblages into faunal zones revealing on average three faunal zones that were broadly similar throughout. Occupying the level between MTL and MHWST were high abundances of *J. macrescens* and *T. inflata* with minimal calcareous taxa. A second faunal zone was also observed which was characterised by high abundances of *J. macrescens* and *T. inflata* together with an increased calcareous component. This mixed assemblage zone spanned the largest large vertical range ranging from around MHWST to below MTL often creating an altitudinal overlap. A third faunal zone was also observed, where calcareous taxa were substantially more abundant with agglutinated forms low in abundance. This faunal zone was also altitudinally constrained below MTL.

Transect datasets were combined to create site specific training sets (JDT and BLT) and a total combined dataset (TCD). Further quantitative measures were employed to test for the significance of environmental variables governing modern foraminiferal distributions. Ordination and partial ordination techniques demonstrated altitude to be significant in explaining variance in all training sets ranging from 13% to 22% of the explained variance. Monte-Carlo permutation tests further confirmed this relationship ($p = <0.05$), suggesting statistically robust transfer functions could be developed. However inter-correlation between the environmental variables was high, ranging from 33% to 71%, implying that altitude cannot not be considered independent of the other variables.

Transfer functions were created for the training sets to assess their reconstructive ability. Using altitude as the only constraining environmental variable, DCCA revealed gradient lengths that indicated strongly linear species distributions. Gradient lengths ranged from between 0.775 and 1.536 SD units for site specific training sets JDT and BLT to 1.173 SD

units for a total combined dataset. As a result, linear regression models (PLS) were developed. These suggested the strength of relationship (r^2_{jack}) between the foraminiferal assemblages and altitude was relatively weak for an unscreened training set (0.32; component 2). However the poor relationships observed were representative of the short environmental gradients of the contemporary training set. In such cases prediction errors may provide a better estimate of model performance. This suggested model predictions of sea-level to within 0.11 m for an unscreened training set. In order to improve model performance, sample outliers were removed. This resulted in an improved strength of relationship to $r^2_{\text{jack}} = 0.54$ whilst prediction errors (RMSEP_{jack}) decreased to 0.08 m (PLS; component 2). Whilst these results were promising, when considering the microtidal regime, prediction errors were actually large by comparison to other research (30%).

The TCD screened transfer function was applied to fossil samples from three sediment cores to produce estimates of palaeo-marsh altitude and finally reconstruct MSL. Prior to this, the MAT was used to assess the degree to which fossil samples showed a strong analogy with modern assemblages. This resulted in a number of levels within each core that contaminated no modern equivalent. This again reflected the short environmental gradients observed in this study. Increasing the sampling range incorporating more modern analogues may circumvent this issue. Estimates of palaeo-marsh altitude revealed an overall increasing trend moving up through the core. To produce estimates of palaeo MSL, the data were converted and plotted against chronology. Ages were established using short-lived radionuclides and radiocarbon dating. Combining this data through age-depth modelling showed a high-resolution record for core JD1 suggesting a sea-level reconstruction possible to AD 1751. Core BL extended to ~AD 1888 whilst core JD2 was restricted to the past 50 years or so due to a hiatus in the record.

Core JD1 suggested relatively stable MSL observations up until the early 20th century where fossil samples with good modern analogues suggest a sharp increase in MSL around AD 1940. Mean sea-level continues to rise up to AD 1968 and then a fall to AD 1987. A fluctuating record is then observed to the present day. In contrast, core JD2 demonstrated a relatively low resolution record when plotted against age. Nonetheless the record showed an increase in MSL up until AD 1971 with stable observations of MSL recorded thereafter. Reconstructed MSL for core BL indicated increasing trends in MSL to AD 1911 after which MSL stabilised up until AD 1962. An increasing trend in MSL is observed thereafter before faster rates of MSL rise are observed from 4 cm depth (AD 1986).

As a final assessment to the reconstruction, the transfer function was compared with instrumental records using tide-gauge data from Split, central Croatia. To provide a longer

time-series, the data were also compared with Trieste. The reconstructions showed comparable trends which were in parts, very similar. The record from core JD1 shows an inflexion around the period AD 1940 where the rate of sea-level dramatically increases. This timing compares well with other proxy records of sea-level change from around the world. Similarly a more recent acceleration from approximately AD 1990 shows further increases in the rate of MSL. This again confirms other observations by both tide-gauge records and satellite altimetry measurements. Ultimately this study has demonstrated the utility of foraminiferal transfer functions in reconstructing sea-level change for the Adriatic Sea.

REFERENCES

- Adam P. (1978) Geographical variations in British saltmarsh vegetation. *Journal of Ecology* 66: 339-366.
- Adam P. (1990) *Saltmarsh Ecology*, Cambridge: Cambridge University Press.
- Admiralty. (2010) *Admiralty tide tables NP 201-07*, United Kingdom hydrographic office, Taunton.
- Albani A, Barbero RS and Donnici S. (2007) Foraminifera as ecological indicators in the Lagoon of Venice, Italy. *Ecological Indicators* 7: 239-253.
- Albani AD, Favero V and Serandrei Barbero R. (1984) Benthonic foraminifera as indicators of intertidal environments. *Geo-Marine Letters* 4: 43-47.
- Allen JRL. (2000) Morphodynamics of Holocene salt marshes: a review sketch from the Atlantic and Southern North Sea coasts of Europe. *Quaternary Science Reviews* 19: 1155-1231.
- Allen JRL, Rae JE, Longworth G, et al. (1993) A Comparison of the ²¹⁰Pb Dating Technique with Three Other Independent Dating Methods in an Oxidic Estuarine Salt-Marsh Sequence. *Estuaries* 16: 670-677.
- Allen JRL and Thornley DM. (2004) Laser granulometry of Holocene estuarine silts: effects of hydrogen peroxide treatment. *The Holocene* 14: 290-295.
- Alve E and Murray JW. (2001) Temporal variability in vertical distributions of live (stained) intertidal foraminifera, southern England. *The Journal of Foraminiferal Research* 31: 12-24.
- Anderson H and Jackson J. (1987) Active tectonics of the Adriatic Region. *Geophysical Journal of the Royal Astronomical Society* 91: 937-983.
- Antonioli F, Anzidei M, Lambeck K, et al. (2007) Sea-level change during the Holocene in Sardinia and in the northeastern Adriatic (central Mediterranean Sea) from archaeological and geomorphological data. *Quaternary Science Reviews* 26: 2463-2486.
- Antonioli F, Ferranti L, Fontana A, et al. (2009) Holocene relative sea-level changes and vertical movements along the Italian and Istrian coastlines. *Quaternary International* 206: 102-133.
- Antonioli F, Garulli GB, Furlani S, et al. (2004) The enigma of submerged marine notches in Northern Adriatic Sea. *Quaternaria Nova* VIII: 263-275.

- Anzidei M, Antonioli F, Benini A, et al. (2010) Sea level change and vertical land movements since the last two millennia along the coasts of southwestern Turkey and Israel. *Quaternary International*. 232, 13-20.
- Appleby PG. (2001) Chronostratigraphic Techniques in Recent Sediments. In: Last W and Smol J (eds) *Tracking Environmental Change Using Lake Sediments*. Dordrecht: KluwerAcademic Publishers, 171-203.
- Appleby PG. (2002) Chronostratigraphic Techniques in Recent Sediments. In: Last W and Smol J (eds) *Tracking Environmental Change Using Lake Sediments*. Springer Netherlands, 171-203.
- Appleby PG, Nolan PJ, Gifford DW, et al. (1986) 210Pb dating by low background gamma counting. *Hydrobiologia* 143: 21-27.
- Appleby PG and Oldfield F. (1978) The calculation of lead-210 dates assuming a constant rate of supply of unsupported 210Pb to the sediment. *CATENA* 5: 1-8.
- Appleby PG and Oldfield F. (1992) Application of lead-210 to sedimentation studies. In: Ivanovich M and Harmon RS (eds) *Uranium Series Disequilibrium: Applications to Environmental Problems*. Clarendon Press, 731-778.
- Appleby PG, Oldfield F, Thompson R, et al. (1979) 210Pb dating of annually laminated lake sediments from Finland. *Nature* 280: 53-55.
- Appleby PG, Richardson N and Nolan PJ. (1992) Self-absorption corrections for well-type germanium detectors. *Nuclear Instruments and Methods in Physics Research Section B: Beam Interactions with Materials and Atoms* 71: 228-233.
- Arabelos DN, Papazachariou DZ, Contadakis ME, et al. (2011) A new tide model for the Mediterranean Sea based on altimetry and tide gauge assimilation. *Ocean Science* 7: 429-444.
- Artegiani A, Paschini E, Russo A, et al. (1997) The Adriatic Sea General Circulation. Part I: Air–Sea Interactions and Water Mass Structure. *Journal of Physical Oceanography* 27: 1492-1514.
- Bačani A, Koch G, Bergant S, et al. (2004) Origin of Recent Organic-Rich Sediments from Morinje Bay (Northern Dalmatia, Croatia): Aspects of Hydrological and Hydrogeological Impact. *32nd International Geological Congress*. Florence, Italy.
- Ball DF. (1964) Loss-on-ignition as an estimate of organic matter and organic carbon in non-calcareous soils. *Journal of Soil Science* 15: 84-92.
- Baric A, Grbec B and Bogner D. (2008) Potential Implications of Sea-Level Rise for Croatia. *Journal of Coastal Research* 24: 299–305.
- Barka A and Reilinger R. (1997) *Active tectonics of the Eastern Mediterranean region: deduced from GPS, neotectonic and seismicity data*.

- Barlow NLM, Shennan I, Long AJ, et al. (2013) Salt marshes as late Holocene tide gauges. *Global and Planetary Change* 106: 90-110.
- Bartholdy J. (2012) Salt Marsh Sedimentation. In: Davis Jr RA and Dalrymple RW (eds) *Principles of Tidal Sedimentology*. Springer Netherlands, 151-185.
- Battaglia M, Murray MH, Serpelloni E, et al. (2004) The Adriatic region: An independent microplate within the Africa-Eurasia collision zone. *Geophysical Research Letters* 31: L09605.
- Benac C, Juracic M and Blaskovic I. (2008) Tidal notches in Vinodol Channel and Bakar Bay, NE Adriatic Sea: Indicators of recent tectonics. *Marine Geology* 248: 151-160.
- Bennett KD. (1994) Confidence intervals for age estimates and deposition times in late-Quaternary sediment sequences. *The Holocene* 4: 337-348.
- Berkeley A, Perry CT, Smithers SG, et al. (2007) A review of the ecological and taphonomic controls on foraminiferal assemblage development in intertidal environments. *Earth-Science Reviews* 83: 205-230.
- Bernhard JM. (2000) Distinguishing Live from Dead Foraminifera: Methods Review and Proper Applications. *Micropaleontology* 46: 38-46.
- Bernhard JM, Ostermann DR, Williams DS, et al. (2006) Comparison of two methods to identify live benthic foraminifera: A test between Rose Bengal and CellTracker Green with implications for stable isotope paleoreconstructions. *Paleoceanography* 21: PA4210.
- Bindoff NL, Willebrand J, Artale V, et al. (2007) Observations: Oceanic Climate Change and Sea Level. In: Solomon S, Qin D, Manning M, et al. (eds) *Climate Change 2007: The Physical Science Basis. Contribution of Working Group I to the Fourth Assessment Report of the Intergovernmental Panel on Climate Change* Cambridge, United Kingdom and New York, NY, USA. Cambridge University Press.
- Birks HJB. (1986) Numerical zonation, comparison and correlation of Quaternary pollen-stratigraphical data. *Handbook of Holocene Palaeoecology and Palaeohydrology*.
- Birks HJB. (1992) Some reflections on the application of numerical methods in Quaternary palaeoecology. *Joensuu yliopisto, Karjalan tutkimuslaitoksen julkaisu - University of Joensuu, Publications of Karelian Institute* 102: 7-20.
- Birks HJB. (1995) Quantitative palaeoenvironmental reconstructions. *Statistical Modelling of Quaternary Science Data*: 161-254.
- Birks HJB. (1998) D.G. Frey and E.S. Deevey Review 1: Numerical tools in palaeolimnology – Progress, potentialities, and problems. *Journal of Paleolimnology* 20: 307-332.
- Birks HJB. (2010) Numerical methods for the analysis of diatom assemblage data. In: Smol JP and Stoermer EF (eds) *The Diatoms: Applications for the Environmental and Earth Sciences, Second ed.* Cambridge, UK: University Press, 23-54.

- Birks HJB, Line JM, Juggins S, et al. (1990) Diatoms and pH reconstruction. *Philosophical Transactions of the Royal Society of London B* 327: 263-278.
- Blaauw M. (2010) Methods and code for 'classical' age-modelling of radiocarbon sequences. *Quaternary Geochronology* 5: 512-518.
- Blaauw M and Christen JA. (2005) Radiocarbon peat chronologies and environmental change. *Journal of the Royal Statistical Society: Series C (Applied Statistics)* 54: 805-816.
- Blaauw M and Christen JA. (2011) Flexible paleoclimate age-depth models using an autoregressive gamma process. *Bayesian Analysis* 6: 457-474.
- Blaauw M and Heegaard E. (2012) Estimation of Age-Depth Relationships. In: Birks HJB, Lotter AF, Juggins S, et al. (eds) *Tracking Environmental Change Using Lake Sediments*. Springer Netherlands, 379-413.
- Blott SJ and Pye K. (2001) GRADISTAT: a grain size distribution and statistics package for the analysis of unconsolidated sediments. *Earth Surface Processes and Landforms* 26: 1237-1248.
- Borcard D, Legendre P and Drapeau P. (1992) Partialling out the Spatial Component of Ecological Variation. *Ecology* 73: 1045-1055.
- Boyle J. (2000) Rapid elemental analysis of sediment samples by isotope source XRF. *Journal of Paleolimnology* 23: 213-221.
- Boyle JF. (2002) Inorganic Geochemical Methods in Palaeolimnology. In: Last W and Smol J (eds) *Tracking Environmental Change Using Lake Sediments*. Springer Netherlands, 83-141.
- Brain MJ, Long AJ, Petley DN, et al. (2011) Compression behaviour of minerogenic low energy intertidal sediments. *Sedimentary Geology* 233: 28-41.
- Bronk Ramsey C. (2001) Development of the radiocarbon calibration program OxCal. *Radiocarbon* 43: 355-363.
- Bronk Ramsey C. (2008) Deposition models for chronological records. *Quaternary Science Reviews* 27: 42-60.
- Bronk Ramsey C. (2009a) Bayesian analysis of radiocarbon dates. *Radiocarbon* 51: 337-360.
- Bronk Ramsey C. (2009b) Dealing with Outliers and Offsets in Radiocarbon Dating. *Radiocarbon* 51: 1023-1045.
- Buble G, Bennett RA and Hreinsdóttir S. (2010) Tide gauge and GPS measurements of crustal motion and sea level rise along the eastern margin of Adria. *Journal of Geophysical Research*. 115: B02404.
- Buck CE, Litton CD and Smith AFM. (1992) Calibration of radiocarbon results pertaining to related archaeological events. *Journal of Archaeological Science* 19: 497-512.

- Buck. CE, Kenworthy. JB, Litton. CD, et al. (1991) Combining archaeological and radiocarbon information: a Bayesian approach to calibration. *Antiquity* 65: 808-821.
- Callard SL, Gehrels WR, Morrison BV, et al. (2011) Suitability of salt-marsh foraminifera as proxy indicators of sea level in Tasmania. *Marine Micropaleontology* 79: 121-131.
- Cazenave A, Bonnefond P, Mercier F, et al. (2002) Sea level variations in the Mediterranean Sea and Black Sea from satellite altimetry and tide gauges. *Global and Planetary Change* 34: 59-86.
- Cazenave A, Cabanes C, Dominh K, et al. (2001) Recent sea level change in the Mediterranean Sea revealed by Topex/Poseidon satellite altimetry. *Geophysical Research Letters*. 28: 1607-1610.
- Cazenave A and Llovel W. (2010) Contemporary Sea Level Rise. *Annual Review of Marine Science* 2: 145-173.
- Cazenave A and Nerem RS. (2004) Present-day sea level change: Observations and causes. *Reviews of Geophysics*. 42: RG3001.
- Charman DJ, Gehrels WR, Manning C, et al. (2010) Reconstruction of recent sea-level change using testate amoebae. *Quaternary Research* 73: 208-219.
- Charman DJ, Roe HM and Gehrels WR. (1998) The use of testate amoebae in studies of sea-level change: a case study from the Taf Estuary, south Wales, UK. *The Holocene* 8: 209-218.
- Charman DJ, Roe HM and Roland Gehrels W. (2002) Modern distribution of saltmarsh testate amoebae: regional variability of zonation and response to environmental variables. *Journal of Quaternary Science* 17: 387-409.
- Church JA and White NJ. (2006) A 20th century acceleration in global sea-level rise. *Geophysical Research Letters* 33: L01602.
- Church JA, Clark PU, Cazenave A, et al. (2013) Sea Level Change. In: Stocker TF, Qin D, Plattner GK, et al. (eds) *Climate Change 2013: The Physical Science Basis. Contribution of Working Group I to the Fifth Assessment Report of the Intergovernmental Panel on Climate Change*. Cambridge, United Kingdom and New York, NY, USA: Cambridge University Press.
- Ciabatti M, V CP and F. RL. (1987) Quaternary sedimentation in the Central Adriatic Sea. *Giornale di Geologia* 49: 113–125.
- Coccioni R. (2000) Benthic foraminifera as bioindicators of heavy metal pollution - a case study from the Goro Lagoon (Italy). In: Martin RE (ed) *Environmental Micropaleontology: The Application of Microfossils to Environmental Geology*. New York: Kluwer Academic/Plenum Publishers, 71-103.
- Cosovic V, Juracic M, Moro A, et al. (2006) Recent foraminifera from the Croatian Adriatic seacoast. *Anuário do Instituto de Geociências* 29: 532-532.

- Crisciani F, Ferraro S and Raicich F. (1994) Interannual variability of the sea level at Trieste. *Il Nuovo Cimento C* 17: 377-384.
- Culver SJ and Horton BP. (2005) Infaunal marsh foraminifera from the Outer Banks, North Carolina, USA. *Journal of Foraminiferal Research* 35: 148-170.
- Cundy AB and Croudace IW. (1995) Sedimentary and geochemical variations in a salt marsh/mud flat environment from the mesotidal Hamble estuary, southern England. *Marine Chemistry* 51: 115-132.
- Cushman-Roisin B and Naimie CE. (2002) A 3D finite-element model of the Adriatic tides. *Journal of Marine Systems* 37: 279-297.
- Dale AL and Dale B. (2002) Application of ecologically based statistical treatments to micropalaeontology. In: Haslett S.K. (ed) *Quaternary Environmental Micropalaeontology*. London: Arnold, 259-286.
- de Rijk S. (1995) Salinity control on the distribution of salt marsh foraminifera (Great Marshes, Massachusetts). *Journal of Foraminiferal Research* 25: 156-166.
- de Rijk S and Troelstra SR. (1997) Salt marsh foraminifera from the Great Marshes, Massachusetts: environmental controls. *Palaeogeography, Palaeoclimatology, Palaeoecology* 130: 81-112.
- Debenay J-P, Guiral D and Parra M. (2004) Behaviour and taphonomic loss in foraminiferal assemblages of mangrove swamps of French Guiana. *Marine Geology* 208: 295-314.
- Debenay JP, Guiral D and Parra M. (2002) Ecological Factors Acting on the Microfauna in Mangrove Swamps. The Case of Foraminiferal Assemblages in French Guiana. *Estuarine, Coastal and Shelf Science* 55: 509-533.
- Del Río Vera J, Criado-Aldeanueva F, García-Lafuente J, et al. (2009) A new insight on the decreasing sea level trend over the Ionian basin in the last decades. *Global and Planetary Change* 68: 232-235.
- Devoy RJN. (1979) Flandrian sea level changes and vegetational history of the lower Thames Estuary. *Philosophical Transactions of the Royal Society London B* 285: 355-407.
- Di Bella L and Casieri S. (2011) Paleoenvironmental reconstruction of Late Quaternary succession by foraminiferal assemblages of three cores from the San Benedetto del Tronto coast (central Adriatic Sea, Italy). *Quaternary International* 241: 169-183.
- Di Bella L, Casieri S and Carboni MG. (2008) Late Quaternary paleoenvironmental reconstruction of the Tremiti structural high (Central Adriatic Sea) from benthic foraminiferal assemblages. *Geobios* 41: 729-742.
- Donnelly JP, Cleary P, Newby P, et al. (2004) Coupling instrumental and geological records of sea-level change: Evidence from southern New England of an increase in the rate of sea-level rise in the late 19th century. *Geophysical Research Letters* 31: L05203.

- Doody JP. (2008) *Saltmarsh conservation, management and restoration*, Dordrecht: Springer.
- Douglas BC. (1991) Global Sea Level Rise. *Journal Geophysical Research*. 96: 6981-6992.
- Duchemin G, Jorissen FJ, Redois F, et al. (2005) Foraminiferal microhabitats in a high marsh: Consequences for reconstructing past sea levels. *Palaeogeography, Palaeoclimatology, Palaeoecology* 226: 167-185.
- Edwards RJ. (2001) Mid- to late Holocene relative sea-level change in Poole Harbour, southern England. *Journal of Quaternary Science* 16: 221-235.
- Edwards RJ. (2004) Constructing chronologies of sea-level change from salt marsh sediments. In: Buck, C.E. and Millard, A.R. (eds) *Tools for Constructing Chronologies: Crossing Disciplinary Boundaries*. London: Springer Verlag Ltd, 191-213.
- Edwards RJ and Horton BP. (2000) Reconstructing relative sea-level change using UK salt-marsh foraminifera. *Marine Geology* 169: 41-56.
- Edwards RJ and Horton BP. (2006) Developing detailed records of relative sea-level change using a foraminiferal transfer function: an example from North Norfolk, UK. *Philosophical Transactions of the Royal Society A: Mathematical, Physical and Engineering Sciences* 364: 973-991.
- Edwards RJ, van de Plassche O, Gehrels WR, et al. (2004a) Assessing sea-level data from Connecticut, USA, using a foraminiferal transfer function for tide level. *Marine Micropaleontology* 51: 239-255.
- Edwards RJ, Wright AJ and van de Plassche O. (2004b) Surface distribution of salt-marsh foraminifera from Connecticut, USA: modern analogues for high-resolution sea level studies. *Marine Micropaleontology* 51: 1-21.
- Ellison JC. (1989) Pollen analysis of mangrove sediments as a sea-level indicator: assessment from Tongatapu, Tonga. *Palaeogeography, Palaeoclimatology, Palaeoecology* 74: 327-341.
- Engelhart SE, Horton BP, Roberts DH, et al. (2007) Mangrove pollen of Indonesia and its suitability as a sea-level indicator. *Marine Geology* 242: 65-81.
- Fabrizio F and Coccioni R. (2012) The Response of Benthic Foraminiferal Assemblages to Copper Exposure: A Pilot Mesocosm Investigation. *Journal of Environmental Protection* 3: 342-352.
- Faivre S, Fouache E, Ghilardi M, et al. (2010a) Relative sea level change in western Istria (Croatia) during the last millennium. *Quaternary International*. 232: 132-143.
- Faivre S, Fouache E, Kovačević V, et al. (2010b) Geomorphological and archeological indicators of Croatian shoreline evolution over the last two thousand years. *Geology of the Adriatic area, GeoAct special publications* 3: 125-133.

- Farrell WE and Clark JA. (1976) On Postglacial Sea Level. *Geophysical Journal of the Royal Astronomical Society* 46: 647-667.
- Fatela F and Taborda R. (2002) Confidence limits of species proportions in microfossil assemblages. *Marine Micropaleontology* 45: 169-174.
- Fenoglio-Marc L. (2002) Long-term sea level change in the Mediterranean Sea from multi-satellite altimetry and tide gauges. *Physics and Chemistry of the Earth, Parts A/B/C* 27: 1419-1431.
- Fenoglio-Marc L, Braitenberg C and Tunini L. (2012) Sea level variability and trends in the Adriatic Sea in 1993–2008 from tide gauges and satellite altimetry. *Physics and Chemistry of the Earth, Parts A/B/C* 40–41: 47-58.
- Ferla M, Cordella M, Michielli L, et al. (2007) Long-term variations on sea level and tidal regime in the lagoon of Venice. *Estuarine, Coastal and Shelf Science* 75: 214-222.
- Ferranti L, Antonioli F, Mauz B, et al. (2006) Markers of the last interglacial sea-level high stand along the coast of Italy: Tectonic implications. *Quaternary International* 145-146: 30-54.
- Ferranti L, Monaco C, Antonioli F, et al. (2008) Alternating steady and stick-slip up lift in the Messina straits, southern Italy: evidence from raised late Holocene shoreline. *Journal of Geophysical Research* 112:
- Figueira BO, Grenfell HR, Hayward BW, et al. (2012) Comparison of rose bengal and celltracker green staining for identification of live salt-marsh foraminifera. *The Journal of Foraminiferal Research* 42: 206-215.
- Flemming NC and Webb CO. (1986) Tectonic and eustatic coastal changes during the last 10,000 years derived from archaeological data. *Zeitschrift für Geomorphologie, Supplementband* 62: 1-29.
- Franco P, Jertié L, Malanotte-Rizzoli P, et al. (1982) Descriptive model of the northern Adriatic. *Oceanologica Acta* 5: 379-389.
- Frontalini F and Coccioni R. (2008) Benthic foraminifera for heavy metal pollution monitoring: A case study from the central Adriatic Sea coast of Italy. *Estuarine, Coastal and Shelf Science* 76: 404-417.
- Frontalini F and Coccioni R. (2011) Benthic foraminifera as bioindicators of pollution: A review of Italian research over the last three decades. *Revue de Micropaléontologie* 54: 115-127.
- Frontalini F, Coccioni R and Bucci C. (2010) Benthic foraminiferal assemblages and trace element contents from the lagoons of Orbetello and Lesina. *Environmental Monitoring and Assessment* 170: 245-260.

- Furlani S, Biolchi S, Cucchi F, et al. (2011) Tectonic effects on Late Holocene sea level changes in the Gulf of Trieste (NE Adriatic Sea, Italy). *Quaternary International* 232: 144-157.
- Furlani S, Cucchi F, Biolchi S, et al. (2010) Notches in the Northern Adriatic Sea: Genesis and development. *Quaternary International*. 232: 158-168.
- García D, Vigo I, Chao BF, et al. (2007) Vertical Crustal Motion along the Mediterranean and Black Sea Coast Derived from Ocean Altimetry and Tide Gauge Data. *Pure and Applied Geophysics* 164: 851-863.
- Gasse F, Barker P, Gell PA, et al. (1997) Diatom-inferred salinity in palaeolakes: An indirect tracer of climate change. *Quaternary Science Reviews* 16: 547-563.
- Gauch HG and Whittaker RH. (1972) Comparison of Ordination Techniques. *Ecology* 53: 868-875.
- Gehrels RW. (1994) Determining Relative Sea-Level Change from Salt-Marsh Foraminifera and Plant Zones on the Coast of Maine, U.S.A. *Journal of Coastal Research* 10: 990-1009.
- Gehrels RW. (2002) Intertidal foraminifera as palaeoenvironmental indicators. In: Haslett SK (ed) *Quaternary Environmental Micropalaeontology*. New York: Arnold, 91-114.
- Gehrels RW and Newman SWG. (2004) Salt-marsh foraminifera in Ho Bugt, western Denmark, and their use as sea-level indicators. *Danish Journal of Geography* 104: 97-106.
- Gehrels WR. (1999) Middle and Late Holocene Sea-Level Changes in Eastern Maine Reconstructed from Foraminiferal Saltmarsh Stratigraphy and AMS ¹⁴C Dates on Basal Peat. *Quaternary Research* 52: 350-359.
- Gehrels WR. (2000) Using foraminiferal transfer functions to produce high-resolution sea-level records from salt-marsh deposits, Maine, USA. *The Holocene* 10: 367-376.
- Gehrels WR. (2007) SEA LEVEL STUDIES Microfossil Reconstructions. In: Scott AE (ed) *Encyclopedia of Quaternary Science*. Oxford: Elsevier, 3015-3024.
- Gehrels WR, Belknap DF, Black S, et al. (2002) Rapid sea-level rise in the Gulf of Maine, USA, since AD 1800. *The Holocene* 12: 383-389.
- Gehrels WR, Hayward BW, Newnham RM, et al. (2008) A 20th century acceleration of sea-level rise in New Zealand. *Geophysical Research Letters* 35: L02717.
- Gehrels WR, Hendon D and Charman DJ. (2006a) Distribution of testate amoebae in salt marshes along the north American east coast. *The Journal of Foraminiferal Research* 36: 201-214.
- Gehrels WR, Kirby JR, Prokoph A, et al. (2005) Onset of recent rapid sea-level rise in the western Atlantic Ocean. *Quaternary Science Reviews* 24: 2083-2100.

- Gehrels WR, Marshall WA, Gehrels MJ, et al. (2006b) Rapid sea-level rise in the North Atlantic Ocean since the first half of the nineteenth century. *The Holocene* 16: 949-965.
- Gehrels WR, Roe HM and Charman DJ. (2001) Foraminifera, testate amoebae and diatoms as sea-level indicators in UK saltmarshes: a quantitative multiproxy approach. *Journal of Quaternary Science* 16: 201-220.
- Gehrels WR and Woodworth PL. (2013) When did modern rates of sea-level rise start? *Global and Planetary Change* 100: 263-277.
- Godwin H. (1940) Studies in the post-glacial history of British vegetation. III: fenland pollen diagrams. IV: postglacial changes of relative land and sea level in the English Fenland. *Philosophical Transactions of the Royal Society of London* B230: 239-303.
- Goldberg ED. (1963) Geochronology with ²¹⁰Pb. *Radioactive Dating. Proceedings of the Symposium on Radioactive Dating*. International Atomic Energy Agency, Vienna, Austria, 121-131.
- Goldstein ST and Harben EB. (1993) Taphofacies implications of infaunal foraminiferal assemblages in a Georgia saltmarsh, Sapelo Island. *Micropaleontology* 39: 55-62.
- Goldstein ST and Watkins GT. (1998) Elevation and the distribution of salt-marsh foraminifera, St. Catherine's Island, Georgia: a taphonomic approach. *Palaios* 13: 570-580.
- Gray AB, Pasternack GB and Watson EB. (2010) Hydrogen peroxide treatment effects on the particle size distribution of alluvial and marsh sediments. *The Holocene* 20: 293-301.
- Grenfell HR, Hayward BW, Nomura R, et al. (2012) A foraminiferal proxy record of 20th century sea-level rise in the Manukau Harbour, New Zealand. *Marine and Freshwater Research* 63: 370-384.
- Grimm EC. (2004) Tilia View: Version 2.0.2. Research and Collections Center, Illinois State Museum.
- Guilbault J-P, Clague JJ and Lapointe M. (1995) Amount of subsidence during a late Holocene earthquake--evidence from fossil tidal marsh foraminifera at Vancouver Island, west coast of Canada. *Palaeogeography, Palaeoclimatology, Palaeoecology* 118: 49-71.
- Hamilton S and Shennan I. (2005) Late Holocene relative sea-level changes and the earthquake deformation cycle around upper cook inlet, Alaska. *Quaternary Science Reviews* 24: 1479-1498.
- Haslett SK. (2001) The Palaeoenvironmental Implications of the Distribution of Intertidal Foraminifera in a Tropical Australian Estuary: a Reconnaissance Study. *Australian Geographical Studies* 39: 67-74.

- Haslett SK. (2002) *Quaternary Environmental Micropaleontology*, London: Arnold.
- Haslett SK, Cundy AB, Davies CFC, et al. (2003) Salt Marsh Sedimentation over the past C. 120 Years along the West Cotentin Coast of Normandy (France): Relationship to Sea-Level Rise and Sediment Supply. *Journal of Coastal Research* 19: 609-620.
- Hatté C and Jull AJT. (2007) Radiocarbon Dating | Plant Macrofossils. In: Editor-in-Chief: Scott AE (ed) *Encyclopedia of Quaternary Science*. Oxford: Elsevier, 2958-2965.
- Hawkes AD, Horton BP, Nelson AR, et al. (2010) The application of intertidal foraminifera to reconstruct coastal subsidence during the giant Cascadia earthquake of AD 1700 in Oregon, USA. *Quaternary International* 221: 116-140.
- Hayes A, Kucera M, Kallel N, et al. (2005) Glacial Mediterranean sea surface temperatures based on planktonic foraminiferal assemblages. *Quaternary Science Reviews* 24: 999-1016.
- Hayward BW, Grenfell HR and Scott DB. (1990) Tidal range of marsh foraminifera for determining former sea-level heights in New Zealand. *New Zealand Journal of Geology and Geophysics* 42: 395-413.
- Hayward BW, Grenfell HR and Scott DB. (1999) Tidal range of marsh foraminifera for determining former sea-level heights in New Zealand. *New Zealand Journal of Geology and Geophysics* 42: 395-413.
- Hayward BW, Holzmann M, Grenfell HR, et al. (2004) Morphological distinction of molecular types in *Ammonia* – towards a taxonomic revision of the world's most commonly misidentified foraminifera. *Marine Micropaleontology* 50: 237-271.
- Hill MO and Gauch HG, Jr. (1980) Detrended correspondence analysis: An improved ordination technique. *Vegetatio* 42: 47-58.
- Hill TCB, Woodland WA, Spencer CD, et al. (2007) Holocene sea-level change in the Severn Estuary, southwest England: a diatom-based sea-level transfer function for macrotidal settings. *The Holocene* 17: 639-648.
- Hippensteel SP, Martin RE, Nikitina D, et al. (2002) Interannual variation of marsh foraminiferal assemblages (Bombay Hook National Wildlife Refuge, Smyrna, DE): do foraminiferal assemblages have a memory? *Journal of Foraminiferal Research* 32: 97-109.
- Holgate SJ. (2007) On the decadal rates of sea level change during the twentieth century. *Geophysical Research Letters* 34: L01602.
- Holgate SJ, Matthews A, Woodworth PL, et al. (2013) New Data Systems and Products at the Permanent Service for Mean Sea Level. *Journal of Coastal Research* 29: 493-504.
- Holgate SJ and Woodworth PL. (2004) Evidence for enhanced coastal sea level rise during the 1990s. *Geophysical Research Letters* 31: L07305.

- Horton BP. (1997) Quantification of the indicative meaning of a range of Holocene sea-level index points from the western North Sea. Durham University.
- Horton BP. (1999) The distribution of contemporary intertidal foraminifera at Cowpen Marsh, Tees Estuary, UK: implications for studies of Holocene sea-level changes. *Palaeogeography, Palaeoclimatology, Palaeoecology* 149: 127-149.
- Horton BP, Corbett R, Culver SJ, et al. (2006) Modern saltmarsh diatom distributions of the Outer Banks, North Carolina, and the development of a transfer function for high resolution reconstructions of sea level. *Estuarine, Coastal and Shelf Science* 69: 381-394.
- Horton BP and Culver SJ. (2008) Modern Intertidal Foraminifera of the Outer Banks, North Carolina, U.S.A., and their Applicability for Sea-Level Studies. *Journal of Coastal Research* 24: 1110-1125.
- Horton BP and Edwards RJ. (2003) Seasonal distributions of foraminifera and their implications for sea-level studies. *SEPM Special Publication* 75.
- Horton BP and Edwards RJ. (2005) The application of local and regional transfer functions to the reconstruction of Holocene sea levels, north Norfolk, England. *The Holocene* 15: 216-228.
- Horton BP and Edwards RJ. (2006) Quantifying Holocene Sea Level Change Using Intertidal Foraminifera: Lessons from the British Isles. *Cushman Foundation for Foraminiferal Research, Special Publication* 40: 97.
- Horton BP, Edwards RJ and Lloyd JM. (1999a) A foraminiferal-based transfer function: implications for sea-level studies. *Journal of Foraminiferal Research* 29: 117-129.
- Horton BP, Edwards RJ and Lloyd JM. (1999b) Reconstruction of former sea levels using a foraminiferal-based transfer function. *Journal of Foraminiferal Research* 29: 117–129.
- Horton BP, Edwards RJ and Lloyd JM. (1999c) UK intertidal foraminiferal distributions: implications for sea-level studies. *Marine Micropaleontology* 36: 205-223.
- Horton BP, Gibbard PL, Mine GM, et al. (2005) Holocene sea levels and palaeoenvironments, Malay-Thai Peninsula, southeast Asia. *The Holocene* 15: 1199-1213.
- Horton BP, Larcombe P, Woodroffe SA, et al. (2003) Contemporary foraminiferal distributions of a mangrove environment, Great Barrier Reef coastline, Australia: implications for sea-level reconstructions. *Marine Geology* 198: 225-243.
- Horton BP and Murray JW. (2006) Patterns in cumulative increase in live and dead species from foraminiferal time series of Cowpen Marsh, Tees Estuary, UK: Implications for sea-level studies. *Marine Micropaleontology* 58: 287-315.

- Horton BP, Zong Y, Hillier C, et al. (2007) Diatoms from Indonesian mangroves and their suitability as sea-level indicators for tropical environments. *Marine Micropaleontology* 63: 155-168.
- Hua Q. (2009) Radiocarbon: A chronological tool for the recent past. *Quaternary Geochronology* 4: 378-390.
- Hua Q and Barbetti M. (2004) Review of tropospheric bomb C-14 data for carbon cycle modeling and age calibration purposes. *Radiocarbon* 46: 1273-1298.
- Hua Q, McDonald J, Redwood D, et al. (2012) Robust chronological reconstruction for young speleothems using radiocarbon. *Quaternary Geochronology* 14: 67-80.
- Hua Q, Zoppi U, Williams AA, et al. (2004) Small-mass AMS radiocarbon analysis at ANTARES. . *Nuclear Instruments and Methods in Physics Research B* 223–224 284–292.
- Imbrie J and Kipp NG. (1971) A new micropaleontological method for quantitative paleoclimatology. Application to a late Pleistocene Caribbean core. In: Turekian KK (ed) *The Late Cenozoic Glacial Ages*. New Haven Yale University Press, 71-131.
- Imbrie J and Webb T. (1981) Transfer functions: calibrating micropaleontological data in climatic terms. In: Berger A (ed) *Climatic variations and variability: facts and theories*. Dordrecht: D. Reidel, 125-134.
- Institute Hydrographic. (1955–2002) *Report on sea level measurement along the eastern Adriatic coast*. Split.
- Jackson ST and Williams JW. (2004) Modern analogs in Quaternary paleoecology: here today, gone yesterday, gone tomorrow. *Annual Review of Earth and Planetary Science* 32: 495–537.
- Jevrejeva S, Grinsted A, Moore JC, et al. (2006) Nonlinear trends and multiyear cycles in sea level records. *Journal of Geophysical Research* 111: C09012.
- Jones VJ and Juggins S. (1995) The construction of diatom-based chlorophyll transfer function and its application at three lakes on Signy Island (maritime Antarctic) subject to differing degrees of nutrient enrichment. *Freshwater Biology* 34: 433-445.
- Jorissen FJ. (1987) The distribution of benthic foraminifera in the Adriatic Sea. *Marine Micropaleontology* 12: 21-48.
- Jorissen FJ. (1988) Benthic foraminifera from the Adriatic Sea: principles of phenotypic variation. *Utrecht micropaleontological bulletins* 37.
- Jorissen FJ, Asioli A, Borsetti AM, et al. (1993) Late Quaternary central Mediterranean biochronology. *Marine Micropaleontology* 21: 169-189.
- Jorissen FJ and Wittling I. (1999) Ecological evidence from live–dead comparisons of benthic foraminiferal faunas off Cape Blanc (Northwest Africa). *Palaeogeography, Palaeoclimatology, Palaeoecology* 149: 151-170.

- Juggins S. (2003-2011) C2: A Microsoft Windows program for developing and applying palaeoecological transfer functions and for visualising multi-proxy stratigraphic datasets. Newcastle Upon Tyne. University of Newcastle.
- Juggins S. (2007) C2 Version 1.5 User guide. Software for Ecology and Palaeoecological Data Analysis and Visualisation. Newcastle upon Tyne, UK. Newcastle University, 73pp.
- Jurina I, Ivanić M, Troskot-Čorbić T, et al. (2013) Activity concentrations and distribution of radionuclides in surface and core sediments of the Neretva Channel (Adriatic Sea, Croatia). *Geologia Croatica* 66: 143-150.
- Kemp AC, Engelhart SE, Culver SJ, et al. (2013) Modern Salt-Marsh and Tidal-Flat Foraminifera From Sitkinak and Simeonof Islands, Southwestern Alaska. *The Journal of Foraminiferal Research* 43: 88-98.
- Kemp AC, Horton BP, Corbett DR, et al. (2009a) The relative utility of foraminifera and diatoms for reconstructing late Holocene sea-level change in North Carolina, USA. *Quaternary Research* 71: 9-21.
- Kemp AC, Horton BP, Culver SJ, et al. (2009b) Timing and magnitude of recent accelerated sea-level rise (North Carolina, United States). *Geology* 37: 1035-1038.
- Kemp AC, Horton BP, Donnelly JP, et al. (2011) Climate related sea-level variations over the past two millennia. *Proceedings of the National Academy of Sciences*.
- Kemp AC, Horton BP, Vann DR, et al. (2012a) Quantitative vertical zonation of salt-marsh foraminifera for reconstructing former sea level; an example from New Jersey, USA. *Quaternary Science Reviews* 54: 26-39.
- Kemp AC, Sommerfield CK, Vane CH, et al. (2012b) Use of lead isotopes for developing chronologies in recent salt-marsh sediments. *Quaternary Geochronology* 12: 40-49.
- Koide M, Bruland KW and Goldberg ED. (1973) Th-228/Th-232 and Pb-210 geochronologies in marine and lake sediments. *Geochimica et Cosmochimica Acta* 37: 1171-1187.
- Krishnaswamy S, Lal D, Martin JM, et al. (1971) Geochronology of lake sediments. *Earth and Planetary Science Letters* 11: 407-414.
- Lambeck K, Anzidei M, Antonioli F, et al. (2004) Sea level in Roman time in the Central Mediterranean and implications for recent change. *Earth and Planetary Science Letters* 224: 563-575.
- Lambeck K and Purcell A. (2005) Sea-level change in the Mediterranean Sea since the LGM: model predictions for tectonically stable areas. *Quaternary Science Reviews* 24: 1969-1988.
- Lascaratos A, Roether W, Nittis K, et al. (1999) Recent changes in deep water formation and spreading in the eastern Mediterranean Sea: a review. *Progress in Oceanography* 44: 5-36.

- Leorri E and Cearreta A. (2009) Recent sea-level changes in the southern Bay of Biscay: transfer function reconstructions from salt-marshes compared with instrumental data. *Scientia Marina* 73.
- Leorri E, Cearreta A and Horton BP. (2008) A foraminifera-based transfer function as a tool for sea-level reconstructions in the southern Bay of Biscay. *Geobios* 41: 787-797.
- Leorri E, Fatela F, Cearreta A, et al. (2011) Assessing the performance of a foraminifera-based transfer function to estimate sea-level changes in northern Portugal. *Quaternary Research* 75: 278-287.
- Leorri E, Gehrels WR, Horton BP, et al. (2010) Distribution of foraminifera in salt marshes along the Atlantic coast of SW Europe: Tools to reconstruct past sea-level variations. *Quaternary International* 221: 104-115.
- Leps J and Smilauer P. (2005) *Multivariate analysis of ecological data using canoco*, Cambridge: Cambridge University Press.
- Leuliette EW, Nerem RS and Mitchum GT. (2004) Calibration of TOPEX/Poseidon and Jason Altimeter Data to Construct a Continuous Record of Mean Sea Level Change. *Marine Geodesy* 27: 79-94.
- Leyer I and Wesche K. (2007) *Multivariate Statistik in der Ökologie*, Berlin Heidelberg: Springer.
- Lionello P. (2012) *The Climate of the Mediterranean Region: From the past to the future*, London: Elsevier.
- Lionello P, Malanotte-Rizzoli P, Boscolo R, et al. (2004) The Mediterranean climate: basic issues and perspectives. *White Paper on Mediterranean climate variability and predictability, Technical report*. 5-17.
- Loring DH and Rantala RTT. (1992) Manual for the geochemical analyses of marine sediments and suspended particulate matter. *Earth-Science Reviews* 32: 235-283.
- Luz B and Bernstein M. (1976) Planktonic foraminifera and quantitative paleoclimatology of the Eastern Mediterranean. *Marine Micropaleontology* 1: 307-323.
- Manca BB, Kovačević V, Gačić M, et al. (2002) Dense water formation in the Southern Adriatic Sea and spreading into the Ionian Sea in the period 1997–1999. *Journal of Marine Systems* 33–34: 133-154.
- Marcos M, Puyol B, Wöppelmann G, et al. (2011) The long sea level record at Cadiz (southern Spain) from 1880 to 2009. *Journal of Geophysical Research* 116: C12003.
- Marcos M and Tsimplis MN. (2008) Coastal sea level trends in Southern Europe. *Geophysical Journal International* 175: 70-82.
- Marjanović M, Bačić Ž and Bašić T. (2012) Determination of Horizontal and Vertical Movements of the Adriatic Microplate on the Basis of GPS Measurements. In:

- Kenyon S, Pacino MC and Marti U (eds) *Geodesy for Planet Earth*. Springer Berlin Heidelberg, 683-688.
- Marshall WA, Gehrels WR, Garnett MH, et al. (2007) The use of 'bomb spike' calibration and high-precision AMS ^{14}C analyses to date salt-marsh sediments deposited during the past three centuries. *Quaternary Research* 68: 325-337.
- McCormac FG, Hogg AG, Blackwell PG, et al. (2007) *SHCal04 Southern Hemisphere calibration, 0-11.0 cal kyr BP*.
- McKenzie D. (1972) Active Tectonics of the Mediterranean Region. *Geophysical Journal International* 30: 109-185.
- Mihelčič G, Lojen S, Dolenec T, et al. (2006) Trace Metals Conservation in Morinje Bay Sediment: Historical Record of Anthropogenic Emissions into a Shallow Adriatic Bay. *Croatica Chemica Acta* 79: 161-167.
- Miko S, Koch G, Mesić S, et al. (2007) Influence of land use in small karst watersheds on the chemical status of peloid sediments on the eastern Adriatic coast. *Journal of Soils and Sediments* 7: 303-312.
- Milker Y, Schmiedl G and Betzler C. (2011) Paleobathymetric history of the Western Mediterranean Sea shelf during the latest glacial period and the Holocene: Quantitative reconstructions based on foraminiferal transfer functions. *Palaeogeography, Palaeoclimatology, Palaeoecology* 307: 324-338.
- Millot C and Taupier-Letage I. (2005) Circulation in the Mediterranean Sea. In: Saliot A (ed) *The Mediterranean Sea*. Springer Berlin Heidelberg, 29-66.
- Mills H, Kirby JR, Holgate S, et al. (2013) The Distribution of Contemporary Saltmarsh Foraminifera in a Macrotidal Estuary: an Assessment of Their Viability for Sea-Level Studies. *Journal of Ecosystem and Ecography* 3: 1-16.
- Morhange C and Pirazzoli PA. (2005) Mid-Holocene emergence of southern Tunisian coasts. *Marine Geology* 220: 205-213.
- Murray JW. (1971) Living foraminifera in tidal marshes; a review. *The Journal of Foraminiferal Research* 1: 153-161.
- Murray JW. (1973) *An Atlas of British Recent Foraminifera*, London: Heinemann Educational Books.
- Murray JW. (1976) Comparative studies of living and dead benthic foraminiferal distribution. In: Hedley RHA, C. (ed) *Foraminifera*, v.2. London: Academic Press, 45-109.
- Murray JW. (1979) *British Nearshore Foraminifera*, London: Academic Press.
- Murray JW. (1982) Benthic foraminifera: the validity of living, dead or total assemblages for the interpretation of palaeoecology. *Journal of Micropalaeontology* 1: 137-140.
- Murray JW. (1989) Syndepositional dissolution of calcareous foraminifera in modern shallow-water sediments. *Marine Micropaleontology* 15: 117-121.

- Murray JW. (1991) *Ecology and Palaeoecology of Benthic Foraminifera*, Harlow, England: Longman Scientific and Technical.
- Murray JW. (2000) The enigma of the continued use of total assemblages in ecological studies of benthic foraminifera. *The Journal of Foraminiferal Research* 30: 244-245.
- Murray JW. (2003) Patterns in the cumulative increase in species from foraminiferal time-series. *Marine Micropaleontology* 48: 1-21.
- Murray JW. (2006) *Ecology and Applications of Benthic Foraminifera*, New York: Cambridge University Press.
- Nicholls RJ and Cazenave A. (2010) Sea-Level Rise and Its Impact on Coastal Zones. *Science* 328: 1517-1520.
- Oldfield F, Ascoli A, Accorsi CA, et al. (2003) A high resolution late Holocene palaeo environmental record from the central Adriatic Sea. *Quaternary Science Reviews* 22: 319-342.
- Orlić M, Beg Paklar G, Pasarić Z, et al. (2006) Nested modeling of the east Adriatic coastal waters. *Acta Adriatica* 47: 219-245.
- Orlić M, Gačić M and La Violette PE. (1992) The currents and circulation of the Adriatic Sea. *Oceanologica Acta* 15: 109-124.
- Orlić M and Pasarić M. (2000) Sea-level changes and crustal movements recorded along the east Adriatic coast. *Nuovo Cimento della Societa Italiana di Fisica C* 23: 351-364.
- Overpeck JT, Webb T and Prentice IC. (1985) Quantitative interpretation of fossil pollen spectra: dissimilarity coefficients and the method of modern analogues: *Quaternary Research* 23: 87-108.
- Ozarko DL, Patterson RT and Williams HFL. (1997) Marsh Foraminifera from Nanaimo, British Columbia (Canada); implications of infaunal habitat and taphonomic biasing. *Journal of Foraminiferal Research* 27: 51-68.
- Pandža M, Franjić J and Škvorc Ž. (2007) The salt marsh vegetation on the East Adriatic coast. *Biologia* 62: 24-31.
- Parker W and Arnold A. (2003) Quantitative methods of data analysis in foraminiferal ecology. In: Sen Gupta B (ed) *Modern Foraminifera*. Netherlands: Springer 71-89.
- Patterson RT and Fishbein E. (1989) Re-Examination of the Statistical Methods Used to Determine the Number of Point Counts Needed for Micropaleontological Quantitative Research. *Journal of Paleontology* 63: 245-248.
- Peltier WR. (2004) Global glacial isostasy and the surface of the ice-age earth: The ICE-5G (VM2) Model and GRACE. *Annual Review of Earth and Planetary Sciences* 32: 111-149.
- Penaud A, Eynaud F, Sánchez-Goñi M, et al. (2011) Contrasting sea-surface responses between the western Mediterranean Sea and eastern subtropical latitudes of the

- North Atlantic during abrupt climatic events of MIS 3. *Marine Micropaleontology* 80: 1-17.
- Pethick JS. (1981) Long-term accretion rates on tidal salt marshes. *Journal of Sedimentary Research* 51: 571-577.
- Petrucci F, Medioli FS, Scott DB, et al. (1983) Evaluation of the usefulness of foraminifera as sea level indicators in the Venetian Lagoon (N. Italy). *Acta Naturalia Ateneo Parmense* 19: 63-77.
- Pheleger FB and Walton WR. (1950) Ecology of marsh and bay foraminifera, Barnstable Massachusetts. *American Journal of Science* 248: 274-294.
- Pikelj K and Juračić M. (2013) Eastern Adriatic Coast (EAC): Geomorphology and Coastal Vulnerability of a Karstic Coast. *Journal of Coastal Research* 29: 944-957.
- Pirazzoli P. (1996) *Sea Level Changes. The Last 20 000 Years*, Chichester, New York: John Wiley & Sons Ltd.
- Pirazzoli PA. (1986) Marine notches. In: Van de Plassche O (ed) *Sea-level Research: A Manual for the Collection and Evaluation of Data*. Norwich: Geobooks, 361-400.
- Piva A, Asioli A, Trincardi F, et al. (2008) Late-Holocene climate variability in the Adriatic Sea (Central Mediterranean). *The Holocene* 18: 153-167.
- Plater AJ and Appleby PG. (2004) Tidal sedimentation in the Tees estuary during the 20th century: radionuclide and magnetic evidence of pollution and sedimentary response. *Estuarine, Coastal and Shelf Science* 60: 179-192.
- Plater AJ, Horton BP, Haworth EY, et al. (2000) Holocene tidal levels and sedimentation rates using a diatom-based palaeoenvironmental reconstruction: the Tees estuary, northeastern England. *The Holocene* 10: 441-452.
- Plater AJ, Ridgway J, Appleby PG, et al. (1999) Historical Contaminant Fluxes in the Tees Estuary, UK: Geochemical, Magnetic and Radionuclide Evidence. *Marine Pollution Bulletin* 37: 343-360.
- Plater AJ and Shennan I. (1992) Evidence of Holocene sea-level change from the Northumberland coast, eastern England. *Proceedings of the Geologists' Association* 103, Part 3: 201-216.
- Prentice IC. (1980) Multidimensional scaling as a research tool in Quaternary palynology: A review of theory and methods. *Review of Palaeobotany and Palynology* 31: 71-104.
- Pugh DT. (1996) *Tides, surges and mean sea-level (reprinted with corrections)*, Chichester, UK: John Wiley & Sons Ltd.
- R Development Core Team. (2013) R: A language and environment for statistical computing. Vienna, Austria: R Foundation for Statistical Computing. ISBN 3-900051-07-0, URL <http://www.R-project.org/>.

- Raichich F. (2007) A Study of Early Trieste Sea Level Data (1875–1914). *Journal of Coastal Research*: 23: 1067-1073.
- Ranwell DS. (1974) The saltmarsh to tidal woodland transition. *Hydrobiological Journal* 8: 139-151.
- Reimer PJ, Baillie MGL, Bard E, et al. (2009) INTCAL09 and MARINE09 Radiocarbon Age Calibration Curves, 0–50,000 Years CAL BP. *Radiocarbon* 51: 1111-1150.
- Reimer PJ and Reimer RW. (2007a) Radiocarbon Dating | Calibration. In: Editor-in-Chief: Scott AE (ed) *Encyclopedia of Quaternary Science*. Oxford: Elsevier, 2941-2950.
- Reimer PJ and Reimer RW. (2007b) Radiocarbon dating: calibration. In: Elias RW (ed) *Encyclopedia of Quaternary Science*. Amsterdam: Elsevier, 2941-2950.
- Rixen M, Beckers JM, Levitus S, et al. (2005) The Western Mediterranean Deep Water: A proxy for climate change. *Geophysical Research Letters* 32: L12608.
- Robins JA. (1978) Geochemical and geophysical applications of radioactive lead. In: Nriagu JO (ed) *The biogeochemistry of lead in the environment*. Elsevier Press, 285-393.
- Robinson AR, Leslie WG, Theocharis A, et al. (2001) Mediterranean Sea circulation. *Encyclopedia of Ocean Science* 3: 1689-1705.
- Roe HM, Charman DJ and Roland Gehrels W. (2002) Fossil testate amoebae in coastal deposits in the UK: implications for studies of sea-level change. *Journal of Quaternary Science* 17: 411-429.
- Roe HM and van de Plassche O. (2005) Modern pollen distribution in a Connecticut saltmarsh: Implications for studies of sea-level change. *Quaternary Science Reviews* 24: 2030-2049.
- Rohling EJ and Gieskens WWC. (1993) Late Quaternary changes in Mediterranean Intermediate Water density and formation rate. *Paleoceanography* 4: 531-545.
- Romić D, Zovko M, Romić M, et al. (2008) Quality aspects of the surface water used for irrigation in the Neretva Delta (Croatia). *Journal of Water and Land Development* 12: 59-70.
- Romic M and Romic D. (2003) Heavy metals distribution in agricultural topsoils in urban area. *Environmental Geology* 43: 795-805.
- Rossi V and Horton BP. (2009) The application of a subtidal foraminifera-based transfer function to reconstruct holocene paleobathymetry of the PO Delta, Northern Adriatic Sea. *Journal of Foraminiferal Research* 39: 180-190.
- Rossi V, Horton BP, Corbett DR, et al. (2011) The application of foraminifera to reconstruct the rate of 20th century sea level rise, Morbihan Golfe, Brittany, France. *Quaternary Research* 75: 24-35.
- Rožić N. (2001) Fundamental levelling networks and height datums at the territory of the Republic of Croatia. *Acta Geodaetica et Geophysica Hungarica* 36: 231-243.

- Sawai Y, Horton BP and Naqumo T. (2004) The development of a diatom-based transfer function along the Pacific coast of eastern Hokkaido, northern Japan - an aid in paleoseismic studies of the Kuril subduction zone. *Quaternary Science Reviews* 23: 2476-2484.
- Scott DB, Collins ES, Duggan J, et al. (1996) Pacific Rim marsh foraminiferal distributions: implications for sea-level studies. *Journal of Coastal Research* 12: 850–861.
- Scott DB and Hermelin JOR. (1993) A Device for Precision Splitting of Micropaleontological Samples in Liquid Suspension. *Journal of Paleontology* 67: 151-154.
- Scott DB and Medioli FS. (1978) Vertical zonations of marsh foraminifera as accurate indicators of former sea-levels. *Nature* 272: 528-531.
- Scott DB and Medioli FS. (1980a) Living vs. Total Foraminiferal Populations: Their Relative Usefulness in Paleoecology. *Journal of Paleontology* 54: 814-831.
- Scott DB and Medioli FS. (1980b) Quantitative studies of marsh foraminiferal distributions in nova-scotia canada implications for sea level studies. *Cushman Foundation for Foraminiferal Research Special Publication*: 1-58.
- Šepić J, Vilibić I and Strelec Mahović N. (2012) Northern Adriatic meteorological tsunamis: Observations, link to the atmosphere, and predictability. *Journal of Geophysical Research: Oceans* 117: C02002.
- Serandrei-Barbero R, Albani AD and Zecchetto S. (1997) Palaeoenvironmental significance of a benthic foraminiferal fauna from an archaeological excavation in the Lagoon of Venice, Italy. *Palaeogeography, Palaeoclimatology, Palaeoecology* 136: 41-52.
- Serandrei-Barbero R, Carbognin L, Taroni G, et al. (1999) Distribution of Recent Benthic Foraminifera in the Southern Basin of the Venice Lagoon (Italy): Statistical Evaluation of Taxa Significance. *Micropaleontology* 45: 99-111.
- Serandrei-Barbero R, Donnici S and Madricardo F. (2011) Supratidal foraminifera as ecological indicators in anthropically modified wetlands (Lagoon of Venice, Italy). *Ecological Engineering* 37: 1140-1148.
- Serandrei-Barbero R, Morisieri M, Carbognin L, et al. (2003) An inner shelf foraminiferal fauna and its response to environmental processes (Adriatic Sea Italy). *Revista Espanola Micropaleontologia* 35: 1-24.
- Shennan I. (1982) Interpretation of Flandrian sea-level data from the Fenland, England. *Proceedings of the Geologists' Association* 93: 53-63.
- Shennan I. (1986) Flandrian sea-level changes in the Fenland. II: Tendencies of sea-level movement, altitudinal changes, and local and regional factors. *Journal of Quaternary Science* 1: 155-179.
- Smith JN. (2001) Why should we believe 210Pb sediment geochronologies? *Journal of Environmental Radioactivity* 55: 121-123.

- Southall KE, Gehrels WR and Hayward BW. (2006) Foraminifera in a New Zealand salt marsh and their suitability as sea-level indicators. *Marine Micropaleontology* 60: 167-179.
- Šparica M, Bačani A, Koch G, et al. (2005a) Ecosystem of Morinje Bay (Adriatic Sea, Croatia): Aspects of the sediment/water interface. *RMZ - Materials and Geoenvironment* 52: 115-118.
- Šparica M, Koch G, Belak M, et al. (2005b) Recent Sediments of Makirina Cove (Northern Dalmatia, Croatia): Their Origin Viewed Through a Multidisciplinary Approach. *Geologia Croatica* 58: 21-72.
- Stocchi P, Girometti L, Spada G, et al. (2009) Post-glacial readjustment, sea-level variations, subsidence and erosion along Italian coasts. *Bollettino di Geofisica Teorica ed Applicata* 50: 129-144.
- Stocchi P and Spada G. (2009a) Glacio–isostatic Adjustment in the Po Plain and in the Northern Adriatic Region. *Pure and Applied Geophysics* 166: 1303-1318.
- Stocchi P and Spada G. (2009b) Influence of glacial isostatic adjustment upon current sea level variations in the Mediterranean. *Tectonophysics* 474: 56-68.
- Stuiver M and Braziunas TF. (1998) Anthropogenic and solar components of hemispheric ^{14}C . *Geophysical Research Letters* 25: 329-332.
- Stuiver M and Polach HA. (1977) Discussion: reporting of ^{14}C data. *Radiocarbon* 19: 355-363.
- Tamisiea ME and Mitrovica JX. (2011) The moving boundaries of sea level change: Understanding the origins of geographic variability. *Oceanography* 24: 24-39.
- Telford RJ, Andersson C, Birks HJB, et al. (2004a) Biases in the estimation of transfer function prediction errors. *Paleoceanography* 19: PA4014.
- Telford RJ and Birks HJB. (2005) The secret assumption of transfer functions: problems with spatial autocorrelation in evaluating model performance. *Quaternary Science Reviews* 24: 2173-2179.
- Telford RJ, Heegaard E and Birks HJB. (2004b) All age–depth models are wrong: but how badly? *Quaternary Science Reviews* 23: 1-5.
- Telford RJ, Heegaard E and Birks HJB. (2004c) The intercept is a poor estimate of a calibrated radiocarbon age. *The Holocene* 14: 296-298.
- ter Braak CJF. (1986) Canonical Correspondence Analysis: A New Eigenvector Technique for Multivariate Direct Gradient Analysis. *Ecology* 67: 1167-1179.
- ter Braak CJF. (1987) The analysis of vegetation-environment relationships by canonical correspondence analysis. *Vegetation* 69: 69-77.
- ter Braak CJF. (1995) Non-linear methods for multivariate statistical calibration and their use in palaeoecology: a comparison of inverse (k-nearest neighbours, partial least

- squares and weighted averaging partial least squares) and classical approaches. *Chemometrics and Intelligent Laboratory Systems* 28: 165-180.
- ter Braak CJF and Barendregt LG. (1986) Weighted averaging of species indicator values: Its efficiency in environmental calibration. *Mathematical Biosciences* 78: 57-72.
- ter Braak CJF and Juggins S. (1993) Weighted averaging partial least squares regression (WA-PLS): an improved method for reconstructing environmental variables from species assemblages. *Hydrobiologia* 269-270: 485-502.
- ter Braak CJF, Juggins S, Birks HJB, et al. (1993) Weighted averaging partial least squares regression (WA-PLS): definition and comparison with other methods for species-environment calibration. Chapter 25. In: Patil GP and Rao CR (eds) *Multivariate Environmental Statistics*. Amsterdam: North-Holland.
- ter Braak CJF and Prentice IC. (1988) A theory of gradient analysis. *Advances in Ecological Research* 18: 271-317.
- ter Braak CJF and Smilauer P. (1997-2003) Canoco for Windows. Version 4.5.
- ter Braak CJF and Verdonschot PFM. (1995) Canonical correspondence analysis and related multivariate methods in aquatic ecology. *Aquatic Sciences* 57: 255-289.
- Thomas E and Varekamp JC. (1991) Paleo-environmental analyses of marsh sequences (Clinton, Connecticut): evidence for punctuated rise in relative sealevel during the latest Holocene. *Journal of Coastal Research* 81: 125-158.
- Tobin R, Scott DB, Collins ES, et al. (2005) Infaunal benthic foraminifera in some north American marshes and their influence on fossil assemblages. *The Journal of Foraminiferal Research* 35: 130-147.
- Tooley MJ. (1978) *Sea-level Changes – North-West England During the Flandrian Stage*, Oxford: Clarendon Press.
- Tooley MJ. (1982) Sea-level changes in northern England. *Proceedings of the Geologists' Association* 93: 43-51.
- Troëls-Smith J. (1955) Characterization of unconsolidated sediments. *Danmarks Geologiske Undersøgelse Series* 4: 1-73.
- Tsimplis MN and Baker TF. (2000) Sea level drop in the Mediterranean Sea: An indicator of deep water salinity and temperature changes? *Geophysical Research Letters* 27: 1731-1734.
- Tsimplis MN and Josey SA. (2001) Forcing of the Mediterranean Sea by atmospheric oscillations over the North Atlantic. *Geophysical Research Letters*. 28: 803-806.
- Tsimplis MN, Marcos M and Somot S. (2008) 21st century Mediterranean sea level rise: Steric and atmospheric pressure contributions from a regional model. *Global and Planetary Change* 63: 105-111.

- Tsimplis MN, Proctor R and Flather RA. (1995) A two-dimensional tidal model for the Mediterranean Sea. *Journal of Geophysical Research: Oceans* 100: 16223-16239.
- Tsimplis MN, Raicich F, Fenoglio-Marc L, et al. (2012) Recent developments in understanding sea level rise at the Adriatic coasts. *Physics and Chemistry of the Earth, Parts A/B/C* 40–41: 59-71.
- Tsimplis MN and Spencer NE. (1997) Collection and Analysis of Monthly Mean Sea Level Data in the Mediterranean and the Black Sea. *Journal of Coastal Research* 13: 534-544.
- van de Plassche O. (1986) *Sea-level research: a manual for the collection and evaluation of data*, Norwich: Geobooks.
- van der Plicht J. (2007) Radiocarbon Dating | Variations in Atmospheric ^{14}C . In: Editor-in-Chief: Scott AE (ed) *Encyclopedia of Quaternary Science*. Oxford: Elsevier, 2923-2931.
- Vilibić I. (2006a) The role of the fundamental seiche in the Adriatic coastal floods. *Continental Shelf Research* 26: 206-216.
- Vilibić I. (2006b) Seasonal sea level variations in the Adriatic. *Acta Adriatic* 47: 141-158.
- Vilibić I and Šepić J. (2009) Destructive meteotsunamis along the eastern Adriatic coast: Overview. *Physics and Chemistry of the Earth, Parts A/B/C* 34: 904-917.
- Walton WR. (1952) Techniques for recognition of living foraminifera. *Cushman Foundation Foraminiferal Research* 3: 56-60.
- Wang A, Gao S, Jia J, et al. (2005) Sedimentation rates in the Wanggang salt marshes, Jiangsu. *Journal of Geographical Sciences* 15: 199-209.
- Watcham EP, Shennan I and Barlow NLM. (2013) Scale considerations in using diatoms as indicators of sea-level change: lessons from Alaska. *Journal of Quaternary Science* 28: 165-179.
- Weber J, Vrabec M, Pavlovic-Preseren P, et al. (2010) GPS-derived motion of the Adriatic microplate from Istria Peninsula and Po Plain sites, and geodynamic implications. *Tectonophysics* 483: 214-222.
- Wold S, Ruhe H, Wold H, et al. (1984) The collinearity problem in linear regression. The partial least squares (PLS) approach to generalized inverse. *SIAM Journal of Scientific and Statistical Computations*: 735-743.
- Woodroffe SA. (2009) Recognising subtidal foraminiferal assemblages: implications for quantitative sea-level reconstructions using a foraminifera-based transfer function. *Journal of Quaternary Science* 24: 215-223.
- Woodroffe SA, Horton BP, Larcombe P, et al. (2005) Intertidal mangrove foraminifera from the central Great Barrier Reef Shelf, Australia: implications for sea-level reconstruction. *The Journal of Foraminiferal Research* 35: 259-270.

- Woodroffe SA and Long AJ. (2010) Reconstructing recent relative sea-level changes in West Greenland: Local diatom-based transfer functions are superior to regional models. *Quaternary International* 221: 91-103.
- Woodworth PL. (2003) Some Comments on the Long Sea Level Records from the Northern Mediterranean. *Journal of Coastal Research* 19: 212-217.
- Wright AJ, Edwards RJ and van de Plassche O. (2011) Reassessing transfer-function performance in sea-level reconstruction based on benthic salt-marsh foraminifera from the Atlantic coast of NE North America. *Marine Micropaleontology* 81: 43-62.
- Zerbini S, Plag H-P, Baker T, et al. (1996) Sea level in the Mediterranean: a first step towards separating crustal movements and absolute sea-level variations. *Global and Planetary Change* 14: 1-48.
- Zong Y. (1997) Mid- and late-Holocene sea-level changes in Roudsea Marsh, northwest England: a diatom biostratigraphical investigation. *The Holocene* 7: 311-323.
- Zong Y and Horton BP. (1999) Diatom-based tidal-level transfer functions as an aid in reconstructing Quaternary history of sea-level movements in the UK. *Journal of Quaternary Science* 14: 153-167.
- Zong Y and Tooley MJ. (1996) Holocene sea-level changes and crustal movements in Morecambe Bay, northwest England. *Journal of Quaternary Science* 11: 43-58.
- Zovko M and Romic M. (2011) Soil Contamination by Trace Metals: Geochemical Behaviour as an Element of Risk Assessment. In: Dar IA and Dar MA (eds) *Earth and Environmental Sciences*. InTech, 437-456.

APPENDIX A. TROELS-SMITH CORE DESCRIPTIONS

Jadrtnovac Site 1

Core 1. GPS: 43°40.803'N 15°57.426'E

Depth (cm)	Sediment description (after Troels-smith, 1955)	Nig	Strf	Elas	Sicc	Lim Sup
0-13	Dark brown grey very organic clay with abundant roots, occasional sand and gravel. As ₂ , Sh ₁ , Th ⁰ ₁ , Ga ₊ , Ggmin ₊ .	3	0	0	2+	-
13	Bedrock					

Core 2. GPS: 43°40.806'N 15°57.425'E

Depth (cm)	Sediment description (after Troels-smith, 1955)	Nig	Strf	Elas	Sicc	Lim Sup
0-11	Dark brown peat with abundant roots. Th ⁰ ₃ , Sh ₁ , As ₊ .	3+	0	0	2+	-
11-18	Grey brown peaty clay with abundant roots. As ₂ , Th ¹ ₂ , Sh ₊ .	3	0	0	2+	0
18	Bedrock					

Core 3. GPS: 43°40'48.21"N 15°57'24.33"E.

Depth (cm)	Sediment description (after Troels-smith, 1955)	Nig	Strf	Elas	Sicc	Lim Sup
0-11	Dark brown peat with abundant roots. Th ⁰ ₃ , Sh ₁ , As ₊ .	3+	0	0	2+	-
11-19	Grey brown peaty clay with abundant roots. As ₂ , Th ¹ ₂ , Sh ₊ .	3	0	0	2+	0
19	Bedrock					

Core 4 . GPS: 43°40.804'N 15°57.423'E

Depth (cm)	Sediment description (after Troels-smith, 1955)	Nig	Strf	Elas	Sicc	Lim Sup
0-11	Dark brown peat with abundant roots. Th ⁰ ₃ , Sh ₁ , As ₊ , Th ² ₊ .	3+	0	0	2+	-
11-20	Grey brown peaty clay with abundant roots. As ₂ , Th ¹ ₂ , Sh ₊ .	3	0	0	2+	0
20-42	Blue grey slightly mottled silty clay with some rootlets. As ₂ ₊ , Ag ₁ , Th ¹ ₊₊ , Lf ₊ , Sh ₊ .	2	0	0	2	0
42	Bedrock					

Core 5. GPS: 43°40.805'N 15°57.420'E

Depth (cm)	Sediment description (after Troels-smith, 1955)	Nig	Strf	Elas	Sicc	Lim Sup
0-10	Dark brown peat with abundant rootlets. Th ⁰ 3, Sh1, As+, Th ² +	3+	0	0	2+	-
10-17	Grey brown peaty clay with abundant rootlets. As2, Th ¹ 2, Sh+.	3	0	0	2+	0
17-54	Blue grey slightly mottled silty clay with some rootlets. As2 ⁺ , Ag1, Th ¹ ++, Lf+, Sh+.	2	0	0	2	0
54	Bedrock					

Core 6. GPS: 43°40.806'N 15°57.416'E

Depth (cm)	Sediment description (after Troels-smith, 1955)	Nig	Strf	Elas	Sicc	Lim Sup
0-8	Grey brown very peaty clay with abundant rootlets. As2, Th ⁰ 2, Sh+.	3	0	0	2	-
8-30	Mottled grey brown silty clay with abundant rootlets. Orange and black mottles and occasional shells. As3, Ag1, Th ¹ ++, Lf+, Dg+, Tm+.	3	0	0	2	0
30-70	Blue grey clayey silt with rootlets, stems and shells. Ag3, As1, Th ¹ ++, Tm++.	2	0	0	2	0
70	Bedrock					

Core 7. GPS: 43°40.809'N 15°57.408'E

Depth (cm)	Sediment description (after Troels-smith, 1955)	Nig	Strf	Elas	Sicc	Lim Sup
0-8	Dark brown clayey peat. As2, Th ⁰ 2, Sh+.	3	0	0	2+	-
8-35	Light grey silty clay with orange brown mottles, rootlets and stems. As3, Ag1, Lf+, Th ¹ ++.	2+	0	0	2+	0
35-90	Blue grey clayey silt with rootlets and occasional stems and shells. Ag3, As1, Th ² ++, Tm+, Ptm+.	2	0	0	2+	0
90	Bedrock					

Core 8. GPS: 43°40.810'N 15°57.403'E

Depth (cm)	Sediment description (after Troels-smith, 1955)	Nig	Strf	Elas	Sicc	Lim Sup
0-8	Dark brown clayey peat with abundant rootlets. As2, Th ⁰ 1+, Sh++.	3	0	0	2+	-
8-40	Mottled grey silty clay with occasional rootlets and abundant shells. As3, Ag1, Th ¹ ++, Lf+, Tm+.	2	0	0	2+	0
40-98	Blue grey clayey silt with occasional rootlets and stems and abundant shells and fragments. Ag3, As1, Th ¹ +, Tm+, Ptm+, Ggmaj+.	2	0	0	2+	0
98	Bedrock					

Core 9. GPS: 43°40.813'N 15°57.391'E

Depth (cm)	Sediment description (after Troels-smith, 1955)	Nig	Strf	Elas	Sicc	Lim Sup
0-8	Dark brown clayey peat. As1, Th ⁰ 3, Sh++.	3	0	0	2+	-
8-42	Orange brown mottled grey silty clay with rootlets and stems. As3, Ag1, Th ¹ ++, Lf+, Ptm+.	2	0	0	2+	0
42-100	Blue grey clayey silt with occasional rootlets and stems. Very abundant shells and fragments of a variety of types. Ag3, As1, Th ¹ +, Tm++, Ptm++.	2	0	0	2+	0

100-168	Unrecoverable (presumed similar to unit above).					
168	Bedrock					

Core 10. GPS: 43°40.816'N 15°57.379'E

Depth (cm)	Sediment description (after Troels-smith, 1955)	Nig	Strf	Elas	Sicc	Lim Sup
0-14	Grey brown peaty clay. As ₂ , Th ⁰ ₂ .	3	0	0	2+	-
14-28	Grey silty clay with occasional orange/brown to black mottles. Abundant rootlets and stems. As ₂ , Ag ₂ , Th ¹ ₊₊ , Lf ₊ , Sh ₊ .	2+	0	0	2+	0
28-100	Blue grey clay silt with occasional rootlets and stems and shell fragments. Ag ₃ , As ₁ , Th ¹ ₊ , Ptm ₊₊ , Tm ₊ .	2	0	0	2+	0
100-176	Unrecoverable (presumed similar to unit above).					
176	Bedrock					

Core 11. GPS: 43°40.820'N 15°57.366'E

Depth (cm)	Sediment description (after Troels-smith, 1955)	Nig	Strf	Elas	Sicc	Lim Sup
0-10	Brown clayey peat with very abundant rootlets. As ₁ , Sh ₁ , Th ⁰ ₂ .	3	0	0	2	-
10-40	Grey silty clay with orange/brown to black mottles and woody detritus, rootlets and stems. As ₃ , Ag ₁ ₊ , Th ¹ ₊₊ , Lf ₊ , Sh ₊ , DL ₊ .	2+	0	0	2+	0
40-89	Blue grey clay silt with occasional rootlets, stems and abundant shells. Woody detritus. Ag ₃ , As ₁ , Th ¹ ₊ , Ptm ₊₊ , Tm ₊ , DL ₊ .	2	0	0	2+	1
89-100	Shelly silty clay. Ag ₄ , Ptm ₊₊ , As ₊ , Th ¹ ₊ .	2	0	0	2+	0
100-205	Unrecoverable (presumed similar to unit above).					
205	Bedrock					

Core 12. GPS: 43°40.823'N 15°57.352'E

Depth (cm)	Sediment description (after Troels-smith, 1955)	Nig	Strf	Elas	Sicc	Lim Sup
0-10	Grey brown peaty clay with abundant rootlets. As ₂ , Sh ₊₊ , Th ⁰ ₂ .	3	0	0	2+	-
10-38	Grey silty clay with orange/brown to black mottles with abundant rootlets and stems. As ₂ , Ag ₊ , Th ¹ ₊₊ .	2+	0	0	2+	0
38-78	Blue grey clay silt with occasional rootlets, stems and phragmites. Abundant shells. Ag ₃ , As ₁ , Th ¹ ₊ , Thphrag ₊ , Ptm ₊₊ , Tm ₊₊ .	2	0	0	2+	0
78-141	Medium grey shelly silt with occasional rootlets. Ag ₃ , Ptm ₁ , As ₊ , Th ² ₊ , Tm ₊ .	2	0	0	2+	0
141-223	Unrecoverable (presumed similar to unit above).					
223	Bedrock					

Blace Transect 1

Core 1. GPS 43°00.263' N 017°28.466' E

Depth (cm)	Sediment description (after Troels-smith, 1955)	Nig	Strf	Elas	Sicc	Lim Sup
0-22	Dark brown very organic clay with abundant rootlets. As ₃ , Th ¹ ₁ , Ag ⁺ , Sh ⁺⁺ .	3+	0	0	3	-
22	Bedrock					

Core 2. GPS 43°00.263' N 017°28.465' E

Depth (cm)	Sediment description (after Troels-smith, 1955)	Nig	Strf	Elas	Sicc	Lim Sup
0-9	Dark brown peat with abundant rootlets and some clay. Th ¹ ₃ , As ₁ , Sh ⁺ .	3+	0	0	3	-
9-28	Grey brown organic silty clay with abundant rootlets and occasional mottles. As ₂ , Ag ₂ , Th ¹ ₊₊ , Sh ⁺ , Lf ⁺ .	2+	0	0	3	0
28-30	Dark brown organic peaty clay with abundant detrital stems and rootlets. Th ² ₁ , As ₁ , Dh ₁ , Ag ₁ , Sh ⁺ .	3	0	0	2+	0
30	Bedrock					

Core 3. GPS 43°00.264' N 017°28.464' E

Depth (cm)	Sediment description (after Troels-smith, 1955)	Nig	Strf	Elas	Sicc	Lim Sup
0-10	Dark brown clayey peat with abundant rootlets. Th ¹ ₃ , As ₁ , Sh ⁺ .	3	0	0	2	-
10-30	Grey brown organic silty clay with abundant rootlets and detrital stems. Fragments of burnt wood/charcoal. As ₂ , Ag ₁ , Th ¹ ₁₊ , Dh ⁺⁺ , Dg ⁺ , Anth ⁺⁺ .	3	0	0	2+	0
30	Bedrock					

Core 4. GPS 43°00.264' N 017°28.463' E

Depth (cm)	Sediment description (after Troels-smith, 1955)	Nig	Strf	Elas	Sicc	Lim Sup
0-11	Grey-brown peaty clay with abundant rootlets. Th ¹ ₂ , As ₂ , Ag ⁺ .	3	0	0	2	-
11-30	Grey-brown silty clay with abundant rootlets and detrital organics. Occasional small shells and wood fragments. Whole hydrobia shell. As ₂ , Ag ₁ , Th ¹ ₁ , Dh ⁺⁺ , Dl ⁺ , Th ⁺ .	2++	0	0	3	0
30-38	Blue grey very organic silt (micaceous). Ag ₂ , Dh ₂ , Th ² ₊ , Dl ⁺ , Sb ⁺ .	2++	0	0	3	0
38	Bedrock					

Core 5. GPS 43°00.265' N 017°28.461' E

Depth (cm)	Sediment description (after Troels-smith, 1955)	Nig	Strf	Elas	Sicc	Lim Sup
0-26	Grey brown organic clay with abundant rootlets. As ₂ , Th ¹ ₂ .	3	0	0	2+	-
26-37	Grey silty clay with rootlets and detrital organics. As ₂ , Ag ₁₊ , Th ¹ ₁ , Dh ⁺ .	2+	0	0	2+	0
37-45	Blue-grey silt (micaceous), with rootlets and detrital organics. Possibly some lamination. Ag ₄ , Th ² ₊₊ , Dh ⁺ , As ⁺ , Sb ⁺ .	2	0	0	2+	0
45-70	Grey brown organic silt with rootlets plus 'nut'. Ag ₃ , Dh ₁ , Th ² ₊₊ , Sh ⁺⁺ , As ⁺ , Dl ⁺ .	2++	0	0	2+	0

70	Bedrock					
----	---------	--	--	--	--	--

Core 6. GPS 43°00.265' N 017°28.456' E

Depth (cm)	Sediment description (after Troels-smith, 1955)	Nig	Strf	Elas	Sicc	Lim Sup
0-16	Grey brown peaty clay with rootlets. As ₃ , Th ⁰ ₁ , Dh+, Lf+.	2++	0	0	2+	-
16-100	Slightly laminated medium to dark grey (micaceous) silt with occasional rootlets, organic detritus and shells. Ag ₃ , As ₁ , Th ² +, Dh+, Tm+, Sb+.	3	1+	0	2+	0
100-126	Medium to dark gray saturated coarse shelly silt. Ag ₃ , Ptm ₁ , Tm+, As+, Dh+.	3	0	0	1+	0
126	Bedrock					

Core 7. GPS 43°00.266' N 017°28.452' E

Depth (cm)	Sediment description (after Troels-smith, 1955)	Nig	Strf	Elas	Sicc	Lim Sup
0-12	Grey silty clay with abundant rootlets and some detrital organics. As ₂ , Ag ₁ , Th ¹ ++, Dh+, Sh+.	2++	0	0	2	-
12-95	Medium to dark grey slightly laminated silt with organic detritus, shells and mica. Ag ₄ , Th ² ++, Dh++, As ₂ , Ptm+, Dl+, Sb+.	3	1	0	2+	0
95-134	Medium grey saturated silt with occasional organic detritus and shells. Ag ₄ , Tm+, Dh+, Dl+.	3	0	0	1+	0
134	Bedrock					

Core 8. GPS 43°00.273' N 017°28.457' E

Depth (cm)	Sediment description (after Troels-smith, 1955)	Nig	Strf	Elas	Sicc	Lim Sup
0-13	Medium brown clayey peat with abundant rootlets. As ₁ +, Sh ₁ , Th ¹ ₂ +	3	0	0	2+	-
13-42	Grey brown organic clay with abundant rootlets. As ₂ , Ag ₁ , Th ¹ ₁ +	2+	0	0	2+	0
42-53	Medium blue grey silt with rootlets, detrital organics and shell fragments. As+, Ag ₃ , Dh ₁ , Dg+, Ptm+, Th ² +	3	0	0	2+	0
53-76	Grey brown detrital organics with silt. Ag ₂ , Dh ₁ , Dl ₁ , Th ² +	3	0	0	2+	0
76	Bedrock					

Core 9. GPS 43°00.291' N 017°28.462' E

Depth (cm)	Sediment description (after Troels-smith, 1955)	Nig	Strf	Elas	Sicc	Lim Sup
0-9	Medium brown peat with abundant rootlets and clay. Th ⁰ ₃ , As ₁ +, Sh+.	3	0	0	2+	-
9-23	Brown grey mottled organic silty clay with rootlets and orange staining. As ₃ , Ag ₁ , Th ¹ ++, Lf+.	2+	0	0	2+	0
23-30	Grey brown silt with abundant detrital organics. Ag ₃ , Dl ₁ , Dh++, Sh+, Sb+.	3	0	0	3	0
30-43	Medium grey clayey silt with occasional organic detritus, rootlets and shells. Ag ₂ , As ₁ , Th+, Ptm++, Dh+, Th ² ++.	2++	0	0	2+	0
43-87	Grey and brown very organic silt saturated towards the base. Ag ₂ , Dg ₁ , Th ² ₁ , Dh+, Dl++.	3+	0	0	2	0
87	Bedrock					

Core 10. GPS 43°00.272' N 017°28.457' E

Depth (cm)	Sediment description (after Troels-smith, 1955)	Nig	Strf	Elas	Sicc	Lim Sup
0-14	Brown grey mottled silty clay with abundant rootlets. As ₂ , Ag ₁ , Th ¹ ₁ , Lf ₊ .	2+	0	0	2+	-
14-50	Grey brown clayey silt with rootlets, detrital stems and occasional small shells (hydrobia). Mica. Ag ₂ , As ₂ , Th ² ₊₊ , Dh ₊ , Tm ₊ , Sb ₊ .	2	0	0	2+	0
50-78	Brown grey silt with lots of detrital organics and some shells. Fragments of charcoal. Ag ₂ , Dg ₁ , Dl ₁ , Th ² ₊₊ , Tm ₊ , Ptm ₊ , Anth ₊ .	3	0	0	2+	0
78-108	Medium grey shelly silt with occasional rootlets and organic detritus. Ag ₄ , As ₊ , Th ² ₊ , Dg ₊ , Tm ₊₊ , Ptm ₊₊ .	2+	0	0	2	0
108	Bedrock					

Core 11. GPS 43°00.269' N 017°28.455' E

Depth (cm)	Sediment description (after Troels-smith, 1955)	Nig	Strf	Elas	Sicc	Lim Sup
0-11	Grey brown organic clay with abundant rootlets. As ₃ , Th ¹ ₁ , Ag ₊ .	2++	0	0	2	-
11-30	Medium brown grey very silty clay with occasional rootlets and detrital organics. As ₂ , Ag ₂ , Th ² ₊₊ , Sh ₊ , Dg ₊ .	2++	0	0	2	0
30-87	Medium to dark grey silt with occasional shell fragments, organic detritus and shells. Ag ₄ , Th ² ₊ , Dl ₊ .	3	0	0	2+	0
87-120	Very organic grey brown silt. Ag ₂ , Dg ₂ , Th ² ₊ , Dl ₊ .	3	0	0	2+	0
120-158	Medium to dark grey saturated shelly silt. Ag ₄ , Ptm ₊ , Tm ₊₊ , Dg ₊ , As ₊ .	3	0	0	1+	0
158	Bedrock					

APPENDIX B. RAW FORAMINIFERA COUNTS (SURFACE AND CORE)

Table A1. Jadrtovac Site 1 Surface foraminifera dead and live counts.

Foraminifera taxa	Sample Number																					
	1	2	3	4	5	6	7	8	9	10	11	12	13	14	15	16	17	18	19	20	21	22
<i>Balti. pseudomacrescens</i>	0	0	3	0	2	9	1	5	1	0	1	4	0	8	0	3	8	16	0	0	1	8
	0	0	0	0	0	0	0	0	0	0	0	0	0	0	0	0	0	0	0	0	0	0
<i>Haplophragmoides wilberti</i>	0	0	5	0	0	1	1	2	2	2	7	1	0	0	7	3	31	6	1	4	12	13
	0	0	0	0	0	0	0	0	0	0	0	0	0	0	0	0	0	0	1	0	0	0
<i>Miliammina fusca</i>	0	0	34	0	10	69	34	16	13	12	8	5	1	0	0	0	0	1	1	4	0	8
	0	0	0	0	0	0	0	1	2	0	0	0	0	0	0	0	0	0	1	0	0	0
<i>Jadammina macrescens</i>	0	7	83	90	91	108	113	323	184	240	214	143	95	277	265	90	59	162	160	144	199	243
	0	0	0	0	0	4	0	13	11	16	4	4	0	53	4	2	5	1	8	8	19	8
<i>Reophax moniliformis</i>	0	0	0	0	0	0	0	0	0	0	12	30	0	0	0	0	0	0	0	2	0	0
	0	0	0	0	0	0	0	0	0	0	0	0	0	0	0	0	0	0	0	0	0	0
<i>Siphotrochammina lobata</i>	0	0	0	2	0	0	13	7	2	0	0	5	0	0	2	0	2	1	0	0	3	0
	0	0	0	0	0	0	0	0	0	0	0	0	0	0	0	0	0	0	0	0	0	0
<i>Trochammina inflata</i>	0	2	519	515	63	312	232	316	548	60	58	16	28	69	105	235	250	319	570	431	335	1050
	0	0	9	28	0	1	6	36	67	11	7	1	1	15	10	34	37	10	52	64	35	121
<i>Ammonia</i> spp.	0	0	0	4	0	0	0	0	0	231	0	0	0	2	1	67	59	3	1	58	15	23
	0	0	0	0	0	0	0	0	0	25	0	0	0	0	0	11	6	0	3	3	1	0
<i>Brazalina</i> spp.	0	0	0	0	0	0	0	0	0	3	2	0	0	2	2	0	0	8	2	0	7	10
	0	0	0	0	0	0	0	0	0	0	0	0	0	0	0	0	0	0	0	0	0	1
<i>Elphidium</i> spp.	0	0	90	312	0	0	0	0	0	5	0	0	0	0	0	12	17	0	3	19	7	14
	0	0	0	0	0	0	0	0	0	2	0	0	0	0	0	5	3	0	3	6	0	1
<i>Haynesia germanica</i>	0	0	0	0	0	0	0	0	0	35	0	0	0	0	0	11	21	0	0	10	3	4
	0	0	0	0	0	0	0	0	0	0	0	0	0	0	0	0	0	0	0	0	0	0
<i>Quinqueloculina</i> spp.	0	0	14	8	0	0	0	0	0	193	10	0	0	0	3	334	314	1	19	598	63	384
	0	0	0	0	0	0	0	0	0	50	0	0	0	0	1	87	47	2	26	74	10	137
<i>Spirillina vivipara</i>	0	0	0	0	0	0	0	0	0	4	0	1	0	0	1	19	3	0	0	6	1	7
	0	0	0	0	0	0	0	0	0	0	0	0	0	0	0	7	3	0	0	2	2	0
Total Dead	0	9	748	931	166	499	394	669	750	785	312	205	124	358	386	774	765	517	757	1280	646	1764
Total Live	0	0	9	28	0	5	6	50	80	104	11	5	1	68	15	146	101	13	94	157	67	265
Altitude m HVR571	0.48	0.44	0.27	0.22	0.20	0.18	0.19	0.15	0.14	0.09	0.06	0.08	0.05	0.08	0.08	0.11	0.10	0.06	0.05	0.06	0.10	0.04

Table A2. Jadrtovac Site 2 Surface foraminifera dead and live counts.

Foraminifera taxa	Sample number									
	1	2	3	4	5	6	7	8	9	10
<i>Balticamina pseudomacrescens</i>	0	1	0	1	0	0	0	1	0	1
	0	0	0	0	0	0	0	0	0	0
<i>Haplophragmoides wilberti</i>	12	12	20	6	12	9	8	8	7	6
	7	0	0	1	0	0	0	0	1	0
<i>Miliammina fusca</i>	9	9	14	402	355	264	65	18	4	10
	0	0	0	39	21	19	1	3	0	0
<i>Jadammina macrescens</i>	215	293	226	167	104	197	443	211	615	299
	96	29	7	10	2	5	32	23	80	36
<i>Reophax moniliformis</i>	0	0	0	0	0	0	0	0	0	0
	0	0	0	0	0	0	0	0	0	0
<i>Siphotrochammina lobata</i>	0	2	2	0	0	0	0	0	0	0
	0	0	0	0	0	0	0	0	0	0
<i>Trochammina inflata</i>	12	61	926	291	253	419	369	440	82	110
	3	42	0	49	15	14	24	36	8	29
<i>Ammonia</i> spp.	0	0	3	5	18	84	72	86	33	37
	0	0	0	1	0	3	0	14	2	5
<i>Brazalina</i> spp.	0	0	0	7	1	3	6	0	0	3
	0	0	0	0	0	0	3	0	0	0
<i>Elphidium</i> spp.	10	33	297	147	30	5	5	7	0	4
	0	11	0	20	4	1	0	4	0	0
<i>Haynesia germanica</i>	0	0	0	0	1	16	21	17	7	10
	0	0	0	0	0	0	0	0	0	0
<i>Quinqueloculina</i> spp.	2	10	80	12	14	96	147	484	79	74
	0	1	0	0	0	13	6	92	12	31
<i>Spirillina vivipara</i>	0	0	2	15	0	0	3	0	0	1
	0	0	0	9	0	1	1	0	0	0
Total Dead	260	421	1570	1053	788	1093	1139	1272	827	555
Total Live	106	83	7	129	42	56	67	172	103	101
Altitude m HVR571	0.35	0.30	0.23	0.19	0.19	0.17	0.16	0.15	0.14	0.08

Table A3. Jadrtovac Site 1 Random Surface foraminifera dead and live counts.

Foraminifera taxa	Sample number									
	1	2	3	4	5	6	7	8	9	10
<i>Balticamina pseudomacrescens</i>	0	1	0	0	0	0	0	0	0	0
	0	0	0	0	0	0	0	0	0	0
<i>Haplophragmoides wilberti</i>	3	12	6	14	3	0	1	9	45	12
	0	1	0	0	0	0	0	0	2	0
<i>Miliammina fusca</i>	294	68	21	4	3	287	9	2	43	0
	1	0	0	0	0	0	0	0	0	0
<i>Jadammina macrescens</i>	285	228	74	117	110	778	600	126	2043	200
	7	22	3	11	33	9	28	3	32	0
<i>Reophax moniliformis</i>	0	0	0	0	0	0	0	0	0	0
	0	0	0	0	0	0	0	0	0	0
<i>Siphotrochammina lobata</i>	3	7	0	0	0	0	0	0	0	0
	0	0	0	0	0	0	0	0	0	0
<i>Trochammina inflata</i>	245	474	278	308	230	520	640	284	438	377
	35	53	23	74	110	20	14	17	0	0
<i>Ammonia</i> spp.	6	0	0	0	163	20	91	1	3	13
	8	0	0	29	45	6	37	6	1	0
<i>Brazalina</i> spp.	3	10	0	0	7	0	4	0	0	0
	0	0	0	0	0	0	1	0	0	0
<i>Elphidium</i> spp.	8	3	0	0	105	22	32	0	9	36
	3	3	0	1	30	11	20	0	0	0
<i>Haynesia germanica</i>	0	0	0	0	78	5	29	0	0	0
	0	0	0	0	0	0	0	0	0	0
<i>Quinqueloculina</i> spp.	40	98	0	4	638	259	79	0	8	2
	11	24	0	4	135	15	22	0	0	0
<i>Spirillina vivipara</i>	0	12	0	0	4	6	0	0	0	0
	0	2	0	0	0	0	0	0	0	0
Total Dead	887	913	379	447	1341	1897	1485	422	2589	640
Total Live	65	105	26	119	353	61	122	26	35	0
Altitude m HVR571	0.07	0.16	0.16	0.06	0.09	0.14	0.11	0.09	0.18	0.27

Table A4. Blace Transect 1 Surface foraminifera dead and live counts.

Foraminifera taxa	Sample Number																	
	1	2	3	4	5	6	7	8	9	10	11	12	13	14	15	16	17	18
<i>Balticamina pseudomacrescens</i>	0	0	0	0	0	0	0	0	0	0	0	0	0	0	0	0	0	0
	0	0	0	0	0	0	0	0	0	0	0	0	0	0	0	0	0	0
<i>Haplophragmoides wilberti</i>	5	17	17	4	22	7	0	5	9	3	0	0	1	0	0	0	1	1
	0	0	1	2	0	0	0	0	0	0	0	0	0	0	0	0	0	0
<i>Miliammina fusca</i>	45	10	5	3	38	70	34	7	42	0	17	0	0	2	1	30	0	1
	0	0	0	0	0	0	0	0	0	0	0	0	0	0	0	0	0	0
<i>Jadammina macrescens</i>	78	295	200	90	488	289	507	240	280	140	79	25	23	5	4	101	170	240
	1	3	2	1	12	19	18	11	10	21	16	13	22	0	0	4	10	12
<i>Reophax moniliformis</i>	0	0	0	0	0	0	0	0	0	0	0	0	0	0	0	0	0	0
	0	0	0	0	0	0	0	0	0	0	0	0	0	0	0	0	0	0
<i>Siphotrochammina lobata</i>	0	0	0	1	0	0	2	0	0	0	0	0	1	0	0	0	1	0
	0	0	0	0	0	0	0	0	0	0	0	0	0	0	0	0	0	0
<i>Trochammina inflata</i>	695	450	400	139	200	145	303	285	638	245	95	41	24	17	7	343	650	720
	30	9	35	3	10	9	9	12	10	20	13	15	13	1	0	15	16	33
<i>Ammonia</i> spp.	1	0	0	0	0	0	0	0	0	87	103	58	35	98	78	0	25	74
	0	0	0	0	0	0	0	0	0	1	0	15	13	13	13	0	1	4
<i>Brazalina</i> spp.	0	0	0	0	1	0	1	0	2	0	3	5	3	4	4	0	0	0
	0	0	0	0	0	0	0	0	0	0	0	0	0	1	2	0	0	0
<i>Elphidium</i> spp.	1	0	1	0	0	0	0	0	0	5	16	30	6	7	29	0	0	0
	0	1	2	0	0	0	0	0	0	2	2	15	0	0	0	0	0	0
<i>Haynesia germanica</i>	0	0	0	0	0	0	0	0	0	33	42	12	16	17	8	0	4	13
	0	0	0	0	0	0	0	0	0	0	0	0	0	0	0	0	0	0
<i>Quinqueloculina</i> spp.	643	178	50	0	0	0	0	0	0	240	1117	95	68	21	39	1	197	510
	0	19	4	0	0	0	0	0	0	34	14	36	45	19	25	0	9	30
<i>Spirillina vivipara</i>	10	3	1	0	0	0	0	0	0	31	170	8	4	3	5	0	13	5
	0	2	1	0	0	0	0	0	0	7	0	0	0	0	1	0	7	0
Total Dead	1478	953	674	237	749	511	847	537	971	784	1642	274	181	174	175	475	1061	1564
Total Live	31	34	45	6	22	28	27	23	20	84	46	79	95	34	41	19	43	83
Altitude m HVR571	0.37	0.37	0.36	0.34	0.32	0.29	0.28	0.29	0.3	0.26	0.2	0.17	0.18	0.05	0.01	0.4	0.34	0.29

Note - Samples 16, 17 and 18 – high marsh samples taken adjacent to samples 1, 2 and 3.

Table A5. Blace Transect 2 Surface foraminifera dead and live counts.

Foraminifera taxa	Sample Number									
	1	2	3	4	5	6	7	8	9	10
<i>Balticamina pseudomacrescens</i>	2	0	0	0	0	0	0	0	0	0
	0	0	0	0	0	0	0	0	0	0
<i>Haplophragmoides wilberti</i>	15	16	8	11	1	3	0	0	0	0
	5	0	0	2	1	0	0	0	0	0
<i>Miliammina fusca</i>	2	1	0	3	21	1	0	0	0	1
	0	0	0	0	0	0	0	0	0	0
<i>Jadammina macrescens</i>	128	155	258	215	69	9	0	1	0	0
	44	10	71	50	12	5	0	0	0	0
<i>Reophax moniliformis</i>	0	0	0	0	0	0	0	0	0	0
	0	0	0	0	0	0	0	0	0	0
<i>Siphotrochammina lobata</i>	0	0	0	0	0	0	0	0	0	0
	0	0	0	0	0	0	0	0	0	0
<i>Trochammina inflata</i>	71	27	26	105	89	14	0	1	0	0
	18	2	7	25	9	7	1	1	0	0
<i>Ammonia</i> spp.	15	3	8	84	387	16	108	49	0	7
	4	0	0	2	18	2	0	0	0	1
<i>Brazalina</i> spp.	0	1	0	0	6	0	0	0	0	0
	0	0	0	0	0	0	0	0	0	0
<i>Elphidium</i> spp.	6	2	0	2	42	102	12	12	0	0
	6	1	1	5	7	43	0	0	0	0
<i>Haynesia germanica</i>	0	0	0	11	86	4	27	10	0	0
	0	0	0	0	0	0	0	0	0	0
<i>Quinqueloculina</i> spp.	201	164	127	143	217	24	4	0	0	1
	89	15	47	37	18	3	0	0	0	0
<i>Spirillina vivipara</i>	0	0	0	0	8	1	0	0	0	0
	1	1	0	0	0	0	0	0	0	0
Total Dead	440	369	427	574	926	174	151	73	0	9
Total Live	167	29	126	121	65	58	1	1	0	1
Altitude m HVR571	0.4	0.34	0.26	-0.01	-0.14	-0.16	-0.16	-0.15	-0.16	-0.07

Table A6. Jadrtovac Site 1 Core fossil foraminifera dead counts.

Foraminifera taxa	Sample Depth (cm)																					
	1	2	3	4	5	6	7	8	9	10	11	12	13	14	15	16	17	18	19	20	21	22
<i>Balticammina pseudomacrescens</i>	0	1	2	0	0	0	0	0	0	0	0	0	0	0	0	0	0	0	0	0	1	0
<i>Haplophragmoides wilberti</i>	0	12	4	2	4	0	0	0	0	5	0	0	0	1	0	8	2	5	1	19	1	0
<i>Miliammina fusca</i>	20	8	24	94	34	19	39	103	178	347	100	180	236	117	248	210	191	355	414	156	115	87
<i>Jadammina macrescens</i>	42	127	195	158	214	56	77	95	178	172	113	177	218	196	283	61	35	59	43	60	57	65
<i>Reophax moniliformis</i>	0	0	0	0	0	0	0	0	0	0	0	0	0	0	0	0	0	0	0	0	0	0
<i>Siphotrochammina lobata</i>	1	4	1	11	0	0	0	0	0	2	0	0	0	1	0	14	4	6	12	1	0	0
<i>Trochammina inflata</i>	146	272	215	186	334	62	87	85	107	102	71	240	199	529	571	175	133	81	114	28	56	4
<i>Ammonia</i> spp.	0	0	0	0	0	0	0	0	0	0	0	3	2	0	0	0	0	0	0	0	1	15
<i>Brazalina</i> spp.	0	0	0	0	0	0	0	0	0	0	0	0	0	0	0	0	0	0	0	0	0	0
<i>Elphidium</i> spp.	0	0	0	0	0	0	0	0	0	0	0	1	0	0	0	0	0	0	0	0	0	0
<i>Haynesia germanica</i>	0	0	0	0	0	0	0	0	0	0	0	0	0	0	0	0	0	0	0	0	1	0
<i>Quinqueloculina</i> spp.	0	0	0	0	0	0	0	0	0	0	0	13	0	0	0	0	0	0	0	0	0	0
<i>Spirillina vivipara</i>	0	0	0	0	0	0	0	0	0	0	0	0	0	0	0	0	0	0	0	0	0	0
Total	209	424	446	453	586	137	203	283	463	628	284	614	655	844	1102	471	366	509	584	264	233	171

Table A6. Jadrtovac Site 1 Core fossil foraminifera dead counts continued.

Foraminifera taxa	Sample Depth (cm)																					
	23	24	25	26	27	28	29	30	31	32	33	34	35	36	37	38	39	40	41	42		
<i>Balticammina pseudomacrescens</i>	0	0	0	0	0	0	0	0	0	0	0	0	0	0	0	0	0	0	0	0	0	0
<i>Haplophragmoides wilberti</i>	1	0	0	0	0	0	0	2	0	0	0	0	0	0	0	0	0	0	0	0	0	0
<i>Miliammina fusca</i>	34	35	52	27	11	11	3	14	14	8	2	4	1	6	8	6	0	0	0	0	0	0
<i>Jadammina macrescens</i>	98	84	99	89	130	37	21	57	28	7	1	1	0	2	0	1	0	0	0	0	0	0
<i>Reophax moniliformis</i>	0	0	0	0	0	0	0	0	0	0	0	0	0	0	0	0	0	0	0	0	0	0
<i>Siphotrochammina lobata</i>	0	0	0	0	0	0	0	0	0	0	0	0	0	0	0	0	0	0	0	0	0	0
<i>Trochammina inflata</i>	4	8	20	2	1	6	2	4	3	1	0	0	0	0	2	0	0	1	0	0	0	0
<i>Ammonia</i> spp.	16	7	5	3	4	74	33	59	63	61	77	101	89	110	168	149	148	68	98	130		
<i>Brazalina</i> spp.	0	0	0	0	0	0	0	0	0	0	0	0	0	0	0	0	0	0	0	0	0	0
<i>Elphidium</i> spp.	0	0	0	0	2	4	10	15	2	8	53	34	30	23	58	96	75	16	57	41		
<i>Haynesia germanica</i>	0	12	15	11	22	14	92	55	77	183	250	223	195	172	275	359	358	136	172	273		
<i>Quinqueloculina</i> spp.	0	0	0	0	0	0	0	0	1	0	0	0	1	0	0	0	0	0	3	0		
<i>Spirillina vivipara</i>	0	0	0	0	0	0	0	0	0	0	0	0	0	0	0	0	0	0	0	0	0	0
Total	153	146	191	132	170	146	161	206	188	268	383	363	316	313	511	611	581	221	330	444		

Table A7. Jadrtovac Site 2 Core fossil foraminifera counts.

Foraminifera taxa	Sample Depth (cm)																					
	1	2	3	4	5	6	7	8	9	10	11	12	13	14	15	16	17	18	19	20	21	22
<i>Balticammina pseudomacrescens</i>	0	0	0	0	0	0	0	0	0	0	0	0	0	0	0	0	0	0	0	0	0	0
<i>Haplophragmoides wilberti</i>	5	1	17	32	25	53	26	11	55	27	11	11	21	12	4	15	7	7	4	22	18	14
<i>Miliammina fusca</i>	144	315	399	686	998	925	833	730	1326	545	242	21	45	76	263	64	60	28	46	262	80	141
<i>Jadammina macrescens</i>	115	147	114	462	318	186	122	115	271	140	131	112	108	115	321	157	77	98	128	257	160	91
<i>Reophax moniliformis</i>	0	0	0	0	0	0	0	0	0	0	0	0	0	0	0	0	0	0	0	0	0	0
<i>Siphotrochammina lobata</i>	2	0	0	0	0	27	10	15	21	7	3	18	0	11	0	17	6	3	6	0	2	0
<i>Trochammina inflata</i>	220	290	318	417	679	915	628	636	869	750	535	419	517	720	633	628	342	368	397	345	405	372
<i>Ammonia</i> spp.	9	0	0	0	1	6	4	0	7	14	13	2	5	1	2	3	4	2	2	5	9	24
<i>Brazalina</i> spp.	0	0	0	0	0	0	0	0	0	0	5	0	0	1	0	0	0	0	0	0	0	0
<i>Elphidium</i> spp.	5	0	0	0	0	0	0	0	0	0	0	0	0	0	0	0	0	0	0	1	2	
<i>Haynesia germanica</i>	0	1	0	0	0	0	0	0	6	3	3	0	1	0	0	1	2	0	1	0	4	4
<i>Quinqueloculina</i> spp.	23	0	0	0	0	0	0	0	0	0	0	0	0	0	0	0	0	0	0	0	0	0
<i>Spirillina vivipara</i>	0	0	0	0	0	0	0	0	0	0	0	0	0	0	0	0	0	0	0	0	0	0
Total	523	754	848	1597	2021	2112	1623	1507	2555	1486	943	583	697	936	1223	882	498	506	584	891	679	648

Table A7. Jadrtovac Site 2 Core fossil foraminifera counts continued.

Foraminifera taxa	Sample Depth (cm)																					
	23	24	25	26	27	28	29	30	31	32	33	34	35	36	37	38	39	40	41	42	43	44
<i>Balticammina pseudomacrescens</i>	0	0	0	0	0	0	0	0	0	0	0	0	0	0	0	0	0	0	0	0	0	0
<i>Haplophragmoides wilberti</i>	11	8	0	0	6	4	1	0	2	2	2	0	4	3	2	1	2	0	0	0	0	0
<i>Miliammina fusca</i>	130	99	29	89	55	79	80	9	43	41	84	75	141	45	55	84	81	36	79	18	23	6
<i>Jadammina macrescens</i>	171	68	44	132	23	32	24	5	137	116	80	33	68	68	43	53	41	15	17	3	11	5
<i>Reophax moniliformis</i>	0	0	0	0	0	0	0	0	0	0	0	0	0	0	0	0	0	0	0	0	0	0
<i>Siphotrochammina lobata</i>	0	0	0	0	0	0	0	0	0	0	0	0	0	0	0	0	0	0	0	0	0	0
<i>Trochammina inflata</i>	515	200	85	97	65	92	55	15	85	56	121	55	117	42	25	34	21	12	54	14	8	10
<i>Ammonia</i> spp.	30	29	47	30	65	95	163	232	262	382	185	111	192	158	495	401	416	307	72	154	92	155
<i>Brazalina</i> spp.	0	0	0	0	0	0	0	0	0	0	0	0	0	0	0	0	0	0	0	0	0	0
<i>Elphidium</i> spp.	0	6	1	0	0	1	5	4	27	18	20	6	0	3	17	5	6	27	0	1	1	3
<i>Haynesia germanica</i>	8	13	10	4	3	12	22	61	24	27	21	10	22	18	23	22	11	22	7	10	11	16
<i>Quinqueloculina</i> spp.	0	0	0	0	0	0	0	0	0	0	0	0	0	0	0	0	0	0	0	0	0	0
<i>Spirillina vivipara</i>	0	0	0	0	0	0	0	0	0	0	0	0	0	0	0	0	0	0	0	0	0	0
Total	865	424	216	352	217	315	350	326	581	644	514	290	549	337	661	601	578	419	229	200	149	195

Table A7. Jadrtovac Site 2 Core fossil foraminifera counts continued.

Foraminifera taxa	Sample Depth (cm)											
	45	46	47	48	49	50	51	52	53	54	55	56
<i>Balticammina pseudomacrescens</i>	0	0	0	0	0	0	0	0	0	0	0	0
<i>Haplophragmoides wilberti</i>	0	0	0	0	0	0	0	0	0	0	0	0
<i>Miliammina fusca</i>	2	0	0	0	0	0	0	0	0	0	2	4
<i>Jadammina macrescens</i>	0	0	0	0	0	0	0	0	0	0	0	0
<i>Reophax moniliformis</i>	0	0	0	0	0	0	0	0	0	0	0	0
<i>Siphotrochammina lobata</i>	0	0	0	0	0	0	0	0	0	0	0	0
<i>Trochammina inflata</i>	2	1	0	0	0	1	0	0	0	0	3	1
<i>Ammonia</i> spp.	237	157	375	638	487	490	490	485	434	442	380	232
<i>Brazalina</i> spp.	0	0	0	0	0	0	0	0	0	0	0	0
<i>Elphidium</i> spp.	6	41	80	122	105	25	52	32	28	13	7	13
<i>Haynesia germanica</i>	19	21	32	31	18	4	31	23	37	58	30	27
<i>Quinqueloculina</i> spp.	0	0	0	0	0	0	0	0	0	0	0	0
<i>Spirillina vivipara</i>	0	0	0	0	0	0	0	0	0	0	0	0
Total	266	220	487	791	610	520	573	540	499	513	422	277

Table A8. Blace Core fossil foraminifera counts.

Foraminifera taxa	Sample Depth (cm)																					
	1	2	3	4	5	6	7	8	9	10	11	12	13	14	15	16	17	18	19	20	21	22
<i>Balticammina pseudomacrescens</i>	0	0	0	0	0	0	0	0	0	0	0	0	0	0	0	0	0	0	0	0	0	0
<i>Haplophragmoides wilberti</i>	8	10	5	2	12	0	1	11	10	9	3	3	0	0	8	7	0	0	3	8	0	1
<i>Miliammina fusca</i>	37	10	5	169	244	406	587	307	300	419	212	155	250	267	704	420	442	233	255	852	145	139
<i>Jadammina macrescens</i>	207	715	595	137	120	49	23	87	34	35	25	14	21	12	17	26	25	2	21	33	30	15
<i>Reophax moniliformis</i>	0	0	0	0	0	0	0	0	0	0	0	0	0	0	0	0	0	0	0	0	0	0
<i>Siphotrochammina lobata</i>	0	15	3	0	0	0	0	0	0	0	0	0	0	0	0	0	0	0	0	0	0	0
<i>Trochammina inflata</i>	132	240	165	450	315	655	652	456	255	192	165	120	185	111	240	160	118	34	48	220	36	13
<i>Ammonia</i> spp.	3	0	0	0	0	0	0	0	0	2	0	0	0	0	0	0	0	0	0	0	0	0
<i>Brazalina</i> spp.	2	0	0	0	1	0	0	0	0	0	0	0	0	0	0	0	0	0	0	0	0	0
<i>Elphidium</i> spp.	1	0	0	0	0	0	0	0	0	2	0	0	0	0	0	0	0	0	0	0	0	0
<i>Haynesia germanica</i>	0	0	0	0	0	0	0	0	0	0	0	0	0	0	0	0	0	0	0	0	0	0
<i>Quinqueloculina</i> spp.	9	0	0	0	0	0	0	0	0	0	2	0	0	0	0	0	0	0	0	0	0	0
<i>Spirillina vivipara</i>	0	0	0	0	0	0	0	0	0	0	0	0	0	0	0	0	0	0	0	0	0	0
Total	399	990	773	758	692	1110	1263	861	599	659	407	292	456	390	969	613	585	269	327	1113	211	168

Table A8. Blace Core fossil foraminifera counts continued.

Foraminifera taxa	Sample Depth (cm)									
	23	24	25	26	27	28	29	30	31	32
<i>Balticammina pseudomacrescens</i>	0	0	0	0	0	0	0	0	0	0
<i>Haplophragmoides wilberti</i>	1	0	0	0	0	0	0	0	0	0
<i>Miliammina fusca</i>	236	210	323	61	35	54	1	2	3	17
<i>Jadammina macrescens</i>	27	52	117	82	30	9	6	3	3	17
<i>Reophax moniliformis</i>	0	0	0	0	0	0	0	0	0	0
<i>Siphotrochammina lobata</i>	0	0	0	0	0	0	0	0	0	0
<i>Trochammina inflata</i>	131	19	28	31	26	30	14	24	19	40
<i>Ammonia</i> spp.	0	1	1	2	22	55	193	332	217	397
<i>Brazalina</i> spp.	0	0	0	0	0	0	2	9	4	7
<i>Elphidium</i> spp.	0	0	0	1	0	3	24	110	74	142
<i>Haynesia germanica</i>	0	0	0	2	2	3	2	15	17	48
<i>Quinqueloculina</i> spp.	0	0	0	1	0	0	0	3	1	0
<i>Spirillina vivipara</i>	0	0	0	0	0	0	0	0	0	0
Total	277	282	469	179	116	154	242	498	338	668

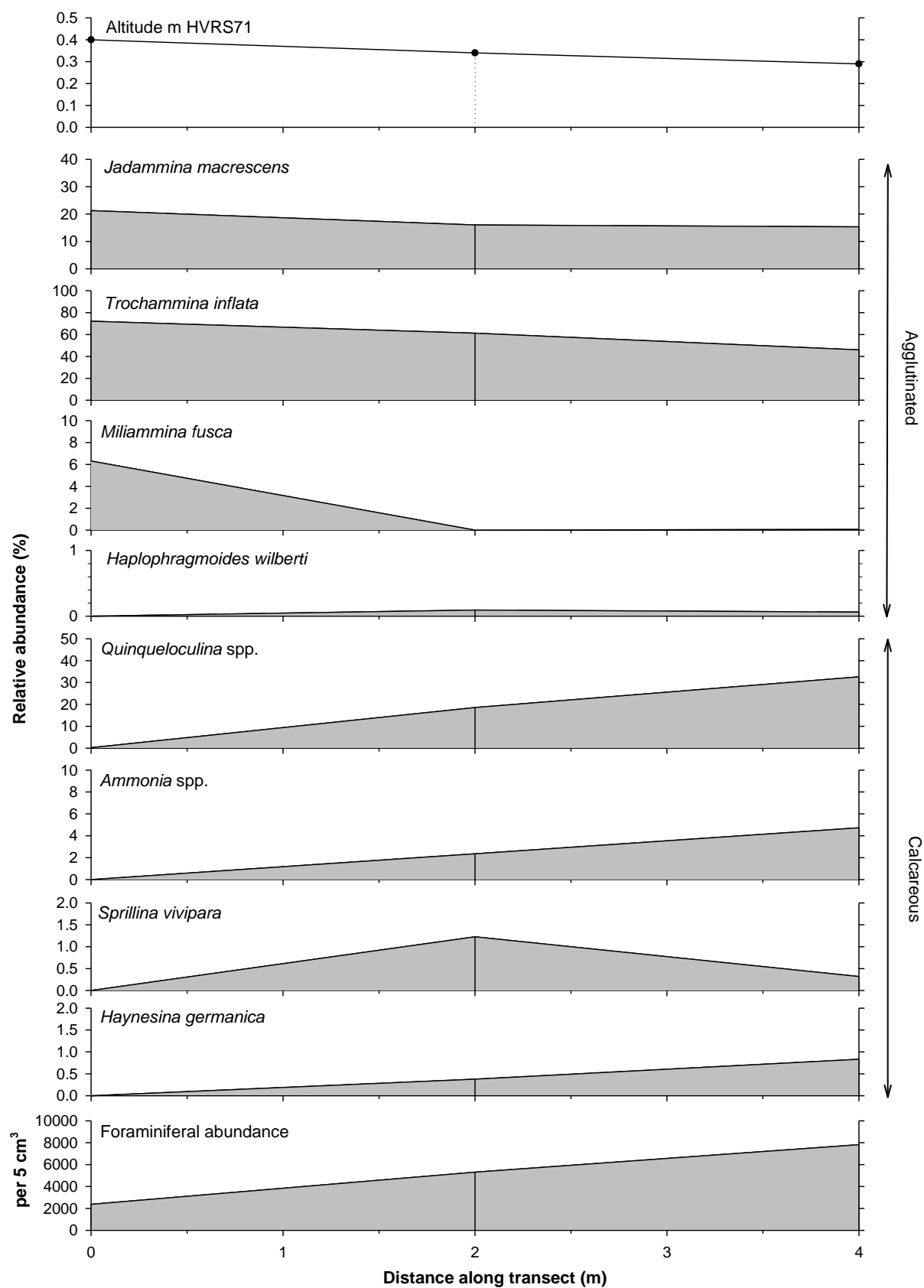


Figure A1. Relative abundance (%) of 'dead' foraminifera and concentration (per 5 cm³) for samples 16, 17 and 18 from BL1. Altitude (m hvrs71) also shown.

APPENDIX C. RADIOCARBON ANALYTICAL REPORT

SGM/1678.1012.001

3rd April 2013

Dr AJ Plater
School of Environmental Sciences
Roxby Building
University of Liverpool
Liverpool
L69 3BX



**NATURAL
ENVIRONMENT
RESEARCH COUNCIL**

Radiocarbon Facility
Scottish Enterprise Technology Park
Rankine Avenue
East Kilbride
G75 0QF

Phone: +44 (0) 1355 260037
Fax: +44 (0) 1355 229829
Email: c.bryant@nerc.rl.gla.ac.uk
Webpage: www.gla.ac.uk/nercrl

Dear Andy

Radiocarbon Analysis Allocation Number 1678.1012

I enclose the formal report for the samples submitted under the above project number. The samples were prepared to graphite at the NERC Radiocarbon Facility-East Kilbride and passed to the SUERC AMS Laboratory for ^{14}C analysis. For any appropriate accounting exercise the full economic cost of the three ^{14}C measurements is £1,740.

In keeping with international practice the result is reported as conventional radiocarbon years BP (relative to AD 1950) and % modern ^{14}C , both expressed at the $\pm 1\sigma$ level for overall analytical confidence. Unless otherwise noted the result has been corrected to $\delta^{13}\text{C}_{\text{VPDB}}\text{‰} -25$ using the $\delta^{13}\text{C}$ values provided in the report. The $\delta^{13}\text{C}$ value was measured on a dual inlet stable isotope mass spectrometer (Thermo Fisher Delta V) and is representative of $\delta^{13}\text{C}$ in the original, pre-treated sample material. The quoted precision is the uncertainty of repeated measurements of the same CO_2 aliquot, ie machine error only. Please let me know if you have any questions concerning the numerical significance of the results and/or the experimental procedures used.

Publication is the prime indicator of science supported by NRCF and therefore an important means by which the value of the facility to the scientific community is judged. Please send us bibliographic reference to and/or copies of any publications (including those not peer-reviewed) and PhD theses, which discuss or describe the results in this report. If you have any comments on the significance of the results in the context of your original research objectives and/or on the report itself please also let us know. Such response will be fed back to the appropriate awarding Committee(s) at NERC. The above project allocation number should be quoted in any correspondence.

May I remind you that, to avoid ambiguity, the uniquely assigned lab codes (SUERC-) and also the facilities where the samples were prepared to graphite and analysed should be quoted as an essential component in the publication/discussion of these data. Likewise, the support provided through NERC should be acknowledged in all relevant publications. The fulfilment of this requirement will be considered in the allocation of future NERC support.

Best wishes,

Dr Steve Moreton
Enc Radiocarbon Analytical Report

1678.1012.001

NERC Radiocarbon Facility (Environment)

RADIOCARBON ANALYTICAL REPORT

Allocation No: 1678.1012 **Submitter:** AJ Plater
University of Liverpool

Project Title: Establishing Holocene and Historical Sea-level Trends for the Croatian Coast of the Adriatic.

Sampling location: Jadrtovac, Croatia

Sample composition: Scirpus seeds from saltmarsh sediment cores.

Pre-treatment of raw samples: Samples were digested in 1M HCl (80°C, 30 minutes), washed free from mineral acid with deionised water. Then samples were digested in 0.2M KOH (80°C, for a maximum of 20 minutes). The digestion was repeated using deionised water until no further humics were extracted. The residue was rinsed free of alkali, digested in 1M HCl (80°C, 1 hours) then rinsed free of acid, transferred to a Ag cup, dried and homogenised.

The total carbon in the pre-treated sample was recovered as CO₂ by heating with CuO in a sealed quartz tube. The gas was converted to graphite by Fe/Zn reduction.

Results:

Publication Code	Sample Identifier	¹⁴ C Enrichment (% Modern ± 1σ)	Conventional Radiocarbon Age (years BP ± 1σ)	Carbon content (% by wt.)	δ ¹³ C _{V-PDB} ‰ ± 0.1‰
SUERC-45020	JD1 25-26	98.86±0.44	256±37	*	-25.3
SUERC-45021	JD1 26-27	97.38±0.45	213±37	*	-26.2
SUERC-45022	JD1 28-30	98.61±0.45	112±37	*	-26.8

* Carbon content not possible to determine accurately due to the small size of the pretreated material

Dr Steve Moreton

3rd April 2013

1678.1012.001

APPENDIX D. TRANSFER FUNCTION RESULTS

Table A9. Palaeo-marsh altitude, standard prediction errors (bootstrap) and minimum dissimilarity coefficient (minDC) values for JD1 core fossil samples.

Core depth (cm)	PMA (PLS)	SE _{pred}	PMA (WA-PLS)	SE _{pred}	minDC	Analogue
1	0.358778	0.090741	0.263176	0.08216	1.23841	good
2	0.344818	0.090248	0.252516	0.082088	0.99712	good
3	0.310159	0.087927	0.220104	0.081293	1.38563	good
4	0.29547	0.08571	0.214406	0.08093	8.78385	good
5	0.330031	0.088866	0.235825	0.081338	1.52705	good
6	0.304887	0.086863	0.215969	0.080965	5.14176	good
7	0.300016	0.086149	0.214007	0.080925	7.53881	good
8	0.273068	0.084305	0.197569	0.082063	16.1939	close
9	0.257936	0.084261	0.184913	0.082855	15.7353	close
10	0.243874	0.083694	0.180769	0.085269	19.0732	close
11	0.261852	0.084443	0.18697	0.082482	12.5937	good
12	0.294182	0.084854	0.213821	0.081094	13.5495	good
13	0.272764	0.084312	0.197143	0.081997	16.4316	close
14	0.343316	0.089006	0.250812	0.081419	0.055834	good
15	0.320063	0.086724	0.233483	0.080928	3.41987	good
16	0.288327	0.084202	0.221394	0.082663	8.24073	good
17	0.287847	0.084187	0.220249	0.083536	9.23383	good
18	0.243959	0.083776	0.188922	0.087899	18.7446	close
19	0.252128	0.083851	0.196472	0.087763	18.3511	close
20	0.230369	0.083594	0.175167	0.087059	23.1114	close
21	0.259821	0.08358	0.192816	0.083672	11.0545	good
22	0.183181	0.084402	0.123738	0.086225	47.4925	poor
23	0.175624	0.08699	0.104124	0.085182	29.1564	poor
24	0.19978	0.086061	0.128719	0.084991	31.3089	poor
25	0.218555	0.085305	0.148398	0.084142	23.4001	close
26	0.199307	0.087623	0.126465	0.086554	29.0673	poor
27	0.193946	0.089382	0.115606	0.087839	24.8083	close
28	0.036663	0.085892	-0.03803	0.083722	46.657	poor
29	0.119837	0.082934	-0.0225	0.083672	97.897	poor
30	0.099394	0.084035	0.006114	0.083156	63.7405	poor
31	0.085202	0.083742	-0.03961	0.083797	77.6329	poor
32	0.110558	0.082727	-0.09381	0.085932	103.439	poor
33	0.110435	0.082367	-0.06901	0.089461	93.4881	poor
34	0.088624	0.082908	-0.10591	0.088085	82.8369	poor
35	0.087759	0.082932	-0.11003	0.088285	82.8558	poor
36	0.066762	0.083512	-0.12013	0.087723	71.9788	poor
37	0.072319	0.083251	-0.10116	0.087988	69.955	poor
38	0.095749	0.082579	-0.07166	0.089201	82.0323	poor
39	0.093634	0.082713	-0.09322	0.089147	83.5163	poor
40	0.081204	0.083219	-0.1269	0.088402	80.4443	poor
41	0.079216	0.0829	-0.07778	0.088826	70.258	poor
42	0.083675	0.083049	-0.11902	0.088649	81.1039	poor

Table A10. Palaeo-marsh altitude, standard prediction errors (bootstrap) and minimum dissimilarity coefficient (minDC) values for JD2 core fossil samples.

Core depth (cm)	PMA (PLS)	SE _{pred}	PMA (WA-PLS)	SE _{pred}	minDC	Analogue
1	0.221685	0.082879	0.300908	0.084755	6.20393	good
2	0.220666	0.08397	0.291817	0.084388	9.90959	good
3	0.223808	0.08474	0.289033	0.084285	8.33166	good
4	0.198412	0.084231	0.263299	0.083855	14.4097	good
5	0.216505	0.084951	0.280068	0.083936	8.17863	good
6	0.234674	0.084631	0.301078	0.085039	9.70352	good
7	0.228312	0.085509	0.290713	0.084518	9.80396	good
8	0.233781	0.085101	0.299734	0.084915	10.8506	good
9	0.220188	0.085566	0.279732	0.083999	8.21891	good
10	0.241017	0.084005	0.315734	0.08609	11.9169	good
11	0.245188	0.083493	0.329016	0.087158	7.21574	good
12	0.269271	0.084861	0.367171	0.090628	1.65503	good
13	0.271731	0.084785	0.371463	0.091174	5.5504	good
14	0.279333	0.084935	0.379792	0.091883	5.65838	good
15	0.234084	0.083103	0.322324	0.08629	3.28848	good
16	0.26778	0.084511	0.365861	0.090369	3.43907	good
17	0.263584	0.084137	0.358475	0.089762	2.64522	good
18	0.267439	0.084641	0.369532	0.090697	2.75941	good
19	0.259403	0.084178	0.358834	0.089529	2.10402	good
20	0.213979	0.083131	0.290568	0.084728	12.7978	good
21	0.244057	0.083575	0.335982	0.08785	2.37469	good
22	0.237147	0.083432	0.322652	0.087446	8.23437	good
23	0.237409	0.083482	0.328952	0.087856	4.60104	good
24	0.209234	0.083082	0.287421	0.085844	13.4305	good
25	0.138093	0.083877	0.221746	0.086138	23.3591	close
26	0.162978	0.083267	0.239345	0.084571	16.9749	close
27	0.099935	0.08528	0.173346	0.085782	26.7812	poor
28	0.097231	0.085326	0.170489	0.085752	29.4098	poor
29	0.012089	0.088682	0.08436	0.087225	43.1596	poor
30	-0.13963	0.0995	-0.02382	0.093002	35.1797	poor
31	0.005716	0.087297	0.08493	0.087313	39.2343	poor
32	-0.05304	0.091176	0.02613	0.089723	31.2172	poor
33	0.059692	0.085496	0.135571	0.086131	39.1494	poor
34	0.050485	0.08653	0.119144	0.085891	41.727	poor
35	0.065328	0.08626	0.136771	0.08561	36.6537	poor
36	-0.00133	0.088343	0.076876	0.087244	43.8563	poor
37	-0.11048	0.096068	-0.03615	0.093311	26.8176	poor
38	-0.07614	0.09371	-0.0036	0.091023	33.7032	poor
39	-0.09345	0.095027	-0.02535	0.092241	33.1523	poor
40	-0.11163	0.09549	-0.03668	0.093048	19.991	close
41	0.088207	0.086229	0.153809	0.085243	36.4766	poor
42	-0.11206	0.097428	-0.03422	0.094239	29.9816	poor
43	-0.07034	0.093425	0.007521	0.090158	38.2574	poor
44	-0.1369	0.099123	-0.04809	0.095088	26.3731	close
45	-0.17716	0.102574	-0.0901	0.097872	16.3934	close
46	-0.13206	0.095408	-0.04742	0.093385	11.6421	good
47	-0.14286	0.096571	-0.06444	0.094787	9.98769	good
48	-0.14704	0.097117	-0.07502	0.095753	7.93063	good

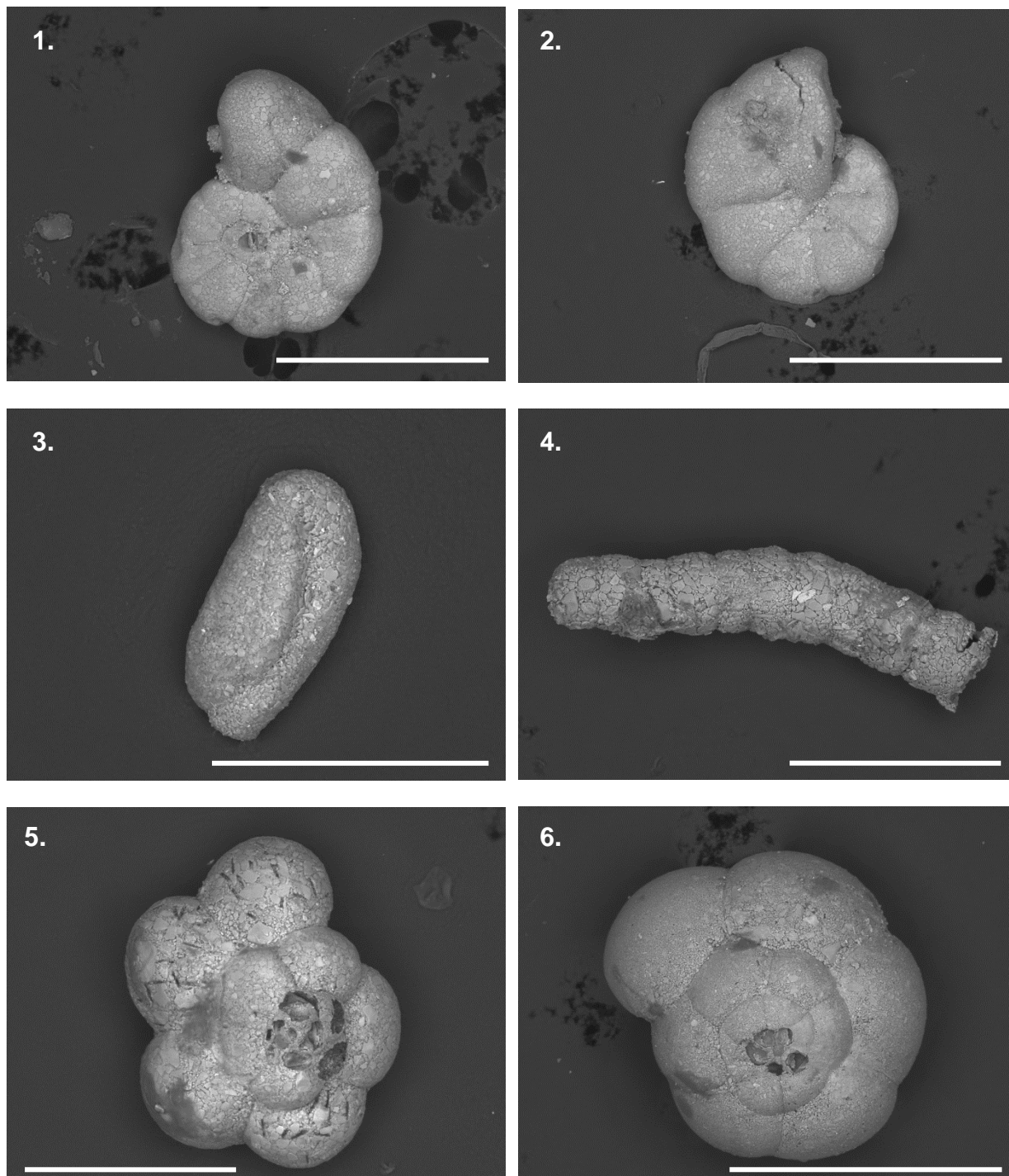
Table A10 continued.

Core depth (cm)	PMA (PLS)	SE _{pred}	PMA (WA-PLS)	SE _{pred}	minDC	Analogue
49	-0.14244	0.096518	-0.07371	0.095569	6.80811	good
50	-0.17668	0.101898	-0.10918	0.099458	7.49407	good
51	-0.16469	0.099738	-0.08569	0.096978	9.3805	good
52	-0.17399	0.101316	-0.09681	0.098158	9.27652	good
53	-0.17434	0.101378	-0.08784	0.097331	11.9724	good
54	-0.1831	0.102984	-0.08324	0.097049	18.1091	good
55	-0.18025	0.103042	-0.09277	0.098156	17.1832	close
56	-0.16873	0.10105	-0.07613	0.096329	16.0025	close

Table A11. Palaeo-marsh altitude, standard prediction errors (bootstrap) and minimum dissimilarity coefficient (minDC) values for BL core fossil samples.

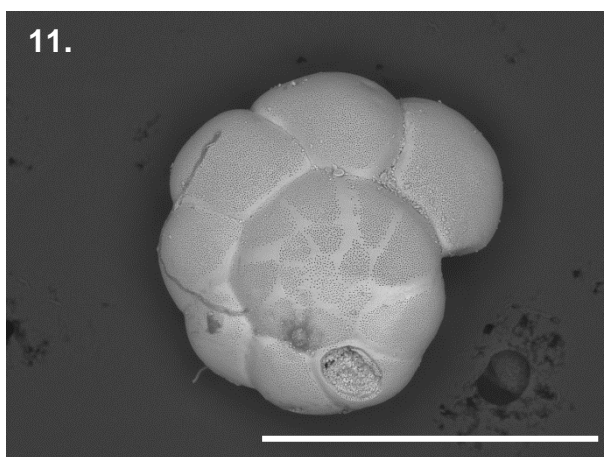
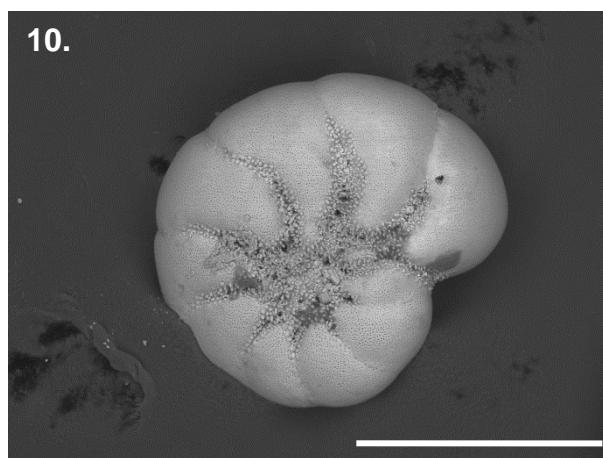
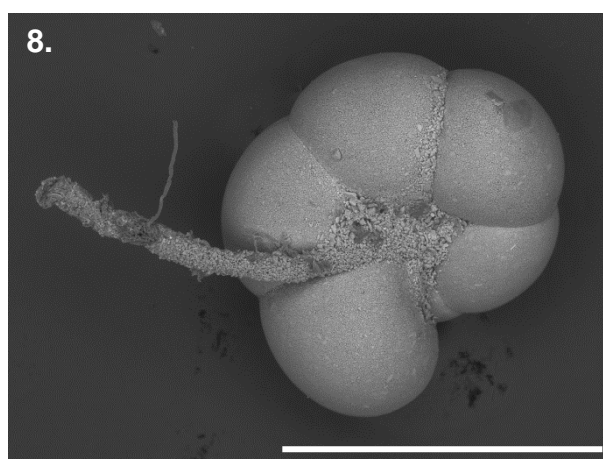
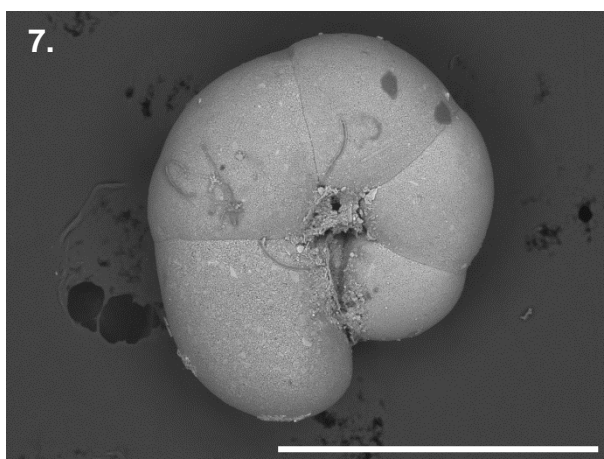
Core depth (cm)	PMA (PLS)	SE _{pred}	PMA (WA-PLS)	SE _{pred}	minDC	Analogue
1	0.26901	0.086587	0.196317	0.082591	4.36298	Good
2	0.247447	0.08877	0.171931	0.085033	2.30708	Good
3	0.241351	0.089367	0.165254	0.08561	1.31219	Good
4	0.327125	0.089116	0.253375	0.082762	2.38762	Good
5	0.298611	0.085676	0.236734	0.08361	11.9415	Good
6	0.328409	0.088518	0.261712	0.084676	21.0714	Close
7	0.313751	0.086683	0.253942	0.086114	21.0573	Close
8	0.314931	0.087081	0.250975	0.084092	14.485	Good
9	0.294334	0.085036	0.240554	0.08656	12.5983	Good
10	0.26588	0.08394	0.221519	0.089806	12.9449	Good
11	0.291207	0.08473	0.237593	0.086845	10.8826	Good
12	0.29166	0.084848	0.238879	0.087163	13.5541	Good
13	0.290935	0.084791	0.237808	0.087431	13.9574	Good
14	0.26656	0.084133	0.223196	0.091049	19.2097	Close
15	0.258991	0.084228	0.219557	0.0926	24.0457	Close
16	0.261251	0.084037	0.219744	0.091267	17.9357	Close
17	0.249554	0.084396	0.211718	0.093313	22.8673	Close
18	0.234757	0.085542	0.204323	0.097463	40.5856	Poor
19	0.237815	0.084742	0.203361	0.094417	25.5143	Close
20	0.248696	0.084455	0.212226	0.093874	25.4418	Close
21	0.241835	0.084194	0.201178	0.091002	17.434	Close
22	0.223464	0.085685	0.192652	0.096172	34.71	Poor
23	0.217236	0.086261	0.188162	0.097106	41.1833	Poor
24	0.219036	0.085401	0.183755	0.093135	31.6722	Poor
25	0.217051	0.085397	0.179026	0.091465	33.8405	Poor
26	0.233188	0.084895	0.1757	0.08413	15.2901	Close
27	0.18584	0.084002	0.128729	0.082903	19.7006	Close
28	0.121311	0.084624	0.070375	0.084233	40.9109	Poor
29	-0.06601	0.090554	-0.12408	0.085268	6.98337	Good
30	-0.03241	0.087593	-0.09828	0.084786	7.06731	Good
31	-0.02298	0.087287	-0.09178	0.084691	9.74278	Good
32	-0.00641	0.086546	-0.07846	0.0844	14.0654	Good

APPENDIX E. SCANNING ELECTRON MICROSCOPE IMAGES



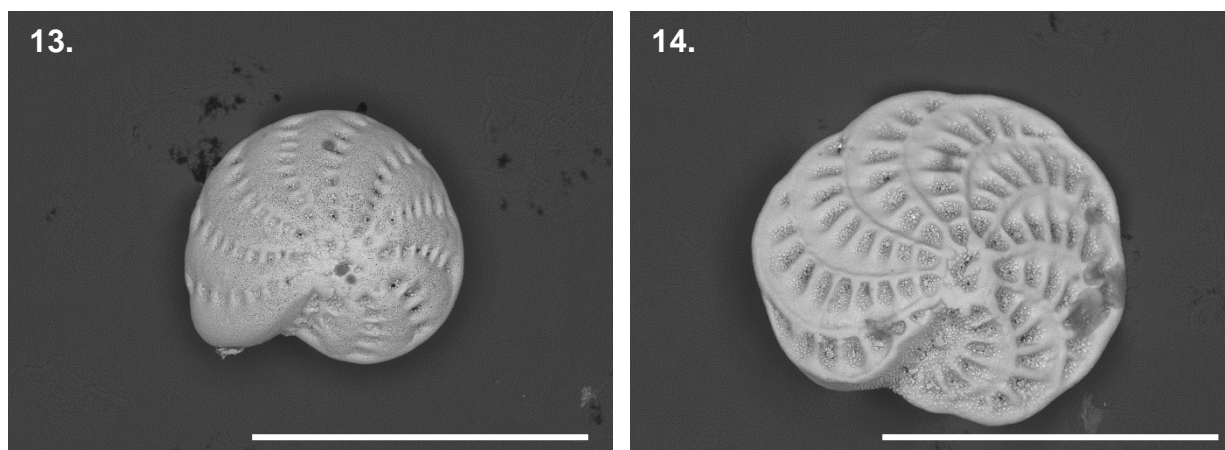
Key:

1. *Jadammina macrescens* (spiral view, scale = 300 μ m).
2. *Haplophragmoides* spp. (side view, scale = 300 μ m).
3. *Miliammina fusca* (side view, scale = 200 μ m).
4. *Reophax moniliformis* (side view, scale = 300 μ m).
5. *Siphrochammina inflata* (spiral view, scale = 300 μ m).
6. *Trochammina inflata* (spiral view, scale = 400 μ m).



Key:

- 7. *Trochammina inflata* (umbilical view, scale = 400µm).
- 8. *Trochammina inflata* (umbilical view showing 'feeding arm', scale = 400µm).
- 9. *Quinqueloculina* spp. (side view, scale = 300µm).
- 10. *Haynesina germanica* (spiral view, scale = 300µm).
- 11. *Ammonia* spp. (spiral view, scale = 400µm).
- 12. *Ammonia* spp. (umbilical view, scale = 400µm).



Key:

13. *Elphidium* spp. (spiral view, scale 300= μm).

14. *Elphidium* spp. (umbilical view, scale = 300 μm).

APPENDIX F. TIDAL LEVELS

Table A12. Details of water level tidal heights recorded and converted into altitude by the Hydrographic Institute, Croatia (Hydrographic Institute, 1955–2002).

Date	Time	Altitude m HVR571
18/01/2010	12:50	-0.08
19/01/2010	15:00	-0.04
21/01/2010	13:20	+0.02